




Faculty of Science and Technology

# MASTER'S THESIS

Study program/ Specialization: Petroleum Engineering/Drilling Technology	Spring semester, 2019 Open
Writer: Simen Moe Strømø	 (Writer's signature)
Faculty supervisor: Mesfin Belayneh	
Title of thesis: Formulation of New Drilling Fluids and Characterization in HPHT	
Credits (ECTS): 30	
Key words: <ul style="list-style-type: none"><li>▪ Viscoelasticity</li><li>▪ Polymers</li><li>▪ Flat rheology</li><li>▪ Barite sag</li><li>▪ Wellbore hydraulics simulations</li><li>▪ Nanoparticles</li><li>▪ Torque &amp; Drag simulations</li></ul>	Pages: 164 + enclosures: 14 Stavanger, 15.06.2019



## ABSTRACT

During the well construction process, a properly designed and formulated drilling fluid is vital in order to successfully drill a well. In HPHT wells, both WBM and OBM properties are significantly affected, specially the rheological and physical properties. Alteration in fluid properties may cause; challenges with respect to maintain the annular pressure, higher potential for barite sagging, as well as poor hole cleaning.

This thesis presents relevant drilling fluid literature study and basic theory for experimental work and simulation studies. Several different fluid systems, both water-based and oil-based, were formulated and characterized with respect to rheology, viscoelasticity, friction and barite sag. Additionally, performance simulation studies, including torque & drag and hydraulics, were performed with some of the best performing fluid systems.

As thermal stability is critical for drilling fluids in order to maintain their physical properties and functions at any given wellbore environment, an optimized lignosulfonates-based flat rheology water-based drilling fluid was formulated. The best thermally stable WBM system was further modified by a MoS<sub>2</sub>-nanofluid. The application of the nanofluid enhanced the lubricity of the fluid system with a total of 40%, resulting in an 6.12% increase in expected maximum measured drilling depth.

In HPHT environments, barite sag is considered one of the most prominent oil-based drilling fluid challenges, as OBMs tend to lose viscosity when heated. In order to avoid this problem, an effort was made to try to identify an anti-sagging agent. The experimental results showed that the application of 0.17 wt% of the polymer poly partial sodium salt increased the sag preventive properties of two different oil-based drilling fluid systems.

## ACKNOWLEDGEMENT

First of all, I would like to express my appreciations to my supervisor Mesfin Belayneh for his never-ending engagement, endless knowledge and continuous support throughout the work with this thesis. Your knowledge and guidance have been of great help.

Additionally, I would like to thank Line Frøland and M-I Swaco for providing oil-based drilling fluids and supplementary additives and chemicals.

Lastly, I would like to thank the University of Stavanger for letting me use their facilities and equipment in order to perform experimental work and simulations.

# TABLE OF CONTENTS

<b>ABSTRACT .....</b>	<b>i</b>
<b>ACKNOWLEDGEMENT .....</b>	<b>ii</b>
<b>LIST OF FIGURES .....</b>	<b>vii</b>
<b>LIST OF TABLES .....</b>	<b>xi</b>
<b>LIST OF NOMENCLATURE.....</b>	<b>xiii</b>
<b>LIST OF ABBREVIATIONS .....</b>	<b>xv</b>
<b>1 INTRODUCTION .....</b>	<b>1</b>
1.1 Background.....	2
1.2 Problem Definition .....	4
1.3 Objective and Scope .....	4
1.4 Research Program .....	5
<b>2 LITERATURE STUDIES.....</b>	<b>6</b>
2.1 Drilling Fluid.....	6
2.1.1 Drilling Fluid Properties .....	6
2.1.2 Drilling Fluid Functions .....	7
2.1.3 Drilling Fluid Types.....	8
2.2 High-Pressure, High-Temperature Drilling Fluid Challenges.....	12
2.2.1 HPHT Density Prediction.....	12
2.2.2 HPHT Viscosity Prediction.....	16
2.3 Barite Sag in Drilling Fluids .....	18
2.3.1 Drilling Parameters Affecting Barite Sag.....	18
2.3.2 Barite Sag in Highly Deviated Wellbores .....	19
2.3.3 Settling of Weight Material in Oil-Based Drilling Fluids.....	19
2.4 Yield Stress of Drilling Fluids.....	21
2.5 Application of Nanoparticles in Drilling Fluids .....	22
<b>3 THEORY.....</b>	<b>24</b>
3.1 Rheology.....	24
3.1.1 Plastic Viscosity.....	24
3.1.2 Yield Point.....	24
3.1.3 Gel Strength.....	24
3.1.4 Shear Stress .....	25

3.1.5	Shear Rate .....	25
<b>3.2</b>	<b>Rheological Models .....</b>	<b>26</b>
3.2.1	Newtonian Fluid .....	26
3.2.2	Non-Newtonian Fluids.....	27
<b>3.3</b>	<b>Viscoelasticity .....</b>	<b>34</b>
3.3.1	Mathematical Representation of Viscoelasticity .....	35
3.3.2	Viscoelastic Models .....	38
3.3.3	Viscoelastic Tests.....	39
<b>3.4</b>	<b>Barite Sag .....</b>	<b>45</b>
3.4.1	Static Testing .....	46
3.4.2	Dynamic Testing .....	48
<b>3.5</b>	<b>Hydraulics .....</b>	<b>50</b>
3.5.1	ECD .....	50
3.5.2	Drilling Fluid Circulation System and Pump Pressure .....	52
<b>3.6</b>	<b>Electrical Stability .....</b>	<b>53</b>
<b>3.7</b>	<b>Tribology and Friction.....</b>	<b>54</b>
<b>3.8</b>	<b>Torque and Drag.....</b>	<b>56</b>
3.8.1	Torque.....	57
3.8.2	Drag.....	58
3.8.3	Tensile and Torsional Limit.....	59
<b>4</b>	<b>EXPERIMENTAL WORK STUDIES.....</b>	<b>61</b>
<b>4.1</b>	<b>Drilling Fluid Formulation .....</b>	<b>61</b>
4.1.1	Water-Based Drilling Fluid Formulation .....	61
4.1.2	Oil-Based Drilling Fluid Formulation.....	63
<b>4.2</b>	<b>Description of Drilling Fluid Additives .....</b>	<b>65</b>
4.2.1	Additives.....	65
4.2.2	Polymer Additives.....	67
4.2.3	Nanoparticle Additives .....	68
<b>4.3</b>	<b>Experimental Equipment and Methodology .....</b>	<b>70</b>
4.3.1	Ofite Viscometer and Rheology Measurement Procedure.....	70
4.3.2	Anton Paar Rheometer and Testing Procedure.....	71
4.3.3	Barite Sag Equipment and Methodology.....	72
4.3.4	Friction CSM Tribometer .....	74
<b>5</b>	<b>RESULTS.....</b>	<b>75</b>
<b>5.1</b>	<b>Flat Rheology Water-Based Drilling Fluid Formulation .....</b>	<b>75</b>
5.1.1	Effect of Lignosulfonates and Temperature on Rheological Parameters .....	75

5.1.2	Effect of Lignosulfonates on Viscoelastic Properties.....	78
<b>5.2</b>	<b>MoS<sub>2</sub>-Nanofluid Based Water-Based Drilling Fluid .....</b>	<b>81</b>
5.2.1	Effect of MoS <sub>2</sub> -Nanofluid on Rheological Properties.....	81
5.2.2	Effect of MoS <sub>2</sub> -Nanofluid on the Lubricity of the Drilling Fluid System.....	82
5.2.3	Effect of MoS <sub>2</sub> -Nanofluid on Viscoelastic Properties - In-situ vs Ex-situ Treated Drilling Fluids.....	83
<b>5.3</b>	<b>Oil-Based Drilling Fluid Characterization and Solution to Sagging Issues .....</b>	<b>84</b>
5.3.1	M-I Swaco OBMs - Escaid Base Oil.....	84
5.3.2	UIS 90/10 OMB - EDC 95/11 Base Oil .....	93
<b>6</b>	<b>RHEOLOGICAL MODELLING AND WELLBORE SIMULATIONS.....</b>	<b>99</b>
<b>6.1</b>	<b>Rheological Modelling .....</b>	<b>99</b>
6.1.1	Rheological Modelling for Lignosulfonates Water-Based Drilling Fluids .....	100
6.1.2	Rheological Modelling for Oil-Based Drilling Fluids .....	107
<b>6.2</b>	<b>Simulation-Well Arrangement for Hydraulic Performance.....</b>	<b>114</b>
<b>6.3</b>	<b>Pump Pressure Simulations .....</b>	<b>115</b>
6.3.1	Pump Pressure for Water-Based Drilling Fluids.....	115
6.3.2	Pump Pressure for Oil-Based Drilling Fluids .....	116
<b>6.4</b>	<b>ECD Simulations.....</b>	<b>119</b>
6.4.1	ECD Simulations for Water-Based Drilling Fluids.....	119
6.4.2	ECD Simulations for Oil-Based Drilling Fluids.....	120
<b>6.5</b>	<b>Torque &amp; Drag Simulations .....</b>	<b>123</b>
6.5.1	Simulation Arrangement .....	123
6.5.2	Torque and Drag Simulation Evaluation .....	123
<b>7</b>	<b>SUMMARY AND DISCUSSION.....</b>	<b>125</b>
<b>7.1</b>	<b>Drilling Fluid Characterization .....</b>	<b>125</b>
7.1.1	Characterization of Flat Rheology Water-Based Drilling Fluids .....	125
7.1.2	Characterization of MoS <sub>2</sub> -Nanofluid - Ex-situ vs In-situ Treatment of Flat Rheology WBM.....	126
7.1.3	Characterization of Oil-Based Drilling Fluids.....	127
7.1.4	Evaluation of Yield Stress.....	130
<b>7.2</b>	<b>Hydraulic Performance.....</b>	<b>132</b>
7.2.1	Hydraulic Performance of Water-Based Drilling Fluids .....	132
7.2.2	Hydraulic Performance of Oil-Based Drilling Fluids .....	133
<b>7.3</b>	<b>Measurement Limitations and Uncertainties .....</b>	<b>136</b>
7.3.1	Uncertainty and Limitations .....	136
7.3.2	Viscometer Measurements .....	136
7.3.3	Rheometer Measurements .....	137
7.3.4	Barite Sag Measurements .....	137

<b>8 CONCLUSION.....</b>	<b>138</b>
<b>8.1 Conclusions for Water-Based Drilling Fluids .....</b>	<b>138</b>
8.1.1 Effect of Lignosulfonates .....	138
8.1.2 Effect of MoS <sub>2</sub> -Nanofluid.....	139
<b>8.2 Conclusions for Oil-Based Drilling Fluids .....</b>	<b>139</b>
8.2.1 Effect of Emulsifier One-Mul .....	139
8.2.2 Effect of the Polymer Poly Partial Sodium Salt (Poly Acrylic).....	139
<b>BIBLIOGRAPHY.....</b>	<b>140</b>
<b>APPENDICES.....</b>	<b>147</b>
APPENDIX A – RHEOLOGICAL MEASUREMENTS.....	147
APPENDIX B - VISCOELASTICITY .....	153
APPENDIX C – BARITE SAG .....	156
APPENDIX D – FRICTION MEASUREMENT AND TORQUE & DRAG SIMULATIONS.....	158



# LIST OF FIGURES

**FIGURE 1.1:** A ILLUSTRATION OF AN ARBITRARY PORE PRESSURE AND FRACTURE PRESSURE GRADIENT PLOT [5]..... 2

**FIGURE 1.2:** SUMMARY OF THE RESEARCH PROGRAM USED FOR THIS THESIS..... 5

**FIGURE 2.1:** ILLUSTRATION OF THE FLUID FLOW THROUGH DRILL PIPE AND RETURN THROUGH ANNULUS [20]..... 14

**FIGURE 2.2:** DRILLING FLUID TEMPERATURE PROFILE DURING CIRCULATION PROCESS ..... 15

**FIGURE 2.3:** EFFECT OF TEMPERATURE ON DRILLING FLUID DENSITY ..... 15

**FIGURE 2.4:** EFFECT OF TEMPERATURE ON THE BUOYANCY FACTOR..... 15

**FIGURE 2.5:** ILLUSTRATION OF EFFECT OF TEMPERATURE AND PRESSURE ON THE VISCOSITY OF DRILLING FLUID..... 17

**FIGURE 2.6:** ILLUSTRATION OF A "FLOW LOOP TEST" [22] ..... 19

**FIGURE 2.7:** VISCOSITY VS. SHEAR STRESS FOR A 10% SUSPENSION OF BENTONITE [25] ..... 21

**FIGURE 3.1:** VELOCITY, SHEAR RATE AND SHEAR STRESS PROFILE ILLUSTRATION OF THE FLUID FLOW IN A TUBE [31] ..... 25

**FIGURE 3.2:** NEWTONIAN FLUID MODEL REPRESENTED IN A SHEAR STRESS VS. SHEAR RATE PLOT [32] ..... 26

**FIGURE 3.3:** NEWTONIAN FLUID AND AN ARBITRARY DRILLING MUD IN A SHEAR STRESS VS. SHEAR RATE PLOT [32] ..... 27

**FIGURE 3.4:** ILLUSTRATION OF PLASTIC, PSEUDOPLASTIC AND DILATANT FLUIDS IN A VISCOSITY VS. STRESS DIAGRAM [33] ..... 28

**FIGURE 3.5:** BINGHAM PLASTIC MODEL REPRESENTED IN A SHEAR STRESS VS. SHEAR RATE PLOT [32]..... 29

**FIGURE 3.6:** POWER LAW MODEL REPRESENTED IN A SHEAR STRESS VS. SHEAR RATE PLOT [32] ..... 30

**FIGURE 3.7:** HERSCHEL-BULKLEY MODEL REPRESENTED IN A SHEAR STRESS VS. SHEAR RATE PLOT [32] ..... 31

**FIGURE 3.8:** THE "RANGE OF MATERIAL BEHAVIOR" [38] ..... 34

**FIGURE 3.9:** STORAGE MODULUS ( $G'$ ) AND LOSS MODULUS ( $G''$ ) AS A FUNCTION OF SHEAR STRAIN AND SHEAR STRESS, RESPECTIVELY [40] ..... 37

**FIGURE 3.10:** COMPLEX SHEAR MODULUS ( $G^*$ ) AND COMPLEX VISCOSITY ( $\eta^*$ ) ILLUSTRATED IN VECTOR DIAGRAMS [40]..... 37

**FIGURE 3.11:** THE MAXWELL MODEL (A) AND THE KELVIN/VOIGT MODEL (B) [40]..... 38

**FIGURE 3.12:** OSCILLATORY RHEOMETER [41] ..... 39

**FIGURE 3.13:** THE TWO-PLATES-MODEL USED FOR OSCILLATORY SHEAR TESTING [40] ..... 40

**FIGURE 3.14:** SHEAR STRAIN AND CORRESPONDING SHEAR STRESS FOR AN OSCILLATORY TEST OF A VISCOELASTIC MATERIAL [40] .... 41

**FIGURE 3.15:** STRAIN AMPLITUDE SWEEP TEST OF A MATERIAL EXHIBITING LIQUID CHARACTERISTICS ( $G'' > G'$ ) [40] ..... 43

**FIGURE 3.16:** BOYCOTT SETTLING [17] ..... 45

**FIGURE 3.17:** TYPICAL DRILLING FLUID CIRCULATION SYSTEM [48]..... 52

**FIGURE 3.18:** ELECTRICAL STABILITY TEST SET-UP [52] ..... 53

**FIGURE 3.19:** TYPICAL STATIC AND KINETIC FRICTIONAL BEHAVIOUR AS A FUNCTION OF TIME [54]..... 55

**FIGURE 3.20:** SEGMENTED DRILL-STRING AND DISTRIBUTION OF LOADS AT EACH SEGMENT [55] ..... 56

**FIGURE 3.21:** DRILL-STRING IN AN INCLINED WELL [55] ..... 58

**FIGURE 3.22:** EXAMPLE OF A TORQUE PLOT WHERE THE LOADS DOES NOT EXCEED THE TORSIONAL LIMIT ..... 59

**FIGURE 3.23:** EXAMPLE OF A TENSION PLOT WHERE THE LOADS DOES NOT EXCEED THE TENSILE LIMIT ..... 60

**FIGURE 4.1:** MOLECULAR STRUCTURE OF THE MAIN COMPONENTS OF LIGNOSULFONATES [72] ..... 67

**FIGURE 4.2:** CHEMICAL STRUCTURE OF POLY (ACRYLAMIDE-CO-ACRYLIC) PARTIAL SODIUM SALT [73]..... 68

**FIGURE 4.3:** SEM PICTURE OF THE  $MOS_2$  NANOPARTICLE (WHITE) ON A PIECE OF PAPER..... 69

**FIGURE 4.4:** SEM PICTURE OF MUD-CAKE FROM  $MOS_2$ -SOLUTION BASED DRILLING FLUID ..... 69

<b>FIGURE 4.5:</b> ELEMENT DISTRIBUTION IN THE $\text{MoS}_2$ NANO-SOLUTION.....	69
<b>FIGURE 4.6:</b> OFITE MODEL 800 VISCOMETER USED FOR RHEOLOGICAL MEASUREMENTS .....	70
<b>FIGURE 4.7:</b> ANTON PAAR MCR 302 RHEOMETER [77] .....	71
<b>FIGURE 4.8:</b> EDC 90/10 AFTER AGING FOR 16 HOURS AT $50^\circ\text{C}$ .....	72
<b>FIGURE 4.9:</b> DYNAMIC SAG TEST EQUIPMENT [78] .....	73
<b>FIGURE 4.10:</b> ILLUSTRATION OF THE PIN-ON-DISC TECHNOLOGY AND A PICTURE OF THE CSM TRIBOMETER.....	74
<b>FIGURE 5.1:</b> VISCOMETER DATA FOR LIGNOSULFONATES WBMs AT FLUID TEMPERATURE OF $50^\circ\text{C}$ .....	75
<b>FIGURE 5.2:</b> YIELD STRESS FOR WBMs AT DIFFERENT TEMPERATURES CALCULATED BASED ON THE ROBERTSON-STIFF MODEL.....	76
<b>FIGURE 5.3:</b> CALCULATED ROBERTSON-STIFF YIELD STRESS FOR WBMs CONTAINING 0.5, 1.0 AND 2.0 GRAMS OF LIGNOSULFONATES .....	76
<b>FIGURE 5.4:</b> VISCOMETER DATA FOR WBMs WITH VARIOUS AMOUNT OF LIGNOSULFONATES AT FLUID TEMPERATURE OF $50^\circ\text{C}$ .....	77
<b>FIGURE 5.5:</b> ROBERTSON-STIFF CALCULATED YIELD STRESS FOR MODIFIED WBMs .....	77
<b>FIGURE 5.6:</b> STORAGE AND LOSS MODULUS VS STRAIN FOR WBMs CONTAINING VARIOUS AMOUNTS OF LIGNOSULFONATES.....	78
<b>FIGURE 5.7:</b> PHASE ANGLE VS. SHEAR STRESS FOR WBMs CONTAINING VARIOUS AMOUNT OF ADDED LIGNOSULFONATES .....	79
<b>FIGURE 5.8:</b> PHASE ANGLE VS. SHEAR STRESS FOR WBMs CONTAINING 0.6-0.9 GRAMS OF ADDED LIGNOSULFONATES .....	79
<b>FIGURE 5.9:</b> ILLUSTRATION OF FLOW POINT AS A FUNCTION OF ADDED LIGNOSULFONATES .....	80
<b>FIGURE 5.10:</b> VISCOMETER DATA FOR THE NANO ENHANCED FLUIDS, EX-SITU, AT FLUID TEMPERATURE OF $22^\circ\text{C}$ .....	81
<b>FIGURE 5.11:</b> VISCOMETER DATA FOR THE NANO ENHANCED FLUIDS, IN-SITU, AT FLUID TEMPERATURE OF $22^\circ\text{C}$ .....	81
<b>FIGURE 5.12:</b> VISUAL REPRESENTATION OF THE COEFFICIENT OF FRICTION AS A FUNCTION OF ADDED $\text{MoS}_2$ , IN-SITU AND EX-SITU ...	82
<b>FIGURE 5.13:</b> AMPLITUDE SWEEP TEST RESULTS FOR THE REF FLUID AND THE NANO MODIFIED FLUIDS, FOR BOTH IN-SITU AND EX-SITU .....	83
<b>FIGURE 5.14:</b> VISCOMETER DATA FOR M-I SWACO'S OBMs AT FLUID TEMPERATURE OF $50^\circ\text{C}$ .....	84
<b>FIGURE 5.15:</b> YIELD STRESS FOR OBMs AT DIFFERENT TEMPERATURES CALCULATED BASED ON THE HERSCHEL-BULKLEY MODEL.....	85
<b>FIGURE 5.16:</b> ELECTRICAL STABILITY AT $50^\circ\text{C}$ BEFORE AND AFTER EMULSION MODIFICATION.....	85
<b>FIGURE 5.17:</b> YIELD STRESS FOR MODIFIED OBMs AT DIFFERENT TEMPERATURES CALCULATED BASED ON THE HERSCHEL-BULKLEY MODEL.....	86
<b>FIGURE 5.18:</b> STORAGE AND LOSS MODULUS AS A FUNCTION OF STRAIN FOR OWRs OF 60/40, 70/30, 80/20 AND 90/10.....	86
<b>FIGURE 5.19:</b> PHASE ANGLE VS. SHEAR STRESS FOR OWRs OF 60/40, 70/30, 80/20 AND 90/10.....	87
<b>FIGURE 5.20:</b> FLOW POINT FOR OWRs OF 60/40, 70/30, 80/20 AND 90/10 .....	87
<b>FIGURE 5.21:</b> TEMPERATURE SWEEP RESULTS FOR THE ONE-MUL MODIFIED M-I SWACO FLUIDS AND THE 90/10 REFERENCE FLUID.....	88
<b>FIGURE 5.22:</b> DAMPING FACTOR VS. TEMPERATURE FOR M-I SWACO OBMs .....	89
<b>FIGURE 5.23:</b> ILLUSTRATION OF THE DYNAMIC SAG FACTOR FOR THE M-I SWACO FLUIDS .....	90
<b>FIGURE 5.24:</b> DYNAMIC SAG POTENTIAL CURVE FOR M-I SWACO FLUIDS .....	91
<b>FIGURE 5.25:</b> ILLUSTRATION OF THE SAG FACTOR FOR THE 90/10 FLUID AND THE POLY ACRYLIC MODIFIED 90/10 FLUIDS.....	92
<b>FIGURE 5.26:</b> DYNAMIC SAG POTENTIAL CURVE FOR THE 90/10 FLUID AND THE POLY ACRYLIC MODIFIED 90/10 FLUIDS .....	92
<b>FIGURE 5.27:</b> VISCOMETER RESPONSE FOR THE EDC 90/10 FLUID AT FOUR DIFFERENT TEMPERATURES.....	93
<b>FIGURE 5.28:</b> CALCULATED YIELD STRESS BASED ON THE ROBERTSON-STIFF MODEL FOR THE EDC 90/10 AND THE M-I SWACO 90/10 FLUIDS .....	93

**FIGURE 5.29:** VISCOMETER RESPONSE FOR POLY ACRYLIC MODIFIED EDC 90/10 FLUIDS AT 50°C ..... 94

**FIGURE 5.30:** CALCULATED YIELD STRESS, BASED ON THE ROBERTSON-STIFF MODEL, FOR THE POLY ACRYLIC MODIFIED EDC 90/10 FLUIDS ..... 94

**FIGURE 5.31:** STORAGE AND LOSS MODULUS AS A FUNCTION OF STRAIN FOR THE POLY ACRYLIC MODIFIED EDC 90/10 FLUIDS ..... 95

**FIGURE 5.32:** PHASE ANGLE VS. SHEAR STRESS FOR MODIFIED EDC 90/10 FLUIDS..... 96

**FIGURE 5.33:** FLOW POINT FOR EDC 90/10 FLUIDS..... 96

**FIGURE 5.34:** ILLUSTRATION OF THE SAG FACTOR FOR THE EDC 90/10 FLUIDS..... 97

**FIGURE 5.35:** DYNAMIC SAG POTENTIAL CURVE FOR THE EDC 90/10 FLUIDS ..... 98

**FIGURE 6.1:** EXAMPLE OF A HERSCHEL-BULKLEY TREND-LINE GAINED FROM RHEOLOGICAL MODELLING OF MEASURED DATA ..... 99

**FIGURE 6.2:** PERCENTAGE DEVIATION BETWEEN MEASURED DATA AND RHEOLOGICAL MODELS FOR GIVEN WATER-BASED MUDS .... 100

**FIGURE 6.3:** TREND-LINES FROM RHEOLOGICAL MODELLING OF THE WBM REFERENCE SYSTEM AT FLUID TEMPERATURE OF 22°C.. 101

**FIGURE 6.4:** TREND-LINES FROM RHEOLOGICAL MODELLING OF THE REF + 0.9 G LS FLUID SYSTEM AT FLUID TEMPERATURE OF 22°C ..... 102

**FIGURE 6.5:** TREND-LINES FROM RHEOLOGICAL MODELLING OF THE REF + 2.0 G LS FLUID SYSTEM AT FLUID TEMPERATURE OF 22°C ..... 103

**FIGURE 6.6:** TREND-LINES FROM RHEOLOGICAL MODELLING OF THE EDC 90/10 REFERENCE FLUID SYSTEM AT FLUID TEMPERATURE OF 22°C..... 107

**FIGURE 6.7:** TREND-LINES FROM RHEOLOGICAL MODELLING OF THE EDC 90/10 + 0.5 G POLY ACRYLIC FLUID SYSTEM AT FLUID TEMP. OF 22°C ..... 108

**FIGURE 6.8:** TREND-LINES FROM RHEOLOGICAL MODELLING OF THE EDC 90/10 + 1.0 G POLY ACRYLIC FLUID SYSTEM AT FLUID TEMP. OF 22°C ..... 109

**FIGURE 6.9:** TREND-LINES FROM RHEOLOGICAL MODELLING OF THE EDC 90/10 + 1.5 G POLY ACRYLIC FLUID SYSTEM AT FLUID TEMP. OF 22°C ..... 110

**FIGURE 6.10:** ILLUSTRATION OF THE SIMULATION-WELL USED FOR THE ECD AND PUMP PRESSURE SIMULATIONS ..... 114

**FIGURE 6.11:** TOTAL PRESSURE DROP AS A FUNCTION OF FLOW RATE FOR SELECTED WATER-BASED DRILLING FLUID SYSTEMS..... 115

**FIGURE 6.12:** PUMP PRESSURE DIFFERENCE BETWEEN THE WBM FLUIDS AT DIFFERENT FLUID TEMPERATURES..... 116

**FIGURE 6.13:** TOTAL PRESSURE DROP AT VARIOUS FLOW RATES FOR M-I SWACO REFERENCE AND MODIFIED FLUIDS AT 100°C..... 116

**FIGURE 6.14:** PUMP PRESSURE DIFFERENCE BETWEEN REFERENCE AND MODIFIED VERSION OF VARIOUS OIL-WATER-RATIO FLUIDS . 117

**FIGURE 6.15:** PUMP PRESSURE FOR EDC 90/10 AND EDC 90/10 + 0.5 G POLY ACRYLIC AT TWO TEMPERATURES..... 117

**FIGURE 6.16:** PUMP PRESSURE DIFFERENCE, IN PSI, BETWEEN THE TWO EDC 90/10 FLUIDS AT THE SAME TEMPERATURE ..... 118

**FIGURE 6.17:** SIMULATED ECD FOR LIGNOSULFONATES CONTAINING WBMs AT TWO DIFFERENT TEMPERATURES ..... 119

**FIGURE 6.18:** ECD PERCENTAGE DEVIATION FOR EACH FLUID BETWEEN THE 22°C AND THE 80°C SIMULATION ..... 120

**FIGURE 6.19:** SIMULATED ECD AT VARIOUS FLOW RATES FOR M-I SWACO REFERENCE AND MODIFIED FLUIDS AT 100°C..... 120

**FIGURE 6.20:** PERCENTAGE ECD DIFFERENCE BETWEEN INITIAL AND MODIFIED FLUIDS FROM M-I SWACO ..... 121

**FIGURE 6.21:** SIMULATED EQUIVALENT CIRCULATION DENSITY FOR EDC 90/10 DRILLING FLUIDS AT 22°C AND 100°C ..... 121

**FIGURE 6.22:** ECD PERCENTAGE DEVIATION BETWEEN THE 22°C AND 100°C SIMULATION FOR EACH OF THE TWO FLUIDS..... 122

**FIGURE 6.23:** DRAG CHART FOR THE REFERENCE AND THE REFERENCE + 1.0 G MOLYBDENUM DISULPHIDE FLUIDS..... 124

**FIGURE 6.24:** MAXIMUM MEASURED DRILLING DEPTH ..... 124

**FIGURE B.1:** PHASE ANGLE VS. SHEAR STRESS FOR WBM CONTAINING 0.6-0.9 GRAMS OF ADDED LIGNOSULFONATES..... 153

**FIGURE B.2:** STORAGE AND LOSS MODULUS VS. STRAIN FOR OWRs OF 60/40, 70/30 AND 80/20 CONTAINING ADDITIONAL ONE-MUL..... 154

**FIGURE B.3:** PHASE ANGLE VS. SHEAR STRESS FOR OWRs OF 60/40, 70/30 AND 80/20 CONTAINING ADDITIONAL ONE-MUL.... 154

**FIGURE B.4:** STORAGE AND LOSS MODULUS VS. STRAIN FOR THE 90/10 FLUID AND THE 90/10 FLUIDS MODIFIED WITH POLY ACRYLIC ..... 155

**FIGURE B.5:** PHASE ANGLE VS. SHEAR STRESS FOR THE 90/10 FLUID AND THE 90/10 FLUIDS MODIFIED WITH POLY ACRYLIC ..... 155

**FIGURE C.6:** OWR 90/10 EDC FLUID AFTER STATIC SAG TEST ..... 157

**FIGURE C.7:** OBMs FROM M-I SWACO AFTER AGING ..... 157

**FIGURE D.8:** ILLUSTRATION OF THE SIMULATION WELL USED FOR TORQUE AND DRAG SIMULATIONS..... 158

**FIGURE D.9:** STRESS TRIP OUT FOR THE REFERENCE FLUID ..... 159

**FIGURE D.10:** STRESS TRIP OUT PLOT FOR THE REFERENCE + 1.0 G MoS<sub>2</sub> FLUID ..... 159

**FIGURE D.11:** TORQUE PLOT FOR THE REFERENCE FLUID..... 160

**FIGURE D.12:** TORQUE PLOT FOR THE REFERENCE + 1.0 G MoS<sub>2</sub> FLUID..... 160

# LIST OF TABLES

**TABLE 2.1:** CORRELATION CONSTANTS [21] ..... 17

**TABLE 3.1:** RELATION BETWEEN  $\tan\delta$  AND MATERIAL STATE [40] ..... 36

**TABLE 3.2:** SUMMARY OF THE PARAMETERS AND EQUATIONS USED IN THE UNIFIED HYDRAULIC MODEL [35] ..... 51

**TABLE 4.1:** RECIPE FOR WBM SYSTEMS CONTAINING VARIOUS AMOUNT OF LIGNOSULFONATES ..... 62

**TABLE 4.2:** RECIPE FOR WBM SYSTEMS CONTAINING 0.6 – 1.0 G OF LIGNOSULFONATES ..... 62

**TABLE 4.3:** RECIPE FOR THE 0.9-GRAM LIGNOSULFONATES SYSTEM MODIFIED WITH MOLYBDENUM DISULPHIDE (MOLY) ..... 62

**TABLE 4.4:** RECIPE FOR OIL-BASED DRILLING FLUID WITH AN OWR OF 90/10 AND EDC 95/11 AS BASE FLUID ..... 63

**TABLE 4.5:** MODIFIED SAMPLES OF EDC 90/10 REFERENCE FLUID ..... 63

**TABLE 4.6:** RECIPE FOR ALL OIL-BASED DRILLING FLUIDS PROVIDED BY M-I SWACO ..... 64

**TABLE 4.7:** POLY ACRYLIC MODIFIED SAMPLES OF M-I SWACO’S 90/10 OWR FLUID ..... 64

**TABLE 4.8:** QUANTITY OF THE DIFFERENT ELEMENTS IN THE  $\text{MOS}_2$  NANO-SOLUTION ..... 69

**TABLE 5.1:** SUMMARY OF IMPORTANT PROPERTIES OBTAINED FROM THE AMPLITUDE SWEEP TESTS FOR LIGNOSULFONATES WBMs. 80

**TABLE 5.2:** SUMMARY OF IMPORTANT PROPERTIES GAINED FROM THE AMPLITUDE SWEEP OF VARIOUS OWR FLUIDS ..... 88

**TABLE 5.3:** SUMMARY OF STATIC SAG PARAMETERS FOR THE M-I SWACO FLUIDS ..... 89

**TABLE 5.4:** SUMMARY OF IMPORTANT PARAMETERS GAINED FROM AMPLITUDE SWEEP TEST OF EDC 90/10 FLUIDS ..... 97

**TABLE 5.5:** SUMMARY OF STATIC SAG PARAMETERS FOR THE EDC 90/10 FLUID ..... 97

**TABLE 6.1:** MODELLED PARAMETERS AND EQUATIONS FOR THE WBM REFERENCE SYSTEM AT FLUID TEMPERATURE OF 22°C ..... 101

**TABLE 6.2:** MODELLED PARAMETERS AND EQUATIONS FOR REF + 0.9 G LS FLUID SYSTEM AT FLUID TEMPERATURE OF 22°C ..... 102

**TABLE 6.3:** MODELLED PARAMETERS AND EQUATIONS FOR REF + 2.0 G LS FLUID SYSTEM AT FLUID TEMPERATURE OF 22°C ..... 103

**TABLE 6.4:** RHEOLOGICAL MODEL SUMMARY FOR WATER-BASED FLUID SYSTEMS TREATED WITH LIGNOSULFONATES ..... 104

**TABLE 6.5:** RHEOLOGICAL MODELLING SUMMARY OF ALL PARAMETERS OF THE LIGNOSULFONATES TREATED WATER-BASED FLUID SYSTEMS ..... 106

**TABLE 6.6:** MODELLED PARAMETERS AND EQUATIONS FOR THE EDC 90/10 FLUID SYSTEM AT FLUID TEMPERATURE OF 22°C ..... 108

**TABLE 6.7:** MODELLED PARAMETERS AND EQUATIONS FOR EDC 90/10 + 0.5 G POLY ACRYLIC FLUID SYSTEM AT FLUID TEMP. OF 22°C ..... 109

**TABLE 6.8:** MODELLED PARAMETERS AND EQUATIONS FOR EDC 90/10 + 1.0 G POLY ACRYLIC FLUID SYSTEM AT FLUID TEMP. OF 22°C ..... 110

**TABLE 6.9:** MODELLED PARAMETERS AND EQUATIONS FOR EDC 90/10 + 1.5 G POLY ACRYLIC FLUID SYSTEM AT FLUID TEMP. OF 22°C ..... 111

**TABLE 6.10:** RHEOLOGICAL MODEL SUMMARY FOR EDC 90/10 FLUID SYSTEMS TREATED WITH POLY ACRYLIC ..... 111

**TABLE 6.11:** RHEOLOGICAL MODELLING SUMMARY OF ALL PARAMETERS OF THE POLY ACRYLIC TREATED EDC 90/10 FLUID SYSTEMS ..... 112

**TABLE 7.1:** CALCULATED YIELD STRESS VALUES, BASED ON ROBERTSON-STIFF MODEL, FOR GIVEN LIGNOSULFONATES WBMs ..... 126

**TABLE 7.2:** PERCENTAGE CHANGE OF THE COEFFICIENT OF FRICTION WITH REGARDS TO THE REFERENCE FLUID ..... 127

**TABLE 7.3:** CALCULATED YIELD STRESS VALUES, BASED ON HERSCHEL-BULKLEY MODEL, FOR MODIFIED OBMs EXHIBITING STABLE VALUES ..... 128

<b>TABLE 7.4:</b> SUMMARY OF YIELD STRESS VALUES FROM DIFFERENT EVALUATION METHODS AND FLOW POINT FOR LIGNOSULFONATES WBMs.....	131
<b>TABLE 7.5:</b> SUMMARY OF YIELD STRESS VALUES FROM DIFFERENT EVALUATION METHODS AND FLOW POINT FOR OBMs PROVIDED BY M-I SWACO.....	131
<b>TABLE 7.6:</b> SUMMARY OF YIELD STRESS VALUES FROM DIFFERENT EVALUATION METHODS AND FLOW POINT FOR OBMs FORMULATED AT UIS.....	131
<b>TABLE 7.7:</b> PRESSURE LOSS FOR WBMs AT SELECTED FLOW RATES AND RELATIVE CHANGE IN PUMP PRESSURE FOR WBM FLUIDS AT 80°C.....	132
<b>TABLE 7.8:</b> TOTAL PRESSURE LOSS FOR WATER-BASED MUD SYSTEMS.....	132
<b>TABLE 7.9:</b> CHANGE IN ECD AT THE SAME FLOW RATE BUT DIFFERENT TEMPERATURE AND ABSOLUTE AVERAGE CHANGE IN ECD...	133
<b>TABLE 7.10:</b> PRESSURE LOSS AT SELECTED PUMP RATES AND TOTAL PRESSURE LOSS FOR ONE-MUL MODIFIED OIL-BASED DRILLING FLUIDS.....	133
<b>TABLE 7.11:</b> RELATIVE CHANGE IN ECD BETWEEN REFERENCE AND ONE-MUL MODIFIED FLUID AND THE ABSOLUTE AVERAGE CHANGE IN ECD.....	134
<b>TABLE 7.12:</b> PUMP PRESSURE AT SELECTED PUMP RATES FOR TWO DIFFERENT TEMPERATURES.....	134
<b>TABLE 7.13:</b> RELATIVE CHANGE IN PUMP PRESSURE WITH REGARDS TO TEMPERATURE ( $P_p^{22^\circ\text{C}} - P_p^{100^\circ\text{C}}$ ) AND PERCENTAGE CHANGE	134
<b>TABLE 7.14:</b> RELATIVE CHANGE IN ECD ( $\text{ECD}_{100^\circ\text{C}} - \text{ECD}_{22^\circ\text{C}}$ ) AND THE ABSOLUTE AVERAGE CHANGE IN ECD.....	135
<b>TABLE A.1:</b> OFITE VISCOMETER READINGS FOR WBMs WITH 0 GRAMS, 0.2 GRAMS AND 0.3 GRAMS OF ADDED LIGNOSULFONATES .....	147
<b>TABLE A.2:</b> OFITE VISCOMETER READINGS FOR WBMs WITH 0.4 GRAMS, 0.5 GRAMS AND 2 GRAMS OF ADDED LIGNOSULFONATES .....	147
<b>TABLE A.3:</b> OFITE VISCOMETER READINGS FOR WBMs WITH 0.6 GRAMS, 0.7 GRAMS, 0.8 GRAMS AND 0.9 GRAMS OF ADDED LS	148
<b>TABLE A.4:</b> OFITE VISCOMETER DATA FOR THE NANO MODIFIED WATER-BASED FLUID, IN-SITU.....	148
<b>TABLE A.5:</b> OFITE VISCOMETER DATA FOR THE NANO MODIFIED WATER-BASED FLUID, EX-SITU.....	149
<b>TABLE A.6:</b> OFITE VISCOMETER READINGS FOR OWRs OF 60/40 AND 70/30.....	149
<b>TABLE A.7:</b> OFITE VISCOMETER READINGS FOR OWRs OF 80/20 AND 90/10.....	150
<b>TABLE A.8:</b> OFITE VISCOMETER READINGS FOR EDC 90/10 AND EDC 90/10 + 0.5 G POLY ACRYLIC.....	150
<b>TABLE A.9:</b> OFITE VISCOMETER READINGS FOR EDC 90/10 + 1.0 G POLY ACRYLIC AND EDC 90/10 + 1.5 G POLY ACRYLIC.....	151
<b>TABLE A.10:</b> OFITE VISCOMETER READINGS FOR 90/10 + 0.5 G POLY ACRYLIC AND 90/10 + 1.0 G POLY ACRYLIC.....	151
<b>TABLE A.11:</b> OFITE VISCOMETER READINGS FOR THE 80/20 ONE-MUL FLUID.....	152
<b>TABLE C.12:</b> SUMMARY OF DYNAMIC SAG MEASUREMENT DATA FOR THE M-I SWACO FLUIDS.....	156
<b>TABLE C.13:</b> SUMMARY OF DYNAMIC SAG MEASUREMENT DATA FOR THE 90/10 FLUIDS.....	156
<b>TABLE C.14:</b> SUMMARY OF DYNAMIC SAG MEASUREMENT DATA FOR THE EDC 90/10 FLUIDS.....	156
<b>TABLE D.15:</b> AVERAGE VALUES FOR THE COEFFICIENT OF FRICTION FOR THE VARIOUS FLUID SYSTEMS.....	158

## LIST OF NOMENCLATURE

$P_{\text{fluid}}$	Pressure exerted by the fluid	[Pa]
$\rho$	Density of the fluid	[kg/m <sup>3</sup> ]
$g$	Gravitational acceleration constant	[m/s <sup>2</sup> ] [ft/s <sup>2</sup> ]
$h_{\text{TVD}}$	True vertical depth	[m]
$\mu$	Newtonian viscosity	[cP]
$\tau$	Shear stress	[lbf/100ft <sup>2</sup> ]
$\dot{\gamma}$	Shear rate	[s <sup>-1</sup> ]
$K$	Consistency index	[ ]
$n$	Flow behaviour index	[ ]
$\mu_p$	Plastic viscosity	[cP]
$\tau_0$	Yield point	[lbf/100ft <sup>2</sup> ]
$\tau_y$	Yield stress	[lbf/100ft <sup>2</sup> ]
$A$	Constant in Robertson-Stiff model similar to $K$	[ ]
$B$	Constant in Robertson-Stiff model similar to $n$	[ ]
$C$	Constant in Robertson-Stiff model, correction factor	[s <sup>-1</sup> ]
$K_a$	Consistency index for Unified model	[ ]
$n_a$	Flow behaviour index for Unified model	[ ]
$\gamma_w$	Specific weight	[lbf/ft <sup>3</sup> ]
$\theta$	Dial reading on viscometer	[ ]
$\Omega$	Share rate on viscometer	[s <sup>-1</sup> ]
$\dot{\gamma}^*$	Average shear rate	[s <sup>-1</sup> ]
$\tau^*$	Average shear stress	[lbf/100ft <sup>2</sup> ]
$G'$	Storage modulus	[Pa]
$G''$	Loss modulus	[Pa]
$\tan\delta$	Damping factor	[1]
$\eta$	Shear viscosity	[cP]
$\eta^*$	Complex viscosity	[cP]
$G^*$	Complex shear modulus	[Pa]
$\omega$	Angular frequency	[s <sup>-1</sup> ]
$\gamma_A$	Shear strain amplitude	[ ]
$\tau_A$	Shear stress amplitude	[lbf/100ft <sup>2</sup> ]

$\gamma_L$	Yield shear strain	[ ]
$M(t)$	Torque	[mNm]
$A_p$	Surface area of the particle	[ft <sup>2</sup> ]
$\tau_g$	Gel strength	[lbf/100ft <sup>2</sup> ]
$\rho_p$	Particle density	[lb/ft <sup>3</sup> ]
$\rho_f$	Fluid density	[lb/ft <sup>3</sup> ]
$V_p$	Particle volume	[ft <sup>3</sup> ]
$D$	True vertical depth to an arbitrary point in the well	[ft] or [m]
$\Delta P_s$	Pressure loss from the flow through the surface equipment	[psi]
$\Delta P_{ds}$	Pressure loss from the flow through the drill string	[psi]
$\Delta P_{dc}$	Pressure loss from the flow through the drill collar	[psi]
$\Delta P_b$	Pressure loss from the flow through the nozzles in the bit	[psi]
$\Delta P_{ac}$	Pressure loss from the flow through annulus	[psi]
$\Delta P_{ads}$	Pressure loss from the flow through annular are between riser and drill string	[psi]
$\Delta P_{tot}$	Total pressure loss through the circulation system	[psi]
$P_{pump}$	Required pump pressure	[psi]
$E_0$	Voltage at which the conductive passageway is formed	[V]
$v_{(x)}$	volume fraction	[ ]
$MW_{top}$	Mud weight at top of the fluid sample	[g]
$MW_{bottom}$	Mud weight at bottom of the fluid sample	[g]
$MW_{initial}$	Initial mud weight before dynamic sag test	[g]
$MW_{final}$	Final mud weight after dynamic sag test	[g]
$\mu_f$	Coefficient of friction	[ ]
$F_f$	Frictional force	lbf
$N$	Normal force	lbf
$\beta$	Buoyancy factor	[ ]
$w_s$	Weight of the drill-string	lbf
$w$	Buoyed weight of the drill-string	lbf
$\mu_a$	Axial coefficient of friction	[ ]
$\mu_t$	Tangential coefficient of friction	[ ]



## LIST OF ABBREVIATIONS

<b>BHP</b>	Bottom-hole pressure	<b>VSST</b>	Viscometric sag “shoe” test
<b>CSR</b>	Controlled shear rate	<b>WBM</b>	Water-based mud
<b>CSS</b>	Controlled shear stress	<b>YP</b>	Yield point
<b>GEL</b>	Gel strength	<b>YS</b>	Yield stress
<b>ECD</b>	Equivalent circulation density		
<b>EDC</b>	Environmental drilling compound		
<b>ES</b>	Electrical stability		
<b>ESD</b>	Equivalent static density		
<b>FP</b>	Flow point		
<b>GPM</b>	Gallons per minute		
<b>H-B</b>	Herschel-Bulkley		
<b>HPHT</b>	High-pressure, high-temperature		
<b>ID</b>	Inner diameter		
<b>LVE</b>	Linear viscoelastic		
<b>LS</b>	Lignosulfonates		
<b>LSYS</b>	Lower shear yield stress		
<b>MD</b>	Measured depth		
<b>MW</b>	Mud weight		
<b>OBM</b>	Oil-based mud		
<b>OD</b>	Outer diameter		
<b>OWR</b>	Oil-water-ratio		
<b>POOH</b>	Pull out of hole		
<b>PPG</b>	Pounds per gallon		
<b>PV</b>	Plastic viscosity		
<b>PVT</b>	Pressure, volume, temperature		
<b>RIH</b>	Run in hole		
<b>ROP</b>	Rate of penetration		
<b>RPM</b>	Revolutions Per Minute		
<b>R-S</b>	Robertson-Stiff		
<b>SG</b>	Specific gravity		
<b>TVD</b>	True vertical depth		
<b>UiS</b>	University of Stavanger		



# 1 INTRODUCTION

Drilling fluids are vital when drilling oil and gas wells, as it is one of the most fundamental elements of the drilling operation. The drilling fluid is the only component of the drilling system that is constantly in contact with the wellbore throughout the entire well-construction process. If properly designed and formulated, the drilling fluid exhibits some crucial functions under anticipated wellbore conditions. The drilling fluids are generally made up of different base liquids, with water and oil being the most common ones. Three key factors are generally used in order to determine which type of fluid to be used for a specific drilling operation in a distinct wellbore environment. These three key factors are:

- cost,
- environmental impact, and
- technical performance.

Water-based muds (WBM) are generally less expensive and more environmentally friendly than oil-based muds (OBM). WBMs are the most frequently used type of drilling fluids and were in 2004 recorded used in approximately 80% of all wells that were being drilled. Oil-based muds are generally used in long-reach wells where the potential for frictional pressure loss is large, as OBMs provides excellent lubricity for the drill-string and the drill bit, reducing the frictional resistance in the system. However, by treating water-based muds with the correct chemicals and additives, WBMs can be modified to perform as good as OBMs in terms of preventing potential drilling problems [1].

Through the last decades, the application of both polymers and nanotechnology have made great progress within lots of scientific fields and within several huge industries. Polymers, for instance, are commonly used in the medicine industry, while nanotechnology is frequently applied in production of technological gadgets and in the medicine industry [2] [3]. Nanotechnology and polymers have also been applied in the petroleum industry, particularly with respect to enhancement of the drilling fluid rheology [4]. This thesis will present lots of different experimental work and simulations studies that have been performed in order to investigate the effect of nanoparticles and polymers on drilling fluid rheology and drilling fluid functions. By the use of rheological measurements and barite sag, friction and viscoelastic testing, as well as ECD & pump pressure and torque & drag simulations, the use of various additives, including polymers and nanoparticles, have been analyzed and evaluated for both oil-based and water-based drilling fluids. In addition to experimental work and simulations studies, a literature study review of previous work and research have been performed, were various drilling fluid challenges have been identified and accounted for.

## 1.1 Background

The sole purpose of drilling a well is to create a pathway from the hydrocarbon reservoir to the surface facilities in order to recover, and produce, hydrocarbons. The aim is to create this pathway, the wellbore, as fast, cheap and safe as possible. During the process of drilling a well there are several important parameters to consider, such as the weight on bit, flow rate, RPM, ROP and so on. However, one of the most important components of the drilling system is the drilling fluid. A properly designed and formulated drilling fluid is vital in order to successfully drill a well in a safe and efficient manner [6].

A drilling fluid needs to possess all the right properties to be able to exhibit the required functions at given wellbore conditions. Amongst others, the fluid should be able to carry, and transport, drilled rock cuttings from the bottom of the wellbore up to the surface. It should provide sufficient hydrostatic pressure in the wellbore to keep within the safe operational window, illustrated by the beige area in **figure 1.1**. The safe operational window, restricted by the formation pore pressure and the formation fracture pressure, is affected by the environment and will be different for every well. For instance, at HPHT conditions and extreme water depths, the safe operational window tends to be very narrow [6].

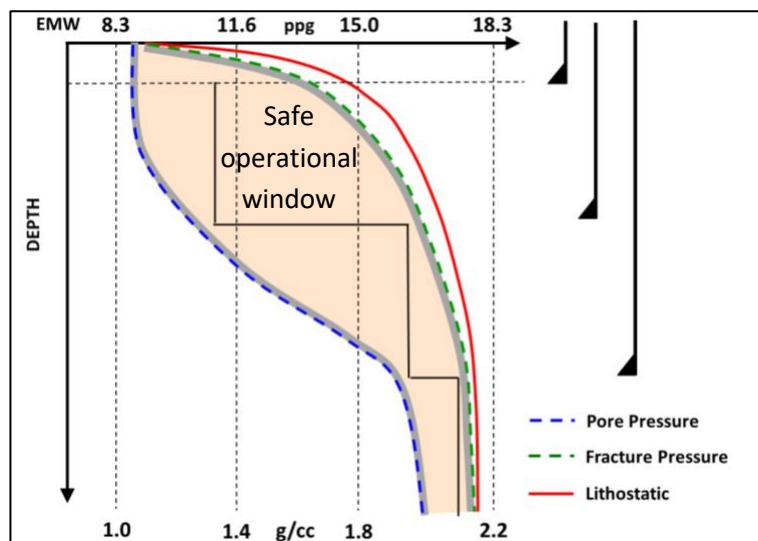


**Figure 1.1:** A Illustration of an arbitrary pore pressure and fracture pressure gradient plot [5]

If the hydrostatic pressure in the well is lower than the pore pressure, this could cause formation fluid influx into the wellbore and cause an increased potential of wellbore collapse due to pressure differentials. On the other hand, if the hydrostatic pressure exceeds the formation fracture pressure, one may experience differential sticking or formation fracturing. In addition to the already mentioned functions, the drilling fluid should also be able to; handle a wide range of environmental conditions, prevent formation damage, lubricate and cool the drill-string & drill-bit and form a good filter-cake at the wellbore walls [6].

The environment is another concern to take into consideration when deciding for which drilling fluid system to be used. Some of the criteria being addressed in terms of health and environment is the cutting treatment system and the mud disposal strategy. In terms of the economical perspective, drilling fluids represent approximately 5 to 15% of the total cost of the drilling operation but might cause 100% of the drilling related problems. As a result, both the environmental concerns and the economic aspects provides favourable arguments for continue to improve the drilling fluid performance [7].

Considering all the essential functions of the drilling fluid, it is of utmost importance to acquire as much knowledge as possible about drilling fluids' behaviour under actual conditions, in order to properly design and formulate fluids with the desirable properties for any given wellbore condition or environment. However, there are some issues related to drilling fluids, which form the background for this thesis' work. These issues are:

**HPHT** - High pressure, high temperature conditions may influence the drilling fluid rheology and the drilling fluid density. For example, HPHT environments can provoke clay flocculation in water-based fluids, making the fluid inoperative. Density fluctuations, as the fluid is temperature and pressure dependent, can lead to wellbore instability issues like wellbore collapse or kick. Additionally, if the rheology is greatly reduced by the HPHT environment, it could lead to poor hole cleaning performance.

**Formation swelling** - Poorly designed drilling fluids may result in clay/shale swelling, as water-based filtrate enters the formation. A swelling formation will cause a reduction of the wellbore diameter, increasing the potential of stuck pipe and wellbore instability [8].

**Sagging** - Barite sag may appear if drilling with oil-based drilling fluids, as OBMs are subject to temperature thinning, causing a reduction in fluid viscosity, which again reduces the fluids' suspension characteristics. If a fluid experience barite sag, this can lead to well-control issues and stuck pipe [9].

**Lost circulation** - If the drilling fluid formulation is poor, this could prevent adequate mud-cake formation at the borehole wall, which again could result in unwanted loss of drilling fluid into the formation. If the fluid column is reduced significantly, this could reduce the pressure exerted by the fluid on to the formation, causing inflow of formation fluids in another part of the well, or even more sever; loss of well control [10].

Therefore, it is crucial to design and formulate a drilling fluid which handles the problems mentioned above.

## 1.2 Problem Definition

The work of this thesis consists of primarily experimental work performed in order to gain important knowledge and characteristics of drilling fluids. Further, this thesis will address issues related to both water-based and oil-based drilling fluids. These are:

- Thermal stability of water-based and oil-based drilling fluids
- Sagging control of oil-based drilling fluids
- Nano fluids effect on the thermal stable water-based drilling fluid

## 1.3 Objective and Scope

The primary objective of the work of this thesis is to describe and solve the issues in the problem definition part. The scope is limited to experimental work and simulation-based studies. The main objectives and activities in this thesis are:

- Formulation of thermally stable rheology drilling fluids
- Formulation of a sag preventive oil-based drilling fluid
- Analyze the frictional performance of nanofluids in the best water-based fluid system
- Drilling fluids rheology modelling, hydraulics and torque & drag performance simulation study

### 1.4 Research Program

The research program consists of three main parts, namely; literature study, experimental work and performance study. A chart of the research program is presented in **figure 1.2**, which represents the approaches used in order to achieve the objectives mentioned above.

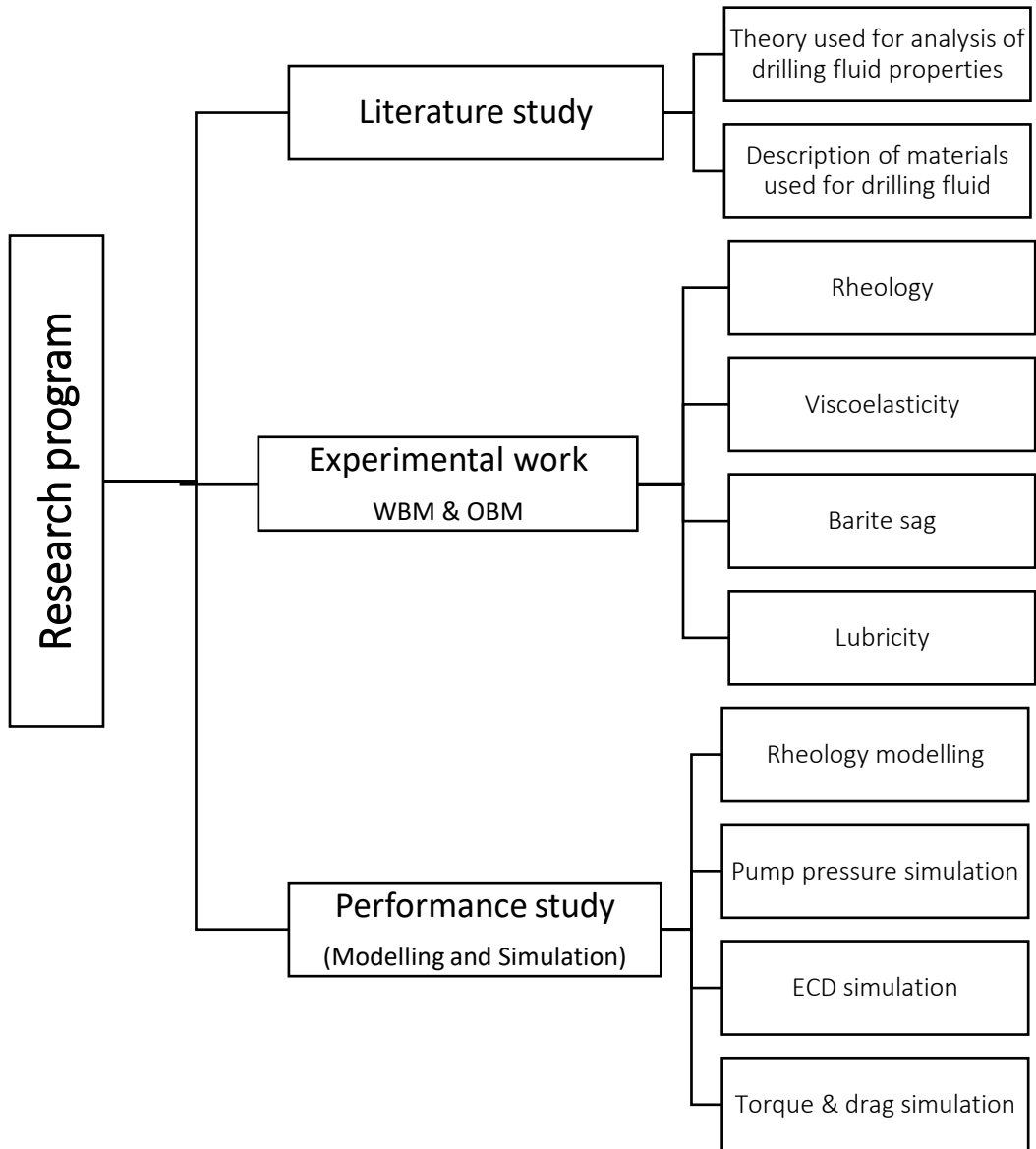


**Figure 1.2:** Summary of the research program used for this thesis

## 2 LITERATURE STUDIES

Through literature study, this chapter will elaborate on industry knowledge and research performed with respect to drilling fluids, its challenges and proposed solutions. It will highlight and account for these challenges and will form the basis for some of the experimental work performed in this thesis.

### 2.1 Drilling Fluid

Drilling fluid, or drilling mud, is defined as the fluid that is used to circulate through the wellbore during the process of drilling a well. The fluid is formulated in such a way that it possesses some important functions that are crucial for the drilling operation to be successful [11]. A drilling fluid is generally composed of a base fluid, weight material, viscosifiers and other chemical products in order to give the fluid its desirable properties [12].

#### 2.1.1 Drilling Fluid Properties

The most important drilling fluid properties are *specific weight*, *viscosity* and *fluid loss control*.

##### 2.1.1.1 Specific Weight

Specific weight ( $\gamma_w$ ) is defined as the density ( $\rho$ ) times the gravitational acceleration ( $g$ ), which means that  $\gamma_w$  works as a force that pulls the mass against the centre of the earth. Supplementary weight material can be used to control the specific weight of any drilling fluid system. The specific weight is a crucial property of the drilling fluid, as too low mud weight could result in influx of formation fluids into the wellbore, and too high mud weight could result in formation fracturing [6].

##### 2.1.1.2 Viscosity

Viscosity ( $\mu$ ) is a measure of a fluid's "thickness" and is defined as frictional forces within a fluid, a resistance of the fluid flow. A fluid that flows easily is less viscous than a fluid that requires some additional forces in order to flow. Viscosity is determined as the ratio between the shear stress ( $\tau$ ) and the shear rate ( $\dot{\gamma}$ ) and has the unit centipoise [cP] [6].

##### 2.1.1.3 Fluid Loss Control

Fluid loss control is defined as the application of additives in the drilling fluid in order to minimize the permeability of the filter-cake and prevent the filter-cake from becoming too thick. The reduction of the filter-cake permeability also helps reducing the fluid loss into the formation [12].



## 2.1.2 Drilling Fluid Functions

A drilling fluid have four main functions, namely:

- Remove cuttings from the bottom of the well
- Prevent well-control issues
- Deposit a mud/filter-cake at the borehole wall
- Cool and lubricate the downhole equipment

By formulating a fluid that maintains these important functions, one will reduce the risk of borehole and well stability issues [12].

### 2.1.2.1 Removal of Cuttings

During the drilling process, there are generated a lot of rock cuttings from drilling through various rock formations. It is then the drilling fluid's job to remove these cuttings from the bottom-hole and bring them up to surface. To do so, the mud need a certain circulation rate and viscosity to be able to suspend the cuttings and carry them with it. Gravity will tend to drag the cuttings downwards and it is therefore important that the circulation rate is adequately high enough to overcome the slip velocity [6]. In order to suspend the cuttings particles during a stop of circulation, it is also important that the drilling fluid has the ability to generate adequate gel strength [12].

### 2.1.2.2 Prevent Well-control Issues

The drilling fluid is also used to prevent well-control issues, by providing an acceptable hydrostatic head to balance between the formation pore pressure and the fracture pressure, as illustrated in **Figure 1.1**. If the pressure applied by the drilling fluid exceeds the fracture pressure, the formation will fracture, and fluid will leak off into the formation and cause the potential for differential sticking. On the other hand, if the pressure is too low, there might be an inflow of formation fluids into the wellbore [6].

The drilling fluid should produce a hydrostatic pressure that places somewhere between the pore pressure and fracture pressure gradient, as represented by the black line in **Figure 1.1**. The density of the drilling fluid is therefore on of the most important fluid properties, as the hydrostatic pressure exerted by the fluid is proportional to the fluid density and is calculated based on the following formula:

$$P_{fluid} = \rho \cdot g \cdot h_{TVD} \quad (2.1)$$

Where:

$P_{\text{fluid}}$	Pressure exerted by the fluid	[Pa]
$\rho$	Density of the fluid	[kg/m <sup>3</sup> ]
$g$	Gravitational acceleration constant	[m/s <sup>2</sup> ]
$h_{\text{TVD}}$	True vertical depth	[m]

### 2.1.2.3 Filter-cake

A filter-cake is the materials that are deposited on the borehole wall when drilling fluid is forced against the wall under a pressure. The filter-cake is formed in the permeable zones in a well, on the borehole walls, and is important as it is used to prevent drilling fluid loss into the formation. As the filter-cake gets thicker, the cake's inflow resistance increases. It is important that the filter-cake does not get too thick, as a too thick filter-cake could cause the drill pipe to get stuck in the wellbore [12].

### 2.1.2.4 Cooling and Lubrication of Equipment

As the drilling process progresses, the drill bit and the drill pipe are heated due to the friction from the bit action and the pipe's contact with the formation walls and rock cuttings. Some of the heat generated will be absorbed by the formation, while the rest is supposed to be taken care of by the circulating drilling fluid. This is important in order to ensure that the drill bit and drill pipe are not overheated and lose some of its important characteristics.

Lubrication is another important function of the drilling fluid. During the circulation process, the moving parts of the drill pipe are lubricated by the mud. This lubrication saves lots of time and money, as the lifetime of the equipment will be extended. A fluid's lubrication properties are determined by its composition and chemical additives [6].

### 2.1.3 Drilling Fluid Types

Drilling fluids are often divided into three main types, namely; water-based mud, oil-based mud and pneumatic drilling fluid. As mentioned, WBMs and OBMs are most commonly used types of fluids and the main difference between these two are which base liquid the fluid is made up of. WBM is composed of fresh water, salt water or brine as base liquid, while OBM is composed of an oil type of liquid as base liquid. From an environmental point of view, WBM are the preferred one as it more environmentally friendly than OBM. However, OBMs have several benefits that makes it a greatly valuable asset in some particularly long and difficult sections of a well [12].

### 2.1.3.1 Water-Based Mud

Water-based mud is a mixture of fresh water, salt water or brine and clay minerals, weight agents and chemicals in order to attain a fluid with the desired drilling fluid properties. Which base fluid that is used depends on the wellbore quality and what properties that are critical for the section to be drilled. For instance, the top section is commonly drilled using sea water as drilling fluid, as the fluid is not circulated back to the rig but discharged to sea [1].

WBM's are typically divided into two main categories, namely; *non-dispersed* and *dispersed*.

#### 2.1.3.1.1 Non-Dispersed

Non-dispersed water-based mud systems are not treated with chemicals to change the flocculation of the clay particles. In a non-dispersed WBM system the clay particles find its own dispersed equilibrium in the aqueous mixture. Non-dispersed water muds are commonly used when drilling the top-hole section of a well [1].

#### 2.1.3.1.2 Dispersed

Dispersed water-based muds are usually treated with chemicals in order to deflocculate the clay particles in the aqueous solution and to improve the rheological parameter control in drilling fluids with higher density. Deflocculation agents are defined as thinning agents that are used to reduce the viscosity of a fluid [1].

Two of the greatest benefits of using WBM's are that it is environmentally friendly and can in some cases be discharged to sea. By discharging to sea, one saves a lot of time and money spent on fluid storage, fluid transportation and fluid treatment after use [12].

### 2.1.3.2 Oil-Based Mud

Oil-based muds are drilling fluids that are made up of solids and chemical additives combined with a mixture of, the usually immiscible liquids, oil and water [13]. The fluid is an oil continuous phase, where the oil-water-ratio (OWR) is mainly somewhere in between 60/40 and 95/5 [14]. The drilling fluids that contains less than 10 percent of water are often referred to as oil muds, while the drilling fluids that contains more than 10 percent are referred to as oil emulsion muds [15].

Oil-based muds are often used in high temperature wells, inclined wells and wells that have potential problems with pipe sticking and hole stabilization. The reason is that OBM has several benefits compared to WBM, and some of the greatest benefits are listed below [6]:

- Oil does not react with clay, hence no swelling formations
- Improved wellbore stability
- Clay-containing sandstone reservoirs exhibit improved production
- More stable mud properties
- Risk of wellbore enlargement is decreased

As mentioned, oil-based muds are constituted by different solids and additives, and the most essential ones will be described in the following paragraphs.

#### *2.1.3.2.1 Base Oil*

Base oil is the main component of an oil-based mud and is the continuous phase of the drilling fluid. In the early days of oil-based drilling fluids, diesel oil and crude oil were used as base oils [14]. Nowadays, more environmental and health friendly non-aromatic- and linear paraffin base oils are generally used [16].

#### *2.1.3.2.2 Weight Agents*

Weight agents are solid particles that are added to the drilling fluid mixture in order to attain a pre-determined mud weight. *Barite* is the most commonly used weighting agent with regards to both oil-based and water-based drilling fluid formulations, as it is a cheap and an effective way of increasing the mud weight [11].

#### *2.1.3.2.3 Wetting Agents*

Wetting agents are surface-active agents that has the primary function to make solids oil-wet to prevent solid particles from accumulate and settle. Wetting agents reduces the contact angle and the interfacial tension between a solid and a liquid, causing the liquid to cover the surface of the solid particle [17].

#### *2.1.3.2.4 Viscosifiers*

Viscosifiers are chemicals used to increase the viscosity of the drilling fluid. For oil-based drilling fluids, the most common viscosifier is organophilic clay, which is surface treated bentonite clay. The bentonite clay is surface treated so that the clay particles are able to disperse into the oil continuous phase and yield. In order for the organophilic clay to generate maximum yield, it will need a polar activator like water. Hence, the yield is a function of the oil-water ratio and increasing OWR will cause a decrease of the clay effect. Organophilic clay yield is also dependent of adequate shear and temperature [17].

#### **2.1.3.2.5 Emulsifiers**

Emulsifiers are chemicals, surface-active agents, that reduces the surface tension between the water droplets and the oil. Emulsifiers are required in oil-based drilling fluids in order to form a heterogenous mixture of two immiscible liquids. Small water droplets are dispersed into the oil continuous phase. Emulsifier chemicals form a film, a thin layer, around the water droplets in order to keep them from coalescing [17].

#### **2.1.3.2.6 Fluid Loss Agents**

Fluid loss agents are added to the drilling fluid to reduce or prevent the tendency of liquid phase loss into the formation. The main fluid loss agents that are used for oil-based mud systems are asphalt (gilsonite), amine-treated lignite and polymers [17].

## 2.2 High-Pressure, High-Temperature Drilling Fluid Challenges

HPHT is a term that was introduced in the Cullen report from 1990 about the Piper Alpha Disaster. From this report, high-pressure, high-temperature wells are defined as wells with bottom-hole temperatures exceeding 150°C and formation pore pressure of at least 690 bar [18]. Operations under these HPHT conditions are often quite challenging, as the downhole conditions affects several parts of the drilling system. Some of these challenges are related to drilling fluids and various HPHT challenges will be described and accounted for in the following two subsections.

### 2.2.1 HPHT Density Prediction

Drilling fluid density is affected by changes in its environment. *Increasing temperature* induces an expansion of the fluid volume. As the volume increases, this will cause a *decrease in fluid density*. While *increasing pressure* leads to a compression of the fluid volume, hence, an *increase in fluid density*. As mentioned in **Chapter 2.1.2.2** the bottom-hole pressure (BHP) is proportional to the wellbore fluid density. Generally, this calculation is a rule of thumb. However, since the fluid density is temperature and pressure dependent, the BHP calculation will require some adjustments in HPHT wells. A correction model was presented by Peters et al. back in 1988, which expresses the density as a function of temperature and pressure, based on PVT-data of the fluid. This model is given by the following equation:

$$\rho = \frac{\rho_o v_o + \rho_w v_w + \rho_s v_s + \rho_c v_c}{1 + v_o \left[ \frac{\rho_o}{\rho_{oe}} - 1 \right] + v_w \left[ \frac{\rho_w}{\rho_{we}} - 1 \right]} \quad (2.2)$$

Where:

$\rho_{(x)}$	density	[kg/m <sup>3</sup> ]
$v_{(x)}$	volume fraction	[ ]

Subscripts:

o	oil	c	chemical	e	elevated temperature and pressure
w	water	s	solids		

By performing density adjustments for every 100 ft, this model has proved to be adequate in order to predict the Equivalent Static Density (ESD). When operating in HPHT wells, high-density fluids are required in order to prevent inflow of formation fluids. High-density fluids require high solids loading that results in higher pressures. This will again lead to a low rate of penetration (ROP), more time at drill site and additional drilling costs [19].

For practical operations, when drilling a well, the density of the drilling fluid measured in laboratory needs to be adjusted for temperature and pressure effects. In order to include these effects, among others, Kaarstad has presented linearized form of the density model [20]:

$$\rho(P, T) = \rho_i [1 + \gamma_p(P - P_i) + \gamma_T(T - T_i)] \quad (2.3)$$

Where:

- $i$  initial condition
- $\gamma_p, \gamma_T$  drilling fluids empirical constants

Figure 2.1 shows the well structure through which a cold drilling fluid is injected through the pipe and the warm drilling fluid flow returns through the annulus. The temperature profiles of the drilling fluid through annulus and drill pipe has been derived by Kaarstad and Aadnøy. The model reads [21]:

Temperature in drill string:

$$T_d(z, t) = \alpha e^{\lambda_1 z} + \beta e^{\lambda_2 z} + g_G z - B g_G + T_{sf} \quad (2.4)$$

Temperature in annulus:

$$T_a(z, t) = (1 + \lambda_1 B) \alpha e^{\lambda_1 z} + (1 + \lambda_2 B) \beta e^{\lambda_2 z} + g_G z - B g_G + T_{sf} \quad (2.5)$$

Where,  $\lambda_1, \lambda_2, \alpha, \beta, A$  and  $B$  can be calculated from:

$$\lambda_1 = \frac{1}{2A} \left( 1 - \sqrt{1 + \frac{4A}{B}} \right) \quad (2.6)$$

$$\lambda_2 = \frac{1}{2A} \left( 1 + \sqrt{1 + \frac{4A}{B}} \right) \quad (2.7)$$

$$\alpha = - \frac{(T_{in} + B g_G - T_{sf}) \lambda_2 e^{\lambda_2 D} + g_G}{\lambda_1 e^{\lambda_1 D} - \lambda_2 e^{\lambda_2 D}} \quad (2.8)$$

$$\beta = -\frac{(T_{in} + B_{gG} - T_{sf})\lambda_1 e^{\lambda_1 D} + gG}{\lambda_1 e^{\lambda_1 D} - \lambda_2 e^{\lambda_2 D}} \quad (2.9)$$

$$A = \frac{w C_{fl}}{2\pi r_c U_a} \left( 1 + \frac{r_c U_a f(t_D)}{K_f} \right) \quad (2.10)$$

$$B = \frac{w C_{fl}}{2\pi r_c U_a} \quad (2.11)$$

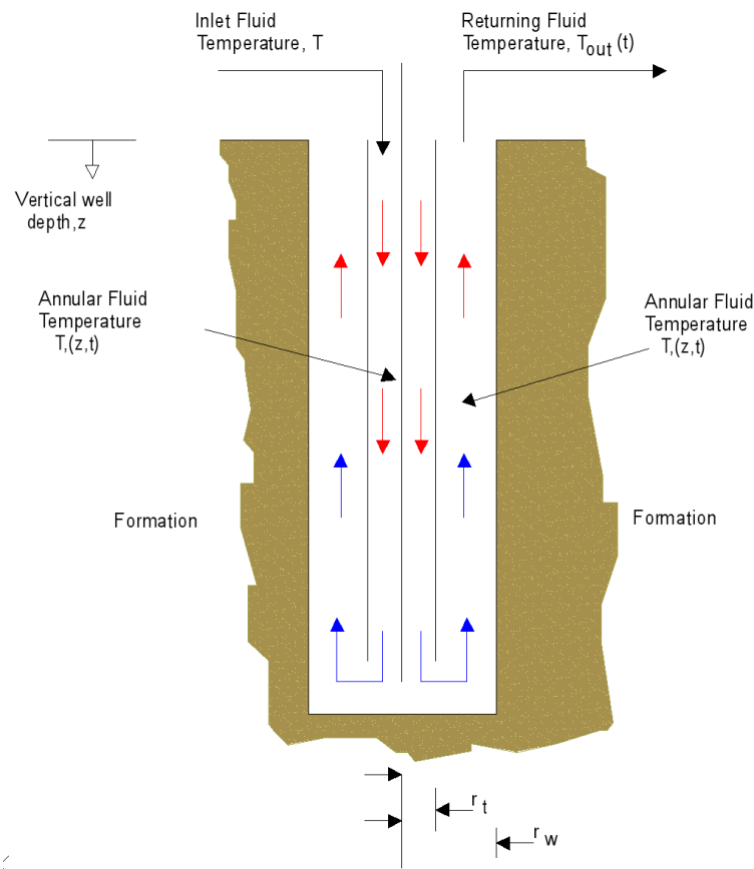


Figure 2.1: Illustration of the fluid flow through drill pipe and return through annulus [20]

Figure 2.2 illustrates the temperature profiles in the annulus and in the pipe. The effect of the temperature profile on the density is shown in figure 2.3. If the density is not accurately predicted, it would be difficult to maintain the well pressure. Moreover, the effect of temperature on the buoyancy factor calculated from the density profile is displayed in figure 2.4. If the buoyancy factor is calculated based solely on the surface density of the drilling fluid, the resulting buoyancy factor would be constant along the depth of the wellbore. This will lead to incorrect torque and drag values. However, as shown, the calculated buoyancy factor from temperature dependent density profile generated different value. This illustrates the need to correct the density and rheological properties of the drilling fluid.



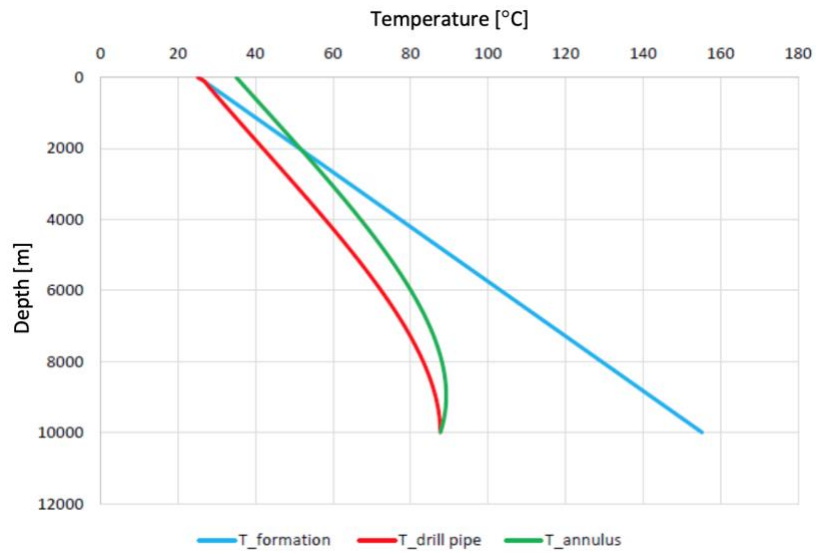


Figure 2.2: Drilling fluid temperature profile during circulation process

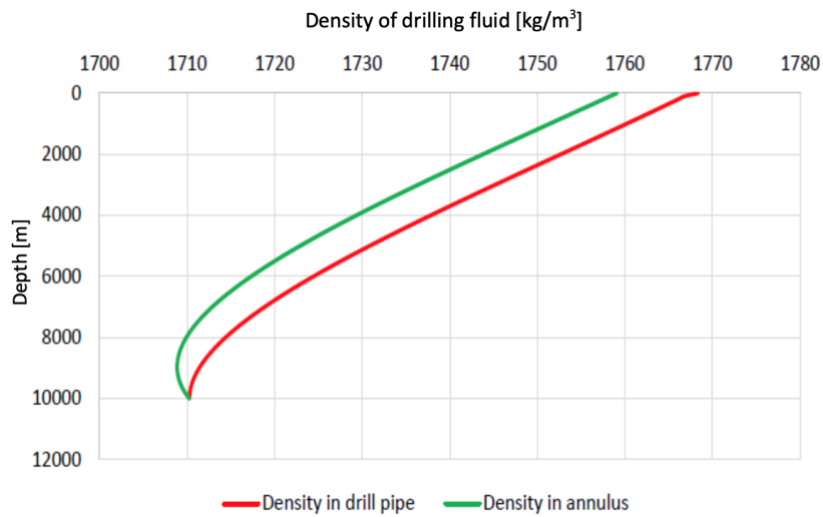


Figure 2.3: Effect of temperature on drilling fluid density

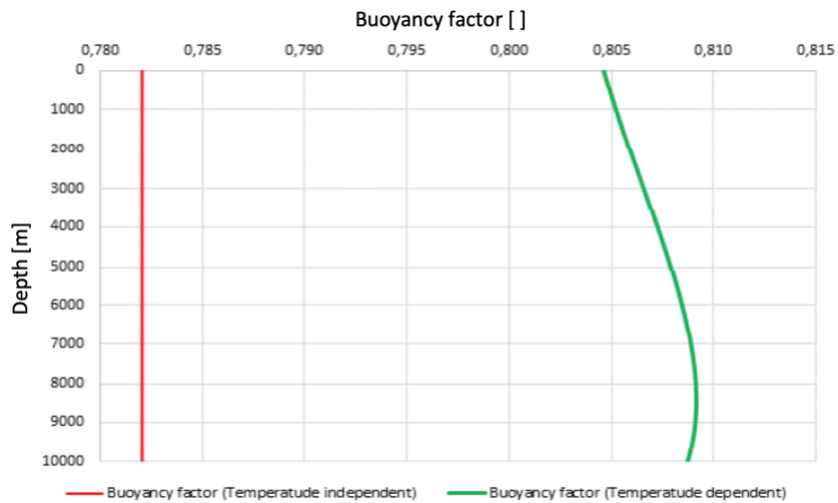


Figure 2.4: Effect of temperature on the buoyancy factor

## 2.2.2 HPHT Viscosity Prediction

In order to adequately predict the rheological parameters down-hole, the viscometer needs to be able to withstand and measure under HPHT conditions. Previously, the viscometers were limited to  $\leq 260^\circ\text{C}/1380$  bar. However, since there has been recorded HPHT wells with temperatures and BHPs approaching  $315^\circ\text{C}$  and  $2760$  bar, respectively, this was then set as the new criteria in order to develop a new HPHT viscometer. Additionally, it was required to accommodate a magnetic coupling in order to allow for precise viscosity measurements of ferromagnetic and magneto-rheological drilling fluids. Six months after this new criteria were suggested, the Chandler 7600 viscometer was designed and finished, meeting the design criteria of  $315^\circ\text{C}$  and  $2760$  bar in order to successfully measure rheological parameters at HPHT conditions [19].

### 2.2.2.1 Temperature and Pressure Dependent Viscosity

As fluid flows into a wellbore, the temperature and pressure increase. These thermodynamic states influence the viscosity and density of the drilling fluid. There are several empirical models, which describe temperature and pressure effect among others the WLF–Barus model reads [21]:

$$n(p, T) = n_o 10 \left( \frac{C_1(T-T_0)}{C_2+(T-T_0)} \right) \exp (\beta (T) (P - P_0)) \quad (2.12)$$

And;

$$\beta(T) = (\beta_0 + \beta_1) (T - T_0) \quad (2.13)$$

Where:

$n_o$	plastic viscosity drilling fluid	[Pa · s]
$P_0$	atmospheric pressure	[psi]
$T_0$	reference temperature	[°C]
$C_1, C_2$	empirical constants	[°C]
$\beta(T)$	viscous coefficient linearized with temperature	[ ]
$\beta_0, \beta_1$	viscous parameters	[1/bar °C]

For an oil-based drilling fluid, the correlation parameters are provided in **table 2.1**.

**Table 2.1:** Correlation constants [21]

Sample	$n_o$	$C_1$	$C_2$	$\beta_0$	$\beta_1$
Sr – 10 oil	0.114	2.54	80.65	$2.62 \times 10^{-3}$	$-1.43 \times 10^{-5}$

For illustration, to study the effect of the temperature profiles shown in figure 2.2 on the viscosity of the drilling fluid, the empirical equation 2.12 was used and the results are displayed in figure 2.5. Assuming the temperature and pressure independent viscosity is 0.114 cP. As the change in pressure increases, the viscosity decreases. This illustrates the need to develop a thermal stable drilling fluid and develop an accurate predictive model to determine the properties of the drilling fluid.

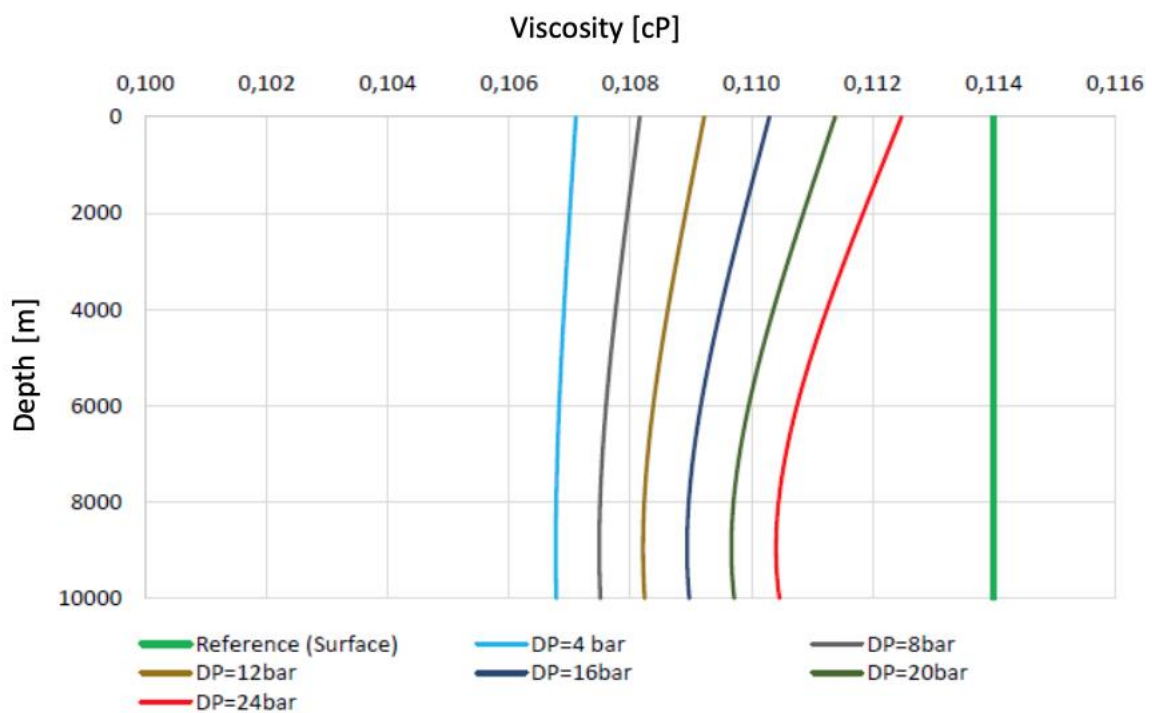


**Figure 2.5:** Illustration of effect of temperature and pressure on the viscosity of drilling fluid

## 2.3 Barite Sag in Drilling Fluids

Barite sag management is identified as one of the most critical problems with regards to drilling fluid challenges. This problem has increased in frequency over the last decades, as there are more high-angle wells being drilled, where the barite sag potential is more severe [20]. In order to better understand how to control and minimize the barite sag, drilling fluid rheology and drilling fluid properties are important to characterize. Through this literature study, different approaches and research work will be presented and accounted for.

### 2.3.1 Drilling Parameters Affecting Barite Sag

In order to determine how to minimize or eliminate the barite sag problem, it is important to know which parameters of the drilling system that influences the sag potential. Bern et al.'s sources have identified that the following parameters are the ones that are most likely to affect the potential of barite sag: hole diameter, wellbore angle, wellbore length, annular velocity, drill pipe rotation, flow regime, mud viscosity, mud gel strength, fluid density, weighting agent density, particle shape and size, particle concentration and time.

Based on this information, Bern et al. developed a flow loop that could conduct continuous measurement of the circulating fluid density in order to simulate the effect of the most dominant parameters influencing the barite sag. Results from extensive testing showed that: significant barite sag was measured at wellbore angles of 0-75°, with 60-75° being the most critical angles, mud weight did not necessarily affect the barite sag over the range of mud weights from 11.6 to 16.0 lbm/gal and that sag was virtually eliminated as lower shear yield stress (LSYS) was increased to 15 lb/100ft<sup>2</sup>. The lower shear yield stress was proposed as an alternative way of measuring the yield stress (YS) by the use of the 6 and 3 RPM Fann-35 readings and is calculated by:

$$LSYS = (2 \cdot \theta_3) - \theta_6 \quad (2.14)$$

From the studies performed by Bern et al. it was suggested that the lower shear yield stress value should be in the interval between 7 and 15 lb/100ft<sup>2</sup> in order to minimize the barite sag potential. Further, lots of studies have been performed trying to understand and better elaborate on the complexity of dynamic sag of weighting agents in drilling fluids. Some of the studies highlights that viscoelastic property analysis could be beneficial in terms of gaining more knowledge about dynamic settling [20].

### 2.3.2 Barite Sag in Highly Deviated Wellbores

In a paper presented by Hanson et al., lots of experimental studies of dynamic barite sag in highly deviated wells have been performed by the use of a flow loop, illustrated in figure 2.6 below. The paper presents historical experiences and tries to establish some guidelines in order to help minimizing the potential of barite sag in the field. Some of these guidelines are addressing operational procedures, like bottoms-up circulations, while others are related to the drilling fluid formulation, like treating the fluid system to prevent flocculation. Results from the extensive flow loop testing indicated that slumping, sliding of sediment beds on the low-side of the tube, was most prominent in angles from 40° to 50°. Further, it was concluded that sag is usually a result of dynamic density stratification and dynamically enhanced Boycott settling [21].

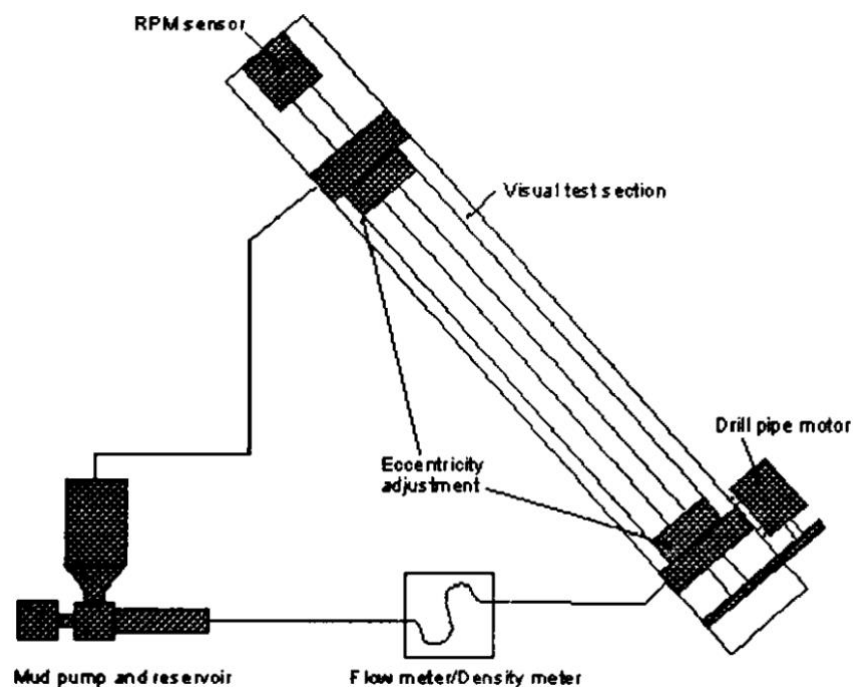


Figure 2.6: Illustration of a "Flow loop test" [22]

### 2.3.3 Settling of Weight Material in Oil-Based Drilling Fluids

Arild Saasen presented in 2002 an article describing the mechanisms of weight material settlement in oil-based drilling fluids and emulsions, also explaining how to treat this problem. For barite sagging in drilling fluids, Boycott settling is highlighted as the primary contributing factor. When particles settle in a deviated part of the well, a denser fluid will at some point be situated above a lighter fluid. In this situation, the gravity will cause a mixing motion that accelerates this separation, hence, accelerating the sagging process.

Further, the effect of drilling fluid density and the effect of gel formation on barite sag were analyzed. For lower drilling fluid densities, the consequences of weight material settlement tend to be smaller, as less dense fluids contains smaller amounts of weight material. As for the effect of the gel strength, it is important that the fluid is able to generate an adequate gel strength. The gel strength, if strong enough, prevents static sag, because in order to initiate static sag, the gravitational force of the weighting particle needs to overcome the fluid gel strength [23]. Saasen also refers to previous studies, performed by Jamison & Clements and Hanson et al., that shows that a reduction of fluid viscosity or gel strength increases the sag potential, and that it is more difficult to prevent dynamic sagging than static sagging [24] [21].

Settlement of weight material in oil-based drilling fluids is greatly dependent of the fluid's rheological behaviour. From the studies Saasen has performed, he recognized a shear thickening effect for oil-based drilling fluids at ultra-low shear rates, opposite of the shear thinning effect that is observed at higher shear rates. The low viscosity environment is created by a Brownian motion that causes a crystalline structure of water-droplets. This crystalline structure is then broken when the shear rate is increased, which results in an increase of fluid viscosity.

Saasen also argues that sag always will happen for weight particles that are larger than one micron, as this is the limited size for self-suspension. A solution to reduce the amount of sag in emulsions is to increase the viscosity of the continuous fluid or try to move the critical shear rate to where the shear thickening occurs at lower values, which can be done in three ways. One way is to add more water to the emulsion in order to prevent the water droplet to move. Both of the two other methods are based on reducing the inter-droplet distance without changing the amount of water in the emulsion, which also restricts the space for the water droplet to move before it collides with other droplets.

## 2.4 Yield Stress of Drilling Fluids

As described in Chapter 3.1.2, the yield stress, or yield point, is defined as the minimum shear stress required to initiate fluid flow, which is a critical factor contributing to cuttings and weight material suspension. This definition indicates that the yield stress is determined at one specific shear stress value. However, this might not be the case.

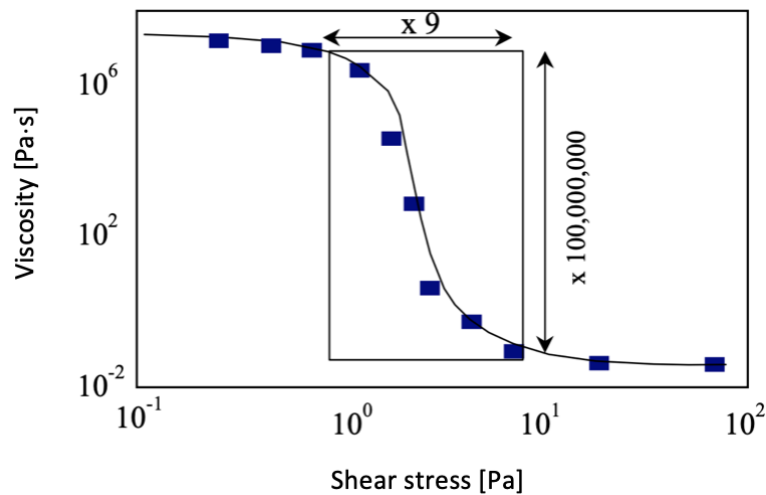


Figure 2.7: Viscosity vs. shear stress for a 10% suspension of bentonite [25]

Illustrated in figure 2.7 is the flow curve of a 10% suspension of bentonite, which is a shear-thinning fluid. These types of fluids tend to exhibit yield stress characteristics as the viscosity drops significantly over a relatively small range of shear stress, as highlighted by the black rectangle in figure 2.7. By conducting applicable measurements below this shear stress, there is found indications of a finite, high value viscosity at low stress. These studies, performed by Howard A. Barnes, therefore suggests that the yield stress might be better defined as a yield stress region, rather than a single yield point [25].

A paper presented by Maxey et al. in 2008 defines yield stress fluids as fluids that are somewhat capable of supporting their own weight. Further, it is argued that both phenomena of yield stress and thixotropy tends to appear in the same fluids. The fluids microstructure that prevents rearrangements, the yield stress, which is broken when flow is initiated, is considered to be the basis of thixotropy. In order to improve the understanding of the “true” yield stress, various experimental methodologies were analyzed, and comparison of the yield stress values obtained from different tests were conducted. Results from the testing showed that drilling fluids, that have been treated as yield stress materials, requires further rheological characterization in order to better predict the fluids’ hydraulic performance [26].

## 2.5 Application of Nanoparticles in Drilling Fluids

Nanotechnology is characterized as the science, technology and engineering that is conducted at nano-scale, by the use of nanoparticles. Nanoparticles are structures with magnitudes in the range of 0.1 – 100 nanometres that can be used to enhance the mechanical, optical and magnetic properties of materials [27]. With its broad field of use, nanotechnology has been adopted into a wide range of industries, including the oil and gas industry. Nanotechnology has been applied in all parts of the petroleum business, from exploration and reservoir engineering to drilling and completion. For drilling fluids in particular, nanotechnology has been used to solve problems regarding fluid loss control and wellbore stability, bit balling, torque and drag issues and various HPHT challenges [28].

A paper from 2012, presented by Long et. al., reviewed some of the many possible applications of nanotechnology in drilling fluids.

*“With the combination of nanotechnology and drilling fluid technology, nanomaterials can significantly increase the high temperature resistance, pollution resistance, fluid loss control as well as cuttings removal ability of drilling fluid systems, improve the drilling at high temperature high pressure conditions, and strengthen the drilling of special reservoirs.” [27]*

From the paper, the latest of nanotechnology, at the time, with regards to drilling and drilling fluid were reviewed. The conclusions drawn from the review were as following:

- Application of nanoscale additives in drilling fluids could potentially solve drilling related problems that are difficult to resolve by the use of conventional methods.
- Nano-modified drilling fluids may enhance the wellbore stability and protect the reservoir.
- It may reduce the environmental impact and increase the safety with regards to drilling operations.
- Highly deviated, horizontal and deep, complex wells are all a part of the future. Nanomaterial based drilling fluids may help to meet the special requirements required to drill these wells.

In 2013, De Stefano et. al. presented a study based on the application of different nanoparticles in order to solve various drilling fluid challenges that occurs frequently during drilling operations. Some of the problem areas that were focused on were: rheology and fluid loss control, HPHT rheology and fluid loss control and shale stability. Different approaches were applied, and the following results/indications were found:



- Application of graphene oxide in a freshwater slurry indicated very positive effects in terms of both the rheology and the fluid loss. For instance, the fluid loss after 30 minutes was reduced by 80% by adding 1.5 grams of graphene oxide to the slurry mixture.
- The application of two different carbon nanotubes (CNTs) showed positive results, even at low loadings, in terms of stabilizing the rheology at extreme HPHT conditions for a non-aqueous invert fluid. One of the fluids exhibited very positive low-shear viscosity, yield point and gel strengths. However, fluid loss control was still an issue.
- For shale stability, nanosilica was applied in order to try to prevent water invasion into shale. The primary results showed positive indications that the nanosilica particles were able to physically plug the nanosized pores, preventing water from invade the shale formation and reduce the wellbore stability.

## 3 THEORY

In order to perform experimental work and simulation studies, and achieve reasonable results, some basic background knowledge is required. This chapter describes and elaborates on the fundamental theories this thesis' experimental work and simulation studies are based on.

### 3.1 Rheology

Rheology is defined as the physical science of deformation and flow of fluids and the deformation of solids [6]. By studying the stress-strain-time relationship of any material, one can identify a material's properties and how they are affected by physical parameters such as pressure and temperature [29]. When discussing the rheology of a drilling fluid, it is meant to focus on the fluid's flowing properties [12]. The most important rheological properties that are used for evaluating and controlling the drilling fluid's functions are; plastic viscosity, yield point and gel strength.

#### 3.1.1 Plastic Viscosity

Plastic viscosity (PV) is defined as a mechanical friction that is generated by solid to solid, fluid to solid or fluid to fluid interactions, that creates a flow resistance within a fluid system. The PV value gives information about the solids content in the drilling fluid and the viscosity of the liquid phase. Plastic viscosity is measured in centipoise [cP] [12].

#### 3.1.2 Yield Point

Yield point (YP) is the minimum shear stress that is required to initiate flow of a fluid [12]. The yield point is also defined as the yield stress (YS) that is given at zero shear rate in the shear stress/shear rate diagram [30]. The yield point occurs due to electrical and chemical forces that arise between the particles in the fluid. YP has the unit [lb/100ft<sup>2</sup>] [12].

#### 3.1.3 Gel Strength

Gel strength (GEL) refers to the fluid's capability to solidify into a jelly texture. This property is also referred to as thixotropy and is a time dependent property. Gel strength is an important drilling fluid property as it helps suspend borehole cuttings during a temporary stop of circulation. Gel strength has the unit [lbf/100ft<sup>2</sup>] [12].

In order to understand the rheological parameters, how they behave and mathematically describe the flow of drilling fluids, the shear stress and shear rate are two essential concepts.

### 3.1.4 Shear Stress

Shear stress is defined as a force or a pressure that is applied to a fluid in order to make it move. From **figure 3.1** one can see that the shear stress increases as one moves closer to the tube wall, this is because the frictional resistance in the tube also increases as one moves towards the tube wall. Shear stress has the unit [lbf/100ft<sup>2</sup>] and is mathematically expressed by **equation 3.1** [6]:

$$\tau = \frac{F}{A} \quad (3.1)$$

Where:

$\tau$	Shear stress	[lbf/100ft <sup>2</sup> ]
$F$	Force applied	[lbf]
$A$	Shear area	[100ft <sup>2</sup> ]

### 3.1.5 Shear Rate

Shear rate is defined as the ratio between velocity ( $v$ ) and distance from the tube wall ( $r$ ), determined by the velocity gradient. The shear rate is dependent of the velocity change from layer to layer inside the fluid, as illustrated by the velocity profile in **figure 3.1** and its unit is [1/s] or [s<sup>-1</sup>]. The shear rate is given by [6]:

$$\dot{\gamma} = \frac{v}{r} \quad (3.2)$$

Where:

$\dot{\gamma}$	Shear rate	[s <sup>-1</sup> ]
$v$	Velocity	[ft/s]
$r$	Distance from the tube wall	[ft]

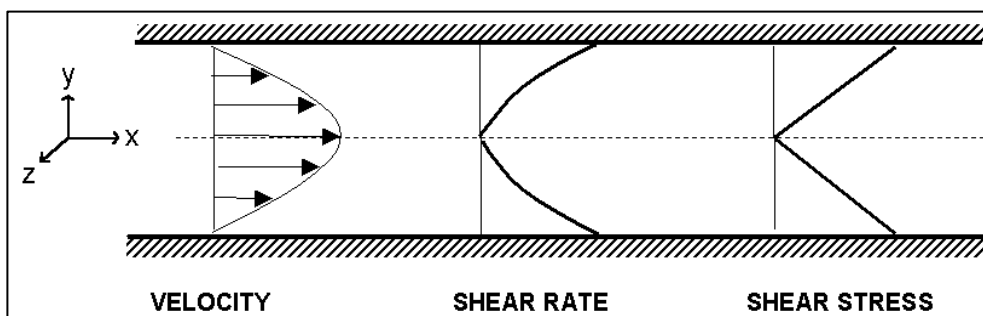


**Figure 3.1:** Velocity, shear rate and shear stress profile illustration of the fluid flow in a tube [31]

## 3.2 Rheological Models

In order to understand a drilling fluid's behaviour, it is important to choose the correct rheological model that correlates with the fluid's rheological data from the lab. Which model to use depends on whether the fluid is Newtonian or non-Newtonian. All the fluid models refer to what is called ideal, theoretical fluids that can be characterized by simple models [11].

### 3.2.1 Newtonian Fluid

A Newtonian fluid is a simple, clean and particle free fluid, such as water or oil. Newtonian fluids do not contain any particles larger than molecules [11]. All Newtonian fluids obey the Newton's law of viscosity, which is a linear relationship where the shear stress is proportional to the shear rate, as illustrated by the plot in figure 3.2 [6]. The Newtonian viscosity relationship is given by:

$$\mu = \frac{\tau}{\dot{\gamma}} \quad (3.3)$$

Where:

$\mu$	Newtonian viscosity	[cP]
$\tau$	Shear stress	[lbf/100ft <sup>2</sup> ]
$\dot{\gamma}$	Shear rate	[s <sup>-1</sup> ]

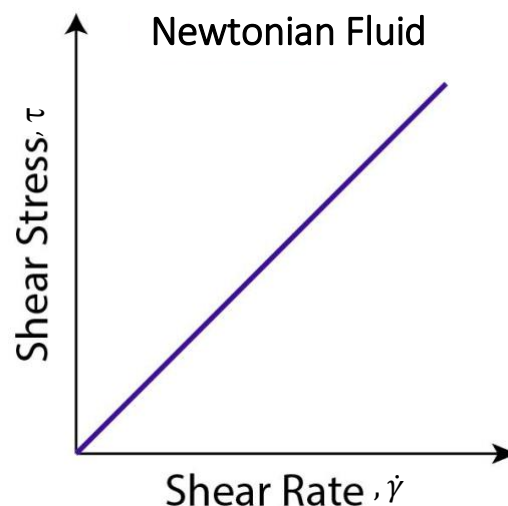


Figure 3.2: Newtonian fluid model represented in a shear stress vs. shear rate plot [32]

All data from Newtonian fluids will give a similar plot with a straight, linear line that runs through the origin of the shear stress/shear rate diagram [12]. To be able to plot the rheological data from the lab

in a shear stress/shear rate plot, the laboratory data have to be converted into engineering field data, which is done by using the following conversion factors:

$$\gamma = 1.703 \cdot \Omega \quad (3.4)$$

$$\tau = 1.067 \cdot \theta \quad (3.5)$$

Where

$\Omega$  shear rate on viscometer [s<sup>-1</sup>]

$\theta$  dial reading on the viscometer [ ]

### 3.2.2 Non-Newtonian Fluids

A non-Newtonian fluid does contain particles larger than of molecules and behaves differently compared to a Newtonian fluid [11]. For instance, the viscosity of a non-Newtonian fluid can change when exposed to different environments. Most drilling fluids are non-Newtonian fluids and have to be characterized by non-Newtonian rheological models. As shown in **figure 3.3**, the Newtonian model does not fit the drilling fluid data very well.

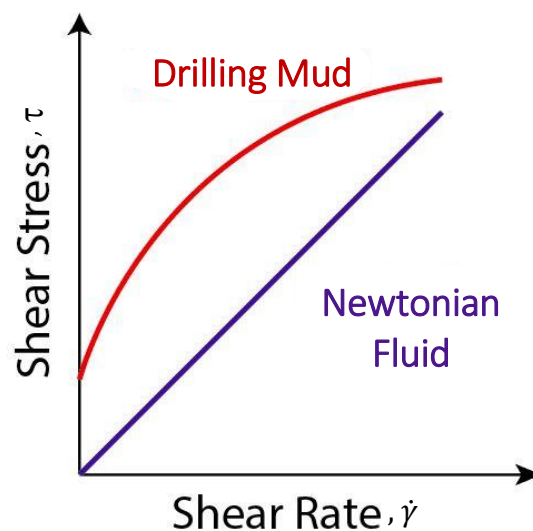


**Figure 3.3:** Newtonian fluid and an arbitrary drilling mud in a shear stress vs. shear rate plot [32]

The behaviour of a non-Newtonian fluid is often split between:

- *Plastic* behaviour – the fluid has a yield point that resists a small shear stress
- *Pseudoplastic* behaviour – the fluid does not have a yield point and the viscosity decreases with increasing velocity gradient
- *Dilatant* behaviour – the fluid viscosity increases with increasing velocity gradient

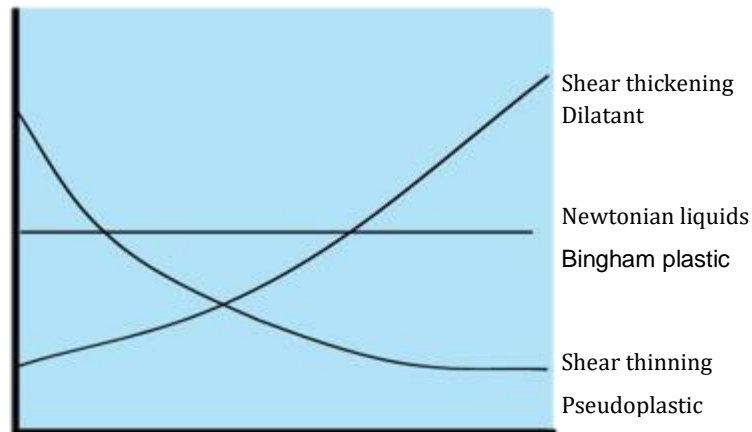


**Figure 3.4:** Illustration of plastic, pseudoplastic and dilatant fluids in a viscosity vs. stress diagram [33]

From **figure 3.4** one observes that pseudoplastic fluids are described as shear thinning fluids and dilatant fluids are described as shear thickening fluids. This refers to the respectively decreasing and increasing viscosity.

In order to characterize fluids with different compositions, various non-Newtonian fluid models are required to be able to describe their behaviour. The most common ones, and the ones used and compared in this thesis are:

- Bingham Plastic model
- Power Law model
- Herschel-Bulkley model
- Robertson & Stiff model
- Unified model

### 3.2.2.1 Bingham Plastic Model

The Bingham Plastic model behaves similarly to the Newtonian model, with a linear relationship between shear stress and shear rate. The only difference is that a Bingham Plastic fluid requires a certain minimum shear stress in order to initiate the fluid flow, hence the fluid has a yield point [12]. The model is illustrated in **figure 3.5**, where the yield point,  $\tau_0$ , is the intersection on the shear stress axis and the slope determines the PV value. The Bingham Plastic model is given by the following relationship:

$$\tau = \mu_p \cdot \dot{\gamma} + \tau_0 \quad (3.6)$$

Where:

$\mu_p$	plastic viscosity	[cP]
$\tau_0$	yield point	[lbf/100ft <sup>2</sup> ]

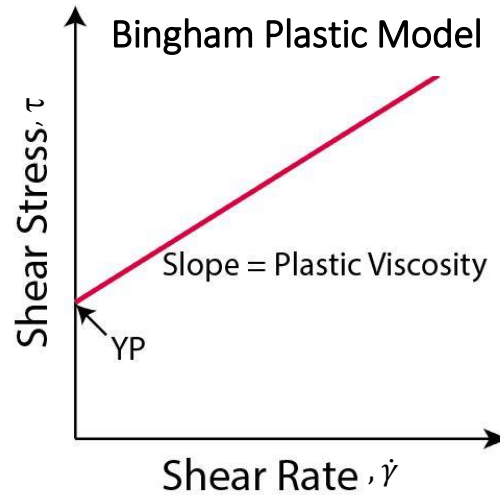


Figure 3.5: Bingham Plastic model represented in a shear stress vs. shear rate plot [32]

The plastic viscosity and the yield point are calculated by using the following equations:

$$\mu_p = \theta_{600} - \theta_{300} \quad (3.7)$$

$$\tau_0 = \theta_{300} - \mu_p \quad (3.8)$$

### 3.2.2.2 Power Law Model

The Power Law model is similar to the Newtonian model and has a line that goes through the origin of the shear stress/shear rate diagram, as shown in figure 3.6. However, it is not described by a linear shear stress/shear rate-relationship, but an exponential relationship. The shear stress/shear rate-relationship is related through the exponent 'n', the flow behaviour index, which expresses the degree of shear thinning [6]. The Power Law model is suited to describe pseudoplastic fluids, hence a good match for most drilling fluids. The Power Law model is given by the following relation:

$$\tau = K \cdot \dot{\gamma}^n \quad (3.9)$$

Where:

- $K$  consistency index  
 $n$  flow behaviour index

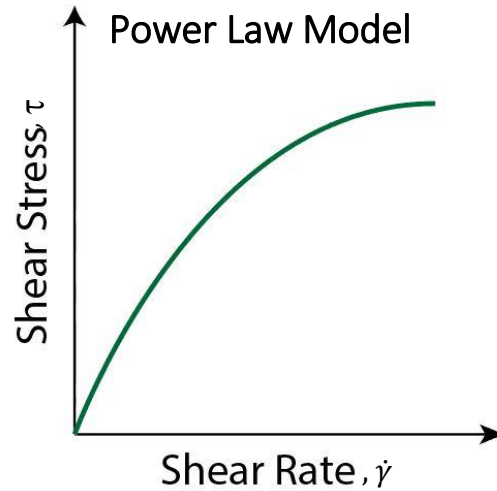


Figure 3.6: Power Law model represented in a shear stress vs. shear rate plot [32]

The consistency index and flow behaviour index can be calculated from the following equations:

$$K = \frac{\theta_{300}}{511^n} = \frac{\theta_{600}}{1022^n} \quad (3.10)$$

$$n = 3,32 \log \left( \frac{\theta_{600}}{\theta_{300}} \right) \quad (3.11)$$

As mentioned, the flow behaviour index,  $n$ , can be used to determine the degree of shear thinning, and that is decided by its numerical value:

- $n < 1$  indicates decreasing viscosity with increase shear rate, hence the fluid is pseudoplastic
- $n = 1$  indicates no change in viscosity with shear rate, hence the fluid is Newtonian
- $n > 1$  indicates increasing viscosity with increasing shear rate, hence the fluid is dilatant

Normally, dilatant flow will not be relevant for the rheological analysis of drilling fluids [6].



### 3.2.2.3 Herschel-Bulkley Model

The Herschel-Bulkley (H-B) model is basically a modified combination of the Power Law and the Bingham Plastic model which, in some cases, better describes the drilling fluid rheology. A minimum shear stress,  $\tau_0$ , is required to initiate flow and once the fluid is in motion, the fluid shear stress/shear rate-relationship behaves very much alike the Power Law. This is illustrated in **figure 3.7**. H-B describes the drilling fluid by the means of three different parameters and is given by the following mathematical equation [34]:

$$\tau = \tau_0 + K \cdot \dot{\gamma}^n \quad (3.12)$$

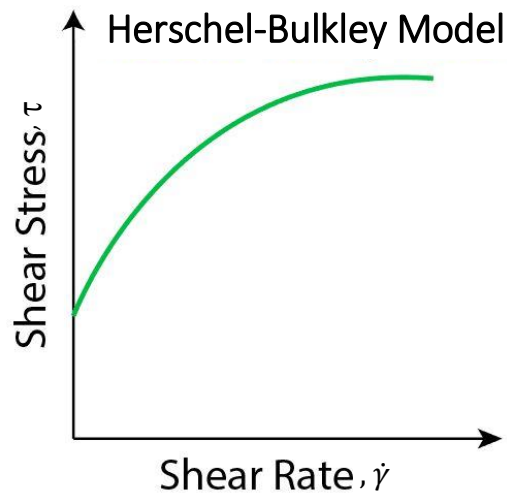


**Figure 3.7:** Herschel-Bulkley model represented in a shear stress vs. shear rate plot [32]

The  $n$  and  $K$  values can be determined graphically.  $\tau_0$  is determined by using the following equation:

$$\tau_0 = \frac{(\tau^*)^2 - \tau_{min}\tau_{max}}{2\tau^* - \tau_{min} - \tau_{max}} \quad (3.13)$$

Where  $\tau^*$  is determined from the corresponding geometric average value of the shear rate,  $\dot{\gamma}^*$ , which is determined by:

$$\dot{\gamma}^* = \sqrt{\dot{\gamma}_{min}\dot{\gamma}_{max}} \quad (3.14)$$

### 3.2.2.4 Robertson-Stiff Model

The Robertson-Stiff (R-S) model is based on a more general approach in order to describe the rheological performance of drilling fluids and cement slurries. Robertson and Stiff's model is given by this basic equation:

$$\tau = A (\dot{\gamma} + C)^B \quad (3.15)$$

Where **A**, **B** and **C** are the R-S constants. **A** and **B** can be compared with the **K** and **n** from the Power Law model accordingly. The constant **C** is used as a correction factor for the shear rate value, and the term  $(\dot{\gamma} + C)$  is regarded as the effective shear rate [35].

**C** and  $\tau_0$  can be calculated by using these equations:

$$C = \frac{\dot{\gamma}_{min}\dot{\gamma}_{max} - (\dot{\gamma}^*)^2}{2\dot{\gamma}^* - \dot{\gamma}_{min} - \dot{\gamma}_{max}} \quad (3.16)$$

$$\tau_0 = AC^B \quad (3.17)$$

Where  $\dot{\gamma}^*$  is the shear rate value corresponding to the geometric average of the shear stress,  $\tau^*$ , which again is calculated from the following equation:

$$\tau^* = \sqrt{\tau_{min}\tau_{max}} \quad (3.18)$$

When the geometric average of the shear stress is obtained, the  $\dot{\gamma}^*$  is read off the plot corresponding  $\tau^*$  value and substituted back into eq. 3.16 in order to calculate **C**.

The constants **A** and **B** can either be calculated or obtained from a plot if the logarithmic form of eq. 3.15 is plotted in a log-log plot, where **B** is the slope and **A** will be the intersection at which  $(\dot{\gamma} + C) = 1.0$  [35]. The logarithmic form of the R-S model is given by:

$$\log \tau = \log A + B \log(\dot{\gamma} + C) \quad (3.19)$$

### 3.2.2.5 Unified Model

The Unified rheological model is a modified version of a simplification of the Herschel-Bulkley model. The intention of the Unified model was to be practical in relation to field work, and that data should be easily generated from field and laboratory viscometers. The Unified model is given by the same equation as H-B, **equation 3.12**:

$$\tau = \tau_0 + K \cdot \dot{\gamma}^n$$

The main difference between the Herschel-Bulkley model and the Unified model is the determination of the parameters  $n$  and  $K$ . According to Zamora and Power's work from 2002,  $n$  and  $K$  can be determined by the following equations for pipe and annular flow respectively:

$$n_p = 3.322 \log \left( \frac{2 \cdot \mu_p + \tau_0}{\mu_p + \tau_0} \right) \quad (3.20)$$

$$K_p = \frac{\mu_p + \tau_0}{511^n} \quad (3.21)$$

$$n_a = 3.322 \log \left( \frac{2 \cdot \mu_p + \tau_0 - \tau_y}{\mu_p + \tau_0 - \tau_y} \right) \quad (3.22)$$

$$K_a = \frac{\mu_p + \tau_0 - \tau_y}{511^n} \quad (3.23)$$

Where  $\mu_p$  is the Bingham plastic viscosity,  $\tau_0$  is the Bingham yield point and  $\tau_y$  is the yield stress. "a" is used as a notation to indicate annular flow and "p" to indicate pipe flow. The yield stress is determined by the low-shear yield point, which is given by [9]:

$$\tau_y = 1.067(2 \cdot \theta_3 - \theta_6) \quad (3.24)$$

### 3.3 Viscoelasticity

Viscoelasticity is defined as a property of materials that exhibit a combination of viscous and elastic behaviour when experiencing deformation. Viscosity is defined as the internal flow resistance in a fluid and is characterized by Newton's law of viscosity, described by **equation 3.3**, while elasticity is a term used in solid mechanics to define a material's capability to return to its initial shape and condition after being exposed to a load [36]. The viscoelastic behaviour is both time and temperature dependent. For example, if a material-test is performed over a longer period of time, the material tends to behave viscous and if the same material-test is performed over a short period of time, the material will tend to behave more elastic. Accordingly, viscoelastic behaviour tends to appear at more intermediate time scales [37].

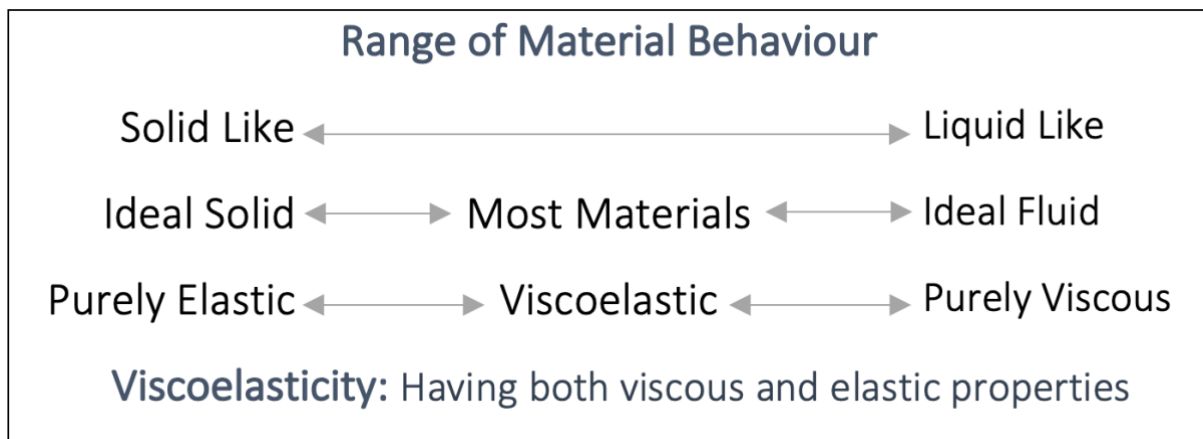


**Figure 3.8:** The “Range of Material Behavior” [38]

From **figure 3.8** one can observe that the viscoelastic behaviour is a physical state that a material experiences in between the two states of either purely elastic or purely viscous. If a material is idealelastic, it means that if the material is exposed to a load it will recover to its initial shape when unloaded [38]. An idealelastic material follows Hooke's law of elasticity, **equation 3.25**, which states that the tensile stress ( $\sigma$ ) of the material is proportional to its partial elongation (strain,  $\varepsilon$ ) multiplied by the materials modulus of elasticity ( $E$ ) [39].

$$\sigma = \varepsilon \cdot E \quad (3.25)$$

An idealelastic material has the capability to store energy. When an elastic material is being exposed to a force that elastically changes its shape, all this energy is stored within the deformed material and will later be used to restore the material to its initial shape. This process is completely reversible [40]. In comparison, an idealviscous (Newtonian) fluid will be deformed and its new shape will be determined

by the shape of its container [38]. During this process all the energy will be lost to frictional heating that occurs due to the frictional forces between the molecules in the fluid. This process is irreversible. An ideal viscous material follows Newton's law, equation 3.3, where the viscosity ( $\mu$ ) is defined as the ratio of the applied shear stress ( $\tau$ ) to the shear rate ( $\dot{\gamma}$ ). Viscosity is defined by:

$$\mu = \frac{\tau}{\dot{\gamma}}$$

Based on the characterizations of the energy conservation in elastic and viscous materials, it is anticipated that a viscoelastic material will be able to store some energy and that the rest will be lost [40].

Considering that a standard drilling fluid usually contains particles larger than molecules, it will exhibit both elastic and viscous behaviours. This makes viscoelasticity an important property in order to determine the drilling fluid's performance with regards to well operations. Viscoelasticity is a highly valuable property in terms of assessing the gel structure and gel strength, barite sag, particle suspension and hydraulic modelling of drilling fluids [37].

### 3.3.1 Mathematical Representation of Viscoelasticity

Viscoelastic behaviour is dependent of both time and applied shear stress, and the viscoelastic behaviour of a fluid is different from a solid. Dynamic rheological measurements are used in order to quantify these different viscoelastic properties, where  $G'$ ,  $G''$  and the complex viscosity,  $\eta^*$ , are the parameters of interest [40].

The *storage modulus*, denoted as  $G'$ , is a measure of the amount of energy that is absorbed and stored by a material during a deformation, as a result of a load that it is exposed to. As the material is unloaded, the stored energy will be utilized to regain its initial shape and the material can be defined as an ideal elastic solid. Storage modulus is measured in shear, in order to separate it from storage modulus ( $E'$ ) which is measured in tension, and represents the elastic behaviour of a material. The storage modulus has the unit [Pa] [40].

$G''$ , the *loss modulus*, is a measure of the energy that is lost during the deformation of a material as a result of the shear process. This energy is consumed as frictional heat when deforming the material due to the internal friction forces, the energy is said to dissipate. During the deformation process, the material is heated as well as some of the heat is lost to the environment. As the energy is lost, the

material will not be able to obtain its initial shape, hence it is an irreversible deformation. The loss modulus is also measured in shear, for the same reason as storage modulus, and it represents the viscous behaviour of a material. The loss modulus has the unit [Pa] [40].

The ratio of the loss modulus and storage modulus is defined as the *damping factor* ( $\tan\delta$ ), or loss factor, and gives information about the portion of viscous and elastic behaviour of the material. The damping factor is used to determine whether a material is behaving like a solid or like a liquid and is given by the following equation:

$$\tan \delta = \frac{G''}{G'} ; \quad 0^\circ \leq \delta \leq 90^\circ \quad (3.26)$$

If  $\delta = 0^\circ$  or  $\tan\delta = 0$ , then the material is 100% solid with an idealelastic behaviour. On the other hand, if  $\delta = 90^\circ$  or  $\tan\delta = \infty$ , the material yields an idealviscous behaviour defining a 100% viscous material. Lastly, if  $\delta = 45^\circ$  or  $\tan\delta = 1$ , i.e.  $G' = G''$ , then the material is in equilibrium between viscous and elastic. **Figure 3.9** shows how the store modulus and loss modulus changes as a function of shear strain and shear stress, respectively. The linear viscoelastic, LVE, range is the part of the graph where  $G'$  and  $G''$  are parallel. To determine the point where  $\delta = 45^\circ$  is an important analysis criterion when considering the gel formation and hardening process, as this is the physical transition from solid to viscous phase [40]. The relation between  $\tan\delta$  and the material state is given in **table 3.1** below:

**Table 3.1:** Relation between  $\tan\delta$  and material state [40]

Idealviscous flow behaviour	Behaviour of a viscoelastic liquid	Viscoelastic behaviour showing 50/50 ratio of the viscous and elastic portions	Behaviour of a viscoelastic gel or solid	Idealelastic deformation behaviour
$\delta = 90^\circ$	$90^\circ > \delta > 45^\circ$	$\delta = 45^\circ$	$45^\circ > \delta > 0^\circ$	$\delta = 0^\circ$
$\tan\delta \rightarrow \infty$	$\tan\delta > 1$	$\tan\delta = 1$	$\tan\delta < 1$	$\tan\delta \rightarrow 0$
$(G' \rightarrow 0)$	$G'' > G'$	$G' = G''$	$G' > G''$	$(G'' \rightarrow 0)$

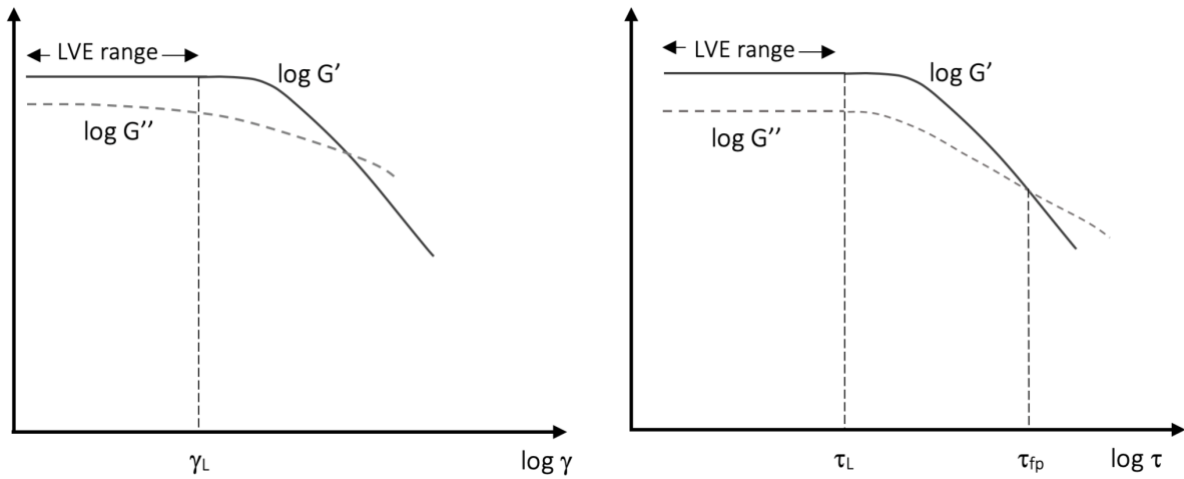


Figure 3.9: Storage modulus ( $G'$ ) and loss modulus ( $G''$ ) as a function of shear strain and shear stress, respectively [40]

The *complex shear modulus*,  $G^*$ , is the vector sum of  $G'$  and  $G''$ , as illustrated in figure 3.10, and is a measure of the complete viscoelastic behaviour of the tested material. Complex shear modulus is given by:

$$G^* = \sqrt{(G')^2 + (G'')^2} \tag{3.27}$$

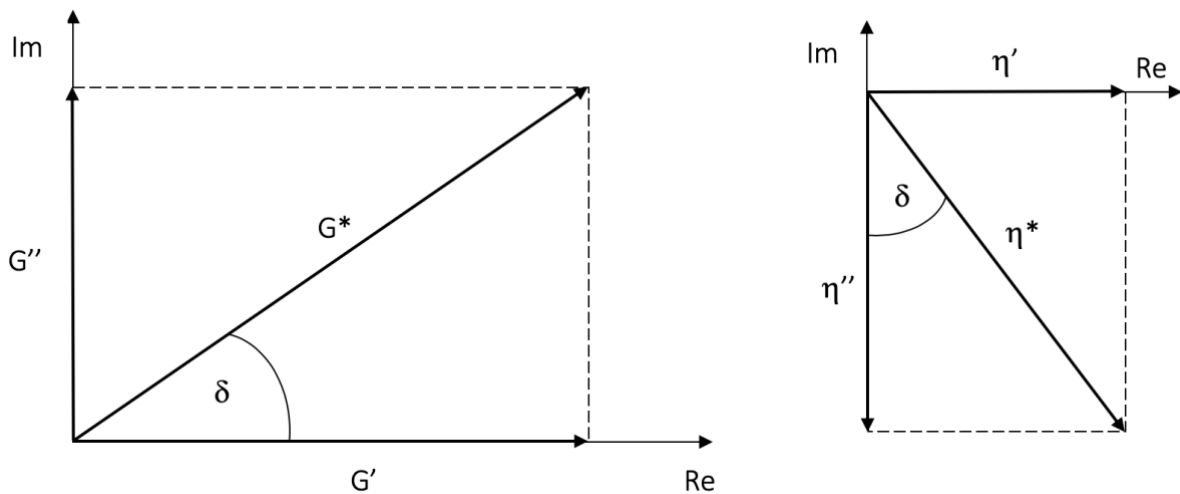


Figure 3.10: Complex shear modulus ( $G^*$ ) and complex viscosity ( $\eta^*$ ) illustrated in vector diagrams [40]

The *complex viscosity*,  $\eta^*$ , is described as the viscoelastic flow resistance and is determined by an oscillatory test. The value is not to be mixed up with the shear viscosity,  $\eta$ , which is determined through a rotational test conducted under steady state conditions. The complex viscosity can be presented in the same way as the complex shear modulus as a vector sum, as shown in figure 3.10.  $\eta'$  and  $\eta''$

represents the viscous behaviour and the elastic behaviour respectively. Complex viscosity is expressed as [40]:

$$|\eta^*| = \sqrt{(\eta')^2 + (\eta'')^2} \quad (3.28)$$

### 3.3.2 Viscoelastic Models

Simple mechanical models are used to understand the basics of viscoelasticity. In these models, springs are generally used to represent the elastic component and dashpots to represent the viscous component. A dashpot is a damper that withstands movement in the form of viscous friction and is characterized by Newton's law for ideal viscous fluids, **equation 3.3**. Elastic components, described by the behaviour of springs, are compliant with Hooke's law where the force applied is proportional to strain, hence **equation 3.25**.

The Maxwell model is the most basic model in terms of describing the viscoelastic behaviour of a liquid. In this model, a spring and a dashpot is combined in a series, as illustrated in **figure 3.11 a)**. In the Kelvin-Voigt model the spring and dashpot is arranged parallel to each other, as shown in **figure 3.11 b)**. The Kelvin-Voigt model is the most elemental model in terms of expressing the viscoelastic behaviour of a solid. The last viscoelastic model, the Burgers model, is a combination of the two previous ones placed in a series [40].

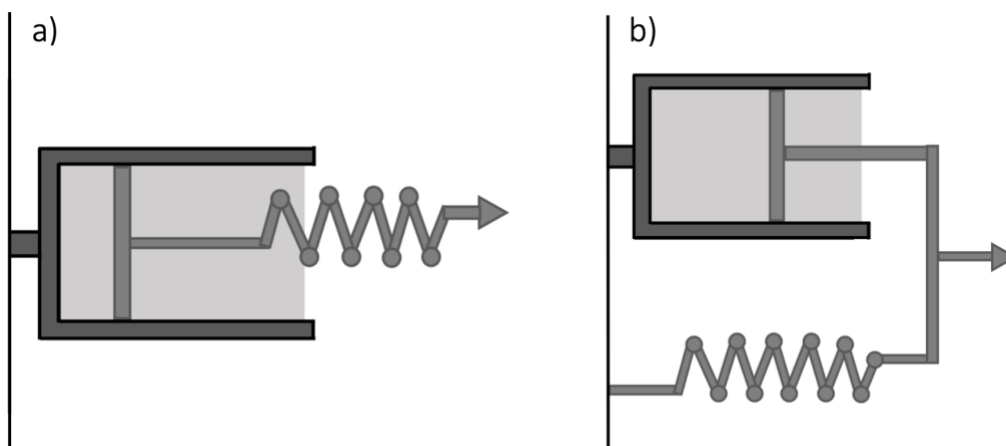


**Figure 3.11:** The Maxwell model (a) and The Kelvin/Voigt model (b) [40]



### 3.3.3 Viscoelastic Tests

In the following paragraphs, some of the elemental methods used for viscoelastic characterization are presented. The data attained from these tests are vital in terms of characterizing viscoelastic materials. When studying viscoelasticity, angular frequency ( $\omega$ ) is an important parameter, as it is used to describe the oscillation frequency. The angular frequency determines the angular displacement as a function of time and has the unit [ $s^{-1}$ ] or [rad/s] [40]:

$$\omega = \frac{2\pi}{T} = 2\pi f \quad (3.29)$$

Where:

$T$	period	[s]
$f$	frequency	[Hz]

#### 3.3.3.1 Oscillatory Tests

Oscillation means to repeatedly change the condition of a material. Oscillatory tests are used to measure the stress response caused by sinusoidal shear deformations in a sample material. The shear deformations are induced by an oscillatory rheometer, illustrated in **figure 3.12** [41].

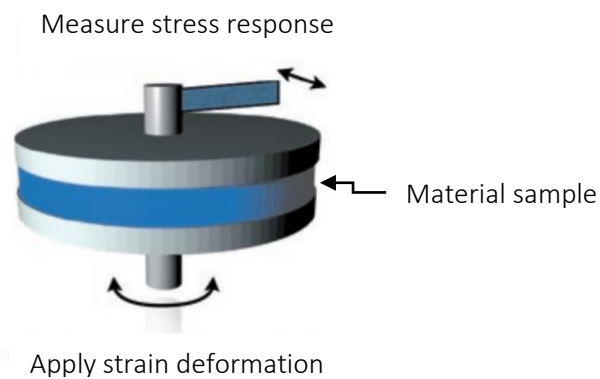


**Figure 3.12:** Oscillatory rheometer [41]

Oscillatory tests are best explained by the *Two-Plates-Model*. As illustrated in **figure 3.13**, the Two-Plates-Model includes a sample placed in between one moving and one stationary plate. In the figure,  $A$  represents the shear area,  $s$  is the deflection path,  $F$  is the shear force,  $h$  is the shear gap and  $\phi$  is the deflection angle.

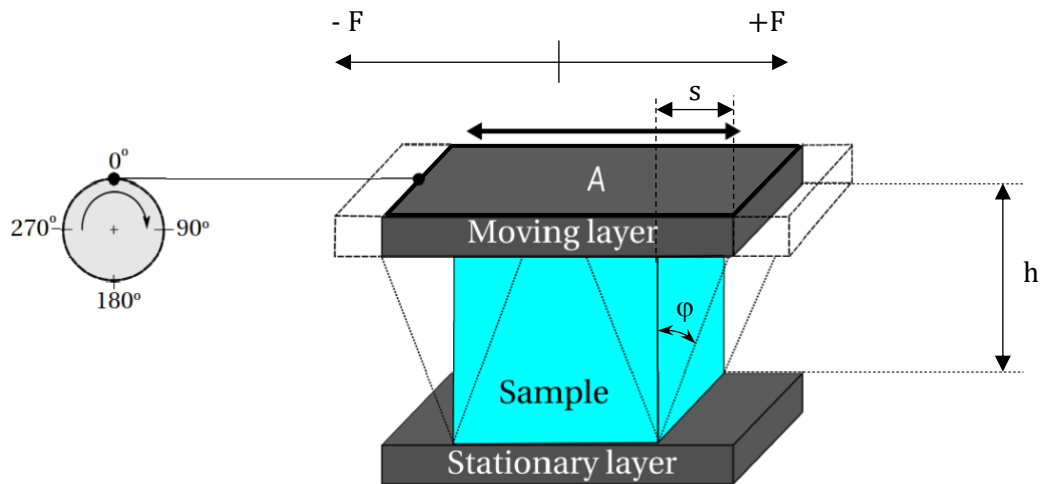


**Figure 3.13:** The Two-Plates-Model used for oscillatory shear testing [40]

The uppermost plate is connected to a rotational wheel, as illustrated to the left in **figure 3.13**. As the wheel is rotated, the upper plate will be set in motion and cause shearing of the sample. When the wheel has completed one revolution around its axis,  $360^\circ$ , this represents one oscillation period. The upper plate moves back and forth according to the force  $\pm F$ , which causes the deflection path  $s$  and deflection angle  $\varphi$ . Since the bottom plate is fixed, the motion of the upper plate will create a shear stress equal to  $\pm\tau$ . The oscillatory motion of the upper plate will behave like a sinusoidal function and the Two-Plates-Model is valid under the assumptions that:

- i. The sample is in contact with both plates without moving along them
- ii. The sample changes shape homogeneously all over the shear gap,  $h$

Shear stress, shear strain and shear rate are all time-dependent parameters, where  $\tau$  and  $\gamma$  are sinusoidal functions. When the rotational wheel's angular position is at  $0^\circ$  or  $180^\circ$ , the shear rate is at its highest. The stress measured for a given strain, at the same angular positions, will vary depending on the material [40]. For an ideal elastic material there will be no phase delay between the  $\tau$ -curve and the  $\gamma$ -curve, they will always be "in phase". However, for an ideal viscous material, there will be a  $90^\circ$  phase angle delay in the  $\tau$ -curve compared to the  $\gamma$ -curve. For a viscoelastic material, the phase angle will be somewhere between  $0^\circ$  and  $90^\circ$ , as illustrated in **figure 3.14** [37].

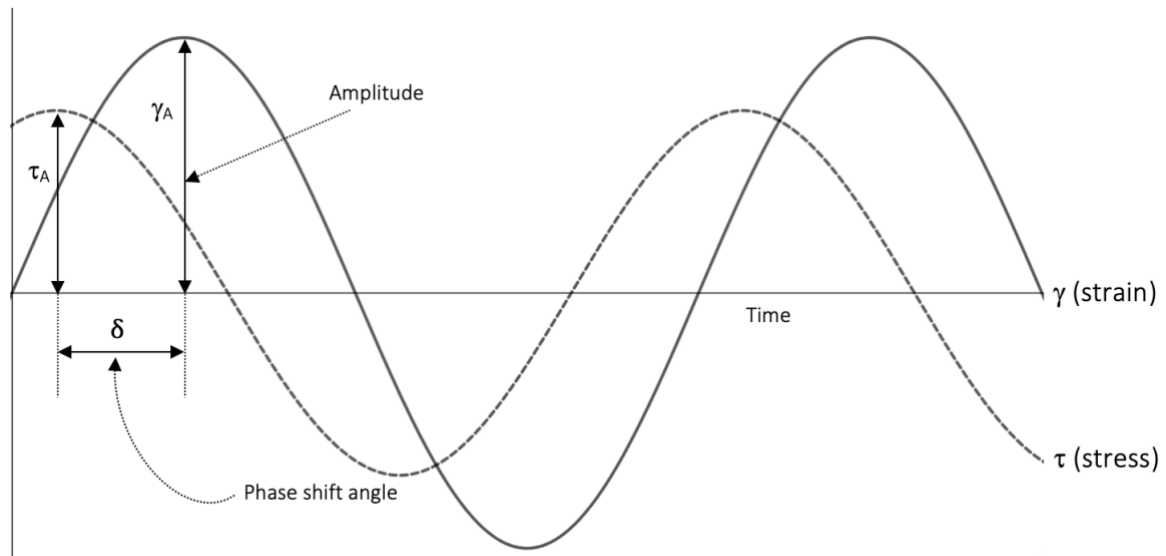


**Figure 3.14:** Shear strain and corresponding shear stress for an oscillatory test of a viscoelastic material [40]

With relation to **figure 3.14**, the applied shear strain,  $\gamma(t)$ , and the corresponding shear stress,  $\tau(t)$ , is given by [37]:

$$\gamma(t) = \gamma_A \sin(\omega t) \quad (3.30)$$

$$\tau(t) = \tau_A \sin(\omega t + \delta) \quad (3.31)$$

Where:

$\gamma_A$	shear rate amplitude	[1]
$\tau_A$	shear stress amplitude	[Pa]
$t$	time	[s]
$\omega$	angular frequency	[rad/s]
$\delta$	phase angle	[°]

Further, the shear stress can be expressed in terms of the shear strain:

$$\tau(t) = \gamma_A [G' \sin(\omega t) + G'' \cos(\omega t)] \quad (3.32)$$

Where storage modulus ( $G'$ ) and loss modulus ( $G''$ ) are defined as:

$$G' = \frac{\tau_A}{\gamma_A} \cos \delta \quad (3.33)$$

$$G'' = \frac{\tau_A}{\gamma_A} \sin \delta \quad (3.34)$$

Ultimately resulting in a shear stress given by equation 3.35:

$$\tau(t) = \gamma_A \left[ \left( \frac{\tau_A}{\gamma_A} \cos \delta \right) \sin(\omega t) + \left( \frac{\tau_A}{\gamma_A} \sin \delta \right) \cos(\omega t) \right] \quad (3.35)$$

Oscillatory rheological measurements can be performed with different presets in order to produce different raw data. These presets are referred to as different test and are called “controlled shear rate” (CSR) and controlled shear stress (CSS). CSR and CSS only produce two different types of raw data. For CSR, the deflection angle and strain are preset, and torque (M(t)) and phase shift angle are the resulting raw data. For CSS, the torque and shear stress are preset, and deflection angle and phase shift angle the resulting raw data. From the raw data, the shear stress and shear strain are calculated respectively from equation 3.31 and equation 3.36 [40].

$$\gamma(t) = \gamma_A \sin(\omega t + \delta) \quad (3.36)$$

There are four different oscillatory tests, and one or more of them will be performed as part of the work with this thesis. These four oscillatory tests are;

- Amplitude sweep
- Frequency sweep
- Time sweep
- Temperature sweep

and they will be presented in the following subsections.

### 3.3.3.1.1 Amplitude Sweep

An amplitude sweep test is an oscillatory test performed by holding a constant frequency,  $\omega$ , but gradually increasing the oscillation amplitude,  $\gamma_A$ . The test is done in order to define the linear viscoelastic range, where both store modulus and loss modulus exhibit constant plateau values, usually at different levels, as shown in figure 3.15 [40]. A viscoelastic deformation is dependent of the sample's internal structure. As long as the internal structure is not broken, during small deformations, the material will behave according to the linear viscoelastic range. As the strain is increased, it will progressively approach the yield strain,  $\gamma_L$ . When surpassing the yield strain of the material, the sample is permanently deformed, which means that the response of the sample is changed from linear viscoelastic to non-linear viscoelastic. In addition to define the LVE range and dynamic yield point, an amplitude sweep test of a drilling fluid will identify the fluids structural stability and its strength [37].

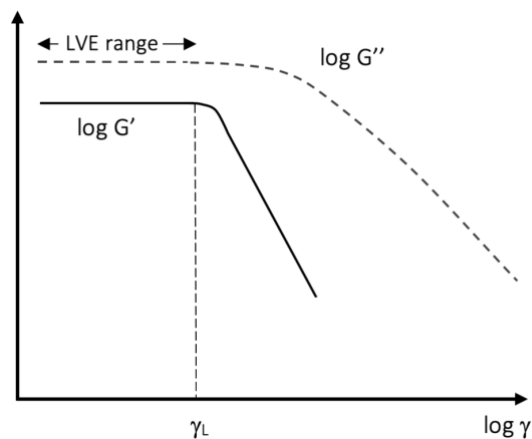


Figure 3.15: Strain amplitude sweep test of a material exhibiting liquid characteristics ( $G'' > G'$ ) [40]

In figure 3.15 the store modulus and loss modulus are plotted against strain in a log-log plot. How  $G'$  and  $G''$  are located relative to each other in the LVE range defines the viscoelastic character of the material.  $G'' > G'$  indicate that the viscous behaviour is more dominant than the elastic behaviour, meaning the material behaves more like a liquid than like a solid. While the opposite,  $G' > G''$ , indicate that the elastic behaviour dominates the viscous behaviour, a material of gel character. If  $G' = G''$  the material exhibit 50/50 viscous and elastic behaviour [40].

### 3.3.3.1.2 Frequency Sweep

A frequency sweep test is an oscillatory test performed by holding a constant oscillation amplitude,  $\gamma_A$ , but gradually decrease the frequency,  $f$ . The frequency sweep test is performed in order to study the time-dependent properties of a material in its linear viscoelastic range. Short- and long-term behaviours of a material are simulated through rapid (high frequencies) and slow oscillations (low frequencies), respectively [40]. The test usually starts off with higher frequencies that are descending towards lower

frequencies. In addition to study the response of time-dependent properties of a material, the test also identifies and measures zero shear viscosity and the structural strength at rest [37]. The results produced from the test are generally plotted in a log-log plot with angular frequency,  $\omega$ , on the x-axis and  $G'$ ,  $G''$  and the complex viscosity,  $\eta^*$ , on the y-axis [40].

As the yield strain,  $\gamma_L$ , is the limiting value for the LVE range and is an important input in the frequency sweep test, an amplitude sweep test always have to be performed prior to the frequency sweep [40].

#### **3.3.3.1.3 Time Sweep**

A time sweep test is an oscillatory test that is performed in order to study a material's behaviour with respect to time, by observing various viscoelastic properties as time progresses. From a time sweep test one can acquire knowledge about a material's gelling time and gelling speed, as well as dispersion settling and structure development [37].

Prior to the oscillatory time sweep test, the sample is pre-sheared, to break the structure of the sample. The time sweep is performed immediately after this, holding the amplitude and frequency constant at isothermal conditions, while monitoring the various property changes as time elapses. As the pre-shearing stops, a thickening, gelling, of the sample can be observed. This situation can be compared to a circulation stop in a well, where the drilling fluid will begin to build gel strength. Therefore, a time sweep test of a drilling fluid is highly valuable in order to assess its barite sag and cuttings suspension capabilities [37].

The results generated from performing a time sweep test are usually presented in a plot with  $G'$ ,  $G''$  and  $\eta^*$  on the y-axis in logarithmic scale and time on the x-axis.

#### **3.3.3.1.4 Temperature Sweep**

A temperature sweep test is an oscillatory test that is performed at constant amplitude and frequency, while the temperature is being increased in steps in order to study the material's structural dependency of its temperature. The test's main objectives are to obtain the sample's flow point, the physical change from viscoelastic gel to viscoelastic liquid, and study the sample's stability in terms of temperature.

As the temperatures that occurs in oil and gas wells are high, a test where one increases the temperature of a drilling fluid will help to anticipate the fluid's behaviour in such an environment. This is particularly important with regards to sagging and settling of weight materials in drilling fluids, as a well formulated drilling fluid should be stable at various temperature ranges [37].

### 3.4 Barite Sag

Barite sag is defined as the settling of weighting agents, most often barite particles, within the drilling fluid [17]. Barite sag is a problem that results in an unstable mud weight that will vary along the depth of the wellbore. The weighting particles will tend to accumulate in the lower parts of the well and as the weight material settles, the fluid density in the upper parts of the wellbore will be reduced and the fluid density in the lower parts will be increased [42]. Barite sag tends to be more prominent in oil-based muds due to its loss of viscosity when heated. However, it does also occur in water-based muds [17].

Barite sag do typically take place in highly deviated wells, especially in wells that have angles from  $50^\circ$  to  $80^\circ$ , low annular velocities and low viscosity drilling fluids. However, sagging does also occur in deviated wells that are drilled with a mud weight greater than  $1.44 \text{ kg/L}$  and have angles that are  $30^\circ$  or more. For wellbores with deviations up to  $75^\circ$ , the barite beds that build up usually slide down towards the bottom of the well. Some of the most typical problems associated with barite sag are well-control issues, pack-offs, loss of circulation, stuck pipe, logging problems and wellbore instability [17].

Previously one thought that barite settling was primarily occurring in static well environments. However, time has shown that wells with low shear rates and inadequate ultra-low shear rate viscosity the contribution to barite sag is even greater [43]. This process is called dynamic settling. In deviated wells, the dynamic barite settling starts at shear rates that are lower than the minimum velocity of a traditional 6-speed viscometer. As a result, viscometers with ultra-low shear rates were developed in order to predict and potentially avoid the development of barite sag [44].

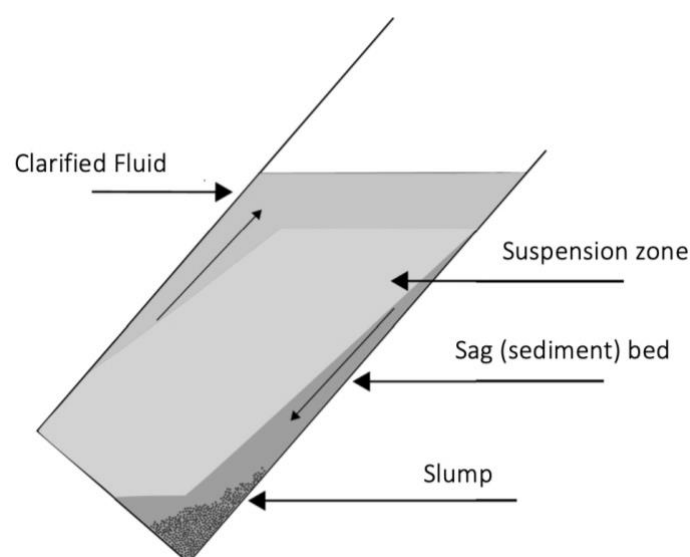


Figure 3.16: Boycott settling [17]

If the weight material is not adequately suspended, it will tend to settle out of a fluid that is stationary. Hindered settling in vertical wells, where the settling speed is reduced due to interactions with other particles in the fluid, is considerably slower than the free settling, where there are no interactions. However, if the same fluid column is tilted into a deviated position, the settling rate will increase compared to a vertical positioned settling. This phenomenon, called Boycott settling, was discovered by A. E. Boycott and is illustrated in **figure 3.16**. What happens is that when the sediments are settled out of the fluid, the light, clarified fluid will tend to move upwards on the high-side of the tube. This movement is caused by a pressure imbalance across the cross-sectional area as barite settles immediately as circulation of the fluid is stopped. The barite sediments will accumulate into a high-density sediment bed that will tend to move downwards on the low side of the tube, called slumping.

Boycott settling in complex, deviated wells is even more prominent, as the flow moves along the high side of the hole, which leads to an even higher pressure difference and an increased barite sediment bed formation. However, this form of Boycott settling can be reduced by increasing the annular velocity and the pipe rotation.

Since the settling of particles is more common during circulation, than in static situations, barite sag is primarily seen as a dynamic settling problem. During drilling of high-pressure, high-temperature (HPHT) wells, a high-density drilling fluid is usually what is used. As the temperatures are high, this will cause the viscosity of the drilling fluid to decrease, hence, increasing the potential for barite sag.

### **Barite Sag Testing**

As mentioned above, potential barite sag in drilling fluids can be predicted and evaluated by modified viscometers with ultra-low shear rates. Even though the information gained from these experiments is valuable, it will not be completely representative in all cases, as there are lots of parameters and conditions that may influence the barite sag potential in a wellbore [17]. However, the methods used for barite sag prediction are usually divided into two main categories, namely; static or dynamic testing.

#### **3.4.1 Static Testing**

Static testing of barite sag is performed by studying a heated drilling fluid sample and how the fluid and its solid particles behave under such conditions. The drilling fluid sample is inserted into a test cell, which again is placed in an oven at a given test angle for a pre-determined amount of time. When the aging process in the oven is completed, the sample is vertically divided into five segments and the density of each segment is measured respectively. By measuring the density, one can evaluate the barite settling under static conditions.



While the drilling fluid is under static conditions, the gravitational force is the only active force affecting the suspended barite particles. To initiate sagging when the fluid is static, the gravitational force minus the buoyancy force will have to overcome the gel strength of the fluid. According to A. Saasen, the highest force the drilling fluid gel can withstand is given by [23]:

$$F = \tau_g \cdot A_p \quad (3.37)$$

Where:

$A_p$	surface area of the particle	[ft <sup>2</sup> ]
$\tau_g$	gel strength	[lbf/100ft <sup>2</sup> ]

Given that the gravity force minus the buoyancy force is equal to:

$$F = (\rho_p - \rho_f) \cdot V_p \cdot g \quad (3.38)$$

Where:

$\rho_p$	density of the particle	[lb/ft <sup>3</sup> ]
$\rho_f$	density of the base fluid	[lb/ft <sup>3</sup> ]
$V_p$	particle volume	[ft <sup>3</sup> ]
$g$	gravitational acceleration	[ft/s <sup>2</sup> ]

By manipulation of **equation 3.37** and **3.38**, one gets a theoretical expression for the gel strength that is required to prevent settlement of weighting particles:

$$\tau_g \geq \frac{(\rho_p - \rho_f)}{6} gD \quad (3.39)$$

However, most OBM drilling fluids will experience static sag even though the gel strength is adequate according to the above equation. The reason is that real gel properties are not measured when following the API procedures for measuring gel strength [23]. **Equation 3.40** presents Stoke's law expressing the terminal velocity of a spherical particle in a Newtonian fluid.

$$v_t = \frac{2(\rho_p - \rho_f)}{18\mu} \cdot gD_p^2 \quad (3.40)$$

The static sag measurements performed in this thesis was done by adapting the approach of Jason Maxey. The fluid sample was aged for 16 hours in vertical direction and the sag factor was calculated by **equation 3.41**:

$$(Sag\ factor)_{static} = \frac{MW_{bottom}}{MW_{top} + MW_{bottom}} \quad (3.41)$$

In this equation,  $MW_{top}$  indicates the mud weight extracted from the top of the fluid sample, while  $MW_{bottom}$  represents the mud weight from the bottom of the sample. Both mud weights are measured in grams and are measured by extracting the same amount of fluid volume from the sample.

From Maxey's study, the ideal sag factor was found to be in the interval from 0.50 to 0.53, in order to adequately suspend solid particles. If the fluid has a sag factor that is greater than 0.53, the fluid is considered to have insufficient particle suspension and will most likely experience barite sag issues [45].

### 3.4.2 Dynamic Testing

Dynamic laboratory testing of barite sag can be measured in two different ways. The first one is performed by using a conventional viscometer and the second one is done by the use of a flow loop.

The Viscometric Sag Shoe Test (VSST) uses a conventional, rotational viscometer with a sag shoe at the bottom. The sag shoe is a thermoplastic cup that is designed in such a way that it better concentrate and collect the settled barite particles in a collection well. The viscometer applies a constant shear rate of 100 RPM, which is pre-determined as the most suitable choice for a 6-speed viscometer. After shearing the sample, the test measures the alteration in fluid density after 30 minutes of shearing. To quantify the degree of barite sag, the dynamic sag factor is determined by **equation 3.42**:

$$(Sag\ factor)_{dynamic} = \frac{MW_{final}}{2 \cdot MW_{initial}} \quad (3.42)$$

The VSST is primarily used to determine a fluid's capability to suspend weighting particles. However, it does not directly measure the fluid's barite sag potential under various well conditions [46]. This procedure is the M-I Swaco procedure used to evaluate the dynamic barite sag.

A flow loop test on the other hand has a more advanced set up and requires more equipment than a simple viscometer. The set-up of a flow loop test is shown in **Chapter 2.3, Figure 2.6**. The flow loop test

produces more realistic results as it takes into account several other parameters, like pipe eccentricity and rotation, flow rate and inclination of wellbore [46]. VSST is the preferred testing method for this thesis, as a flow loop test is more complex and requires more time and equipment to be completed.

### 3.5 Hydraulics

Fluid hydraulics is defined as the application of specific principles from fluid mechanics used to describe how a fluid behave and move. Hydraulics is one of the most important elements that affects the drilling fluid's performance with regards to drilling operations [47]. Hydraulic models are used to describe the flow behaviour of drilling fluids, determining relationships between flow rates and pressure drop for different wellbore geometries and various fluid types [48].

Evaluation and modelling of drilling fluids' hydraulic performance requires several important parameters, such as viscosity, density, slip velocity, friction factor and frictional pressure loss. A study performed by J. Sadigov in 2013 showed that the Unified model better correlates with measured data, compared to other models [49]. Based on Sadigov's work and corresponding results, it was decided that in this thesis, the Unified model will be used when performing hydraulic performance analysis and simulations. A summary of the Unified hydraulics model's most important parameters, equations and relationships are given in **table 3.2** below.

#### 3.5.1 ECD

The resulting fluid pressure in a well is dependent of the true vertical depth, the fluid density, geometry of the wellbore and the fluid's condition, whether it is static or dynamic. If the fluid is static, the exerted pressure is simply characterized by the hydrostatic pressure of the fluid; mud weight multiplied by the TVD [47]. On the other hand, if the fluid is circulating, the term Equivalent Circulation Density (ECD) is introduced. ECD is defined as the effective density exerted against the formation by a circulating drilling fluid. As the fluid is circulated through the well, some pressure will be lost due to friction. This frictional pressure drop is taken into account when calculating the ECD value. Equivalent circulation density is a particular important parameter in formations where the difference between the formation fracture pressure and formation pore pressure gradients is small. ECD is a valuable parameter in order to avoid fluid loss and gas kicks during drilling operations [50]. ECD is given by the following equation:

$$ECD = \rho_f + \frac{\Delta P_{ac}}{0,052 \cdot D} \quad (3.43)$$

Where:

$\Delta P_{ac}$	pressure drop in the annulus between D and the surface	[psi]
$D$	True vertical depth to an arbitrary point in the well	[ft]

**Table 3.2:** Summary of the parameters and equations used in the Unified hydraulic model [35]

Unified Hydraulic Model	
Pipe Flow	Annular Flow
$\mu_p = R_{600} - R_{300}$	$\tau_y = R_{300} - \mu_p$
$n_p = 3.32 \log \left( \frac{2\mu_p + \tau_y}{\mu_p + \tau_y} \right)$	$n_p = 3.32 \log \left( \frac{2\mu_p + \tau_y - \tau_0}{\mu_p + \tau_y - \tau_0} \right)$
$k_p = 1.066 \left( \frac{\mu_p + \tau_y}{511} \right)$	$k_p = 1.066 \left( \frac{\mu_p + \tau_y - \tau_0}{511} \right)$
$G = \left( \frac{(3 - \alpha)n + 1}{(4 - \alpha)n} \right) \left( 1 + \frac{\alpha}{2} \right)$	
$\alpha = 0$ for pipe	$\alpha = 1$ for annuli
$v_p = \frac{24.51 q}{D_p^2} [\text{ft}/\text{min}]$	$v_a = \frac{24.51 q}{D_2^2 - D_1^2} [\text{ft}/\text{min}]$
$\gamma_w = \frac{1.6 \cdot G \cdot v}{D_R} [\text{sec}^{-1}]$	
$\tau_w = \left[ \left( \frac{4 - \alpha}{3 - \alpha} \right) \tau_0 + k \gamma_w^n \right] [\text{lbf}/100\text{ft}^2]$	
$N_{Re} = \frac{\rho v_p}{19.36 \tau_w}$	$N_{Re} = \frac{\rho v_e}{19.36 \tau_w}$
$f_{\text{laminar}} = \frac{16}{N_{Re}}$	$f_{\text{laminar}} = \frac{24}{N_{Re}}$
$f_{\text{transient}} = \frac{16 N_{Re}}{(3470 - 1370 n_p)}$	$f_{\text{transient}} = \frac{16 N_{Re}}{(3470 - 1370 n_p)}$
Turbulent: $f_{\text{turbulent}} = \frac{a}{N_{Re}^b}$	Turbulent: $f_{\text{turbulent}} = \frac{a}{N_{Re}^b}$
$a = \frac{\log(n) + 3.93}{50}$ $b = \frac{1.75 - \log(n)}{7}$	$a = \frac{\log(n) + 3.93}{50}$ $b = \frac{1.75 - \log(n)}{7}$
$f_{\text{partial}} = (f_{\text{transient}}^{-8} + f_{\text{turbulent}}^{-8})^{-1/8}$	
$f_p = (f_{\text{partial}}^{12} + f_{\text{laminar}}^{12})^{1/12}$	$f_a = (f_{\text{partial}}^{12} + f_{\text{laminar}}^{12})^{1/12}$
$\left( \frac{dp}{dL} \right) = 1.076 \cdot \frac{f_p \cdot v_p^2 \cdot \rho}{10^5 \cdot D_p} = [\text{psi}/\text{ft}]$	$\left( \frac{dp}{dL} \right) = 1.076 \cdot \frac{f_a \cdot v_a^2 \cdot \rho}{10^5 \cdot (D_2 - D_1)} = [\text{psi}/\text{ft}]$
$\Delta p = \left( \frac{dp}{dL} \right) \cdot \Delta L = [\text{psi}]$	$\Delta p = \left( \frac{dp}{dL} \right) \cdot \Delta L = [\text{psi}]$
$\Delta p_{\text{Nozzles}} = \frac{156 \cdot \rho \cdot q^2}{(D_{N1}^2 - D_{N2}^2 - D_{N3}^2)^2} = [\text{psi}]$	

### 3.5.2 Drilling Fluid Circulation System and Pump Pressure

A typical drilling fluid circulation system consists of a mud tank, mud pump, stand pipe, drill pipe, drill collar, drill bit and annulus, which is illustrated in even more detail in figure 3.17. The circulation system represents the pathway of the fluid, where it leaves the pumps, through the stand pipe, down the drill pipe, through the nozzles in the drill bit and into the annulus where it is eventually circulated back to the surface [47].

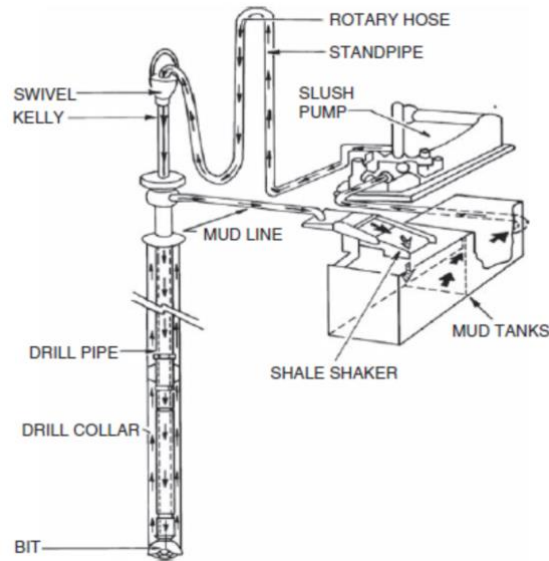


Figure 3.17: Typical drilling fluid circulation system [48]

As the drilling fluid is circulated through the system, a lot of pressure is lost due to friction. The various pressure losses are defined as following:

$\Delta P_s$	pressure loss from the flow through the surface equipment	[psi]
$\Delta P_{ds}$	pressure loss from the flow through the drill string	[psi]
$\Delta P_{dc}$	pressure loss from the flow through the drill collar	[psi]
$\Delta P_b$	pressure loss from the flow through the nozzles in the bit	[psi]
$\Delta P_{ac}$	pressure loss from the flow through annulus	[psi]
$\Delta P_{ads}$	pressure loss from the flow through annular are between riser and drill string	[psi]

In order to circulate the fluid all the way back to surface, the mud pump pressure needs to be adequate to overcome the total pressure loss in the system, hence the pump pressure,  $P_{pump}$ , is given by:

$$P_{pump} = \Delta P_{tot} = \Delta P_s + \Delta P_{ds} + \Delta P_{dc} + \Delta P_b + \Delta P_{ac} + \Delta P_{ads} \quad (3.44)$$

### 3.6 Electrical Stability

When oil-based drilling fluids are formulated, emulsifiers are used to force the two immiscible fluids, oil and water, to mix. Electrical stability (ES) is a parameter that is measured in order to evaluate the level of emulsion and oil-wetting characteristics of a drilling fluid. Generally, an electrical stable drilling fluid will be smooth and have a shiny look, while a drilling fluid with a low degree of electrical stability will have more visible grains and have a duller look. The oil-wetting characteristic of a drilling fluid is often defined as the fluid's ability to absorb external materials into the oil-phase, in this case, absorb water.

#### Electrical Stability Test

The electrical stability is measured by the use of a probe that is inserted into a container that holds the fluid to be tested, as illustrated in **figure 3.18**. The probe has two electrodes where an electrical breakdown is induced between these two electrodes. Several experiments have shown that water forms a conductive passageway for this induced electrical breakdown. The given voltage at which this conductive passageway is created is denoted as  $E_0$  and the current in the system rises suddenly when this value is reached. The test is performed at a fluid temperature of 50°C [51].

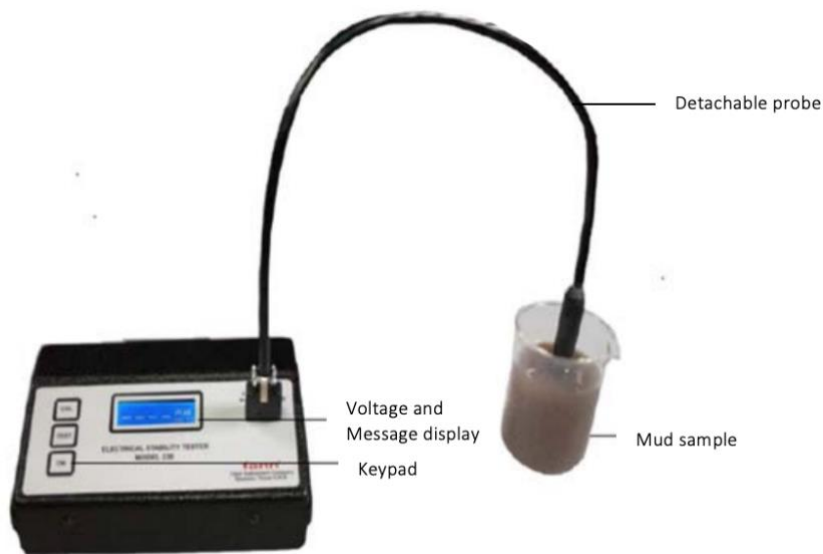


**Figure 3.18:** Electrical stability test set-up [52]

When performing an electrical stability test, it is important that the container does not conduct electricity, as this could affect the electrical stability measurement. The voltage at which the conductive passageway is formed,  $E_0$ , is the parameter of interest.

### 3.7 Tribology and Friction

Tribology is defined as the study of interacting surfaces in relative motion. The French military engineer Amontons published two classical laws of friction in the 17<sup>th</sup> century. Additionally, a third law was introduced in the 18<sup>th</sup> century, by the French physicist and military engineer Coulumb who had been studying static and kinetic friction. These laws stated that [53]:

- Shear resistance between two bodies is independent of the apparent area of contact.
- The shear resistance is proportional to the normal load.
- Dynamic friction is independent of sliding velocity.

Antoine Parent defined the following relation, in order to introduce Amontons work to mechanics [54]:

$$\tan\theta = \frac{F_f}{N} \quad (3.45)$$

Where  $\theta$  is defined as the inclination of the plane,  $F$  the tangential force and  $N$  is the normal force. Euler later showed that the coefficient of friction,  $\mu_f$ , could be determined by the following relationship [54]:

$$\mu_f = \tan\theta \quad (3.46)$$

As of today, the coefficient of friction is determined by the relation between the frictional force and the normal force applied to the objects in contact, and given by [54]:

$$\mu_i = \frac{F_{f,i}}{N} \quad (3.47)$$

Where  $i$  states whether the friction is static or kinetic,  $F_f$  is the frictional force,  $N$  is the normal force and  $\mu$  the friction coefficient.

The coefficient of friction is affected by many factors, such as applied load, surface roughness, humidity, viscosity, temperature and speed [54].



As mentioned, frictional forces can be characterized as either static or kinetic. Static friction is determined as the force counteracting the force applied if the objects are not moving relative to one another. Kinetic friction is described as the force counteracting pushing or pulling force when two objects in contact are moving relative to one another. A typical illustration of the kinetic and static frictional behaviour is given in **figure 3.19** [54]. The coefficient of friction is determined by the use of a CSM tribometer, described further in **Chapter 4.3.4**.

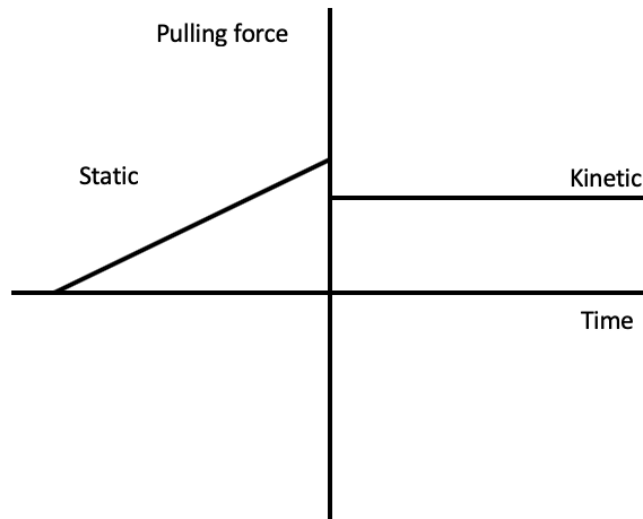


**Figure 3.19:** Typical static and kinetic frictional behaviour as a function of time [54]

### 3.8 Torque and Drag

In this section, some general theory about torque and drag will be presented. Additionally, the tensile and torsional limits will be reviewed.

The figure below, **figure 3.20**, illustrates a drill-string for any curved well which is divided into segments. The segments are loaded with either tensile (+) or compressive (-) loads at the top and at the bottom. These loads are generated by hydrostatic, thermal and fluid flow shear forces causing length changes in the drill-pipe along the wellbore.

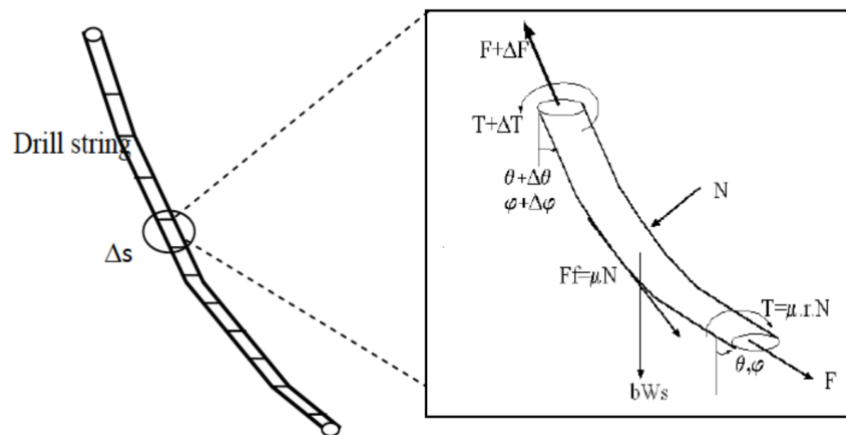


**Figure 3.20:** Segmented drill-string and distribution of loads at each segment [55]

From a drilling perspective, a smooth wellbore is desired, but is seldom the reality as the direction of the wellbore, the azimuth ( $\varphi$ ) and the inclination ( $\theta$ ), is constantly changing. A differential force equation, balancing the vector sum of the axial weight ( $w$ ), the net force and the frictional force ( $\mu_i$ ), were presented and given as following:

$$\frac{dF}{ds} = \pm \mu_a \left[ \sqrt{\left[ \beta w_s \sin(\theta) + F \frac{d\theta}{ds} \right]^2 + \left[ F \sin(\theta) \frac{d\varphi}{ds} \right]^2} \right] + \beta w_s \cos(\theta) \quad (3.48)$$

Where  $\beta$  is the Buoyancy factor,  $w_s$  is the weight of the string and  $\varphi$  and  $\theta$  are the azimuth and the inclination, respectively.  $\mu_a$  is the axial coefficient of friction. The “+”-sign indicates a tension force from pulling the string out of the hole, while the “-”-sign indicates compression from lowering the string into the well. The square-root term from **equation 3.48** represents the normal force per unit length for any inclined wellbore geometry. Further, the normal force for a single drill-string segment can be calculated from the following equation [55]:

$$N_i = \sqrt{\left[ \beta w_i \sin\left(\frac{\theta_{i+1} + \theta_i}{2}\right) + F_i \left(\frac{\theta_{i+1} + \theta_i}{S_{i+1} - S_i}\right) \right]^2 + \left[ F_i \sin\left(\frac{\theta_{i+1} + \theta_i}{2}\right) \left(\frac{\varphi_{i+1} - \varphi_i}{S_{i+1} - S_i}\right) \right]^2} \quad (3.49)$$

Where  $N$  is the normal force and  $S$  represents the drill-string segments.

### 3.8.1 Torque

Torque is the rotational equivalent to a linear force, the result of a force multiplied by an arm. Torque, with regards to drilling operations, is generally characterized as the moment required to rotate the drill-pipe. The required moment, which is applied at the top of the drill-string, needs to overcome the rotational friction resistance in the wellbore and the friction between the drill-bit and the formation. Generally, less rotational force is available at the drill-bit due to the frictional loss along the wellbore [55].

For vertical wellbores, the torque loss is ideally set to zero, apart from small losses due to the viscous forces of the drilling fluid. For deviated and horizontal wellbores, the torque loss may be more significant as the drill-string is more prone to contact with the wellbore walls, causing an increased frictional resistance in the system. In extended-reach drilling, the increasing frictional forces between the drill-string and the borehole wall is a limiting factor, as increasing torque loss may prevent further drilling [56].

The torsional force is dependent on several factors, including; the rotation radius, the coefficient of friction and the normal force above the pipe. The incremental torque is given by [55]:

$$\Delta T = \mu_t N_i r \Delta S \quad (3.50)$$

Where  $\Delta T$  is the added torque,  $\mu_t$  tangential coefficient of friction,  $N$  the normal force,  $r$  the radius of rotation and  $\Delta S$  the change of length. Further, it is possible to calculate the torque loss per unit length for both a non-buckled and a buckled drill-string. This torque loss is expressed as [55]:

$$T_{i+1} = T_i + \sum_{i=1}^n \mu_t r_i N_i (S_{i+1} - S_i) \quad (3.51)$$

Where  $N_i$  is calculated from equation 3.49.

### 3.8.2 Drag

Drag force is defined as the additional load when compared to the free rotating drill-string, the additional load required to move the drill-string. These movements are restricted to either; pull out of hole (POOH) or run into hole (RIH). The drag force is usually defined positive when POOH, because of tension in the drill-string, and is generally defined negative when RIH, because of compression of the drill-string. From a drill-string perspective, great torque and drag forces are generally experienced at the same time.

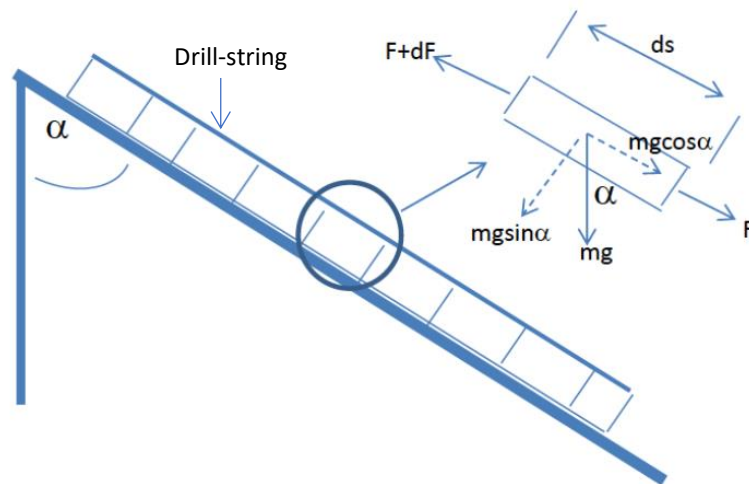


Figure 3.21: Drill-string in an inclined well [55]

The drag force is usually a result of the frictional resistance generated by the drill-string contact with the wellbore wall. By studying the drill-string in figure 3.21 and applying a force balance with the condition of equilibrium along the axial direction, the effective force along the axial direction can be calculated. The additional force,  $dF$ , the drag force, is calculated as:

$$dF = w\Delta S [\cos(\alpha) \pm \mu_a \sin(\alpha)] \quad (3.52)$$

Where the positive sign is used when pulling out of hole and the negative sign is used when running into hole, and where  $w$  is defined as the buoyed weight of the drill-string. The buoyed weight is calculated as following:

$$w = \left(1 - \frac{\rho_{mud}}{\rho_{pipe}}\right) \cdot w_s = \beta w_s \quad (3.53)$$

By integrating the above equation, **equation 3.52**, the contact drag force can be described by the following equation [55]:

$$F_2 = F_1 + w\Delta S [\cos(\alpha) \pm \mu_a \sin(\alpha)] \quad (3.54)$$

Where  $F_2$  is the force at the top of the drill-string and  $F_1$  the force at the bottom. The first term inside the bracket accounts for the weight of the drill-pipe and the second term accounts for the additional friction force required to move the drill-pipe [55].

### 3.8.3 Tensile and Torsional Limit

To ensure a safe drilling operation, it is critical that the drill-string is able to withstand both torsional and axial loads. This means that the drill-string's lower yield strength cannot be exceeded, as this can cause a plastic deformation of the material or impact the material's stability. To prevent problems occurring due to a permanent deformation of the drill-string, the loads experienced during the drilling operation must be within the safe operational window.

The safe operational window, in this context, is limited by the tensile and the torsional limits. The torsional limit is defined by the strength of the material that is subjected to a torsional load, and is the maximum torsional stress that the material withstands before rupture [57]. If the torsional limit is exceeded, the material will fail and could potentially lead to a twist-off of the drill-string. **Figure 3.22** provides an example of a safe operation, where the torque-curves for tripping in and tripping out are both below the torsional limit.

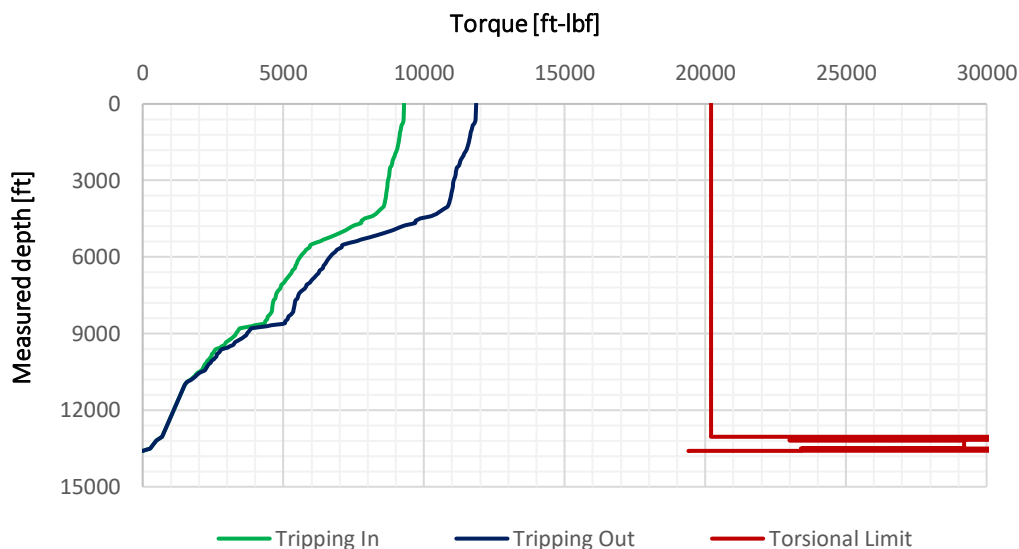


**Figure 3.22:** Example of a torque plot where the loads does not exceed the torsional limit

The tensile limit is defined by the pipe body strength that reaches the maximum yield point [55]. The tensile limit needs to be less than the yield point of the material, meaning it must be inside the material's elastic deformation area, as a plastic deformation of the pipe is undesirable. If the tensile limit is exceeded, the material will fail and could potentially cause a rupture of the drill-string. An example of an operation where all loads are within the safe operational window of the tensile limit is given in figure 3.23.

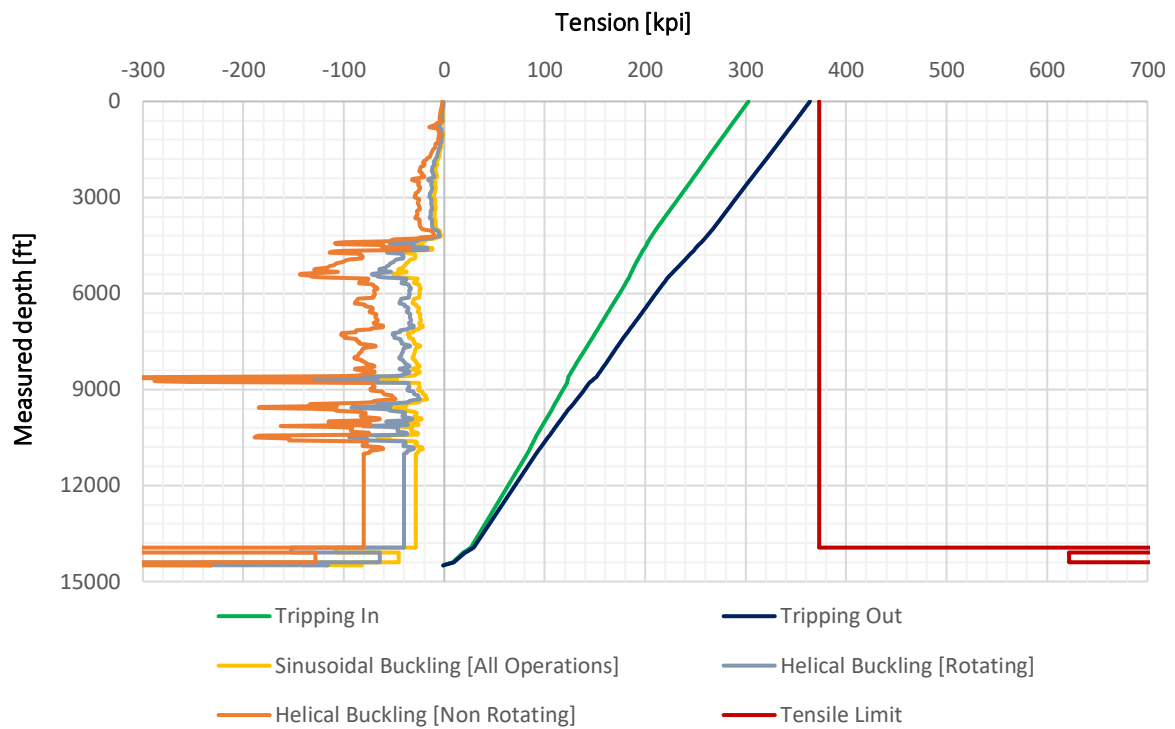


**Figure 3.23:** Example of a tension plot where the loads does not exceed the tensile limit

## 4 EXPERIMENTAL WORK STUDIES

Chapter 4 presents the various experimental work studies that have been performed during the work of this thesis. That includes drilling fluid formulation, description of drilling fluid additives and experimental equipment and methodology for rheology measurements, viscoelastic, barite sag and friction testing.

### 4.1 Drilling Fluid Formulation

#### 4.1.1 Water-Based Drilling Fluid Formulation

All the water-based drilling fluids measured and tested in this these were formulated and mixed at the laboratory at the University of Stavanger (UiS). These fluids were all formulated with a base of water, bentonite, duo-vis, soda ash and barite, while the amount of lignosulfonates was varied. The fluid systems were mixed in the following order:

1. Water, soda ash and lignosulfonates
2. Duo-Vis
3. Bentonite
4. Barite

All additives were accurately measured by using a Mettler Toledo precision weight in order to achieve the desirable concentration. Firstly, water, soda ash and lignosulfonates were mixed together using a spoon, as it is important that polymers are added very carefully, in order to prevent flocculation. Further, the rest of the additives where added and mixed together using a Hamilton beach mixer at various speeds to produce a well-blended fluid mixture. After completed mixing, the various fluids were placed in glass containers to age for 48 hours, to ensure adequate bentonite swelling before performing any testing.

The base fluid, without any lignosulfonates, is referred to as “Ref” and is used as a reference fluid to identify how the fluid system changes and behaves as a function of added lignosulfonates. The amount of lignosulfonates was tested with 0.2, 0.3, 0.4, 0.5 and 2.0 grams, while the amount of the other additives were held constant. Recipes of these various fluid systems are listed in **table 4.1** below.

Further, another five fluids were formulated based on the results obtained from the initial testing. The recipes of these fluids are given in **table 4.2**.

**Table 4.1:** Recipe for WBM systems containing various amount of lignosulfonates

Chemical	Ref	Ref + 0.2 g LS	Ref + 0.3 g LS	Ref + 0.4 g LS	Ref + 0.5 g LS	Ref + 2.0 g LS
Water [mL]	350	350	350	350	350	350
Bentonite [g]	10	10	10	10	10	10
DUO-VIS [g]	0.6	0.6	0.6	0.6	0.6	0.6
Soda Ash [g]	4.0	4.0	4.0	4.0	4.0	4.0
Barite [g]	150	150	150	150	150	150
Lignosulfonates [g]	<b>0</b>	<b>0.2</b>	<b>0.3</b>	<b>0.4</b>	<b>0.5</b>	<b>2.0</b>
wt% lignosulfonates	0.00%	0.04%	0.06%	0.08%	0.10%	0.39%

**Table 4.2:** Recipe for WBM systems containing 0.6 – 1.0 g of lignosulfonates

Chemical	Ref + 0.6 g LS	Ref + 0.7 g LS	Ref + 0.8 g LS	Ref + 0.9 g LS	Ref + 1.0 g LS
Water [mL]	350	350	350	350	350
Bentonite [g]	10	10	10	10	10
DUO-VIS [g]	0.6	0.6	0.6	0.6	0.6
Soda Ash [g]	4.0	4.0	4.0	4.0	4.0
Barite [g]	150	150	150	150	150
Lignosulfonates [g]	<b>0.6</b>	<b>0.7</b>	<b>0.8</b>	<b>0.9</b>	<b>1.0</b>
wt% lignosulfonates	0.12%	0.14%	0.16%	0.18%	0.19%

At a later stage in the process, it was decided to try to enhance the frictional performance of the best performing water-based fluid system by adding nanoparticles. The recipes of these fluids are given in table 4.3, where the Ref + 0.9 g LS fluid is the reference fluid, which is further modified with various amounts of molybdenum disulphide. In the recipe, the molybdenum sulphide is shortened as moly and the reference fluid, Ref + 0.9 g LS, is named REF.

**Table 4.3:** Recipe for the 0.9-gram lignosulfonates system modified with molybdenum disulphide (Moly)

Chemical	REF	REF + 0.5 g MoS <sub>2</sub>	REF + 1.0 g MoS <sub>2</sub>	REF + 1.5 g MoS <sub>2</sub>
Water [mL]	350	349.5	349	348.5
Bentonite [g]	10	10	10	10
DUO-VIS [g]	0.6	0.6	0.6	0.6
Soda Ash [g]	4.0	4.0	4.0	4.0
Barite [g]	150	150	150	150
Lignosulfonates [g]	<b>0.9</b>	<b>0.9</b>	<b>0.9</b>	<b>0.9</b>
Moly [g]	<b>0.0</b>	<b>0.5</b>	<b>1.0</b>	<b>1.5</b>
wt% moly	0.00%	0.10%	0.19%	0.29%

Molybdenum disulphide was added both in-situ and ex-situ, in order to investigate the effect of the method of application. For the in-situ, the nanoparticles were mixed in together with the water, before adding the soda ash and the lignosulfonates. For the ex-situ process, the molybdenum disulphide was added one day after the reference fluid had been made.



### 4.1.2 Oil-Based Drilling Fluid Formulation

For the oil-based drilling fluids, most of them were prepared and provided by M-I Swaco, while some were formulated at the laboratory at the University of Stavanger. The oil-based drilling fluid that was formulated at the UiS laboratory had an OWR of 90/10 and its recipe is given in **table 4.4** below. This recipe is based on a recipe previously given by M-I Swaco, but with the use of a different base oil. M-I Swaco's fluids are formulated by using Escaid 120 ULA as base oil, while the one formulated at UiS used EDC 95/11 as base oil. The main differences of these two base oils will be further described in **Chapter 4.2**. The oil-based fluid system was mixed in the following order:

1. Water and salt
2. EDC 95/11 and One-Mul
3. Lime
4. Versatrol
5. Bentone
6. Barite

All additives were accurately measured in the same way as for the water-based drilling fluids, by the use of a Mettler Toledo precision weight. Firstly, the water and salt were mixed with the Hamilton beach mixer for 10 minutes in order to make the brine. The rest of the additives were then added one by one and mixed for 5 minutes. Finally, the whole mixture was blended for 25 minutes. The fluid was then placed in a glass container for 48 hours in order to ensure proper clay swelling before testing.

**Table 4.4:** Recipe for oil-based drilling fluid with an OWR of 90/10 and EDC 95/11 as base fluid

Chemical	EDC 95/11 [g]	One-Mul [g]	Bentone [g]	Lime [g]	Versatrol [g]	Water [mL]	Salt [g]	Barite [g]
EDC 90/10	498.4	25	7	25	10	67.9	20.9	1095.9

Further, this fluid, hereby referred to as EDC 90/10, was modified by adding various amounts of acrylamide-co-acrylic polymer, shortened as poly acrylic, in order to cope with barite sag issues. Each separate fluid, with its amount and weight-percent of additive, is listed in **table 4.5** below. Additionally, **table 4.6** is provided to present the recipe for the four oil-based drilling fluids that were provided by M-I Swaco.

**Table 4.5:** Modified samples of EDC 90/10 reference fluid

Additive	EDC 90/10	EDC 90/10 + 0.5 g poly acrylic	EDC 90/10 + 1.0 g poly acrylic	EDC 90/10 + 1.5 g poly acrylic
EDC 90/10 [g]	300	300	300	300
Poly acrylic [g]	0.0	0.5	1.0	1.5
wt% poly acrylic	0%	0.17%	0.33%	0.50%

**Table 4.6:** Recipe for all oil-based drilling fluids provided by M-I Swaco

Chemical	60/40	70/30	80/20	90/10
Escaid 120 ULA [g]	373	436	497	559
One-Mul [g]	20	20	20	20
Lime [g]	20	20	20	20
Bentone [g]	12	12	12	12
Versatrol M [g]	10	10	10	10
Water [mL]	305	228	151	71
CaCl <sub>2</sub> [g]	88	66	44	22
Barite [g]	677	709	746	783

Furthermore, the OWR 90/10 M-I Swaco fluid, hereby referred to as 90/10, was also modified by adding various amounts of poly acrylic in order to cope with barite sag issues. These fluid systems are listed in **table 4.7**, presenting the amount and weight percent of poly acrylic added to the reference fluid system.

**Table 4.7:** Poly acrylic modified samples of M-I Swaco's 90/10 OWR fluid

Additive	90/10	90/10 + 0.5 g poly acrylic	90/10 + 1.0 g poly acrylic	90/10 + 1.5 g poly acrylic
90/10 [g]	300	300	300	300
Poly acrylic [g]	0.0	0.5	1.0	1.5
wt% poly acrylic	0%	0.17%	0.33%	0.50%

## 4.2 Description of Drilling Fluid Additives

As presented in the previous subsection, the water-based and oil-based drilling fluids contained various additives and chemicals. This subsection will present these additives and chemicals and describe their most important functions with regards to drilling fluid properties.

### 4.2.1 Additives

#### 4.2.1.1 Bentonite

Bentonite is a clay rock that forms through alteration of volcanic ash and tuff, weathered volcanic rock. Its main component is the clay mineral montmorillonite, but it could also contain some kaolinite or illite as well. When in contact with water, bentonite swells and increases in volume. As the bentonite particles swells, it tends to form a thixotropic, gel like structure [58]. For drilling fluid purposes, bentonite is added to water-based fluid mixtures to create a viscous, shear-thinning fluid and improve its rheological parameters. Addition of bentonite also helps to lubricate downhole equipment, suspend and remove borehole cuttings and to prevent potential blow-outs [59].

#### 4.2.1.2 Bentone

Bentone is a chemically fabricated modification of the bentonite clay. The bentonite clay is chemically changed from being hydrophilic, water soluble, to be organophilic, dispersible in oil-based fluids. Bentone is the oil-based equivalent of bentonite and is used in drilling fluids to improve viscosity, suspend rock cuttings and weight agents and improve the cuttings transport and hole cleaning capabilities [60].

#### 4.2.1.3 Barite

Chemical formula:  $\text{BaSO}_4$

Barite is a soft, non-magnetic sulphate mineral that consists mainly of barium sulphate. It has a specific gravity of 4.3-4.5 and is commonly found as void-filling crystals and concretions in sedimentary rocks and sandstones. As a drilling fluid additive, barite serves the purpose as a weighting agent. By adding barite, the drilling fluid density will increase. The barite particles are small, most of them less than 75  $\mu\text{m}$ , and the weight-percent of barite added increases as a function of the wellbore depth [61].

#### 4.2.1.4 Soda Ash

Chemical formula:  $\text{Na}_2\text{CO}_3$

Soda ash, sodium carbonate, is a water-free, inorganic compound. Soda ash is used as an additive in water-based drilling fluids to treat calcium-ion contamination from drilling anhydrite or gypsum and to control the fluid's pH. Anhydrite and gypsum formations can cause polymer precipitation, clay flocculation and lower pH, which is adjusted and treated by the use of sodium carbonate [62].

#### 4.2.1.5 EDC 95/11

EDC, environmental drilling compound, 95/11 is a type of base oil used in synthetic oil-based drilling fluids. Its chemical composition is made up of a complex solution of various paraffinic and cyclic hydrocarbons with carbon numbers ranging from, generally, C15 to C20. EDC contains n-alkanes, isoalkanes, cyclics and less than 0.03% aromatics. EDC have a boiling point in the range of 240°C to 335°C, is a transparent liquid and is used as the continuous phase in oil-based drilling fluids [63].

#### 4.2.1.6 Escaid 120 ULA

Escaid 120 ULA is a base oil that is developed by ExxonMobil particularly for use in drilling fluids. Its chemical composition is comprised of hydrocarbons ranging from C12 to C16, n-alkanes, isoalkanes, cyclics and less than 0.01 wt% of aromatics. Some of the benefits of the Escaid fluids are that it has low environmental toxicity, improves bit hydraulics by the means of lesser pressure drop, is compatible with elastomers and have minimal effect on drilling fluid rheology at low operating temperatures [64].

#### 4.2.1.7 One-Mul

One-Mul is a very viscous liquid that works as a primary and secondary emulsifier for oil-based drilling fluids. One-Mul, which is a M-I Swaco product, improves the filtration control and is temperature-stable up to 175°C. Some of the greatest benefits of using One-Mul is that it improves the emulsion stability and minimize the dispersion of reactive clays [65].

#### 4.2.1.8 Lime

Chemical formula:  $\text{Ca(OH)}_2$

Calcium hydroxide, lime, is a white powder that is used to increase the pH of drilling fluids. Additionally, it can be used to remove soluble carbonate ions, for corrosion control and flocculation of bentonite muds. Lime is used for alkalinity control in both water- and oil-based drilling fluids [66].

#### 4.2.1.9 Salt

Chemical formula:  $\text{CaCl}_2$

Calcium chloride, salt, is an inorganic compound that is very soluble in water. Salt is used to produce brine that is used as the water phase in the oil-based drilling fluid. Additionally, salt is used as a bridging agent for permeable formations and for control and minimization of formation damage [67].

#### 4.2.1.10 Versatrol

Versatrol, another M-I Swaco product, is a black powder with a specific gravity of 1.04-1.06. Versatrol is used for filtration control in high-pressure, high-temperature oil-based drilling fluid systems. When used in drilling fluids, it exhibits stable properties up to 200°C and enhances the fluid emulsion stability [68].

## 4.2.2 Polymer Additives

Polymers are chemical molecule chains that can be man-made in the laboratory or appear naturally, where the latter is referred to as biopolymers. All polymers consist of repetitious structural units composed by smaller molecules named monomers. Polymers are chained together by covalent bonding's that are repeated throughout the whole structure [69]. The polymer chemistry has made great progress the last two decades, resulting in more common and broadened application of polymers in drilling fluids. For drilling fluid purposes, polymers can be used for filtration loss control, as viscosifiers, enhanced fluid rheology when subject to high temperatures, improve yielding of clay or for flocculation or deflocculation of solid particles [70].

### 4.2.2.1 Duo-Vis

Duo-Vis is a dispersible, high-molecular-weight biopolymer. It has a specific gravity of 1.5, a bulk density of 800 kg/m<sup>3</sup> and appear in powder form. For the use in water-based drilling fluids, Duo-Vis is added in order to provide weight material suspension and increased viscosity. Only small quantities are required in order to successfully achieve a fluid with thixotropic and shear-thinning characteristics. As a result of enhanced rheological parameters, addition of Duo-Vis may increase ROP and optimize hydraulics in terms of lesser pressure drop [71].

### 4.2.2.2 Lignosulfonates

Lignosulfonates, often shortened as LS, are water-soluble polyelectrolyte polymers, illustrated with its main building blocks in **figure 4.1**. Lignosulfonates are formed as a by-product from the manufacturing of wood pulp, paper, by the use of a sulphite process. Lignosulfonates appears as a brown powder with a molecular weight varying from 10<sup>3</sup>-10<sup>6</sup> g/mol. For drilling fluid purposes, lignosulfonates are commonly used as dispersants to prevent flocculation of clay particles [72].

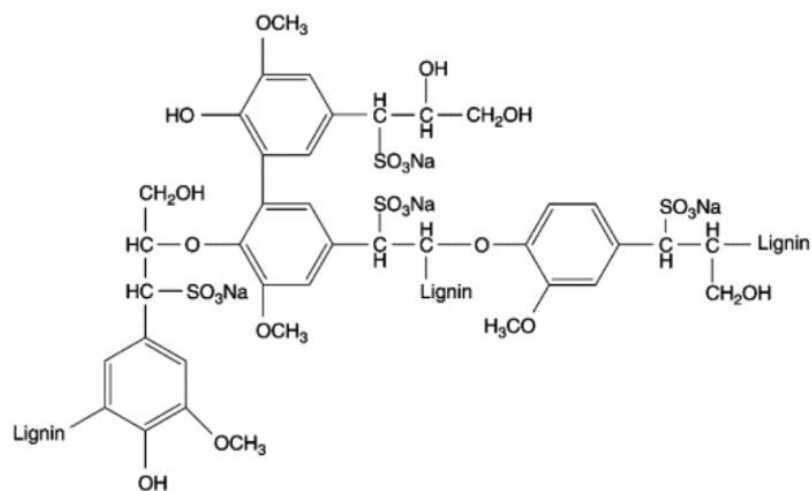


**Figure 4.1:** Molecular structure of the main components of lignosulfonates [72]

#### 4.2.2.3 Poly (acrylamide-co-acrylic) Partial Sodium Salt

Poly partial sodium salt, hereby shortened as poly acrylic, is a polymer that appears in white powder form. Poly acrylic consists of approximately 80 wt% acrylamide and its chemical structure is illustrated in **figure 4.2**. For drilling fluid purposes, poly acrylic used as a thickening agent, or flocculant, used to increase both viscosity and gel structure in order to better suspend solid particles [73].

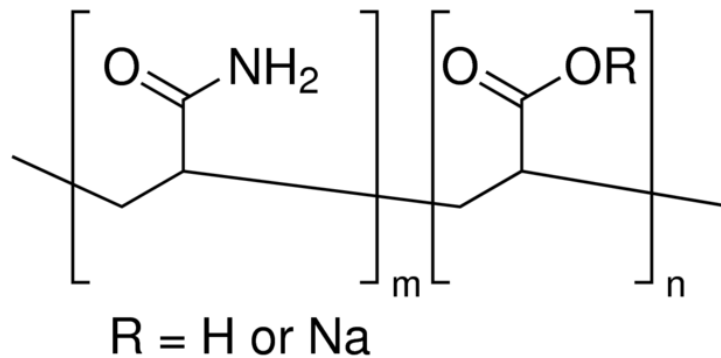


**Figure 4.2:** Chemical structure of poly (acrylamide-co-acrylic) partial sodium salt [73]

#### 4.2.3 Nanoparticle Additives

As described in **Chapter 2.5**, nanotechnology is widely used in lots of industries, including the oil and gas industry. For drilling fluid purposes, nanoparticles are applied in order to solve various drilling fluid issues, such as temperature and shale instability. Nanoparticles have the ability to suspend in solvents because of the interaction between the particle surface and the solvent is able to withstand the difference in densities. This causes either material sinking or suspension, forming a nanofluid. In the oil and gas industry, nanofluids are defined as fluids used for petroleum recovery purposes that contains at least one nano-sized additive [74].

##### 4.2.3.1 Molybdenum Disulphide

Chemical formula:  $MoS_2$

Molybdenum disulphide, often shortened as moly, is an inorganic compound composed of the two elements molybdenum and sulphur and it is naturally occurring in considerable volumes as the mineral molybdenite. Moly has a specific gravity of 4.6-4.75 and has a melting point at 2375°C [75]. Because of its low frictional properties, molybdenum disulphide has been used as lubricant in several fields of science and industries, with automotive fields as the most important one [76]. The molybdenum disulphide used in this thesis was provided in a 30 wt% water solution. **Figure 4.3** shows a SEM picture of the  $MoS_2$  solution after being dried. **Figure 4.4** shows a SEM picture of a mud-cake from  $MoS_2$  based drilling fluid formulated in section and analyzed in section 5.2. As shown in **figure 4.5**, the element

analysis indicated that the MoS<sub>2</sub> contains oxygen, aluminium, silicon, molybdenum and sulphide. Table 4.8 presents the weight percent distribution of these elements along with the percentage error.

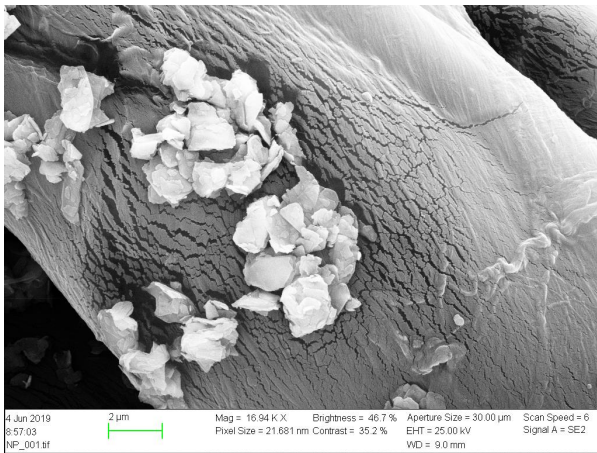


Figure 4.3: SEM picture of the MoS<sub>2</sub> nanoparticle (white) on a piece of paper

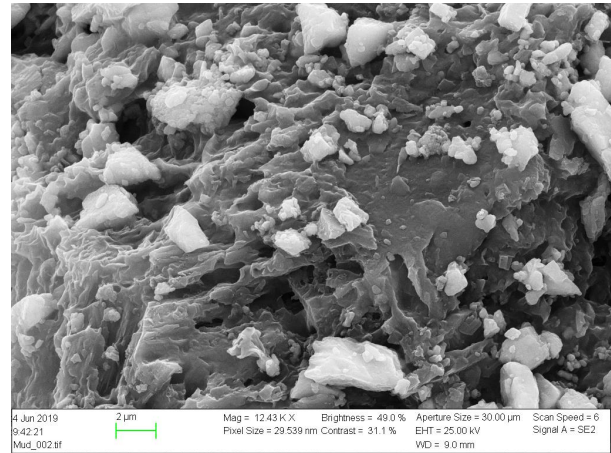


Figure 4.4: SEM picture of mud-cake from MoS<sub>2</sub>-solution based drilling fluid

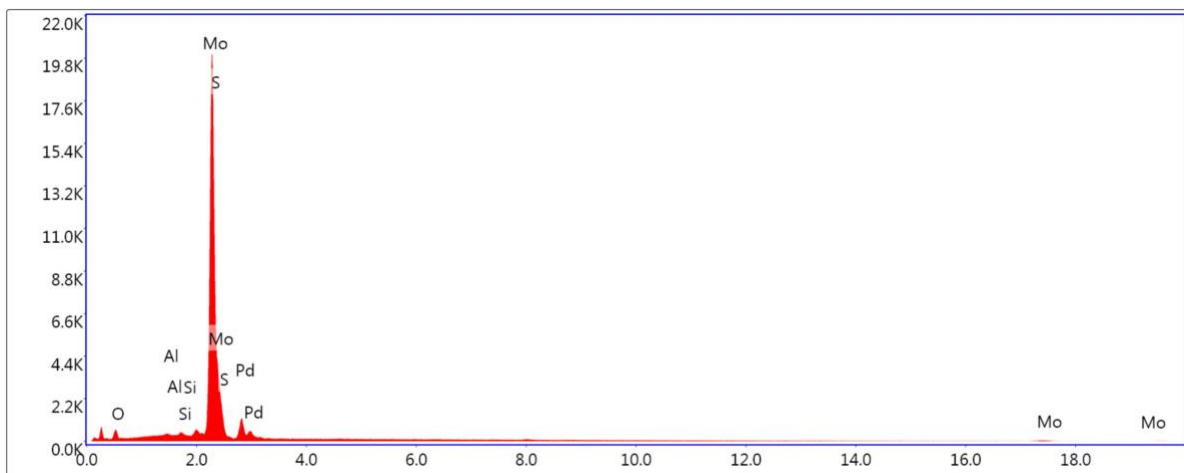


Figure 4.5: Element distribution in the MoS<sub>2</sub> nano-solution

Table 4.8: Quantity of the different elements in the MoS<sub>2</sub> nano-solution

Element	Weight %	Error %
Oxygen (O)	5.46	18.26
Aluminium (Al)	0.47	19.38
Silicon (Si)	0.83	13.55
Molybdenum	25.75	2.18
Sulphide (S)	56.96	2.59

## 4.3 Experimental Equipment and Methodology

### 4.3.1 Ofite Viscometer and Rheology Measurement Procedure

All rheological measurements were performed by the use of a standard Ofite model 800, 8-speed viscometer, depicted in **figure 4.6**. The viscometer has a rotational cylinder that is capable of producing shear rates of 600, 300, 200, 100, 60, 30, 6 and 3 RPM. Prior to the rheological measurements, the drilling fluids were all mixed for 2 minutes in order to ensure proper particle dispersion.

The different fluid systems and their variations were all measured at three different fluid temperatures, 22°C, 50°C and 80°C and at all eight shear rates. The oil-based drilling fluids were also measured at 100°C, as OBMs usually are the ones used in the reservoir section, where this kind of temperatures are common. The temperature was varied in order to analyze the various fluids' dependency of temperature. In order to increase and maintain the temperature of the drilling fluid during the rheological measurement, a heating apparatus was used. The fluid was placed in a cup, which again was placed in to the heating apparatus, where the fluid temperature was increased and measured by the use of a digital thermometer. When the fluid reached each of the desired temperatures, it was held as constant as possible by having the cup inside the heating apparatus during the rheological measurements.

The results from the rheological measurements, for both water-based and oil-based drilling fluids, are presented in **Chapter 5**. Graphs, figures and tables are used to visualize and explain the results and how they are interpreted.

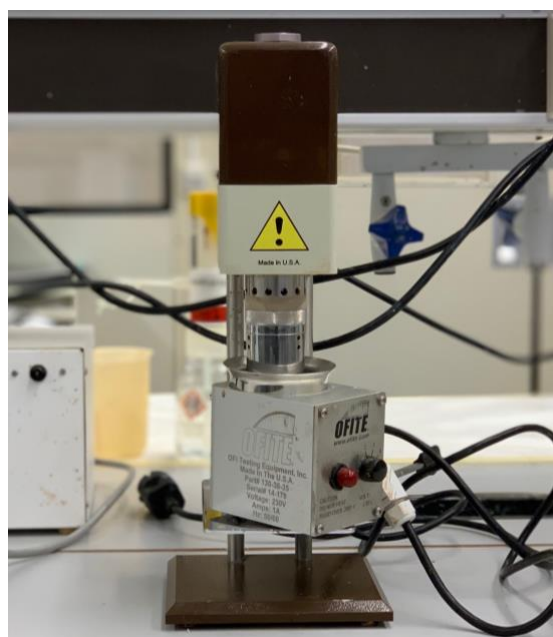


**Figure 4.6:** Ofite model 800 viscometer used for rheological measurements



### 4.3.2 Anton Paar Rheometer and Testing Procedure

All the oscillatory viscoelastic tests were performed by the use of an Anton Paar MCR 302 rheometer, illustrated in **figure 4.7**. The rheometer is highly technological, having several advanced functions and is capable of performing tests in a wide range of temperatures in both rotational and oscillatory mode. The temperature is accurately controlled by the use of a temperature element and a circulating fluid that runs through the system [77]. For this thesis' work, the Anton Paar rheometer was used to perform oscillatory amplitude sweep and temperature sweep tests.

These tests were performed by the use of two flat plates pressed against each other, similar to the Two-plates-model described in **Chapter 3.3.3**. The bottom plate was stationary, while the top plate was oscillating. All fluid samples were pre-sheared and then placed at the bottom plate by the use of a spoon. In order to get realistic and useful results, it was important that the fluid was properly mixed to ensure homogeneously distribution of solid particles within the fluid. Hence, pre-shearing of every sample was necessary. The temperature of the test specimen was held constant by the use of a thermo-cap, isolating the fluid sample and preserving the temperature.



**Figure 4.7:** Anton Paar MCR 302 rheometer [77]

The oscillatory amplitude sweep test was performed in order to identify the LVE range of each fluid. The test was carried out at a constant frequency,  $\omega$ , of 10 rad/s and with increasing oscillation amplitude from 0.001 to 100%. The temperature was held constant at 22°C. The oscillatory temperature sweep test was performed at a constant frequency of 10 rad/s and constant oscillation amplitude of 0.1%, with a temperature gradient of 0.05°C/sec, from a start temperature of 20°C to end temperature of 100°C.

### 4.3.3 Barite Sag Equipment and Methodology

#### 4.3.3.1 Static Sag Measurement

For the static sag measurements, the second method described in **Chapter 3.4.1** was used. The fluid samples were all aged at 50°C for 16 hours at a vertical position in a plastic container. After aging, two data points, one at the top and one at the bottom, were used in order to calculate the static sag factor. The top sample was extracted just below the free oil, as illustrated in **figure 4.8** below.

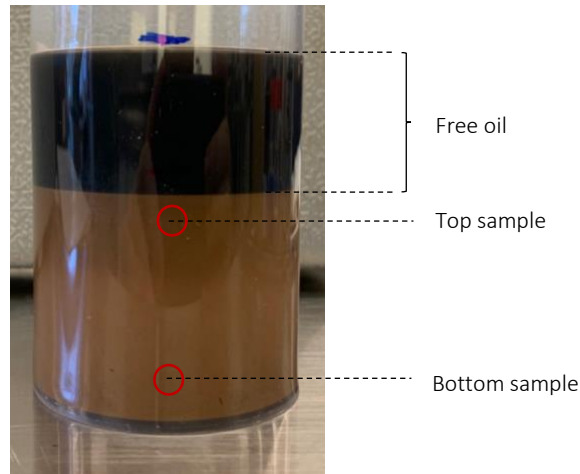


**Figure 4.8:** EDC 90/10 after aging for 16 hours at 50°C

The free oil at the top separates from the drilling fluid as a result of the density differences and the gravitational forces. For a fluid with barite sag issues, the top mud weight sample will be drilling fluid consisting of less solid particles and less base oil, as lots of the particles will have accumulated and settled at the bottom, while the base will be separated from the fluid and is placed on top of the drilling fluid itself. The bottom mud weight sample is assumed to contain larger quantities of solid particles and less base oil, for the same reasons as mentioned above.

For this test, 1 mL of fluid was extracted for both the top and the bottom mud weight sample. To quantify the degree of barite settlement, the static sag factor was calculated by the use of **equation 3.41**:

$$(\text{Sag factor})_{static} = \frac{MW_{bottom}}{MW_{top} + MW_{bottom}}$$

#### 4.3.3.2 Dynamic Sag Measurement

The dynamic sag measurement was performed in accordance with the Viscometric Sag Shoe Test. The sag shoe, borrowed from M-I Swaco, was placed in the bottom of a heating cup that is used for viscometer measurements. The heating cup and sag shoe were pre-heated to 50°C before 140 mL fluid, also pre-heated, were poured into the cup. The system was then placed on the viscometer plate and raised so that distance between the viscometer and the sag shoe was 7 mm. The test was then completed while the viscometer was running at 100 RPMs for 30 minutes.

To evaluate the amount of barite sag at dynamic conditions, one needed to know the initial and final mud weight. Further, the dynamic sag factor was determined by equation 3.42:

$$(\text{Sag factor})_{\text{dynamic}} = \frac{MW_{\text{final}}}{2 \cdot MW_{\text{initial}}}$$

The initial mud weight,  $MW_{\text{initial}}$ , was measured by extracting 20 mL of fluid and weighing it at a Mettler Toledo precision weight. Finally, as the viscometer had been running for 30 minutes, the weight of the fluid accumulated in the collection well of the sag shoe was determined by extracting another 20 mL of fluid. This weight,  $MW_{\text{final}}$ , was also measured, and the dynamic sag factor was calculated based on equation 3.42.

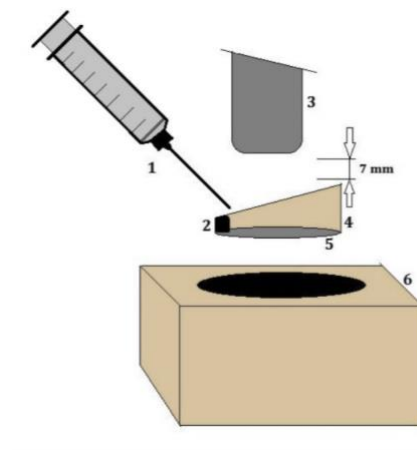


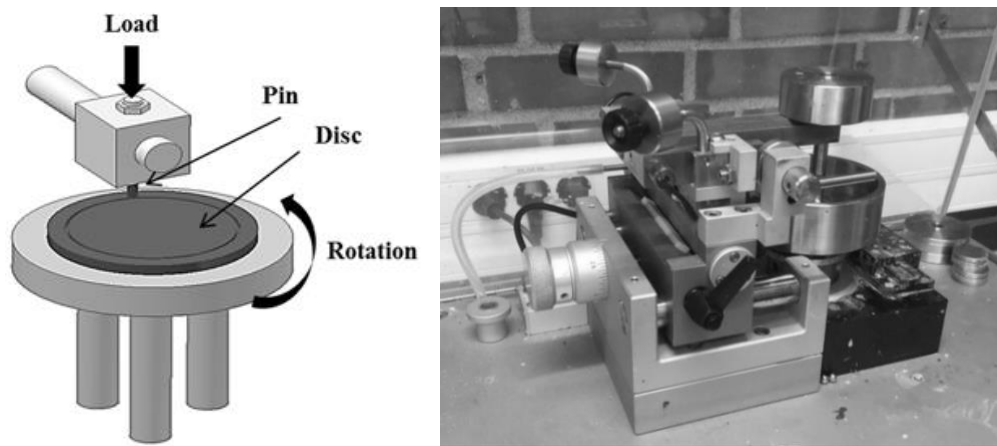
Figure 4.9: Dynamic sag test equipment [78]

Figure 4.9 illustrates the viscometric sag shoe test equipment. The number on the figure correspond to following equipment:

- |             |                                    |                            |
|-------------|------------------------------------|----------------------------|
| 1. Syringe  | 2. Collection well of the sag shoe | 3. Viscometer              |
| 4. Sag shoe | 5. Metal plat of the sag shoe      | 6. Heating cup/thermos-cup |

#### 4.3.4 Friction CSM Tribometer

As mentioned in **Chapter 3.7**, the coefficient of friction was quantified by the use of a CSM tribometer. The tribometer methodology is based on a pin-on-disc technology illustrated to the left in **figure 4.10**. The tribometer instrument is depicted to the right in **figure 4.10**. The metal-ball is made out of chromium-steel and has a diameter of 6 mm. The instrument is computer controlled and the frictional measurements were performed at a constant temperature of 22°C, with a 5 N normal force at 3 cm/s for 10 minutes. All the friction tests were repeated at least two times for each fluid system in order to ensure repeatability and produce numerical average values.



**Figure 4.10:** Illustration of the pin-on-disc technology and a picture of the CSM tribometer

## 5 RESULTS

This chapter presents the experimental results obtained from addressing the three issues presented in Chapter 1.2. These are; formulation of thermally stable water-based drilling fluid, and analyses of the performance of MoS<sub>2</sub> nanofluid on the best thermally stable fluid system, as well as solutions to the sagging issues associated with the EDC 90/10 OBM and the M-I Swaco 90/10 OBM fluid systems.

### 5.1 Flat Rheology Water-Based Drilling Fluid Formulation

This subsection presents the experimental results of the water-based drilling fluids that are described in Chapter 4.1, including viscometer readings, calculated yield stresses and viscoelastic properties. The drilling fluid formulations are provided in section 4.1.1 (Table 4.1 and Table 4.2).

#### 5.1.1 Effect of Lignosulfonates and Temperature on Rheological Parameters

Firstly, the effect of added lignosulfonates was investigated by analyzing how it influenced the viscometer response of the rheological data, as well as the calculated yield stress.

In figure 5.1 the viscometer response, shear stress, is plotted as a function of the RPM. From this figure one can identify a trend indicating that the viscometer response decreases as a function of added lignosulfonates. This result was expected, as the lignosulfonates works as a disperser for the clay particles and prevent them from flocculate, hence, resulting in a less viscous fluid.

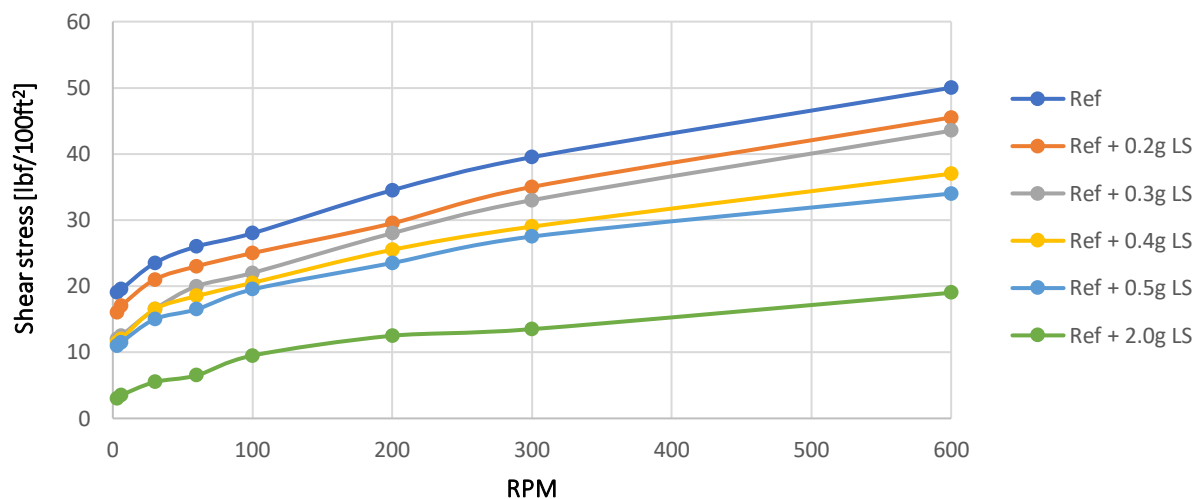


Figure 5.1: Viscometer data for lignosulfonates WBMs at fluid temperature of 50°C

Figure 5.2 illustrates the Robertson-Stiff yield stress for the same six fluids that are represented in figure 5.1. From this plot, one can see that the yield stress of the all fluids, except Ref + 2.0 g LS, is dependent

of the fluid temperature. For fluids Ref to Ref + 0.5 g LS, the yield stress increases as the temperature increases, which is not desirable. Commonly, the yield stress of a water-based drilling fluid should be in the interval between 11 and 20 lbf/100ft<sup>2</sup> and should be temperature stable in order to exhibit the desired functions at all depths of the well. Since Ref + 2.0 g lignosulfonates display stable yield stress values as a function of temperature, but not exhibiting a value inside the desired interval, it was suggested to investigate if a better solution could be found between 0.5 and 2 grams of added lignosulfonates. The desired result is to try to increase the yield stress value of the Ref + 2.0 g LS fluid, while keeping it temperature stable.

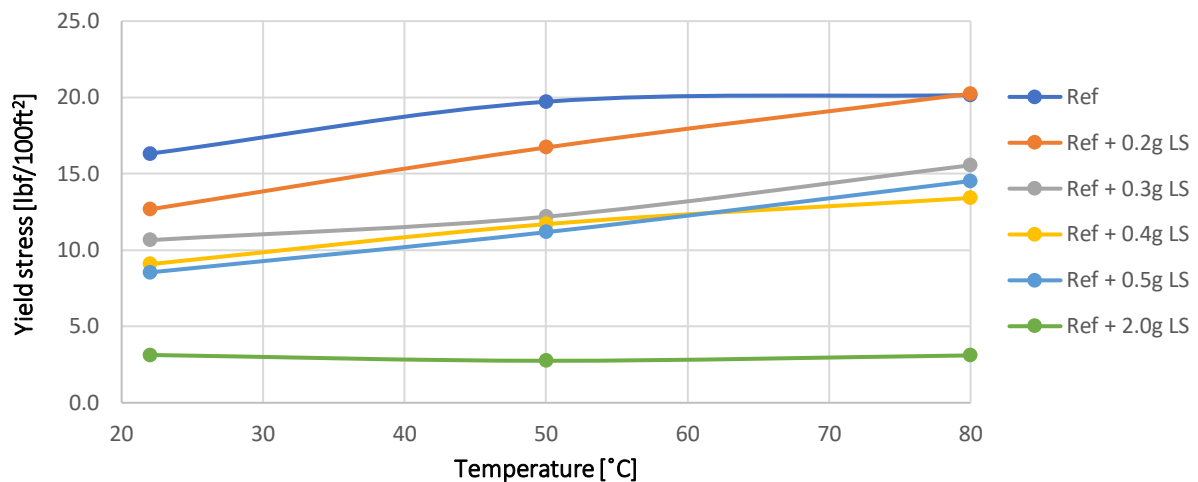


Figure 5.2: Yield stress for WBMs at different temperatures calculated based on the Robertson-Stiff model

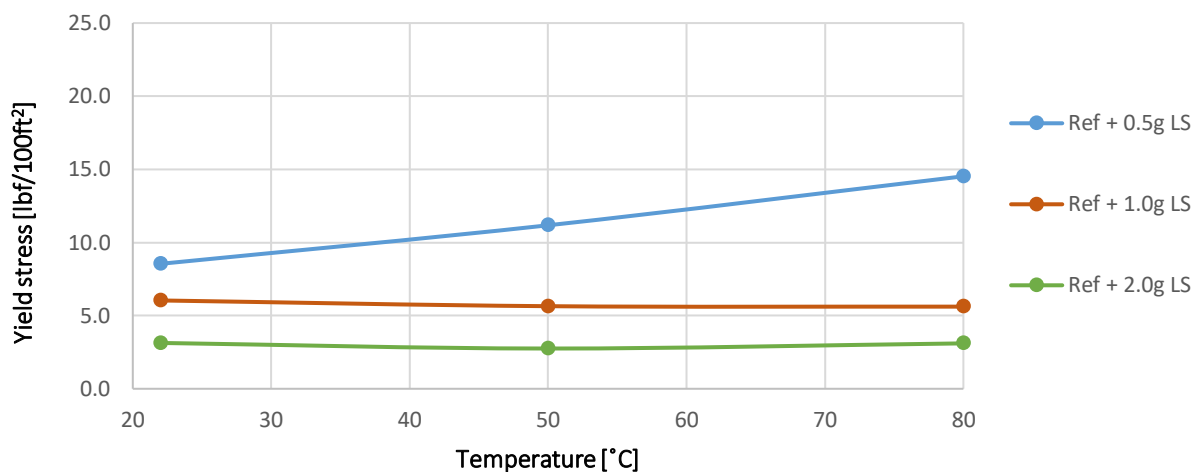


Figure 5.3: Calculated Robertson-Stiff yield stress for WBMs containing 0.5, 1.0 and 2.0 grams of lignosulfonates

Figure 5.3 shows how the yield stress of the reference fluid plus 1.0 gram of added lignosulfonates places in between Ref + 0.5 g LS and Ref + 2.0 g LS. This fluid does exhibit a stable yield stress as a function of increased temperature. However, the numerical value of the yield stress does not comply

within the recommended range of yield stress for water-based drilling fluids. Therefore, it was decided to further investigate with various quantities of lignosulfonates between 0.5 and 1 gram, in order to identify if the “perfect” amount could increase the yield stress even more and still be temperature stable.

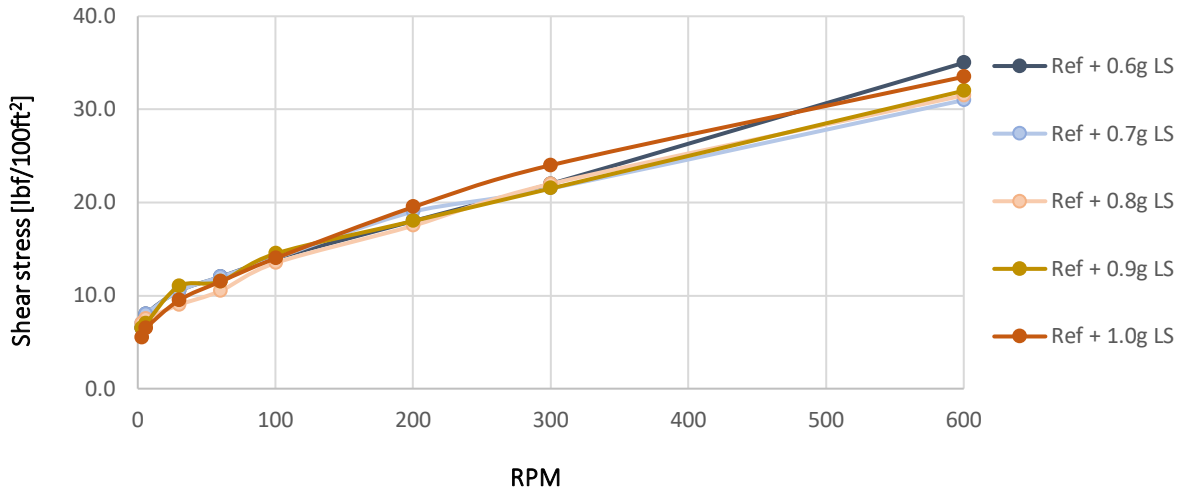


Figure 5.4: Viscometer data for WBMs with various amount of lignosulfonates at fluid temperature of 50°C

The interval was now restricted to 0.6-0.9 grams of added lignosulfonates. It was formulated four new fluids with 0.6, 0.7, 0.8 and 0.9 grams of added lignosulfonates. The viscometer response of these fluids, and the Ref + 1.0 g LS, are illustrated in figure 5.4. From this, it was found that the reference fluid plus 0.9 grams of added lignosulfonates exhibited the most temperature stable yield stress and further increased the yield stress value compared to Ref + 1.0 g LS, as seen in figure 5.5. From this point on, it was decided to proceed with Ref + 0.9 g LS as the best performing drilling fluid system and try to modify this fluid system with nanoparticle treatment. These results are presented in Chapter 5.2.

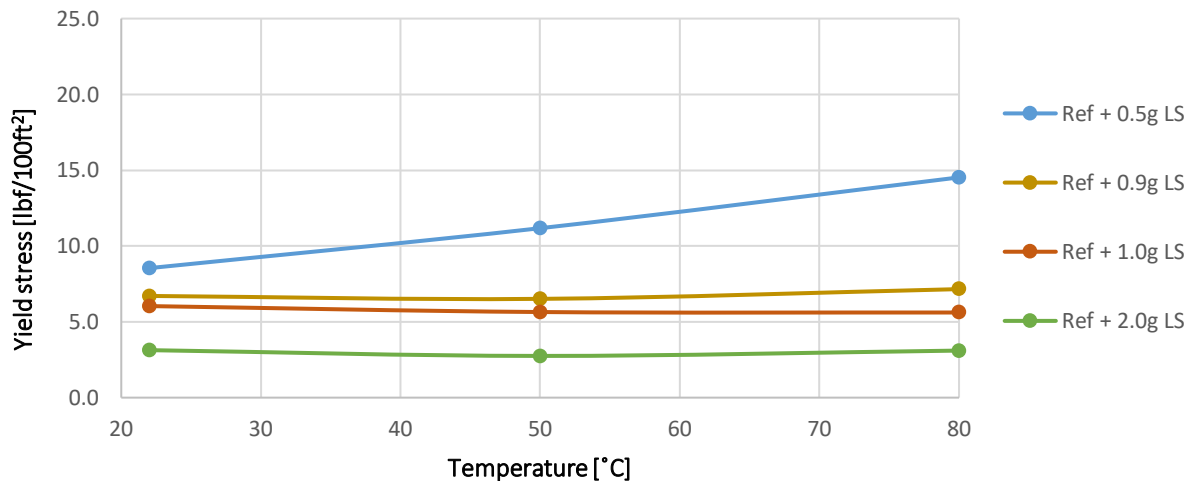


Figure 5.5: Robertson-Stiff calculated yield stress for modified WBMs

### 5.1.2 Effect of Lignosulfonates on Viscoelastic Properties

The results from the amplitude sweep tests of the water-based drilling fluids from Table 4.1 are illustrated in figure 5.7. Storage,  $G'$ , and loss modulus,  $G''$ , are plotted against strain. From the plot one can identify the LVE range, where storage and loss modulus are parallel, which is less than 2% for all the fluid samples. In the LVE range, the storage modulus is greater than loss modulus, which indicates that all the fluids behaves more like viscoelastic gels than like viscoelastic liquids.

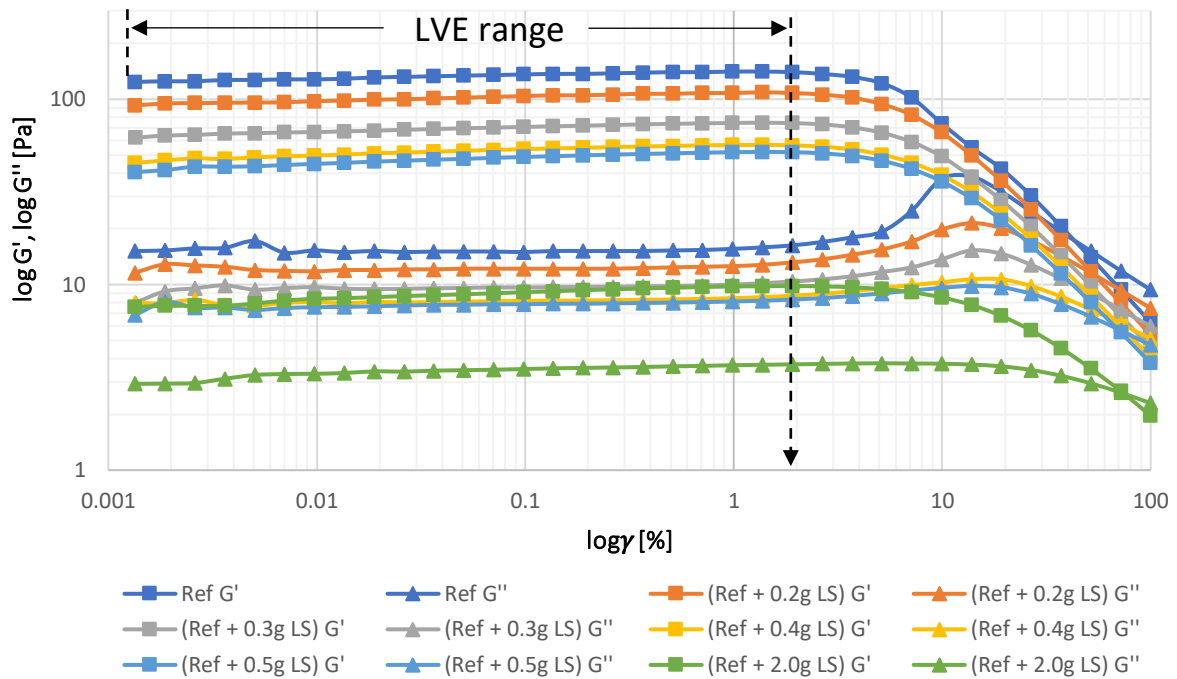


Figure 5.6: Storage and loss modulus vs strain for WBMs containing various amounts of lignosulfonates

The shear yield stress of each sample can be attained by utilizing the strain value at where the LVE range ends. By interpolation, one determines the shear stress value that corresponds to the yield strain and thereby extract the shear yield stress of the sample. A summary of the values of shear yield stress, yield strain, flow point and the value at where  $G' = G''$  for all water-based fluids tested in this thesis are given in table 5.1 below.

The flow point,  $\tau_{fp}$ , where  $G' = G''$ , can easily be determined by plotting the phase angle vs. the shear stress. The shear stress corresponding to a phase angle equal to  $45^\circ$ , is determined as the samples' flow point. This approach is illustrated in figure 5.7 and figure 5.8, where the dashed arrows represents the flow point for each of the fluids.



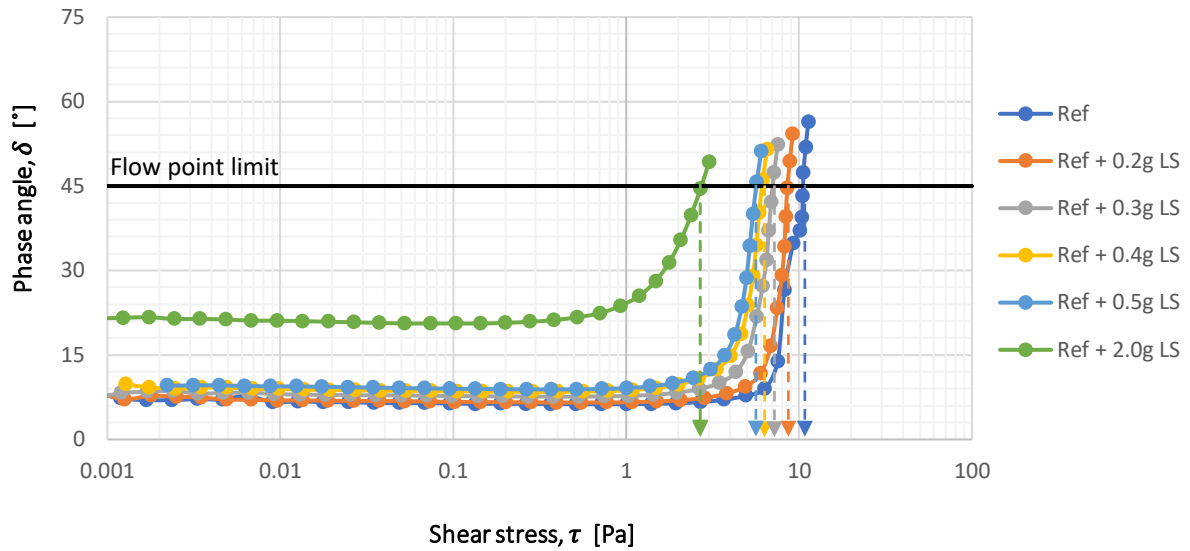


Figure 5.7: Phase angle vs. shear stress for WBM containing various amount of added lignosulfonates

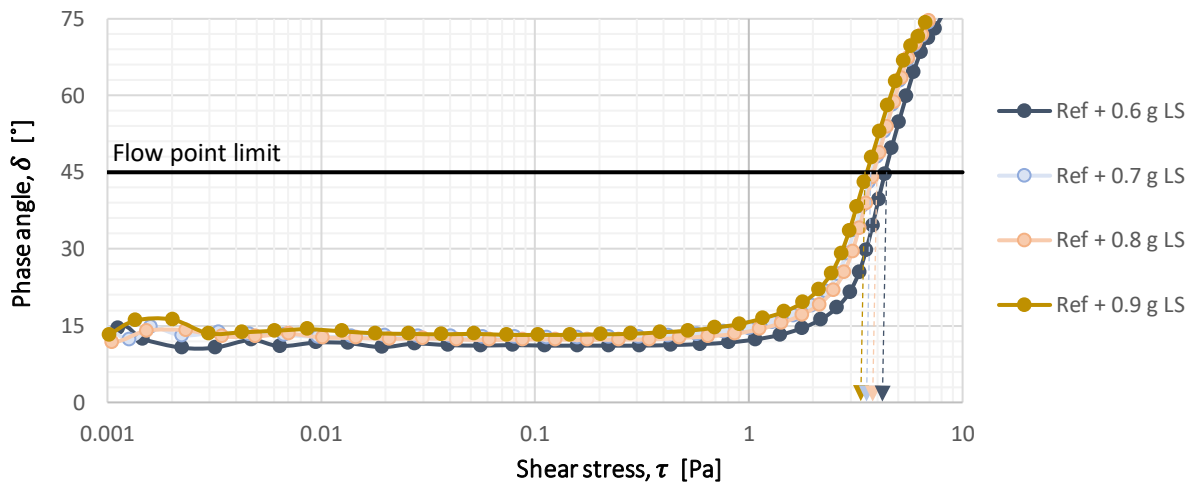


Figure 5.8: Phase angle vs. shear stress for WBM containing 0.6-0.9 grams of added lignosulfonates

Figure 5.9 illustrates the flow point for all the lignosulfonates water-based drilling fluids that were tested and analyzed in this thesis. It shows how the flow point is reduced as a function of increased amount of lignosulfonates.

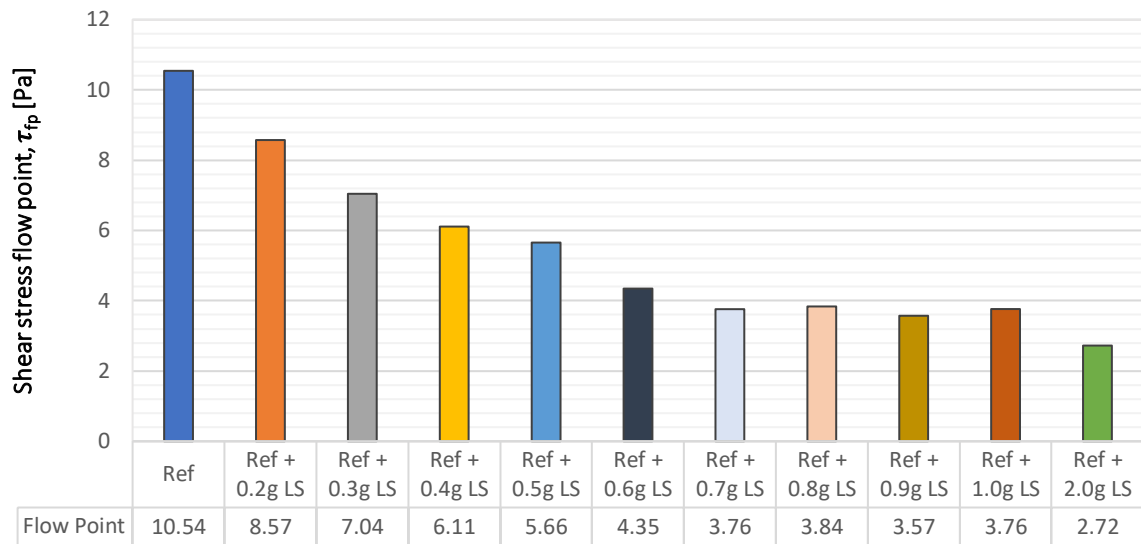


Figure 5.9: Illustration of flow point as a function of added lignosulfonates

Table 5.1: Summary of important properties obtained from the amplitude sweep tests for lignosulfonates WBMs

Fluid	$\tau_{ys}$ [Pa]	$\gamma_{ys}$ [%]	$\tau_{fp}$ [Pa]	$G' = G''$ [Pa]
Ref	4.09	3.00	10.54	17.25
Ref + 0.2g LS	2.88	2.70	8.57	10.47
Ref + 0.3g LS	1.57	2.10	7.04	8.16
Ref + 0.4g LS	1.14	2.00	6.11	6.77
Ref + 0.5g LS	0.42	0.80	5.66	6.20
Ref + 0.6g LS	0.79	1.90	4.35	3.91
Ref + 0.7g LS	0.56	1.89	3.76	3.22
Ref + 0.8g LS	0.53	1.56	3.84	3.37
Ref + 0.9g LS	0.40	0.55	3.57	3.05
Ref + 1.0g LS	0.73	1.80	3.76	4.58
Ref + 2.0g LS	0.01	0.15	2.72	2.46

## 5.2 MoS<sub>2</sub>-Nanofluid Based Water-Based Drilling Fluid

Further on, the Ref + 0.9 g LS fluid system was modified by the use of nanofluid, nanoparticles suspended in a water solution. The nanofluid was added to the fluid system in order to try to enhance the fluid’s lubricity properties. The recipe for these fluid systems can be found in **Table 4.3**.

### 5.2.1 Effect of MoS<sub>2</sub>-Nanofluid on Rheological Properties

**Figure 5.10** presents the viscometer response for the ex-situ nano treated fluids. The results show that there is little difference in the measured data for these fluids and that no linear trend can be identified. The viscometer response for the in-situ nano fluids are presented in **figure 5.11**, exhibiting no linear trends and very small differences in the viscometer response for the different fluids.

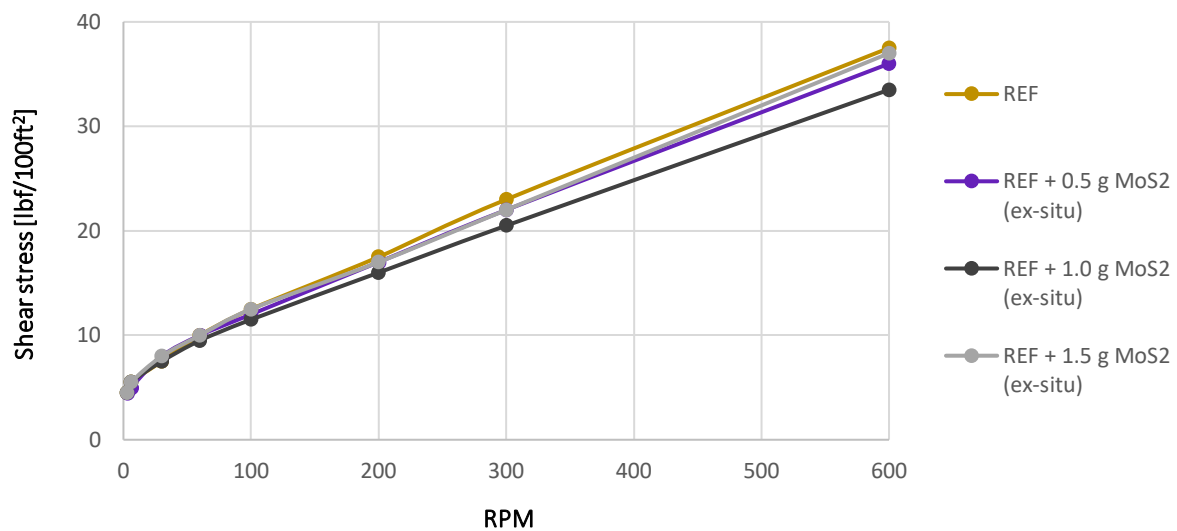


**Figure 5.10:** Viscometer data for the nano enhanced fluids, ex-situ, at fluid temperature of 22°C

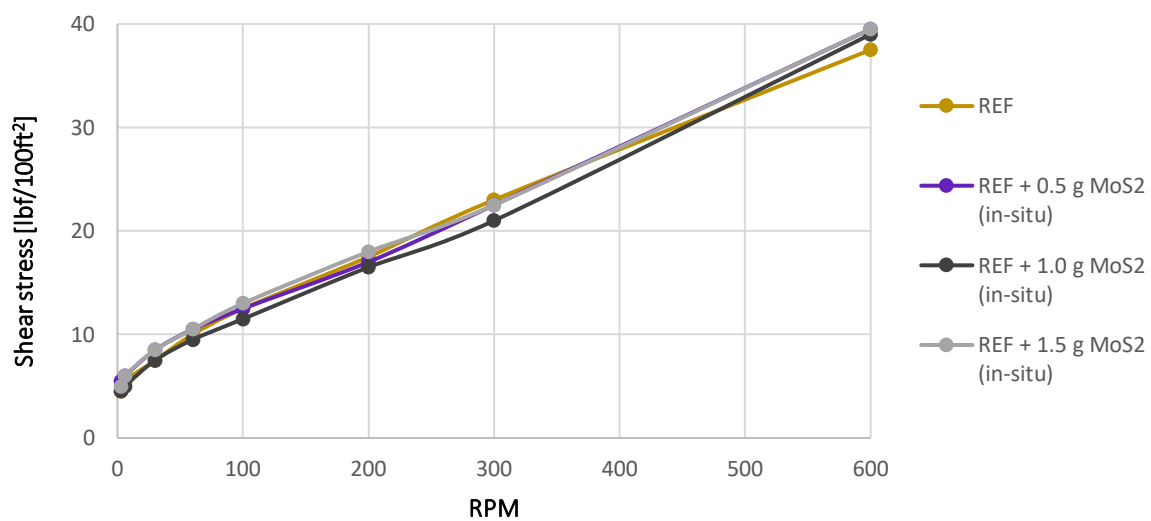


**Figure 5.11:** Viscometer data for the nano enhanced fluids, in-situ, at fluid temperature of 22°C

### 5.2.2 Effect of MoS<sub>2</sub>-Nanofluid on the Lubricity of the Drilling Fluid System

The coefficient of friction is a vital parameter in terms of drilling performance, as less friction will result in less mechanical wear and better drilling performance, ultimately leading to reduced costs. For oil-based drilling fluids, the lubricity is much higher compared to water-based fluids. Friction-reducing additives, typically fatty acid derivatives, are often used in order to improve the lubricity for both water-based and oil-based drilling fluids [79]. This section will evaluate the effect on the coefficient of friction for water-based drilling fluids modified with the nanoparticle molybdenum disulphide, in a water solution, as a friction-reducing additive.

The tribometer data for the MoS<sub>2</sub> modified water-based drilling fluids are presented in **figure 5.12**, illustrating the coefficient of friction as a function of added MoS<sub>2</sub>. The test results show that introduction of MoS<sub>2</sub> at 0.5 gram and 1.0 gram, both in-situ and ex-situ, reduces the coefficient of friction compared to the reference fluid. However, for the addition of 1.5 gram of MoS<sub>2</sub>, the coefficient of friction is reduced when the nanofluid is applied ex-situ but increased when the nano fluid is added in-situ.

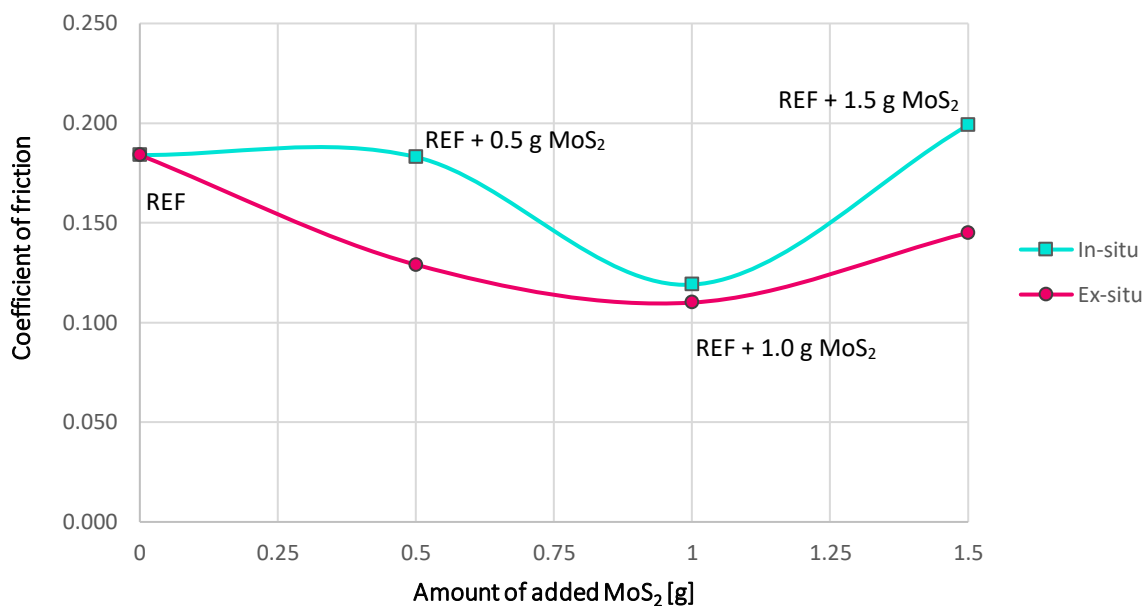


**Figure 5.12:** Visual representation of the coefficient of friction as a function of added MoS<sub>2</sub>, in-situ and ex-situ

### 5.2.3 Effect of MoS<sub>2</sub>-Nanofluid on Viscoelastic Properties - In-situ vs Ex-situ Treated Drilling Fluids

The results from the viscoelastic amplitude sweep test of the reference fluid and the nano treated water-based drilling fluids are illustrated in figure 5.13. From these results, one can see how both the storage and the loss modulus curves shifts upwards, relative to the reference fluid curve, when the MoS<sub>2</sub> is added ex-situ, and how the storage and the loss modulus curves moves downwards, with respect to the reference fluid curve, as the MoS<sub>2</sub> is added in-situ.

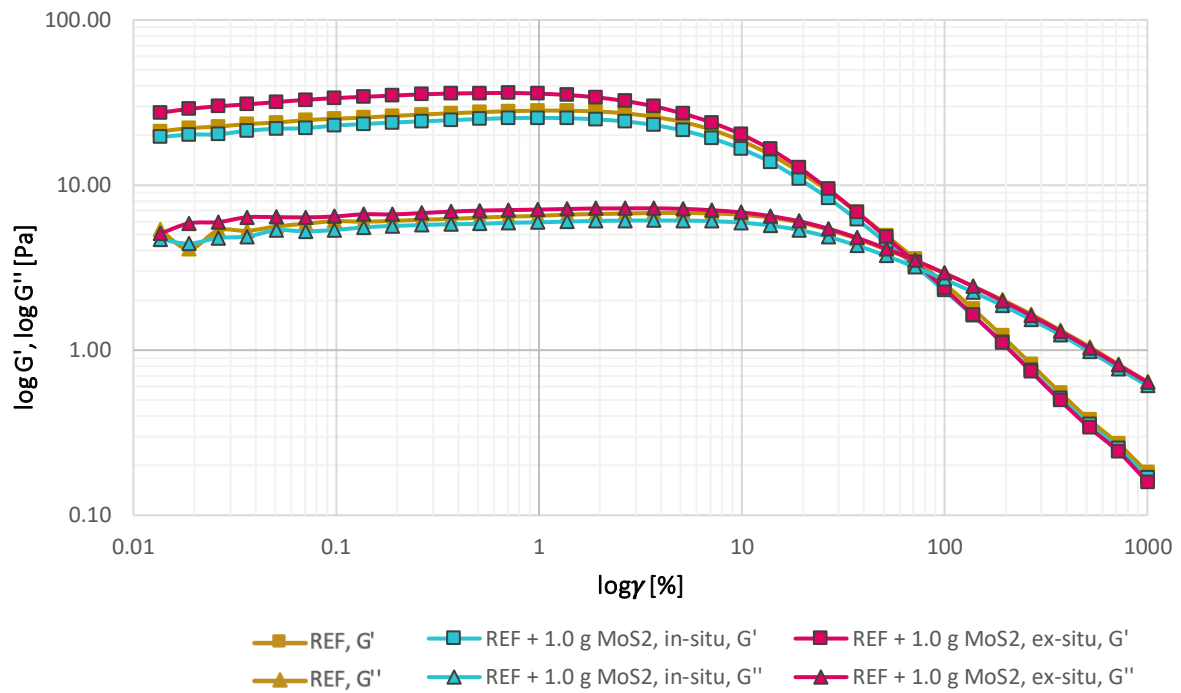


**Figure 5.13:** Amplitude sweep test results for the REF fluid and the nano modified fluids, for both in-situ and ex-situ

These results indicate that fluid treating method plays an important role in terms of the fluid properties. By treating the fluid system with nanofluid ex-situ, it provides a stronger fluid, better capable of storing energy, with greater gel characteristics. While an in-situ treatment causes the fluid system to lose strength, makes it less capable of storing energy and loses some of its gel characteristics, with respect to the reference fluid.

### 5.3 Oil-Based Drilling Fluid Characterization and Solution to Sagging Issues

This subsection will present the rheological and viscoelastic results for the oil-based drilling fluids provided by M-I Swaco and the oil-based drilling fluids formulated at the laboratory at UiS, as well as electrical stability for some of the fluids. Additionally, barite sag issues will be accounted for and the solutions to these issues will be provided.

#### 5.3.1 M-I Swaco OBMs - Escaid Base Oil

The drilling fluid formulation recipe of the M-I Swaco fluid systems can be found in **Chapter 4.1.2** in **Table 4.6**, with modified versions of the 90/10 fluid found in **Table 4.7**.

##### 5.3.1.1 Effect of Temperature on the Rheological Properties of M-I Swaco OBMs

**Figure 5.14** illustrates the viscometer response for the M-I Swaco fluids at the fluid temperature of 50°C. From this plot one can see how the oil-water-ratio affects the viscometer response, with a quite large gap between OWR 60/40 down to the rest. However, there is not identified any linear trend indicating a decrease in viscometer response as a function of increased OWR, as the 90/10 response is located above both the 70/30 and the 80/20 fluid responses.

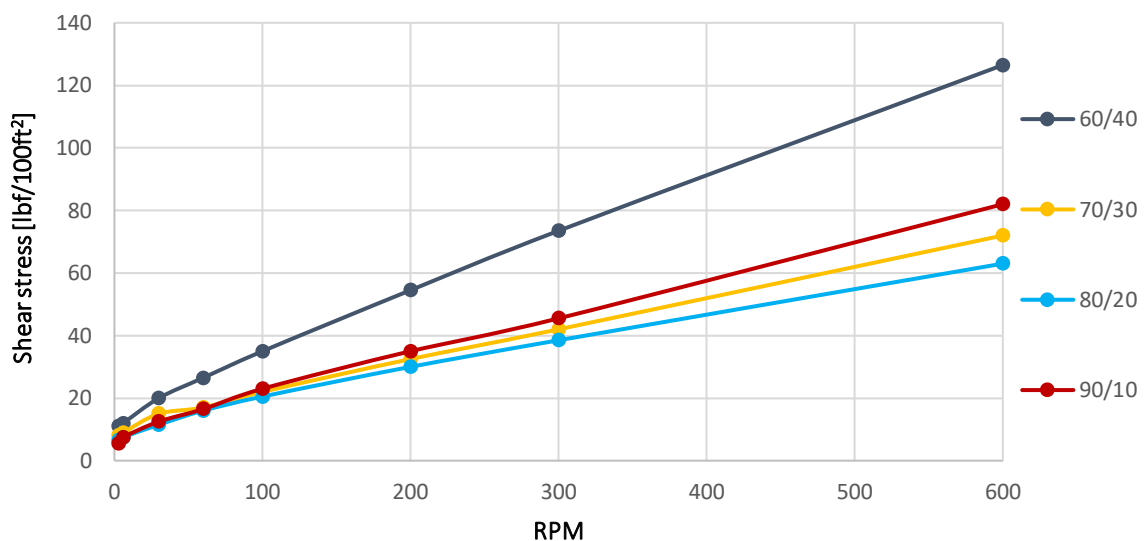


**Figure 5.14:** Viscometer data for M-I Swaco's OBMs at fluid temperature of 50°C

Generally, one would expect to find a linear trend with decreasing viscometer response as a function of increased OWR. The reason why the 90/10 fluid response is located above the 70/30 and the 80/20 fluids might be a result of poor mixing or inhomogeneous solid dispersion, as the curves are located in the same order at all fluid temperatures. In **figure 5.15** below, one can see the calculated Herschel-Bulkley yield stress for the various oil-water-ratio fluids at different fluid temperatures.

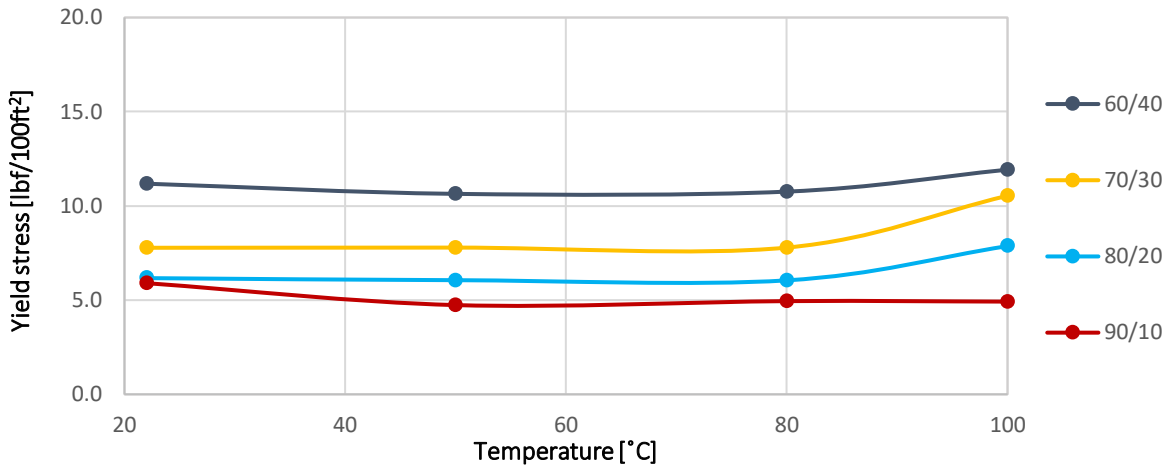


Figure 5.15: Yield stress for OBMs at different temperatures calculated based on the Herschel-Bulkley model

As observed from the plot in figure 5.15, the yield stress is temperature stable for all four fluids up until 80°C. However, when the temperature exceeds 80°C, the yield stress tends to increase for the fluids with oil-water-ratio lower than 90/10. This behaviour is not desired, as it indicates that the fluid functions changes with respect to the fluid temperature.

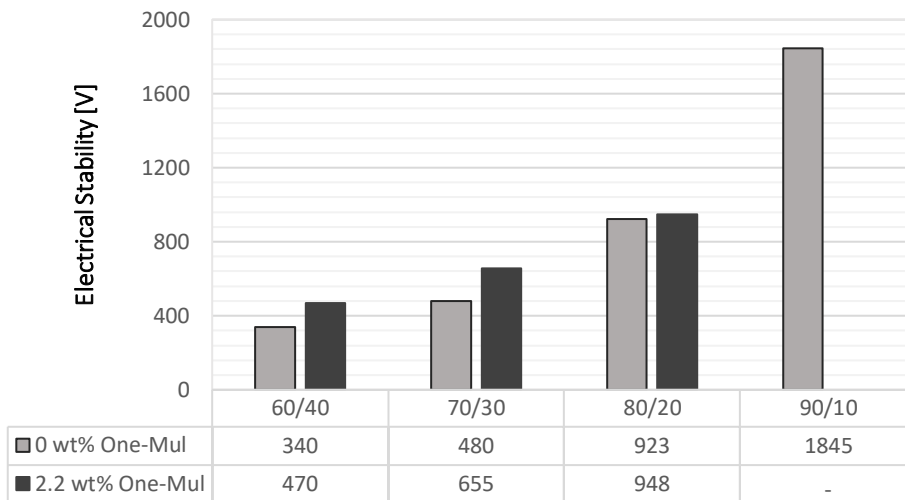


Figure 5.16: Electrical stability at 50°C before and after emulsion modification

By testing all the fluids’ electrical stability, one could recognize a trend were the same fluids that were identified as temperature dependent, also exhibited a lower electrical stability than the temperature stable 90/10 fluid. The initial electrical stability of the fluids is represented by the light grey posts in figure 5.16. It was decided to try to add more emulsifier, M-I Swaco’s One-Mul, in order to make the fluids temperature stable. The results, given in figure 5.17 below, shows that all the fluids exhibit fairly temperature stable yield stress after being modified by addition of 2.2 wt% One-Mul. Additionally, the electrical stability was also increased for all the One-Mul modified fluids, as observed in figure 5.16.

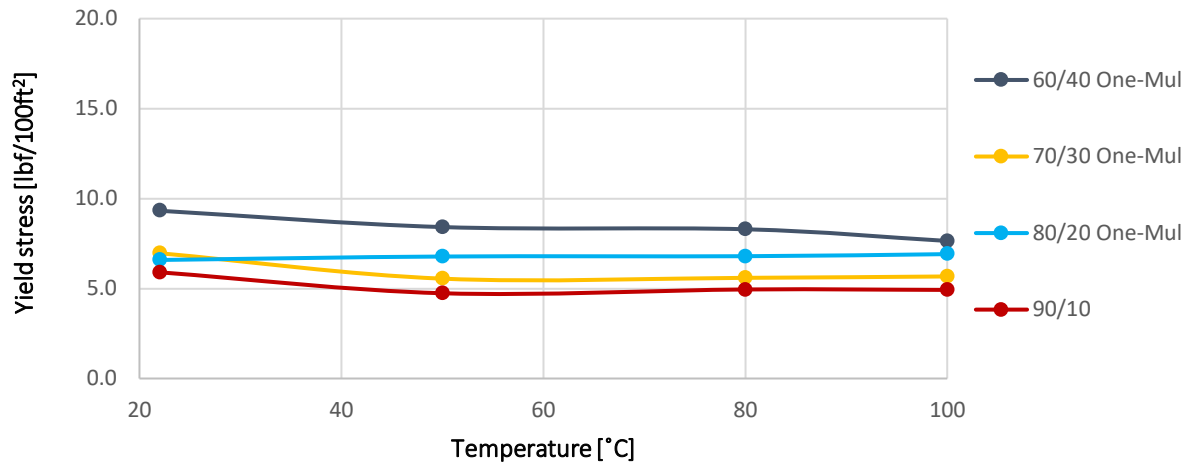


Figure 5.17: Yield stress for modified OBMs at different temperatures calculated based on the Herschel-Bulkley model

### 5.3.1.2 Viscoelastic Properties of the M-I Swaco OBMs

This subsection will present the amplitude sweep and temperature sweep results for the oil-based drilling fluids provided by M-I Swaco.

#### 5.3.1.2.1 Amplitude Sweep of the M-I Swaco OBMs

In figure 5.18, storage and loss modulus are plotted against strain for the M-I Swaco oil-based drilling fluids with various OWRs. The LVE range for each oil-water-ratio fluid is illustrated by the use of a dashed arrow, where the color of the arrow corresponds to the color of the  $G'$  and  $G''$  curve for the same fluid.

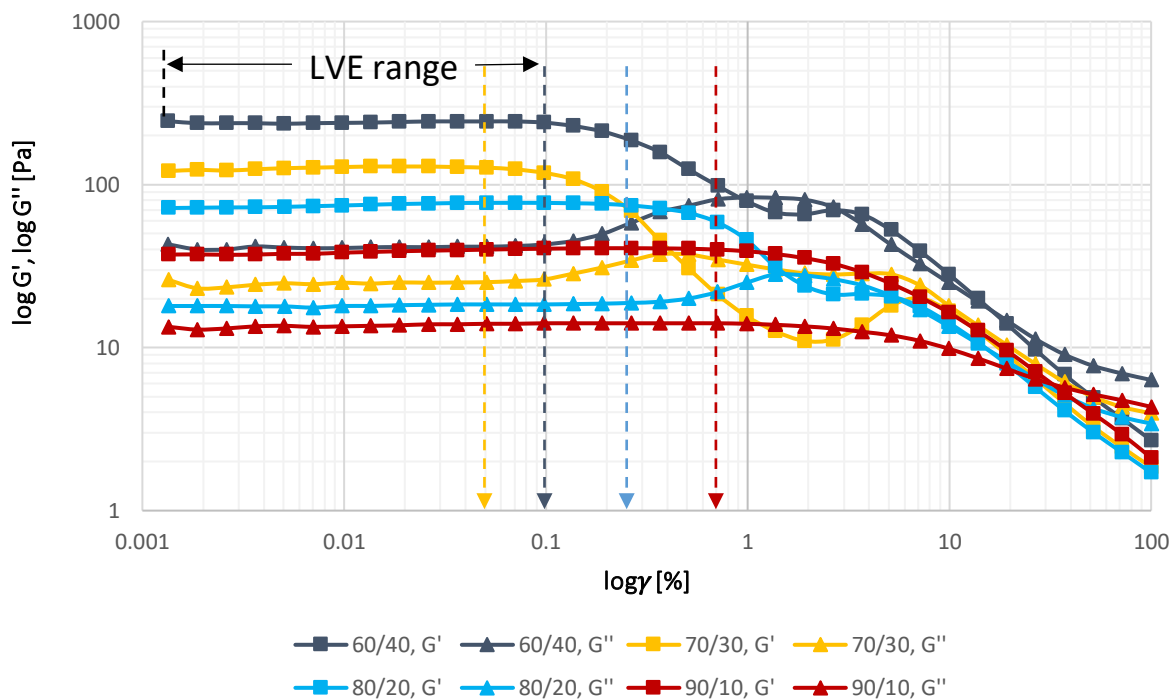


Figure 5.18: Storage and loss modulus as a function of strain for OWRs of 60/40, 70/30, 80/20 and 90/10



As seen from figure 5.18, the linear viscoelastic range is different for each of the four fluids. Additionally, the storage and loss modulus curves cross over each other twice for some of the fluids, making it difficult to interpret what that really means. However, the same approach as for water-based fluids was used in order to obtain the shear yield stress. The strain value at where the LVE range ends was used as the value corresponding to the shear yield stress, and the shear yield stress was interpolated from this value. A summary of the flow point, yield strain, shear yield stress and  $G' = G''$  is given in table 5.2 below.

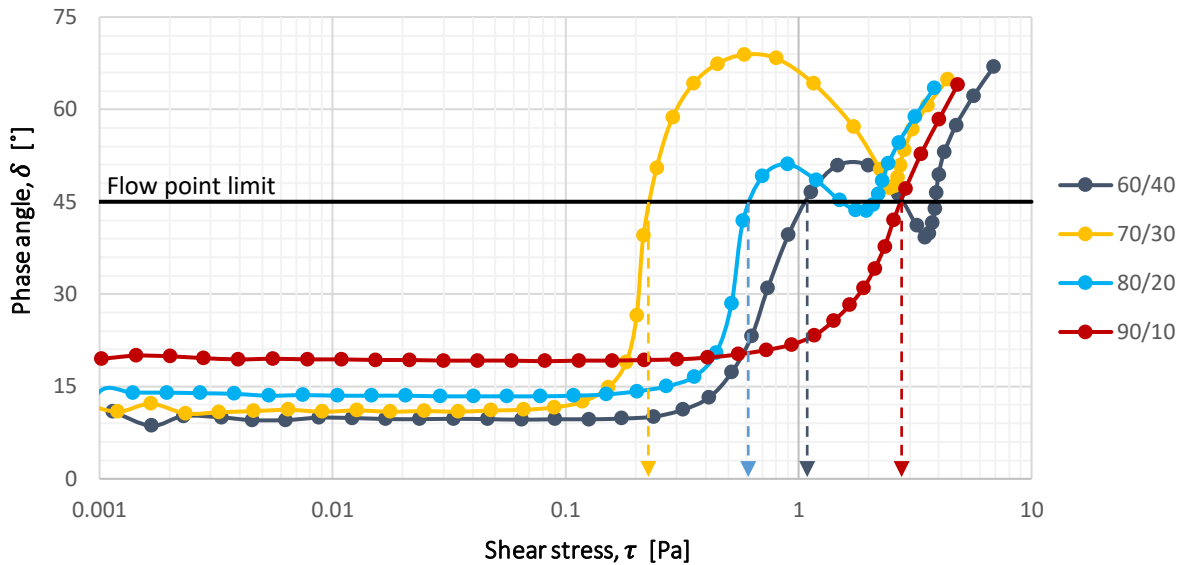


Figure 5.19: Phase angle vs. shear stress for OWRs of 60/40, 70/30, 80/20 and 90/10

The fluids’ flow points,  $\tau_{fp}$ , were determined in the same way as for the water-based fluids and the approach is illustrated in figure 5.19. As some of the curves crosses the flow-point-limit-line twice, it was decided to use the first cross-over as the flow point. All the flow point values are represented as bar graphs in figure 5.20, indicating no linear trend. The amplitude sweep results for the One-Mul modified OBM’s are given in APPENDIX B - VISCOELASTICITY.

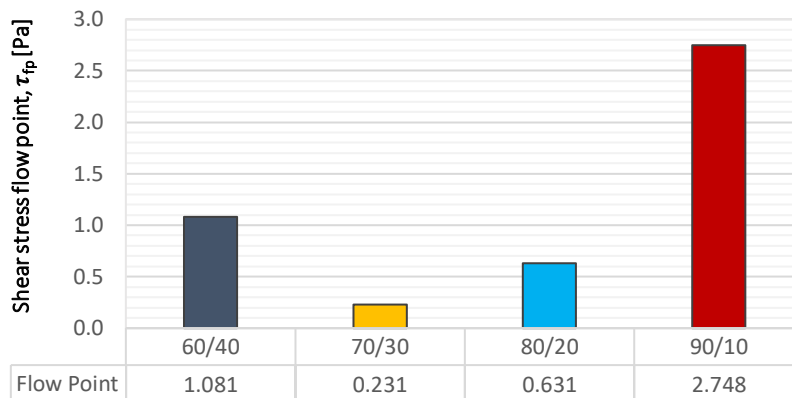


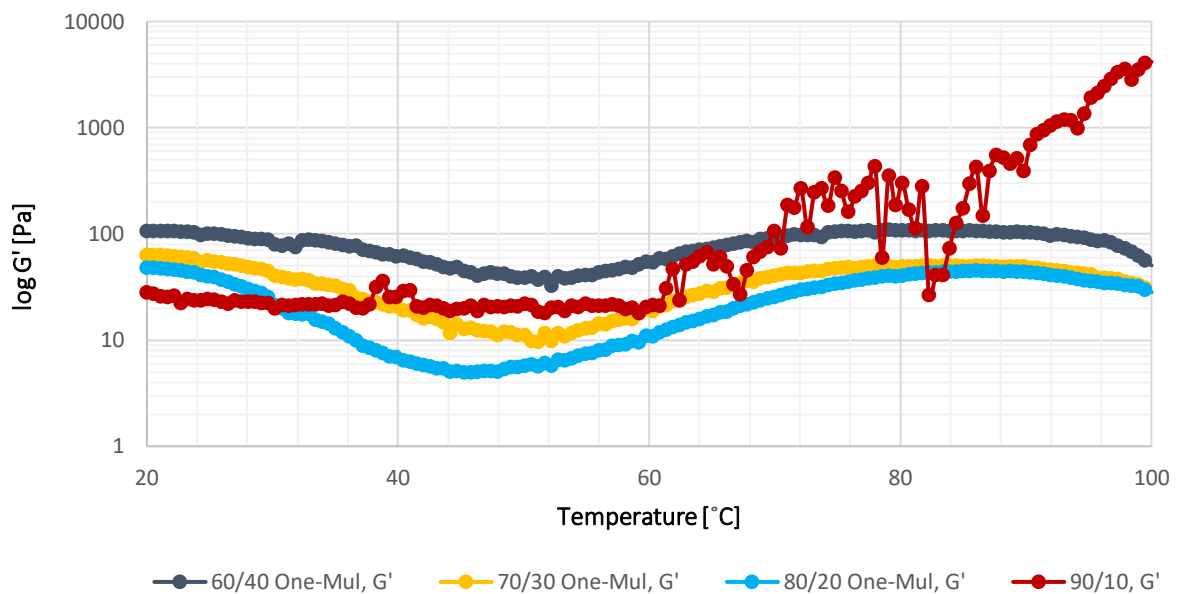
Figure 5.20: Flow point for OWRs of 60/40, 70/30, 80/20 and 90/10

**Table 5.2:** Summary of important properties gained from the amplitude sweep of various OWR fluids

Fluid	$\tau_{ys}$ [Pa]	$\gamma_{ys}$ [%]	$\tau_{fp}$ [Pa]	$G' = G''$ [Pa]
60/40	0.40	0.19	1.08	82.00
70/30	0.11	0.09	0.23	37.10
80/20	0.13	0.17	0.63	27.90
90/10	0.23	0.55	2.75	6.00

### 5.3.1.2.2 Temperature Sweep of the M-I Swaco OBMs

Figure 5.21 presents the results for the temperature sweep test of the M-I Swaco oil-based drilling fluids. For the 90/10 fluid, the storage modulus is quite stable from 20°C to approximately 60°C, before the response starts to get quite noisy. For the One-Mul modified 60/40, 70/30 and 80/20 fluids the storage modulus decreases until reaching a minimum at approximately 50°C, where the value increases up to 80°C before it stabilizes.

**Figure 5.21:** Temperature sweep results for the One-Mul modified M-I Swaco fluids and the 90/10 reference fluid

From figure 5.22 one can see the damping factor as a function of temperature. This representation was used to indicate at which temperature the flow point appears. The flow point was determined as the point where the damping factor-curve crosses the value 1. As seen from the figure, it looks like the 70/30 and the 80/20 fluid has dual performance, with flow point at approximately 42°C and 32°C, respectively, before going back to having gel like characteristics at 54°C and 55°C. The 60/40 and 90/10 fluids behave like viscoelastic gels at all given temperatures.

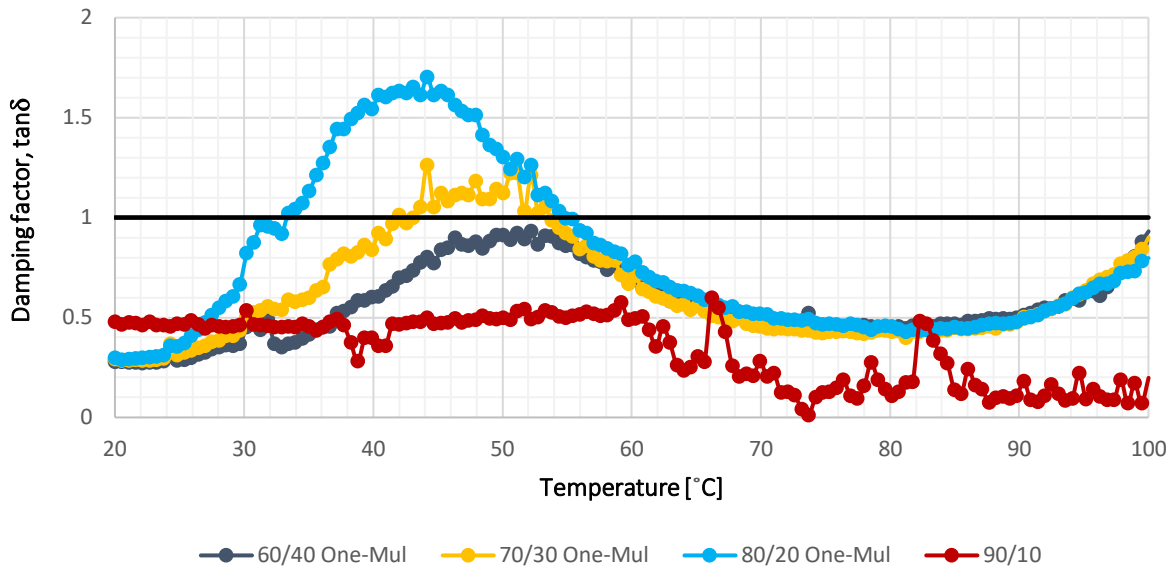


Figure 5.22: Damping factor vs. temperature for M-I Swaco OBMs

### 5.3.1.3 Barite Sag Evaluation of the M-I Swaco’s OBMs

For the barite sag evaluation, it was performed both static and dynamic sag tests. The test results presented in this chapter will be solely from tests performed with the M-I Swaco fluids.

#### 5.3.1.3.1 Static Sag Evaluation of the M-I Swaco’s OBMs

The test methodology and calculation methods for the static sag evaluation were presented in Chapter 4.3.3.1. The expected result from a fluid that is anticipated to have a sag issue is that the mud weight at the top will have a lower density than the mud weight at the bottom, as the barite particles presumably have accumulated and settled at the bottom. The results obtained from static sag measurements of the M-I Swaco fluids are presented in table 5.3 below.

Table 5.3: Summary of static sag parameters for the M-I Swaco fluids

Fluid	MW <sub>top</sub> [g]	MW <sub>bottom</sub> [g]	Static sag factor
60/40	1.60	1.62	0.503
70/30	1.71	1.72	0.501
80/20	1.71	1.72	0.501
90/10	1.72	1.75	0.506

As the static sag factor for all the M-I Swaco fluids were found to be less than 0.53, indicating that all the fluids possess adequate suspension characteristics in static environments. However, as the dynamic

sag is determined to be the most critical, the sag issue of the same fluids was further investigated by performing a dynamic viscometric sag shoe test [43].

### 5.3.1.3.2 Dynamic Sag Measurement of the M-I Swaco's OBMs

#### 5.3.1.3.2.1 Dynamic Sag Evaluation of the M-I Swaco's OBMs

The dynamic sag measurement procedure is well explained and accounted for in **Chapter 4.3.3.2**. Based on the results gained from the dynamic measurements, the dynamic sag factor for the M-I Swaco fluids were calculated and are illustrated in **figure 5.23**. From this figure one can see how the increase in oil-water-ratio increases the dynamic sag factor. In the figure, the sag factor limit illustrates the critical sag factor limit of 0.53. The dynamic sag factor values for the 60/40 fluid and the 70/30 fluid are both below the sag factor limit, indicating that these fluids are not prone to sag issues and that these fluids exhibit adequate suspension characteristics in dynamic environments as well in static environments. However, for the 80/20 fluid and the 90/10 fluid, the dynamic sag factor is well above the sag factor limit, indicating that these fluids may experience challenges with regards to sagging.

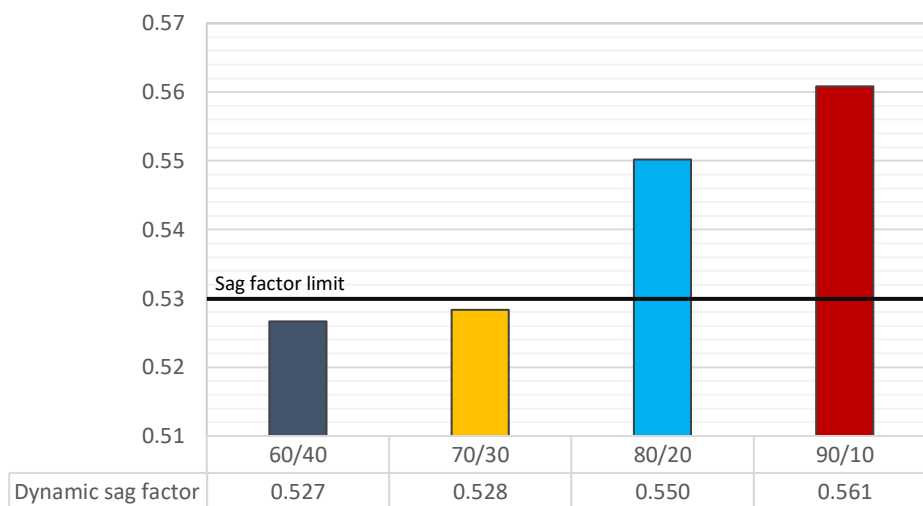


**Figure 5.23:** Illustration of the dynamic sag factor for the M-I Swaco fluids

In addition to the sag factor only, there is another way of indicating the sag potential of a fluid system. This method uses a combined plot where the dynamic sag factor is plotted as the y-axis and the storage modulus/loss modulus-ratio is used as the x-axis. This method was presented in a paper by Belayneh et al. [80] in 2016, based on combination of Saasen et al. [81] and Maxey's [45] work. **Figure 5.24** illustrates this plot for the M-I Swaco drilling fluids.

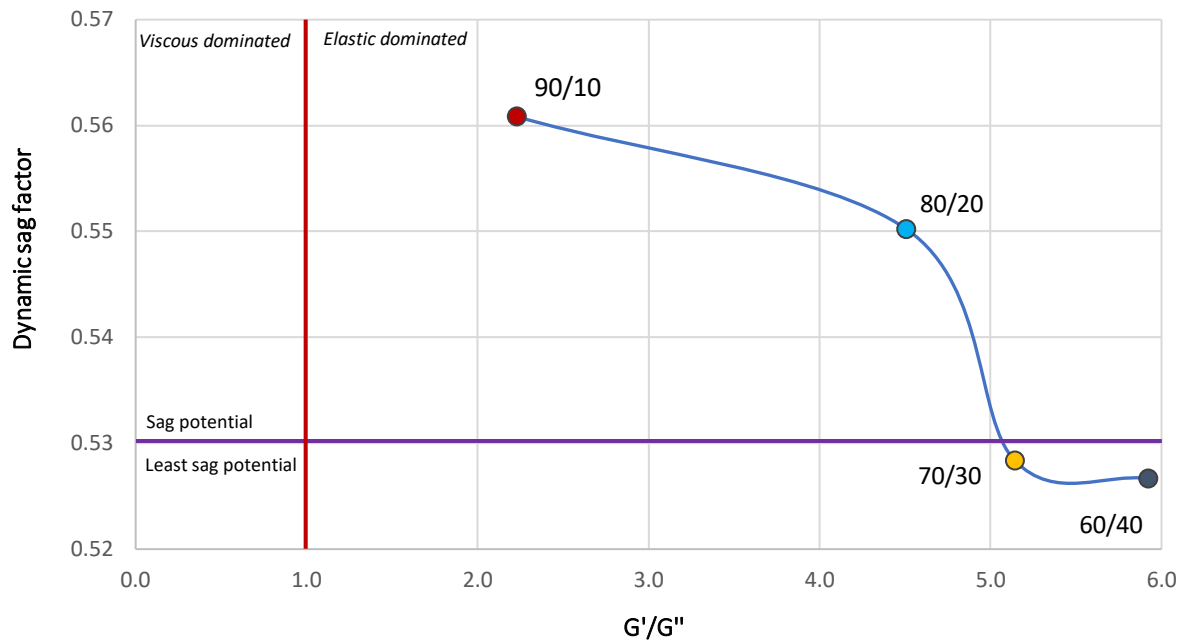


Figure 5.24: Dynamic sag potential curve for M-I Swaco fluids

In figure 5.24 the red, vertical line marks the transition between the viscous dominated and elastic dominated regions, where  $G' = G''$ . The purple, horizontal line defines the regions of sag potential and least sag potential, the sag factor limit of 0.53. As seen from the figure, all the M-I Swaco fluids are located within the elastic dominated region, which indicates that the fluids exhibit moderate gel characteristics and are able to store some energy. The higher the  $G'/G''$ -ratio, the higher is the energy storage potential of the fluid. From the same plot, there is a trend, illustrated by the blue line, indicating that the sag potential decreases with increasing storage/loss-ratio.

Tables of the dynamic sag measurement data for all fluids are given in APPENDIX C – BARITE SAG.

#### 5.3.1.3.2.1 Solution to the M-I Swaco's 90/10 OBM Sag Issues

As both the 80/20 fluid and the 90/10 fluid from M-I Swaco presumably have sag issues in dynamic environments, it was decided to investigate if this sag issue could be solved or controlled. In this section, the application of poly acrylic in the M-I Swaco 90/10 OBM fluid system have been studied.

From figure 5.25 one can see how the addition of poly acrylic gradually reduces the dynamic sag factor of the fluid systems. However, it was found that fluid containing the smallest amount of poly acrylic, 0.5 gram, was the one providing the smallest sag factor. Additionally, the 90/10 + 0.5 g poly acrylic dynamic sag factor value was small enough to fit inside the preferred sag factor interval of 0.50-0.53 and thereby indicating that this fluid exhibits sufficient suspension characteristics in order to prevent sagging.

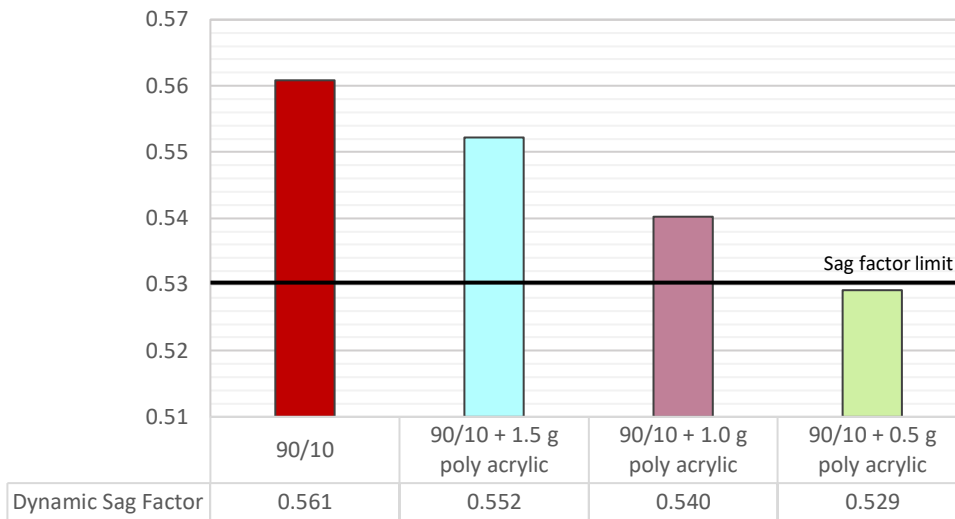


Figure 5.25: Illustration of the sag factor for the 90/10 fluid and the poly acrylic modified 90/10 fluids

Further, in figure 5.26, the dynamic sag potential plot for the 90/10 fluid and the 90/10 poly acrylic modified fluids are presented. As seen from the figure, all the fluids are located within the elastic dominated region, indicating high energy storage potential. The same trend, as for the M-I Swaco fluids, can be observed here; indicating that an increase in storage/loss-ratio decreases the sag potential for the fluid system. However, in this case, the storage/loss-ratio is most likely also a function of added poly acrylic, which indicates that addition of the right amount of poly acrylic increases the storage/loss-ratio and reduces the sag potential.

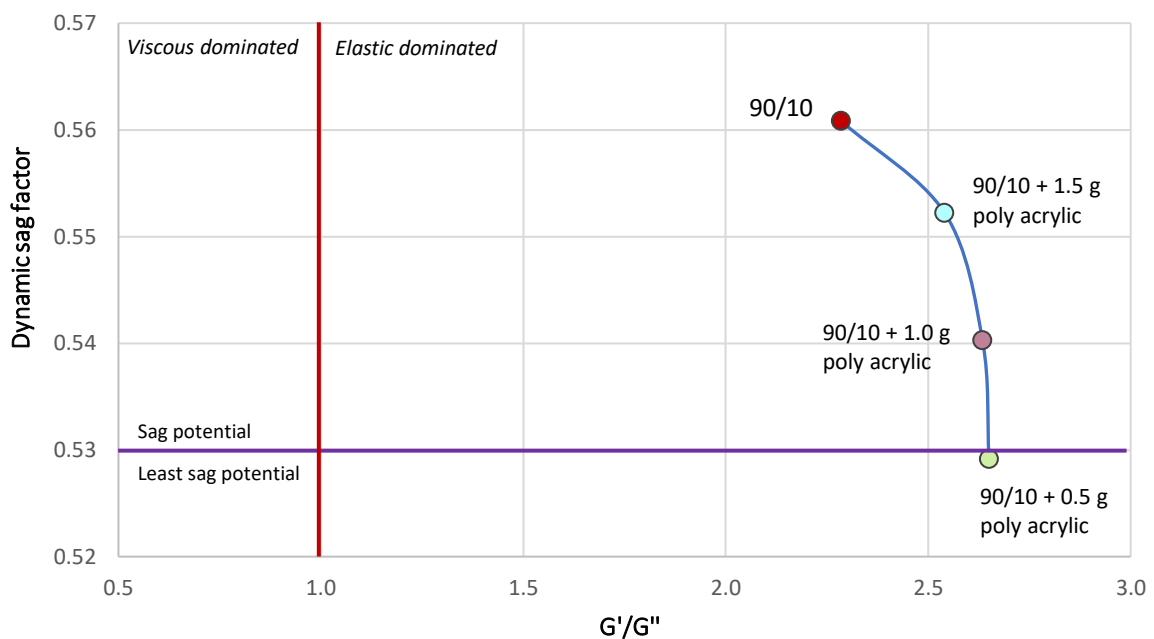


Figure 5.26: Dynamic sag potential curve for the 90/10 fluid and the poly acrylic modified 90/10 fluids

### 5.3.2 UiS 90/10 OMB - EDC 95/11 Base Oil

#### 5.3.2.1 Effect of Temperature on the Rheological Properties of the EDC 90/10 Fluid

The drilling fluid formulation of this fluid is provided in Chapter 4.1.2, Table 4.4. The rheological measurement results presented in this subsection corresponds to the oil-based drilling fluids that were formulated at the laboratory at UiS. The main difference from the 90/10 fluid provided by M-I Swaco compared to the one presented in this subsection, is the base oil. Cause where M-I Swaco used Escaid 120 ULA as base oil, EDC 95/11 was used for this fluid. That resulted in the following rheological measured data, plotted in figure 5.27.

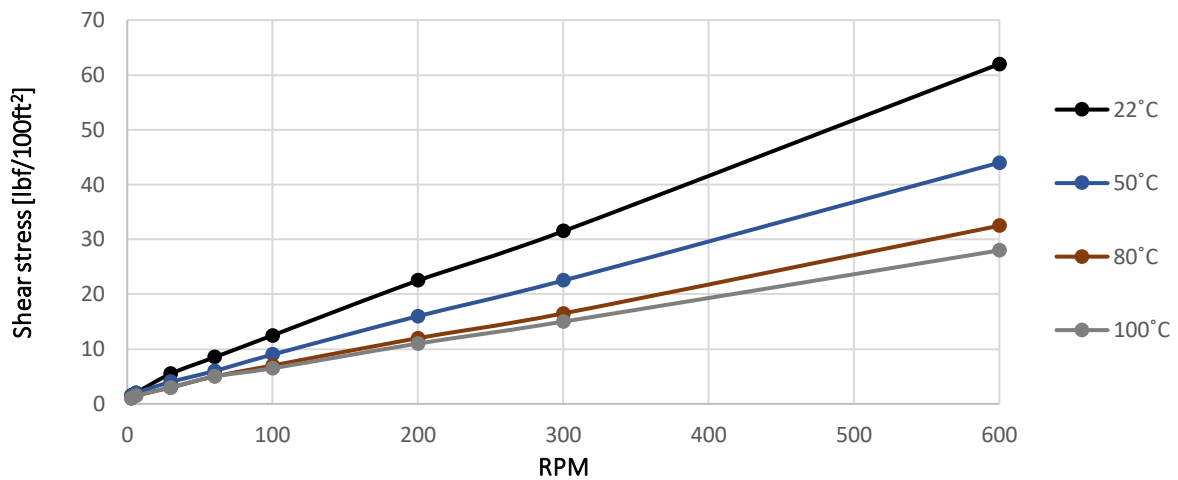


Figure 5.27: Viscometer response for the EDC 90/10 fluid at four different temperatures

As seen from figure 5.27, there is a linear trend indicating that the viscometer response is reduced as a function of increased temperature. However, the relative change of the viscometer response is gradually reduced as the temperature is increased. Figure 5.28 presents a comparison of the calculated yield stress for both the EDC 90/10 fluid and the M-I Swaco 90/10 fluid. These results indicate that there is a quite large difference in yield stress for the two fluids, but that both are temperature stable.

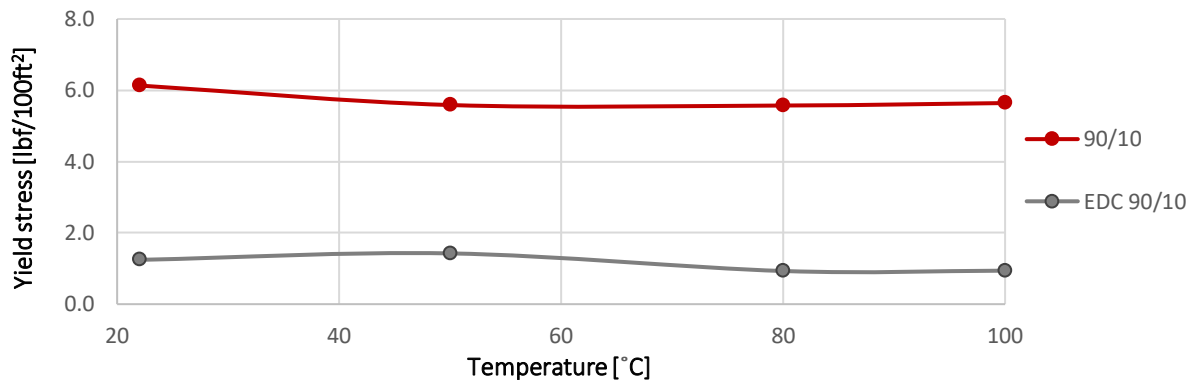
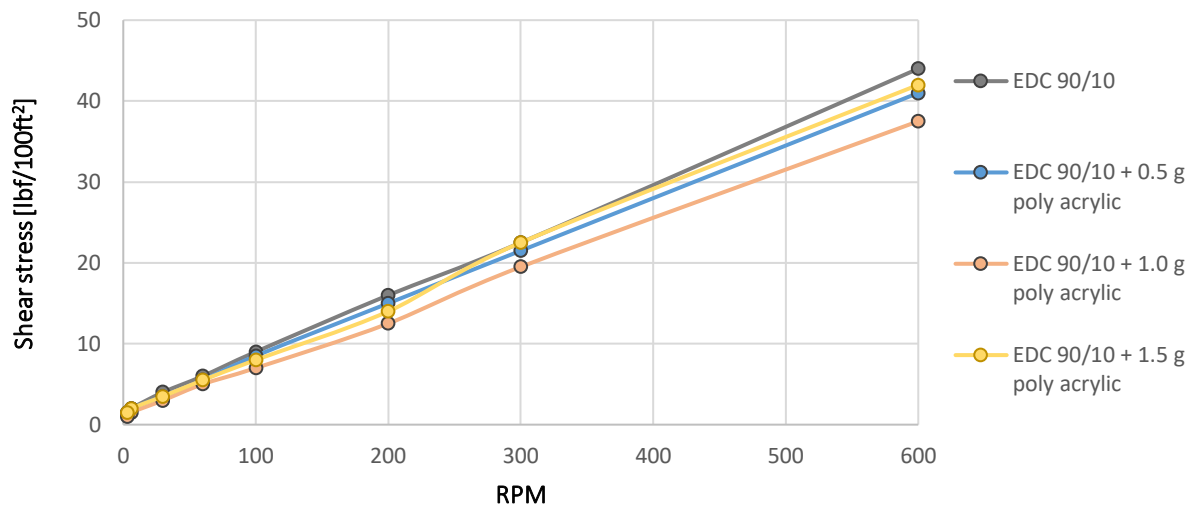


Figure 5.28: Calculated yield stress based on the Robertson-Stiff model for the EDC 90/10 and the M-I Swaco 90/10 fluids

### 5.3.2.2 Effect of Polymer and Temperature on the Rheological Properties of the EDC 90/10 Fluid

Recipes for the polymer modified EDC 90/10 fluids are given in **Table 4.5**. The viscometer response for these fluids are presented in **figure 5.29**. From this figure it is difficult to interpret how the addition of poly acrylic affects the rheology, as there is no linear trend observed. The reference fluid exhibits the highest values, while the reference plus 1.0 gram added poly acrylic provides the lowest values, placing 0.5 and 1.5 grams of added poly acrylic in the middle. However, the results are fairly close to each other, indicating that the addition of poly acrylic have very little effect on the rheological parameters.



**Figure 5.29:** Viscometer response for poly acrylic modified EDC 90/10 fluids at 50°C

This assumption is further confirmed in **figure 5.30**, where the calculated Robertson-Stiff yield stress is practically identical for the four fluids. All the fluids exhibit quite stable yield stresses as the temperature is increased, indicating that the fluid exhibits quite stable properties at various wellbore temperatures.

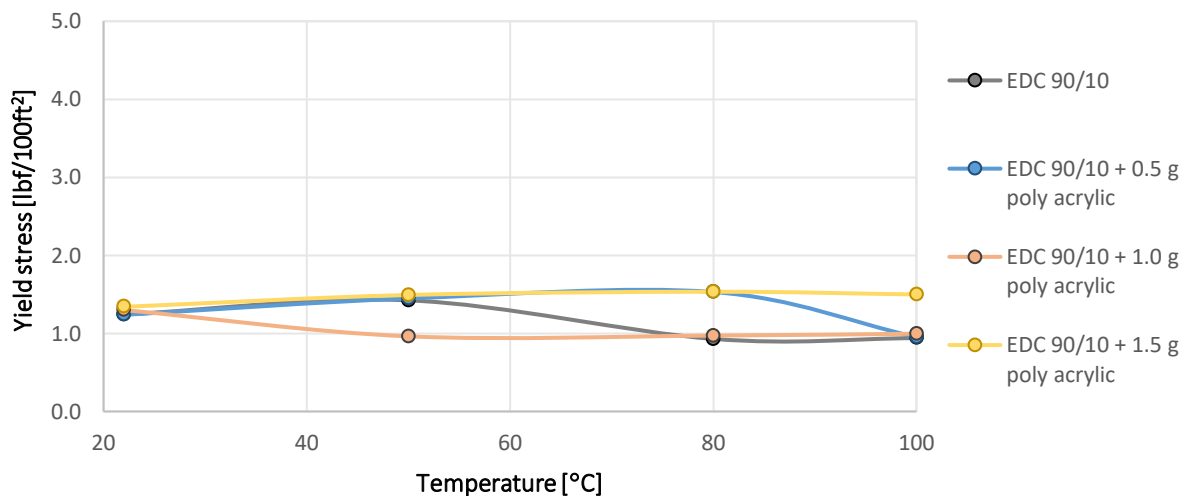


**Figure 5.30:** Calculated yield stress, based on the Robertson-Stiff model, for the poly acrylic modified EDC 90/10 fluids



### 5.3.2.3 Effect of Polymer on Viscoelastic Properties of the EDC 90/10 Fluid

Figure 5.31 shows the oscillatory rheometer response obtained by performing amplitude sweep test of the EDC 90/10 reference fluid, as well as the modified fluids containing various amounts of added poly acrylic. As seen from the plot, the storage and loss modulus behave differently for all the four different fluids.

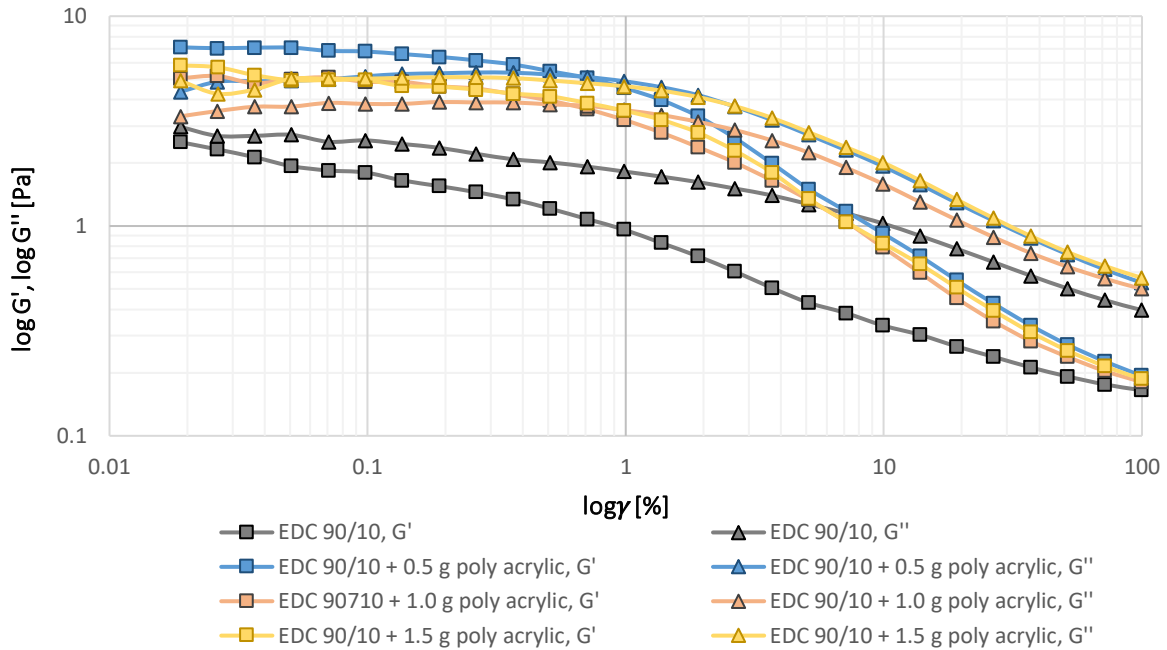
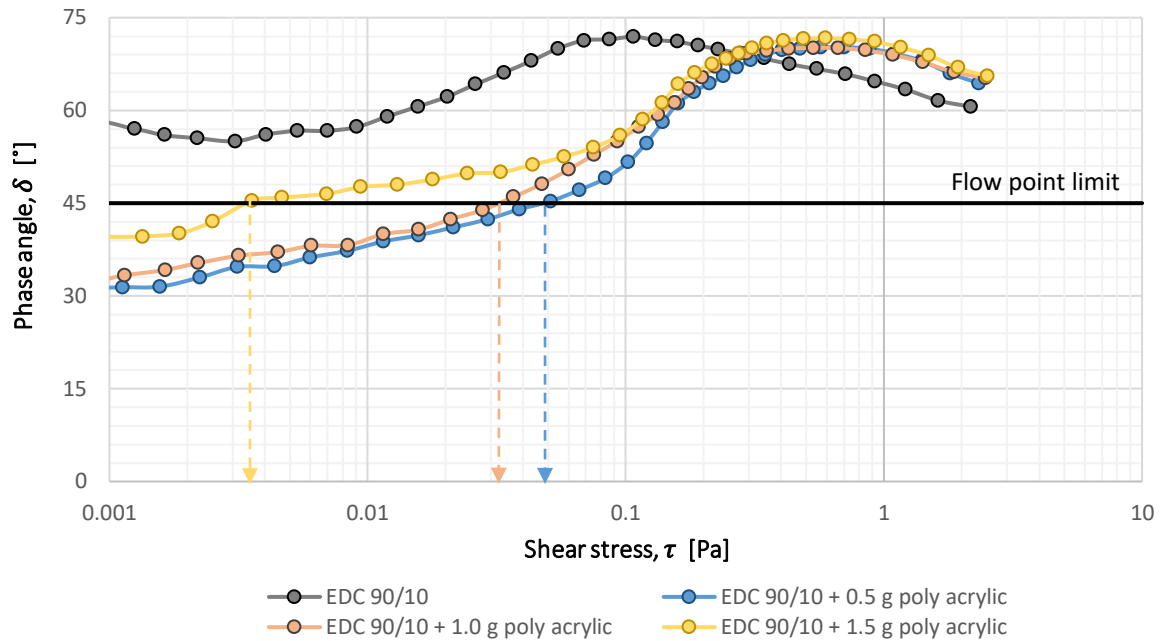


Figure 5.31: Storage and loss modulus as a function of strain for the poly acrylic modified EDC 90/10 fluids

For the EDC 90/10 reference fluid, the loss modulus is greater than the storage modulus for the whole duration of the test, indicating that the fluid behaves like a viscoelastic liquid. As a result of this, the fluid does not possess a flow point, as the flow point indicates the transition from a viscoelastic gel to a viscoelastic liquid. However, for all the poly acrylic fluids, the storage modulus is greater than the loss modulus for small strain values. As the storage and loss modulus cross-over at some point, the flow point can be obtained. By extracting the strain value at where the  $G' = G''$  and interpolate, one can estimate the fluids' flow point.

The LVE range of these fluids are very difficult to acquire, as the measurements performed at very low strain rates, smaller than 0.01%, were incredibly noisy, resulting in unreliable data. As a result, it was decided to read off the yield stress from figure 5.32. This is done by identifying the point in the graph where the phase angle stops being constant and starts increasing towards the flow point limit. This is an alternative way of estimate the yield stress value. From this point, the yield strain is interpolated in the same way as the shear yield stress have been before. A summary of the findings is given in table 5.4 below.

The flow point is determined in the same way as for the M-I Swaco oil-based drilling fluids and the water-based drilling fluids, by plotting phase angle vs. the shear stress. **Figure 5.32** illustrates this plot for the EDC 90/10 fluids, where the dashed arrows indicates the flow point,  $\tau_{fp}$ . As the EDC 90/10 reference fluid is above the flow-point-limit-line for all given shear stress values, this supports the conclusion drawn from **figure 5.31**, that the fluid does not possess a flow point.



**Figure 5.32:** Phase angle vs. shear stress for modified EDC 90/10 fluids

For the poly acrylic EDC 90/10 fluids, the flow points are represented as bar graphs in **figure 5.33** below. All the important parameters gained from the amplitude sweep of the EDC 90/10 fluids are summarized in **table 5.4**.

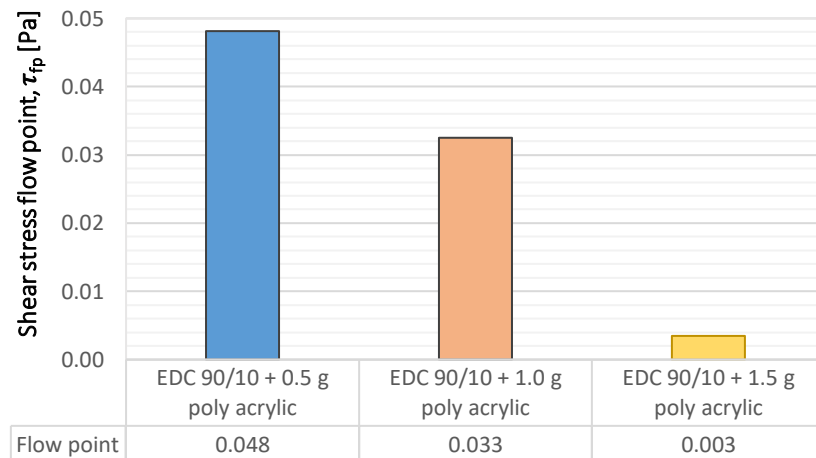


**Figure 5.33:** Flow point for EDC 90/10 fluids

**Table 5.4:** Summary of important parameters gained from amplitude sweep test of EDC 90/10 fluids

Fluid	$\tau_{ys}$ [Pa]	$\gamma_{ys}$ [%]	$\tau_{fp}$ [Pa]	$G' = G''$ [Pa]
EDC 90/10	N/A	N/A	N/A	N/A
EDC 90/10 + 0.5 g poly acrylic	0.0019	0.0202	0.048	5.20
EDC 90/10 + 1.0 g poly acrylic	0.0012	0.0197	0.033	3.77
EDC 90/10 + 1.5 g poly acrylic	0.0017	0.0268	0.003	4.75

5.3.2.4 Barite Sag Evaluation of the 90/10 - EDC 95/11 Base Oil

5.3.2.4.1 Static Sag Evaluation of the EDC 90/10 Fluid

The test results from the static sag measurement of the EDC 90/10 fluid is summarized in table 5.5. Based on the results, the sag factor for the EDC 90/10 fluid was found to be greater than 0.53, indicating that the fluid possesses inadequate suspension characteristics in a static environment. The sag issue of the EDC 90/10 fluid was then further investigated by performing dynamic sag measurements.

**Table 5.5:** Summary of static sag parameters for the EDC 90/10 fluid

Fluid	MW <sub>top</sub> [g]	MW <sub>bottom</sub> [g]	Sag factor
EDC 90/10	1.67	2.14	0.561

5.3.2.4.2 Dynamic Sag Evaluation and Sag Issue Solution to the EDC 90/10 Fluid

For the EDC 90/10 fluids, the dynamic sag factors are illustrated in figure 5.34. As shown in this figure, the same trend, as for the 90/10 fluids, can be found here. The sag factor decreases as a function of added poly acrylic, but with the lowest concentration producing the best result. The EDC 90/10 + 0.5 g poly acrylic sag factor is less than 0.53, as it was for the 90/10 fluid, indicating that this fluid system provides adequate solid suspension characteristics.

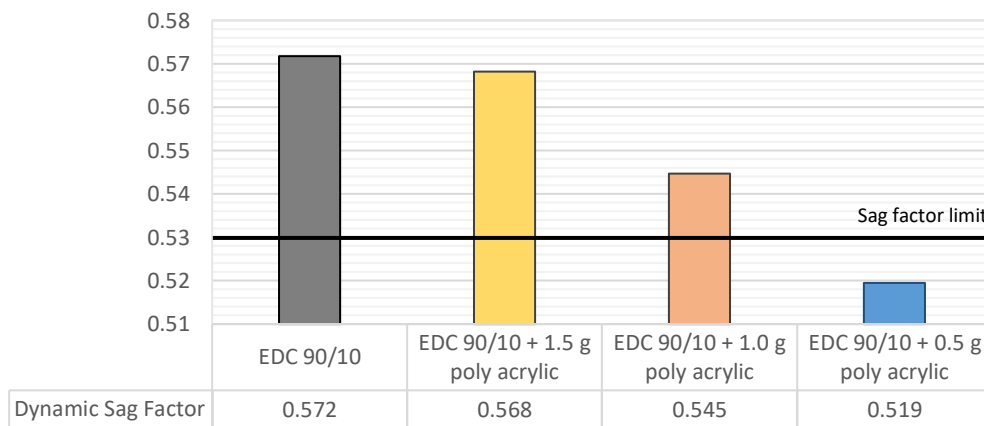


**Figure 5.34:** Illustration of the sag factor for the EDC 90/10 fluids

From the combined plot with the dynamic sag factor and storage/loss-ratio, figure 5.35, one can see that all the poly acrylic modified fluids are located within the elastic dominated region, while the reference fluid is located within the viscous dominated region. As the reference fluid exhibits viscous behaviour, this means the fluid is incapable of storing energy and that all energy is lost during a deformation process. From the plot the same trend, illustrated by the blue line, indicates that an increasing storage/loss-ratio causes a reduction in sag potential.

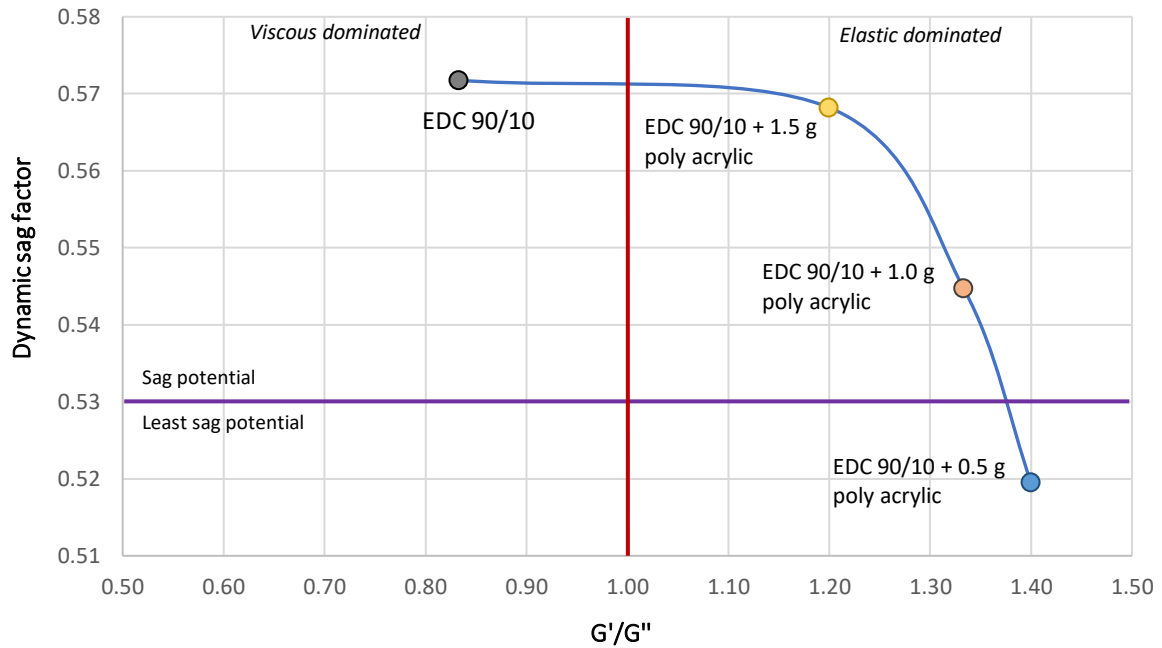


Figure 5.35: Dynamic sag potential curve for the EDC 90/10 fluids

## 6 RHEOLOGICAL MODELLING AND WELLBORE SIMULATIONS

Rheological modelling and wellbore simulation studies were performed with some of the fluid systems that exhibited the best performance in terms of thermal stability, yield stress and barite sag for both oil-based and water-based systems. The results from the rheological modelling and the simulation studies will be presented in this chapter, where the simulation studies include ECD and pump pressure simulations based on the Unified hydraulics model described in **Chapter 3.5** and summarized in **Table 3.2**.

### 6.1 Rheological Modelling

This section will present the results from the rheological modelling, which was performed in order to identify which rheological model that best describes each of the drilling fluids. By calculation and simulation in excel, each of the individual rheological models;

- Bingham Plastic,
- Power Law,
- Herschel-Bulkley,
- Unified and
- Robertson-Stiff,

have been applied in order to calculate and compare the rheological parameters for the drilling fluids in this thesis. All the calculations are based on the rheological formulas presented back in **Chapter 3.2**. From these calculations, a trend-line, which best matches the measured data, is found and the percentage deviation is recorded. An example of a simulated and calculated trend-line according to the Herschel-Bulkley model is illustrated in **figure 6.1**, where the percentage deviation is equal to 2.12%.

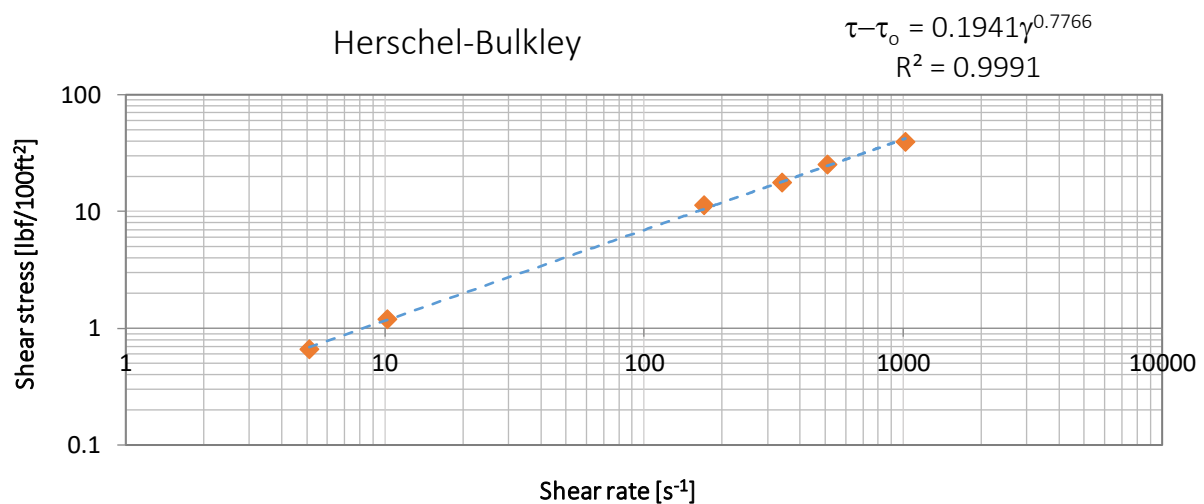


**Figure 6.1:** Example of a Herschel-Bulkley trend-line gained from rheological modelling of measured data

A general trend identified from the excel-calculations was that Herschel-Bulkley, Unified and Robertson-Stiff were the models that generally gave the most accurate characterization of both the water-based and oil-based drilling fluids. Tables of all the measured data from the Ofite 8-speed viscometer, for both water-based and oil-based drilling fluids, are given in APPENDIX A – RHEOLOGICAL MEASUREMENTS.

### 6.1.1 Rheological Modelling for Lignosulfonates Water-Based Drilling Fluids

This subsection will provide rheological models and calculated parameters for selected water-based fluids treated with lignosulfonates. From the results obtained from the experimental work, the following fluid systems were selected for rheological modeling: Reference, Ref + 0.9 g LS and Ref + 2.0 g LS. Firstly, a general curve fitting for the water-based lignosulfonates fluid systems will be performed.

#### 6.1.1.1 Curve Fitting for Lignosulfonates Water-Based Drilling Fluids

From an average value gained from the excel-calculations, based on the rheological Ofite viscometer data, it was indicated that the *Robertson-Stiff* model singles out as the model that best describes the lignosulfonates water-based drilling fluids analyzed in this thesis. From figure 6.2, one can observe how the percentage deviation of the measured data and rheological models varies from fluid to fluid, for some given fluid samples. The total average deviation is definitely smallest for the Robertson-Stiff model, with an average deviation of 1.66%, compared to 2.85% and 3.78% for Herschel-Bulkley and Unified model, respectively.

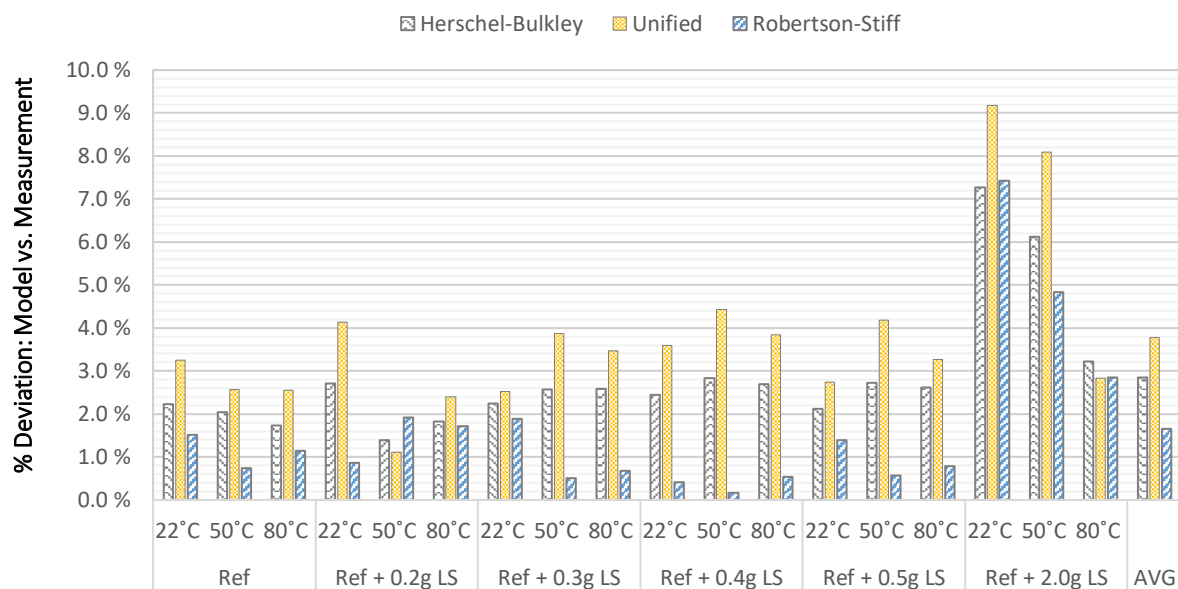


Figure 6.2: Percentage deviation between measured data and rheological models for given water-based muds

### 6.1.1.2 WBM Reference Fluid System

All the trend-lines for the various rheological models for the Ref fluid are illustrated in figure 6.3, while the corresponding parameters and equations are given in table 6.1.

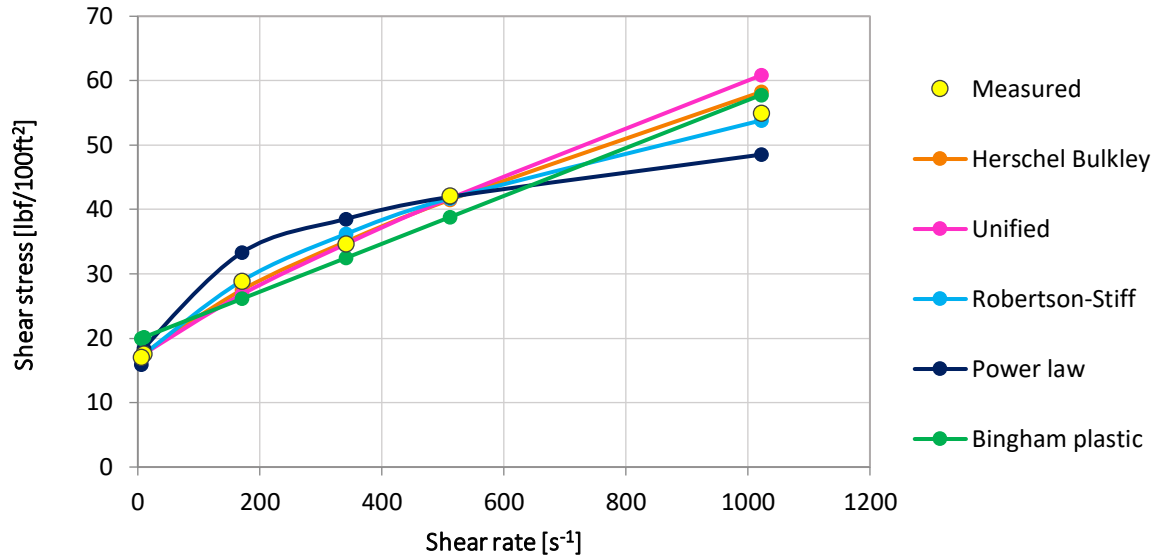


Figure 6.3: Trend-lines from rheological modelling of the WBM reference system at fluid temperature of 22°C

Model	Equation	Parameters				% Deviation	cP
		$\tau_0, \tau_y, A$	$k, C$	$n, B$	$\mu_p, \mu$		
Herschel-Bulkley	$16.23 + 0.2576 \cdot \gamma^{0.7352}$	16.23	0.2576	0.7352		2.22	
Unified	$16.54 + 0.1547 \cdot \gamma^{0.8164}$	16.54	0.1547	0.8164		3.25	
Power Law	$11.313 \cdot \gamma^{0.2101}$		11.313	0.2101		8.37	
Bingham	$0.0372 \cdot \gamma + 19.78$	19.78			0.0372	10.1	17.81
Robertson-Stiff	$4.408 \cdot (52.52 + \gamma)^{0.3954}$	4.408	52.52	0.3954		1.52	

Table 6.1: Modelled parameters and equations for the WBM reference system at fluid temperature of 22°C

Additionally, the table presents the percentage deviation for each of the rheological models. The Bingham plastic model yields the largest deviation, as expected, as this model is overestimating the yield point and the plastic viscosity. As seen from the table, the Herschel-Bulkley, Unified and the Robertson-Stiff models are the ones providing the best match for the measured data. However, as Robertson-Stiff has the lowest percentage deviation, 1.52%, this model is the most suitable model in order to describe the water-based reference system.

### 6.1.1.3 Ref + 0.9 g LS Fluid System

Trend-lines for all the various rheological models for the Ref + 0.9 g LS fluid are illustrated in figure 6.4, while table 6.2 presents the corresponding parameters and equations.

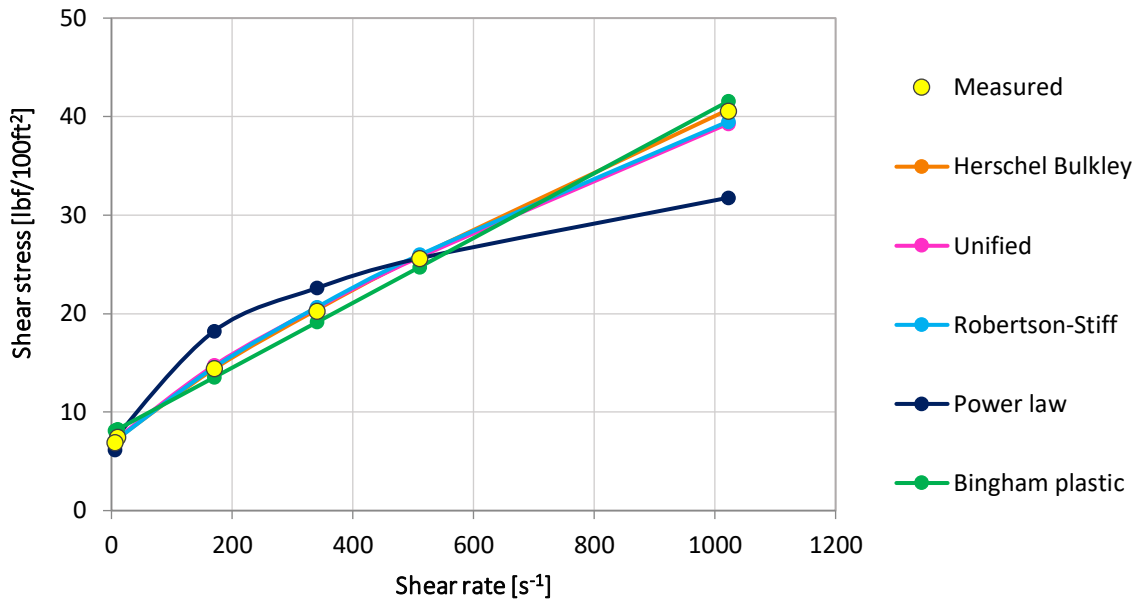


Figure 6.4: Trend-lines from rheological modelling of the Ref + 0.9 g LS fluid system at fluid temperature of 22°C

Model	Equation	Parameters					% Deviation	cP
		$\tau_0, \tau_y, A$	$k, C$	$n, B$	$\mu_p, \mu$			
Herschel-Bulkley	$6.554 + 0.1151 \cdot \gamma^{0.8215}$	6.554	0.1151	0.8215		0.80		
Unified	$6.402 + 0.1634 \cdot \gamma^{0.7655}$	6.402	0.1634	0.7655		1.56		
Power Law	$3.716 \cdot \gamma^{0.3098}$		3.716	0.3098		12.2		
Bingham	$0.0329 \cdot \gamma + 7.926$	7.926			0.0329	7.48	15.75	
Robertson-Stiff	$1.903 \cdot (106.4 + \gamma)^{0.4587}$	0.3573	78.58	0.6719		1.72		

Table 6.2: Modelled parameters and equations for Ref + 0.9 g LS fluid system at fluid temperature of 22°C

For the Ref + 0.9 g LS fluid system, the percentage deviation is actually largest for the Power Law model, with its 12.2%. As the lignosulfonates works as a disperser, causing the fluid to become less viscous, the n-value for the Power Law model is increased, may resulting in the large deviation from the measured data. The results from the rheological modelling of the Ref + 0.9 g LS fluid indicates that the Herschel-Bulkley model provides the best fit for the measured data, with a percentage deviation of just 0.80%.



### 6.1.1.4 Ref + 2.0 g LS Fluid System

All the trend-lines for the various rheological models for the Ref + 2.0 g LS are represented in figure 6.5, while the parameters and equations corresponding to the curves in figure 6.5 are given in table 6.3.

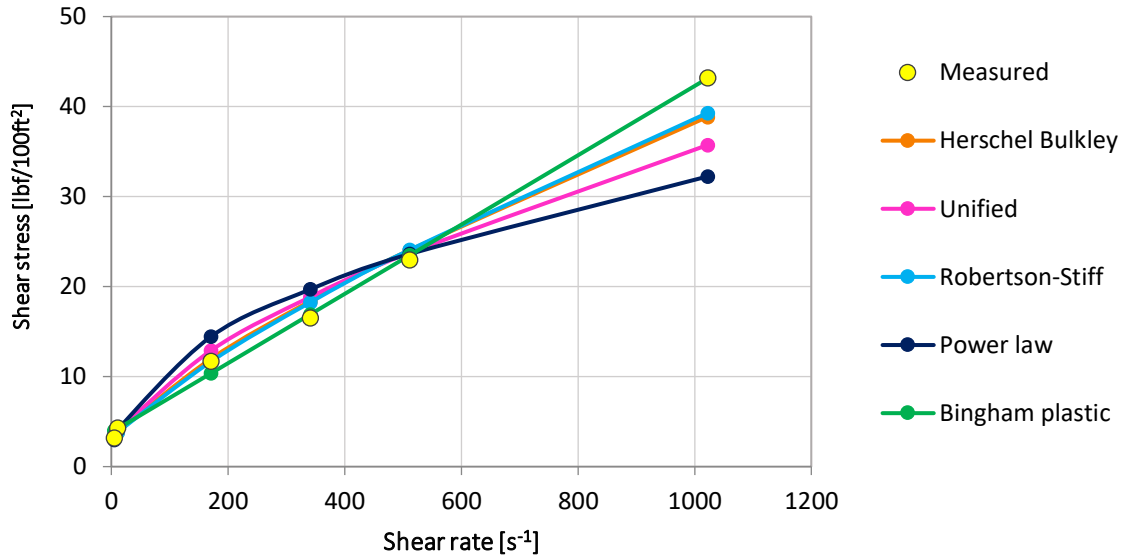


Figure 6.5: Trend-lines from rheological modelling of the Ref + 2.0 g LS fluid system at fluid temperature of 22°C

Model	Equation	Parameters				% Deviation	cP
		$\tau_0, \tau_y, A$	$k, C$	$n, B$	$\mu_p, \mu$		
Herschel-Bulkley	$2.712 + 0.1854 \cdot \gamma^{0.7609}$	2.712	0.1854	0.7609		7.27	
Unified	$2.134 + 0.4086 \cdot \gamma^{0.76363}$	2.134	0.4086	0.6363		9.18	
Power Law	$1.4357 \cdot \gamma^{0.4490}$		1.4357	0.4490		13.6	
Bingham	$0.0385 \cdot \gamma + 3.786$	3.786			0.0385	7.17	18.43
Robertson-Stiff	$0.2241 \cdot (35.0 + \gamma)^{0.7420}$	0.2241	35.00	0.7420		7.42	

Table 6.3: Modelled parameters and equations for Ref + 2.0 g LS fluid system at fluid temperature of 22°C

The same results are obtained for the Ref + 2.0 g LS fluid, where the Power Law model provides the largest percentage deviation of 13.6%, as a result of the added lignosulfonates. Generally large deviations are recorded for this fluid. However, the Herschel-Bulkley model is registered to have the lowest percentage deviation, indicating that this model provides the best match for the measured data for the Ref + 2.0 g LS fluid system.

### 6.1.1.5 Lignosulfonates Water-Based Drilling Fluids Rheological Modelling Summary and Comparison

Table 6.4 presents a summary of the rheological models that were found to be best suited for describing each of the lignosulfonates fluid systems, also presenting the mathematical equation for the corresponding model.

**Table 6.4:** Rheological model summary for water-based fluid systems treated with lignosulfonates

Fluid	Model	Equation
Ref	Robertson-Stiff	$4.408 \cdot (52.52 + \gamma)^{0.3954}$
Ref + 0.9 g LS	Herschel-Bulkley	$6.554 + 0.1151 \cdot \gamma^{0.8215}$
Ref + 2.0 g LS	Herschel-Bulkley	$2.712 + 0.1854 \cdot \gamma^{0.7609}$

Further, a summary of all the calculated parameters and their percentage deviation for all the rheological models are given in table 6.5 below. Based on the data given in table 6.5, following observations were made:

#### Herschel-Bulkley model

The Herschel-Bulkley yield stress,  $\tau_0$ , is reduced with more than 50% for both of the fluids modified with lignosulfonates. When the yield stress is reduced, this indicates that the internal frictional resistance in the fluid systems is reduced and that less pressure/force is required to initiate flow. For the consistency index,  $k$ , and the flow behaviour index,  $n$ , there is not found any linear trend.

#### Unified model

The low shear yield stress follows the same trend as the Herschel-Bulkley yield stress and is reduced as a function of added lignosulfonates. For the consistency index, the value was increased for both the Ref + 0.9 g LS and the Ref + 2.0 g LS fluids, with 5.62% and 164.1% respectively. The flow behaviour index was reduced for both fluids. As the  $n$ -value for all the fluids are below 1, this indicates pseudoplastic fluid behaviours.

#### Power Law model

The Power Law model has an opposite trend for both the consistency index and flow behaviour index, when compared to the Unified model. The  $k$ -value is reduced for both fluids and the  $n$ -value is increased for both fluids. When comparing the  $n$ -values to the Herschel-Bulkley model and the Unified model, the values are quite low.

### **Bingham model**

The Bingham yield stress decreases as a function of added lignosulfonates. The yield stress was reduced by 59.9% and 80.9% for the Ref + 0.9 g LS and the Ref + 2.0 g LS fluids respectively. For the plastic viscosity, there was not found any trend, as the PV for the Ref + 0.9 g LS fluid was reduced by 11.6% and the PV for the Ref + 2.0 g LS fluid was increased with 3.49%.

### **Robertson-Stiff model**

In the Robertson-Stiff model the A-parameter corresponds to the k-value for other models. This A-parameter was reduced for both of the fluids containing lignosulfonates. The B-parameter, corresponding to the n-value of other models, was increased for both fluids, with 69.9% for the Ref + 0.9 g LS fluid and 87.7% for the Ref + 2.0 g LS fluid. As the B-parameter was found to be lower than 1 for all fluids, this indicates a pseudoplastic fluid behaviour.

**Table 6.5:** Rheological modelling summary of all parameters of the lignosulfonates treated water-based fluid systems

Model		Ref	Ref + 0.9 g LS	Ref + 2.0 g LS
<b>Herschel-Bulkley</b>	$\tau_0$	16.23	6.554	2.712
	% deviation		-59.62	-83.29
	k	0.2576	0.1151	0.1854
	% deviation		-55.32	-28.03
	n	0.7352	0.8215	0.7609
	% deviation		11.73	3.50
<b>Unified</b>				
<b>Unified</b>	$\tau_y$	16.54	6.402	2.134
	% deviation		-61.29	-87.10
	k	0.1547	0.1634	0.4086
	% deviation		5.62	164.1
	n	0.8164	0.7655	0.6363
	% deviation		-6.23	-22.06
<b>Power Law</b>				
<b>Power Law</b>	k	11.31	3.711	1.436
	% deviation		-67.19	-87.30
	n	0.2101	0.3098	0.4490
	% deviation		47.45	113.7
<b>Bingham Plastic</b>				
<b>Bingham Plastic</b>	$\tau_y$	19.78	7.926	3.786
	% deviation		-59.92	-80.86
	$\mu_p$	0.0372	0.0329	0.0385
	% deviation		-11.56	3.49
<b>Robertson-Stiff</b>				
<b>Robertson-Stiff</b>	A	3.408	0.3573	0.2241
	% deviation		-89.52	-93.42
	C	52.52	78.58	35.00
	% deviation		49.62	-33.36
	B	0.3954	0.6719	0.7420
	% deviation		69.93	87.65

## 6.1.2 Rheological Modelling for Oil-Based Drilling Fluids

### 6.1.2.1 Curve Fitting for Oil-Based Drilling Fluids

The same procedure for rheological model fitting was performed for the oil-based drilling fluids. Firstly, by comparing the rheological measured data and the calculated model values for the fluids provided by M-I Swaco, it was identified that *Herschel-Bulkley* describes these fluids best. *Herschel-Bulkley* had an average deviation of 2.33%, while *Robertson-Stiff* and *Unified* had average deviations of 2.62% and 3.01%, respectively. Further, for the EDC 90/10 oil-based drilling fluids formulated at the university laboratory, the *Robertson-Stiff* rheological model provided the best match for the measured data. This illustrates the importance of evaluating all rheological models for all fluids, as each fluid behaves differently, and just small modifications could be enough to change which model provides the best match and best describes the behaviour of the fluid.

Further, the same rheological modelling, as performed above for the water-based drilling fluid systems, will be performed on the EDC 90/10 oil-based drilling fluids in order to analyze the effect of added poly acrylic on the rheological parameters. The average values of the curve fitting performed above is conducted using data from measurements at both 22°C, 50°C, 80°C and 100°C, thus exhibiting a different result than what is found from the rheological modelling based on only data from the 22°C measurements.

### 6.1.2.2 EDC 90/10 Reference Fluid System

Trend-lines for all the various rheological models for the EDC 90/10 reference fluid are illustrated in figure 6.6, while table 6.6 presents the corresponding parameters and equations.

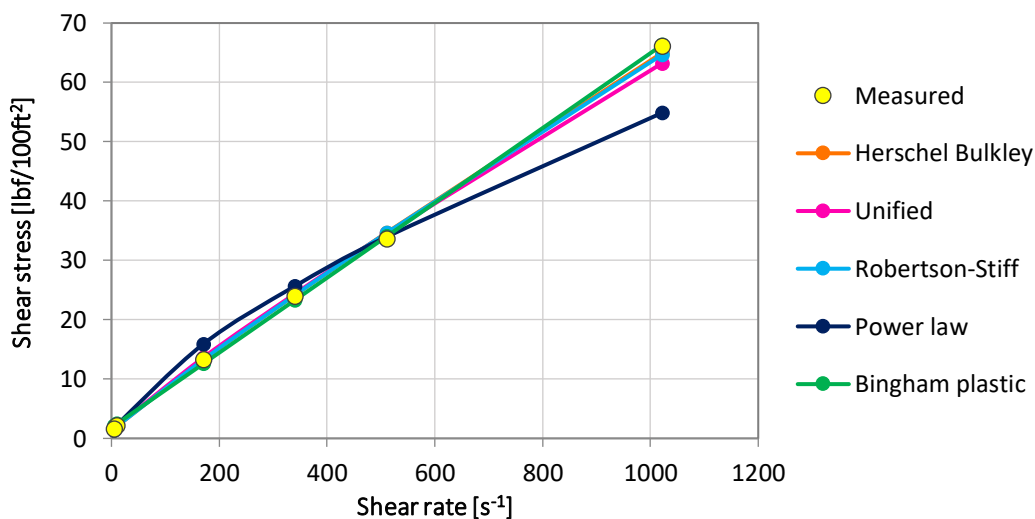


Figure 6.6: Trend-lines from rheological modelling of the EDC 90/10 reference fluid system at fluid temperature of 22°C

Model	Equation	Parameters				% Deviation	cP
		$\tau_0, \tau_y, A$	$k, C$	$n, B$	$\mu_p, \mu$		
Herschel-Bulkley	$1.167 + 0.1025 \cdot \gamma^{0.9285}$	1.167	0.1025	0.9285		2.02	
Unified	$1.067 + 0.1277 \cdot \gamma^{0.8930}$	1.067	0.1277	0.8930		2.34	
Power Law	$0.4554 \cdot \gamma^{0.6915}$		0.4554	0.6915		10.5	
Bingham	$0.0631 \cdot \gamma + 1.827$	1.827			0.0631	10.1	17.81
Robertson-Stiff	$0.1099 \cdot (14.0 + \gamma)^{0.9186}$	0.1099	14.00	0.9186		2.27	

**Table 6.6:** Modelled parameters and equations for the EDC 90/10 fluid system at fluid temperature of 22°C

For the EDC 90/10 reference system, the largest percentage deviation is given by the Power Law model and the Bingham model, both with deviations slightly above 10%. All of the other models deviate with values below 2.50%. However, the Herschel-Bulkley model yield the lowest deviation with its 2.02% and is therefore the model most suitable for describing the EDC 90/10 reference system.

### 6.1.2.3 EDC 90/10 + 0.5 gram Poly Acrylic Fluid System

All the trend-lines for the various rheological models for the EDC 90/10 + 0.5 g poly acrylic fluid are illustrated in figure 6.7, while the corresponding parameters and equations are given in table 6.7.

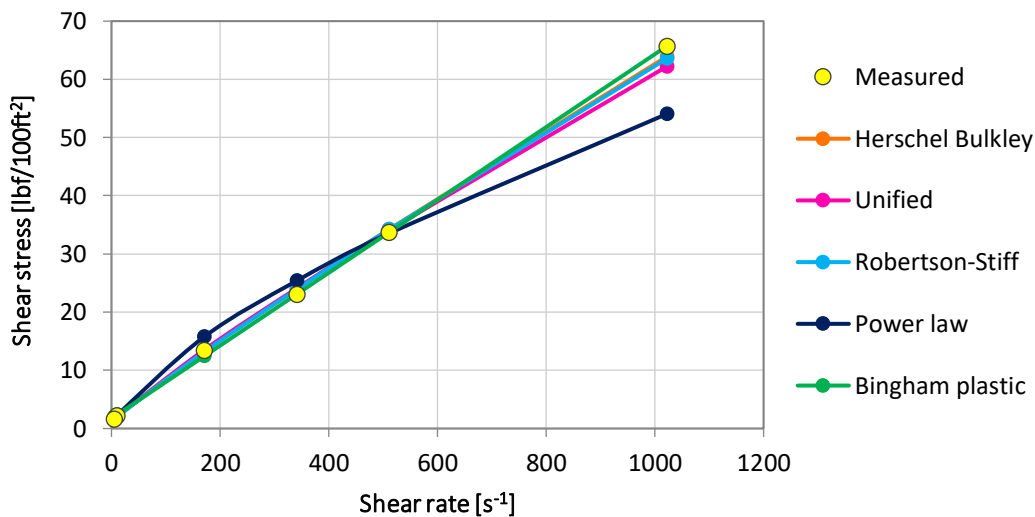


**Figure 6.7:** Trend-lines from rheological modelling of the EDC 90/10 + 0.5 g poly acrylic fluid system at fluid temp. of 22°C

Model	Equation	Parameters				% Deviation	cP
		$\tau_0, \tau_y, A$	k, C	n, B	$\mu_p, \mu$		
Herschel-Bulkley	$1.163 + 0.1041 \cdot \gamma^{0.9238}$	1.163	0.1041	0.9238		2.64	
Unified	$1.067 + 0.1283 \cdot \gamma^{0.8899}$	1.067	0.1283	0.8899		2.64	
Power Law	$0.4576 \cdot \gamma^{0.6886}$		0.4576	0.6886		10.8	
Bingham	$0.0626 \cdot \gamma + 1.726$	1.726			0.0626	7.78	29.97
Robertson-Stiff	$0.1129 \cdot (13.8 + \gamma)^{0.9122}$	0.1129	13.80	0.9122		2.89	

**Table 6.7:** Modelled parameters and equations for EDC 90/10 + 0.5 g poly acrylic fluid system at fluid temp. of 22°C

As seen from **table 6.7**, the Power Law model yields the largest percentage deviation for the EDC 90/10 + 0.5 g poly acrylic fluid system, with its 10.8%. The Bingham model does account for the yield stress, but as the model is linear, it still deviates with 7.78%. Both the Herschel-Bulkley model and the Unified model has deviations of 2.64%, indicating that both of the models can be used to describe the EDC 90/10 + 0.5 g poly acrylic fluid system.

#### 6.1.2.4 EDC 90/10 + 1.0 g Poly Acrylic Fluid System

Trend-lines for all the various rheological models for the EDC 90/10 + 1.0 g poly acrylic fluid are illustrated in **figure 6.8**, while **table 6.8** presents the corresponding parameters and equations.

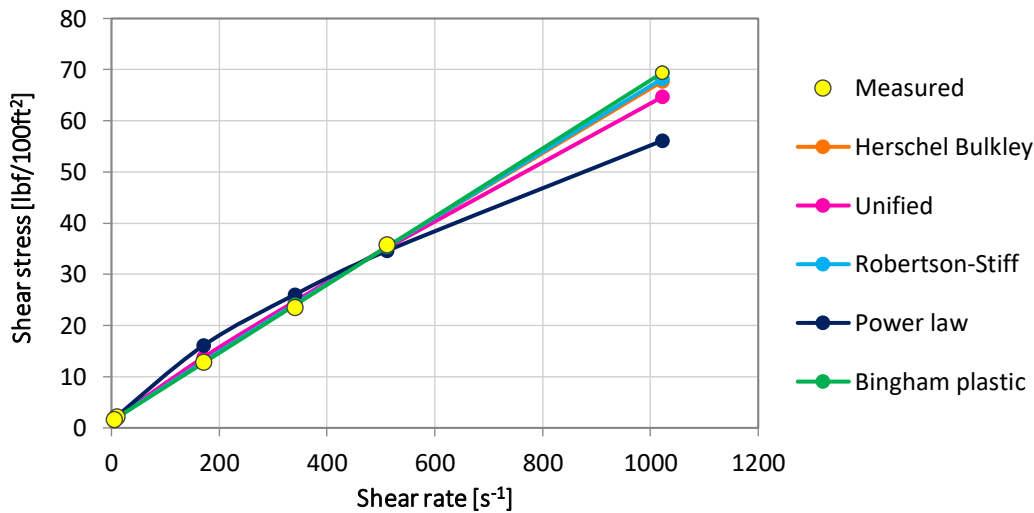


**Figure 6.8:** Trend-lines from rheological modelling of the EDC 90/10 + 1.0 g poly acrylic fluid system at fluid temp. of 22°C

Model	Equation	Parameters				% Deviation	cP
		$\tau_0, \tau_\gamma, A$	k, C	n, B	$\mu_p, \mu$		
Herschel-Bulkley	$1.227 + 0.0856 \cdot \gamma^{0.9604}$	1.227	0.0856	0.9604		2.85	
Unified	$1.067 + 0.1247 \cdot \gamma^{0.8997}$	1.067	0.1247	0.8997		4.06	
Power Law	$0.4449 \cdot \gamma^{0.6981}$		0.4449	0.6981		12.9	
Bingham	$0.0666 \cdot \gamma + 1.328$	1.328			0.0666	2.43	31.89
Robertson-Stiff	$0.0795 \cdot (17.7 + \gamma)^{0.9724}$	0.0795	17.70	0.9724		2.66	

**Table 6.8:** Modelled parameters and equations for EDC 90/10 + 1.0 g poly acrylic fluid system at fluid temp. of 22°C

The EDC 90/10 + 1.0 g poly acrylic fluid system is actually best described by the Bingham Plastic model, as the model yield the lowest percentage deviation of 2.43%. The Power Law model continues to increase in deviation as a function of added poly acrylic and is by far the model with the highest deviation with its 12.9%. Further, it is observed from **table 6.8** that both the Herschel-Bulkley and the Robertson-Stiff model provides good approximations to the measured data, with 2.85% and 2.66% deviation respectively.

#### 6.1.2.5 EDC 90/10 + 1.5 g Poly Acrylic Fluid System

All the trend-lines for the various rheological models for the EDC 90/10 + 1.5 g poly acrylic are illustrated in **figure 6.9**, while the corresponding parameters and equations are given in **table 6.9**.

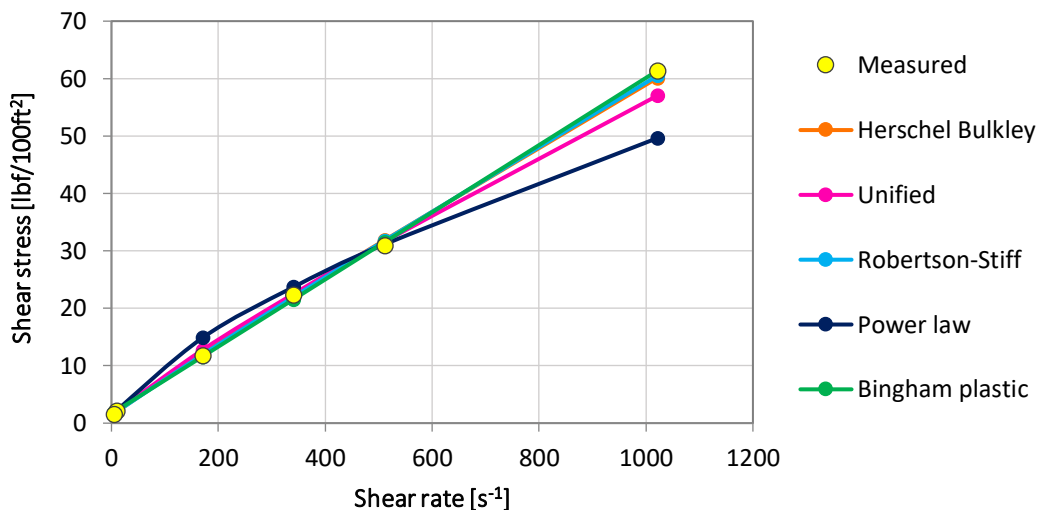


**Figure 6.9:** Trend-lines from rheological modelling of the EDC 90/10 + 1.5 g poly acrylic fluid system at fluid temp. of 22°C



Model	Equation	Parameters				% Deviation	cP
		$\tau_0, \tau_\gamma, A$	k, C	n, B	$\mu_p, \mu$		
Herschel-Bulkley	$1.247 + 0.0852 \cdot \gamma^{0.9436}$	1.247	0.0852	0.9436		2.97	
Unified	$1.067 + 0.1311 \cdot \gamma^{0.8741}$	1.067	0.1311	0.8741		3.70	
Power Law	$0.4675 \cdot \gamma^{0.6733}$		0.4675	0.6733		11.5	
Bingham	$0.0585 \cdot \gamma + 1.629$	1.629			0.0585	5.30	28.01
Robertson-Stiff	$0.0801 \cdot (19.2 + \gamma)^{0.9539}$	0.0801	19.20	0.9539		3.02	

**Table 6.9:** Modelled parameters and equations for EDC 90/10 + 1.5 g poly acrylic fluid system at fluid temp. of 22°C

Lastly, for the EDC 90/10 + 1.5 g poly acrylic the Herschel-Bulkley model is found to provide the best match to the measured data, with a percentage deviation of 2.97%. The Power Law model yield the largest percentage deviation with its 11.5%. Further, it is observed that the Herschel-Bulkley, Unified and the Robertson-Stiff model provides the lowest deviations, as was the general trend observed for all the fluids.

#### 6.1.2.6 EDC 90/10 Rheological Modelling Summary and Comparison

**Table 6.10** presents a summary indicating which rheological model is best suited for each of the fluid systems, also presenting the equation for the corresponding models.

**Table 6.10:** Rheological model summary for EDC 90/10 fluid systems treated with poly acrylic

Fluid	Model	Equation
EDC 90/10	Herschel-Bulkley	$1.167 + 0.1025 \cdot \gamma^{0.9285}$
EDC 90/10 + 0.5 g poly acrylic	Herschel-Bulkley	$1.163 + 0.1041 \cdot \gamma^{0.9238}$
EDC 90/10 + 1.0 g poly acrylic	Bingham Plastic	$0.0666 \cdot \gamma + 1.328$
EDC 90/10 + 1.5 g poly acrylic	Herschel-Bulkley	$1.247 + 0.0852 \cdot \gamma^{0.9436}$

As observed from **table 6.10**, the Herschel-Bulkley model is the most suitable model for three of the fluid systems tested at a fluid temperature of 22°C. This result is likely, as the Herschel-Bulkley model is well known to provide a suitable description of drilling fluids. Further, a summary of all the calculated parameters and their percentage deviations from the reference fluid are given in **table 6.11**.

**Table 6.11:** Rheological modelling summary of all parameters of the poly acrylic treated EDC 90/10 fluid systems

Model		EDC 90/10	EDC 90/10 + 0.5 g poly acrylic	EDC 90/10 + 1.0 g poly acrylic	EDC 90/10 + 1.5 g poly acrylic
<b>Herschel-Bulkley</b>	$\tau_0$	1.167	1.163	1.227	1.247
	% deviation		-0.34	5.14	6.86
	<b>k</b>	0.1025	0.1041	0.0856	0.0852
	% deviation		1.56	-16.5	16.9
	<b>n</b>	0.9285	0.9238	0.9604	0.9436
	% deviation		-0.51	3.43	1.63
<b>Unified</b>	$\tau_y$	1.067	1.067	1.067	1.067
	% deviation		0.0	0.0	0.0
	<b>k</b>	0.1277	0.1283	0.1247	0.1311
	% deviation		0.47	-2.35	2.66
	<b>n</b>	0.8930	0.8899	0.8997	0.8741
	% deviation		-0.35	0.75	-2.12
<b>Power Law</b>	<b>k</b>	0.4554	0.4576	0.4449	0.4675
	% deviation		0.48	-2.30	2.66
	<b>n</b>	0.6915	0.6886	0.6981	0.6733
	% deviation		-0.42	0.95	-2.63
<b>Bingham Plastic</b>	$\tau_y$	1.827	1.726	1.328	1.629
	% deviation		-5.53	-27.3	-10.8
	$\mu_p$	0.0631	0.0626	0.0666	0.0585
	% deviation		-0.79	5.55	-7.29
<b>Robertson-Stiff</b>	<b>A</b>	0.1099	0.1129	0.0795	0.0801
	% deviation		2.73	-27.7	-27.1
	<b>C</b>	14.0	13.80	17.70	19.2
	% deviation		-1.43	26.4	37.1
	<b>B</b>	0.9186	0.9122	0.9724	0.9539
	% deviation		-0.70	5.86	3.84

Based on the data given in **table 6.11**, following trends and/or observations were made:

### **Herschel-Bulkley model**

The yield stress,  $\tau_0$ , is reduced for the EDC 90/10 + 0.5 g poly acrylic fluid with 0.34% relative to the EDC 90/10 reference fluid. However, for both the 1.0 gram fluid and 1.5 grams fluid, the yield stress value increased, with 5.14% and 6.86% respectively. This indicates that the addition of 0.5 gram of poly acrylic reduces the internal frictional resistance in the fluid system, while the addition of 1.0gram and 1.5 grams increases the flow resistance. In terms of the consistency index, it is increased for the 0.5 gram and 1.5 grams fluid, while it is decreased by 16.5 for the 1.0 gram fluid system.

### **Unified model**

The low shear yield stress is constant for all the fluids, with 0% deviation. The consistency index,  $k$ , increased for both the 0.5 gram and the 1.5 grams fluids, but decreased for the 1.0 gram fluid. The flow behaviour index,  $n$ , behaves completely opposite of the consistency index, decreasing for the 0.5 gram and 1.5 grams fluids and increasing for the 1.0 gram fluid. As all the  $n$ -values are lower than 1, this indicates that the fluids behave like pseudoplastic fluids.

### **Power Law model**

A similar trend as for the Unified model is identified for the Power Law model, with increasing consistency index and decreasing flow behaviour index for the 0.5 gram and 1.5 grams fluids and decreasing  $k$ -value and increasing  $n$ -value for the 1.0 gram fluid. The  $n$ -values are low when compared to the Herschel-Bulkley model and the Unified model.

### **Bingham model**

For the Bingham model, the yield stress decreases for all the fluid systems treated with poly acrylic. The yield stress of the EDC 90/10 + 0.5 g poly acrylic fluid exhibits the lowest percentage reduction with 5.53%. This indicates that the flow resistance is reduced for all poly acrylic modified fluid systems. For the plastic viscosity, the value is reduced for the 0.5 gram fluid and the 1.5 grams fluid and increased for the EDC 90/10 + 1.0 g poly acrylic fluid.

### **Robertson-Stiff model**

The A-parameter, corresponding to the  $k$ -value for other models, is increased for the 0.5 gram fluid system and reduced for the 1.0 gram fluid and 1.5 grams fluid, while the B-parameter, corresponding to the  $n$ -value, is decreased for the 0.5 gram fluid and increased for the 1.0 gram and 1.5 grams fluid. As the B-parameter is lower than 1 for all fluids, this indicates a pseudoplastic behaviour.

## 6.2 Simulation-Well Arrangement for Hydraulic Performance

For the hydraulics simulations, an 8.5-inch, vertical wellbore of 10 000 feet was used. This simulation-well is illustrated in **figure 6.10**, also depicting the mud pump and the mud pit. The drill string inside the wellbore has an outer diameter of 5-inch and a 4.8-inch inner diameter, which is typical drill string dimensions for drilling of an 8.5-inch hole. The simulation considers that the surface pressure is equal to zero, as the pump discharge line is connected to the top of the drill string. Further, it is assumed that the drill bit has three 28/32-inch nozzles. For the simulations, the hydraulic performance was studied at flow rates varying from 100 to 600 gallons per minute (GPM), with an increment of 50 GPM for each simulation.

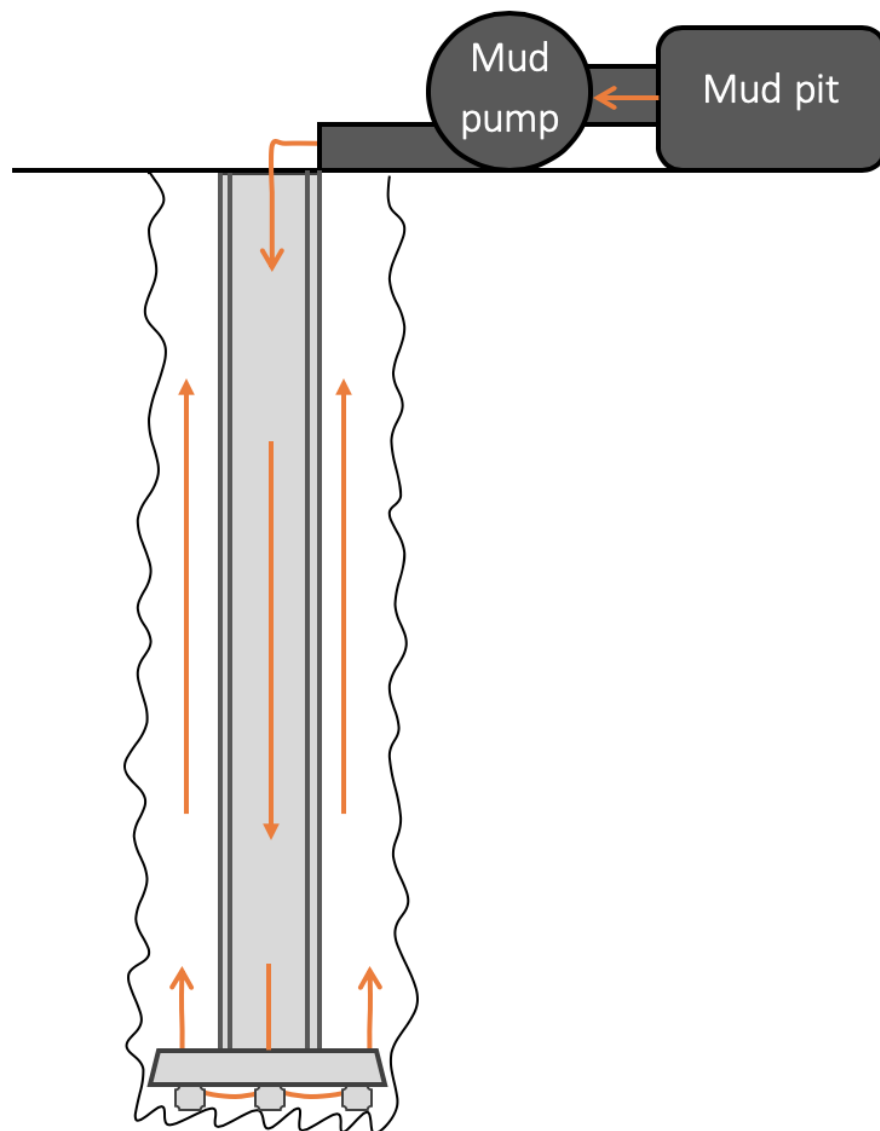


**Figure 6.10:** Illustration of the simulation-well used for the ECD and pump pressure simulations

### 6.3 Pump Pressure Simulations

The pump pressure required to pump fluid through a hydraulic system of a well is equal to the sum of the total frictional pressure drop in the whole system. The simulations performed in this thesis were performed based on the use of constant fluid densities, with  $\rho_{WBM} = 1.35$  SG,  $\rho_{OBM, M-I Swaco} = 1.50$  SG and  $\rho_{OBM, EDC} = 1.75$  SG. Additionally, the wellbore was assumed to be free of cuttings and that no rotation is applied to the drill string. These simplifications are acceptable, as the sole purpose of the simulations were to compare the hydraulic performance of the fluids relative to each other.

#### 6.3.1 Pump Pressure for Water-Based Drilling Fluids

Figure 6.11 shows the simulated pump pressure required for the reference fluid, and additionally, Ref + 0.9 g LS and Ref + 2.0 g LS, at both 22°C and 80°C. The simulation results show a relatively small change in pump pressure for the reference fluid as the fluid temperature is increased. However, the change is larger than for both of the poly acrylic fluids up to 300 GPM.

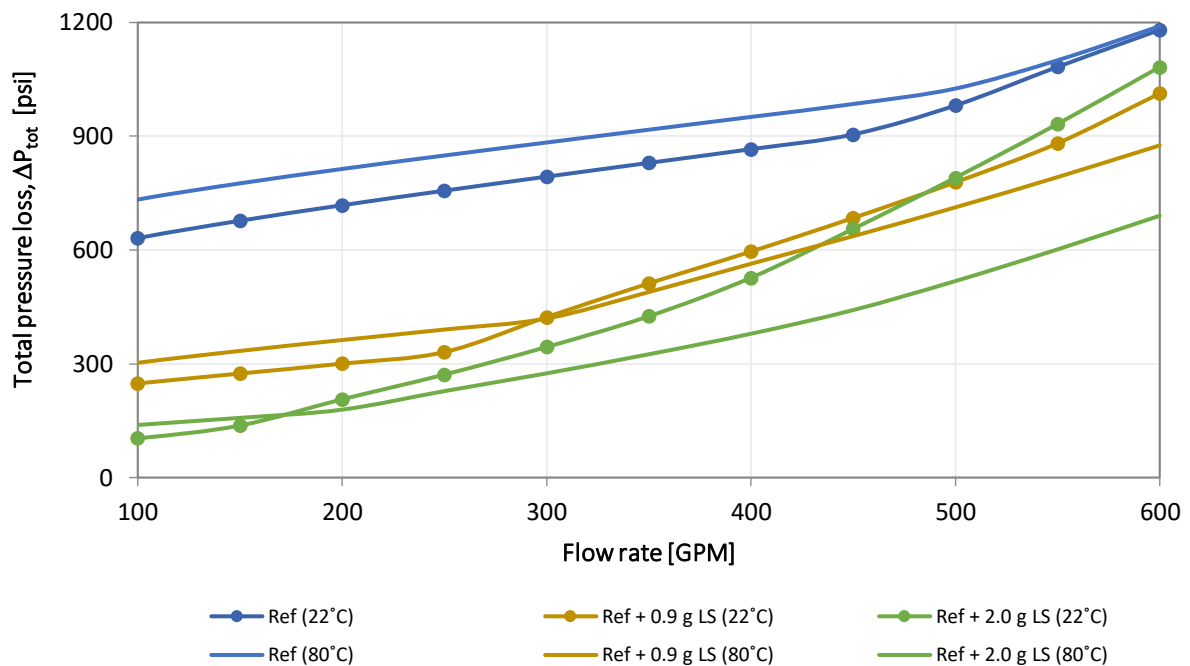


Figure 6.11: Total pressure drop as a function of flow rate for selected water-based drilling fluid systems

The extreme case of 2.0 grams of added lignosulfonates exhibit very similar pressure drop at both temperatures for flow rates up to 200 GPM, from this point on the difference in pressure drop starts to increase and continues to increase until the flow rate reaches 600 GPM. This is clearly indicated in figure 6.12, where the pressure difference is plotted against the flow rate. Further, it is indicated that for the best system, Ref + 0.9 g LS, the pump pressure exhibits the best performance of the three fluids up to 450 GPM. From this point on there is recorded an increase in pressure difference as the flow rate is

approaching 600 GPM. For the reference fluid, the pump pressure difference is quite stable, and the graph in figure 6.12 indicates that the difference decreases as the flow rate increases. These results support previous outcomes that indicated that the Ref + 0.9 g LS fluid exhibited stable performance as a function of increased temperature.

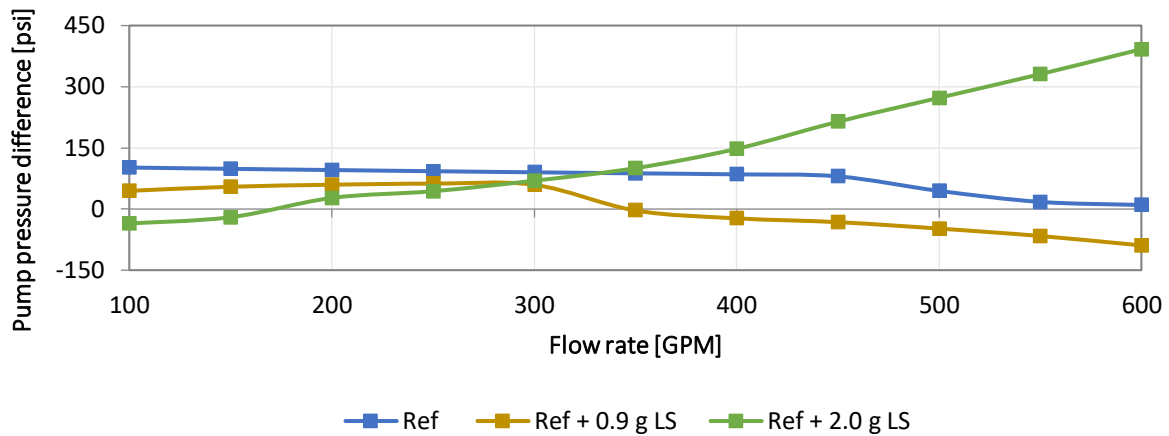


Figure 6.12: Pump pressure difference between the WBM fluids at different fluid temperatures

### 6.3.2 Pump Pressure for Oil-Based Drilling Fluids

#### 6.3.2.1 Simulated Pump Pressure for M-I Swaco Fluids

For this simulation, M-I Swaco oil-based fluids have been compared to the One-Mul-modified versions of the same fluids with the same OWR. All these simulations are based on rheological measurements performed at fluid temperature of 100°C. From figure 6.13, one can see that both 60/40 and the 80/20 fluid exhibit similar pressure loss before and after modification with One-Mul. However, for the 70/30 fluid, the pressure loss difference is quite large for flow rates in the region of 100-300 GPM.

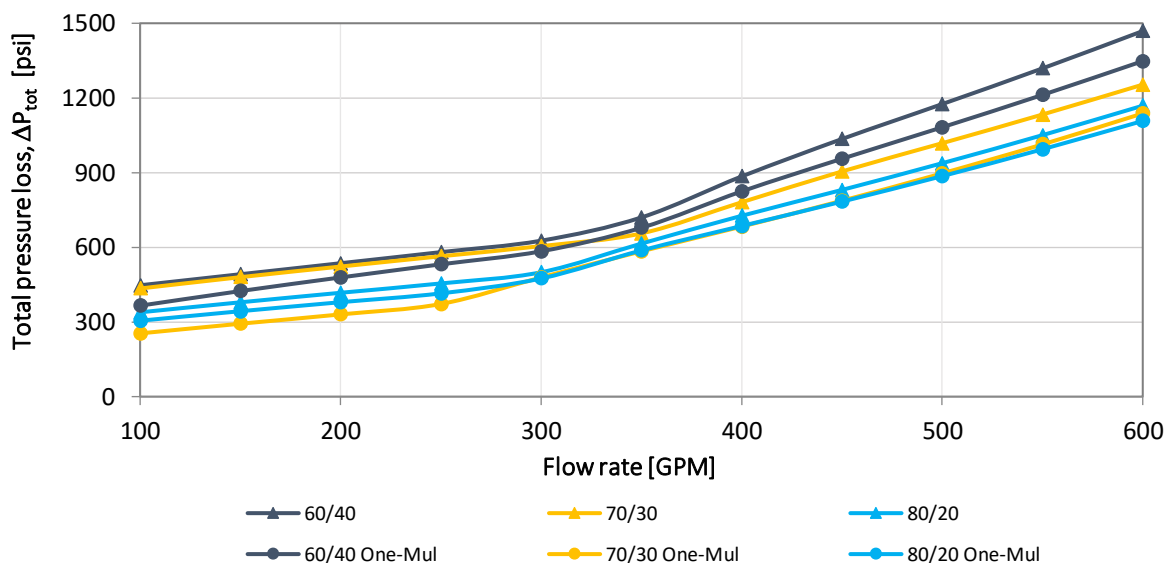
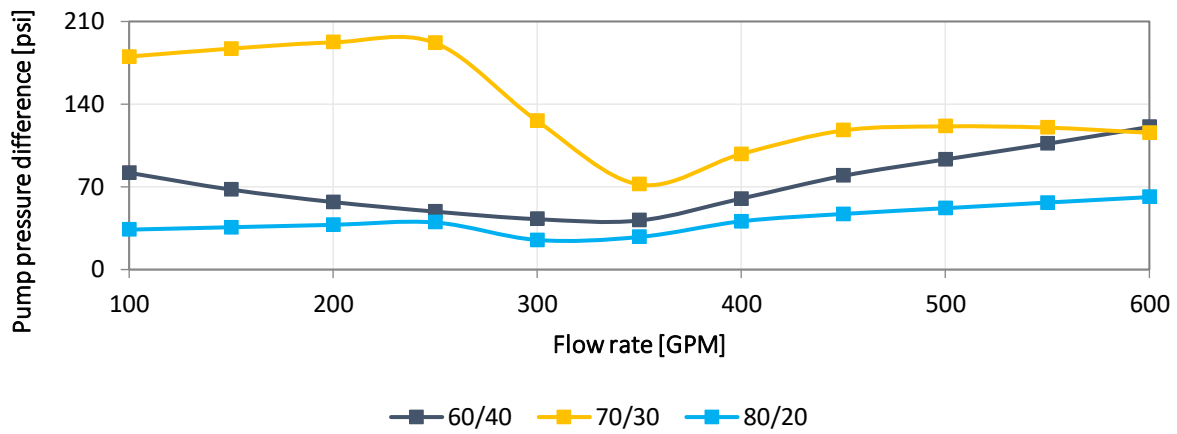


Figure 6.13: Total pressure drop at various flow rates for M-I Swaco reference and modified fluids at 100°C

As indicated in **figure 6.14**, the pump pressure difference is as large as 190 psi for the 70/30 fluid at lower flow rates, while the largest pressure difference for the 60/40 and 80/20 fluid is 120 psi and 60 psi, respectively. This indicates that the 70/30 fluid is most sensitive to rheological modifications in terms of hydraulic performance, while the 60/40 and 80/20 fluids are less affected by the same modifications.



**Figure 6.14:** Pump pressure difference between reference and modified version of various oil-water-ratio fluids

### 6.3.2.2 Simulated Pump Pressure for Fluids Formulated at UiS

The simulations were also performed on the EDC 90/10 reference fluid and the EDC 90/10 + 0.5 g poly acrylic, at both 22°C and 100°C. The pump pressure results are given in **figure 6.15** below. As the figure illustrates, the pump pressure at both temperatures for both fluids are approximately the same. The trend for both fluids is that the total pressure loss is reduced as the fluid temperature increases.

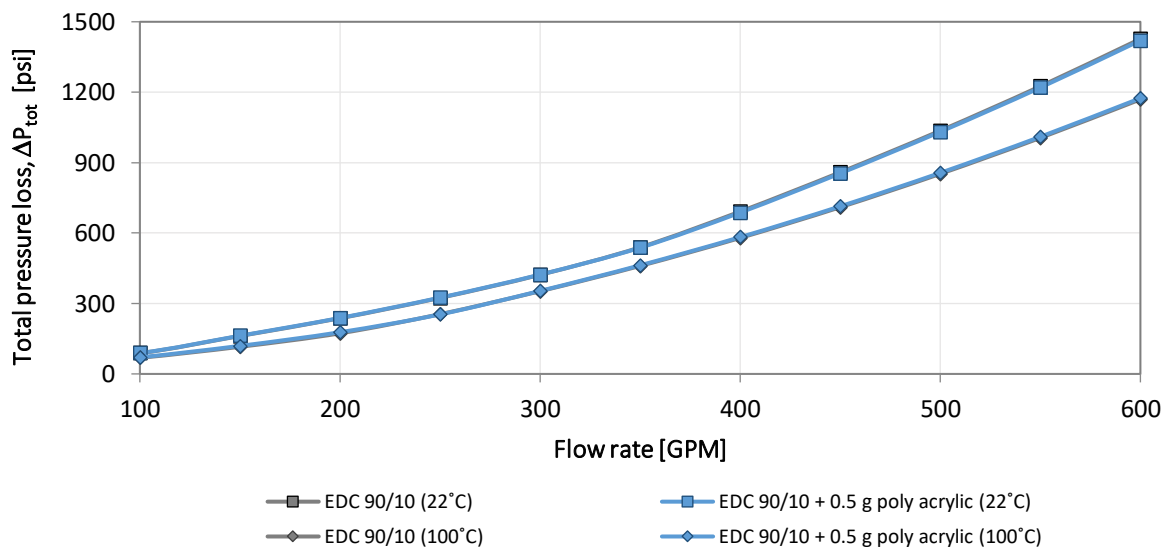


**Figure 6.15:** Pump pressure for EDC 90/10 and EDC 90/10 + 0.5 g poly acrylic at two temperatures

To illustrate the difference between the two fluids, at the same temperature, the pump pressure difference between each fluid at both temperatures is plotted vs. flow rate in figure 6.16. As read from the graph, the maximum pump pressure deviation between the two fluids is recorded as approximately 7 psi at the flow rate of 600 GPM, indicating that the pump pressure requirements are almost identical before and after modification.

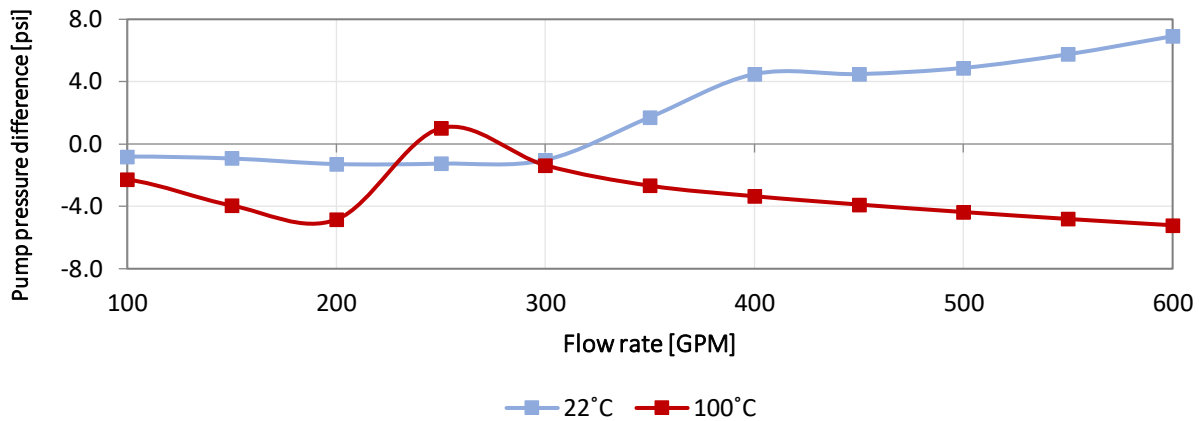


Figure 6.16: Pump pressure difference, in psi, between the two EDC 90/10 fluids at the same temperature



## 6.4 ECD Simulations

The ECD values are determined by utilizing the simulated annular pressure drop and calculated by the use of equation 3.43 given in Chapter 3.5.1. Furthermore, the ECD simulations are based on the same assumptions as the pump pressure simulations, with constant densities, no cuttings in the wellbore and no drill pipe rotation.

### 6.4.1 ECD Simulations for Water-Based Drilling Fluids

For the water-based drilling fluids the ECD was simulated at various flow rates for both 22°C and 80°C. The results, presented in figure 6.17 below, shows that both the reference fluid and Ref + 0.9 g LS exhibit ECDs that are relatively similar for different temperatures. However, the Ref + 2.0 g LS fluid have very similar ECD up to approximately 400 GPM. From this point on, the difference in ECD increases almost linearly, but at different rates for the Ref + 2.0 g LS fluid at the two different temperatures.

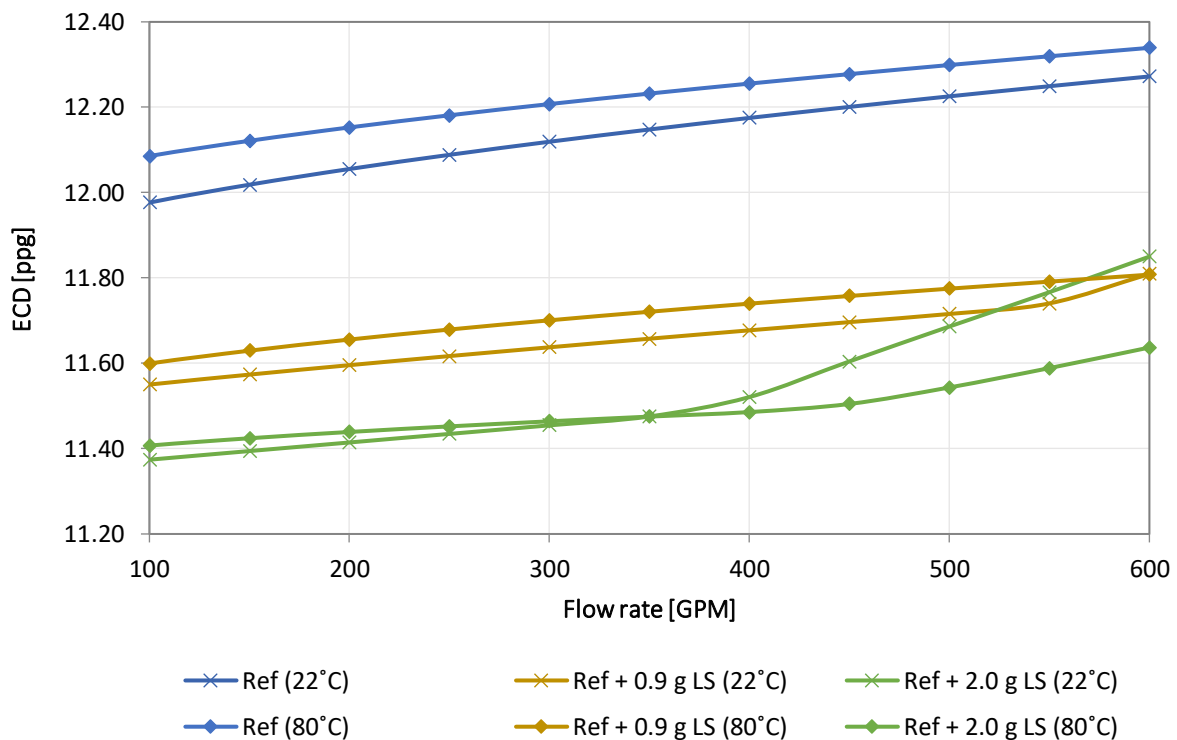


Figure 6.17: Simulated ECD for lignosulfonates containing WBMs at two different temperatures

Further, in figure 6.18, the ECDs are compared relative to each other, where the percentage deviation between the ECD for the two different temperatures is plotted against flow rate. These results show that the Ref + 0.9 g LS fluid has the smallest, most consistent deviation, while Ref + 2.0 g LS has an increasing deviation with increasing flow rate. The average deviation is equal to 0.73%, 0.45% and 0.58% for Ref, Ref + 0.9 g LS and Ref + 2.0 g LS, respectively.

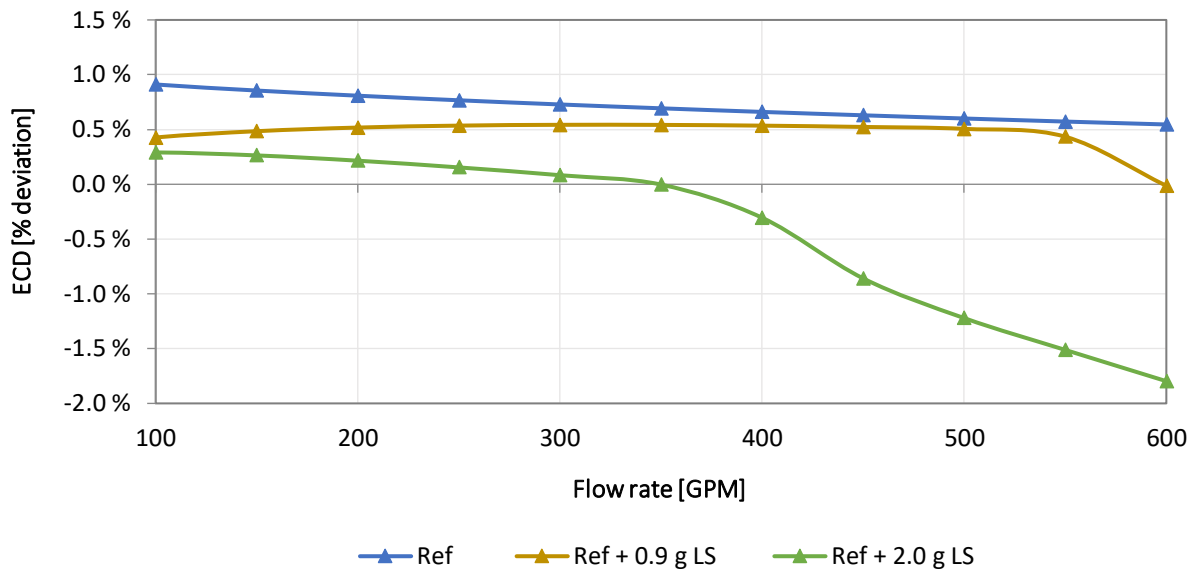


Figure 6.18: ECD percentage deviation for each fluid between the 22°C and the 80°C simulation

## 6.4.2 ECD Simulations for Oil-Based Drilling Fluids

### 6.4.2.1 Simulated ECD for M-I Swaco Fluids

The ECD simulation performed by the use of the M-I Swaco fluids were done solely at fluid temperature of 100°C, in order to analyse the effect of added One-Mul on the equivalent circulation density. As read from the graph in figure 6.19, the difference in ECD for the 70/30 and 70/30 One-Mul fluids is quite large compared to the other two fluids, which again indicates that the 70/30 fluid is more sensitive to rheological modifications. For the 60/40 fluid, the ECDs for the two fluid variations approaches each other as the flow rate increases.

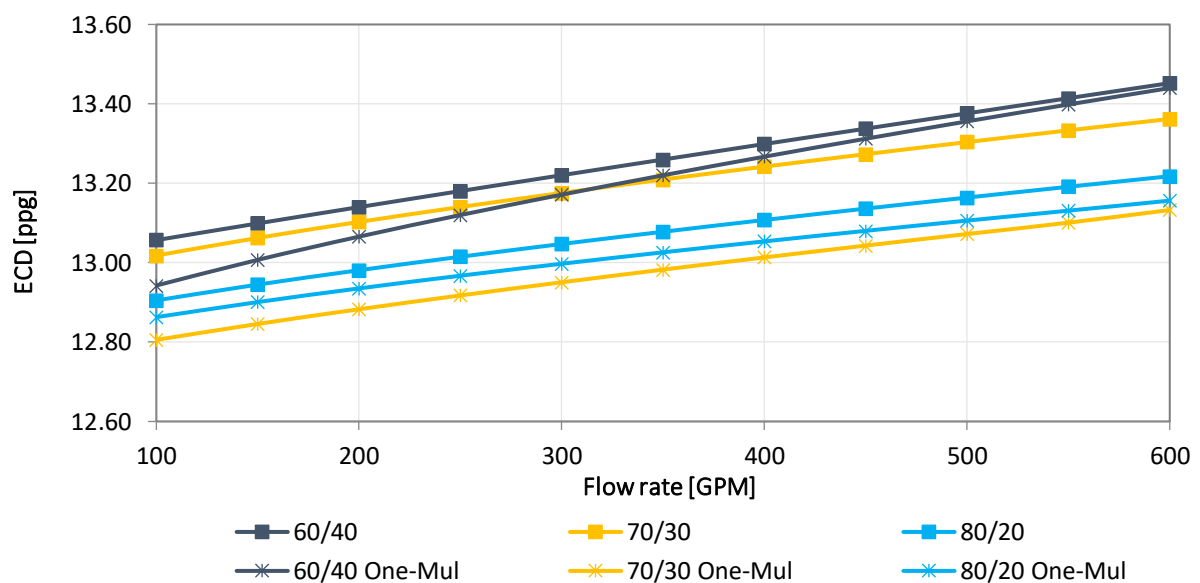


Figure 6.19: Simulated ECD at various flow rates for M-I Swaco reference and modified fluids at 100°C

The percentage ECD difference between the initial fluids and the One-Mul modified fluids are presented in figure 6.20. The figure indicates that the ECD difference for the 80/20 and 70/30 fluids are almost constant for all flow rates, while the 60/40 ECD difference decreases with increasing flow rate. The average deviation is equal to 0.37%, 1.7% and 0.40% for the 60/40, 70/30 and 80/20 fluids, respectively.

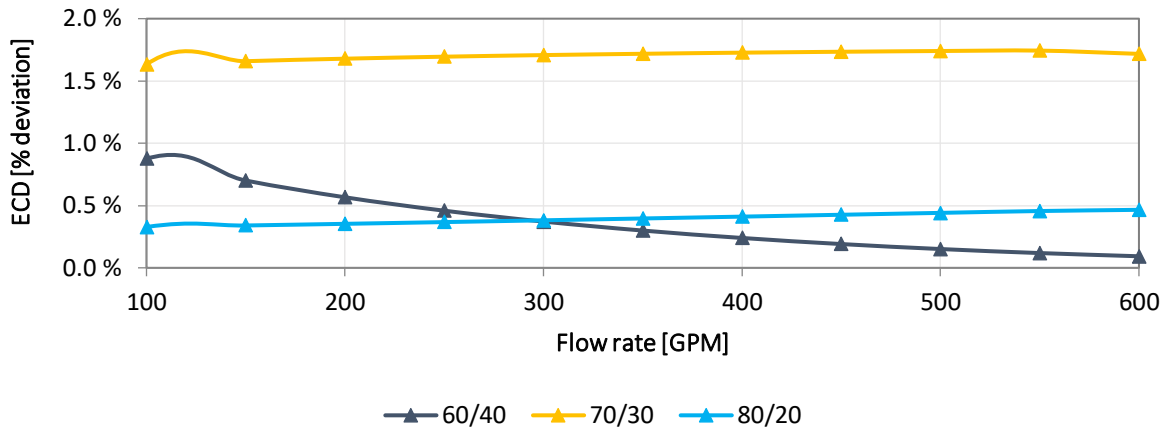


Figure 6.20: Percentage ECD difference between initial and modified fluids from M-I Swaco

#### 6.4.2.2 Simulated ECD for Fluids Formulated at UiS

For the UiS oil-based drilling fluids the ECD was simulated for flow rates varying from 100 to 600 GPM for both 22°C and 100°C, and the results are presented in figure 6.21. As read from the graph, the ECDs are very similar for both fluids. There is some difference in the equivalent circulation density as a function of temperature, but this difference is quite small.

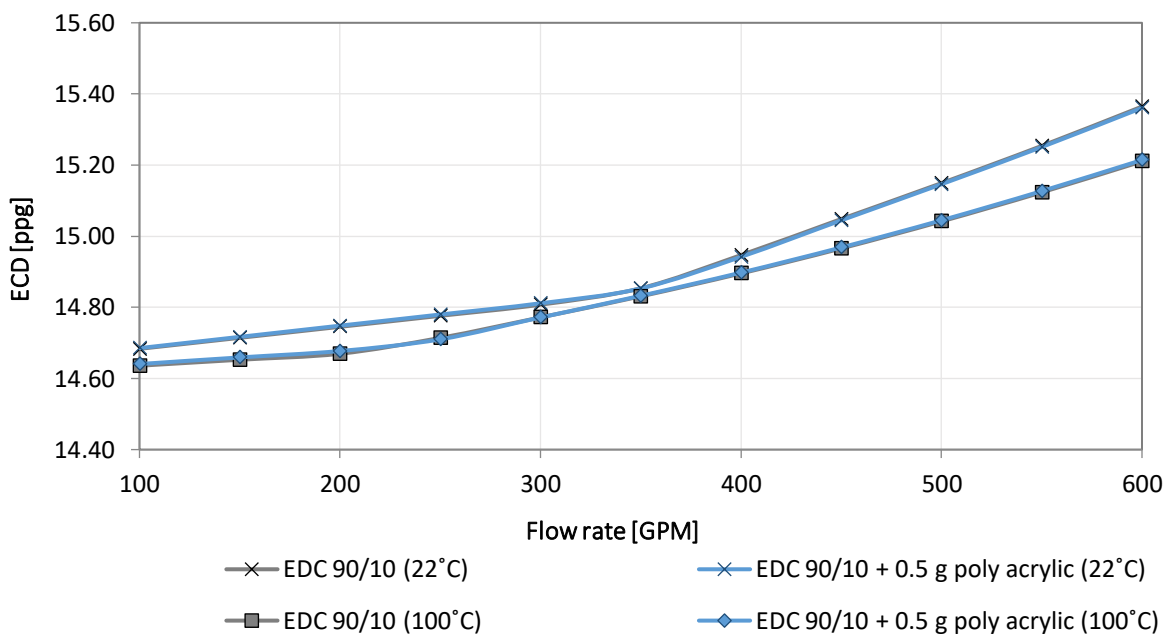


Figure 6.21: Simulated equivalent circulation density for EDC 90/10 drilling fluids at 22°C and 100°C

Figure 6.22 presents the percentage deviation between the ECD value simulated for the two different temperatures. The results show that the deviation is almost identical for the two fluids. EDC 90/10 reference fluid has a slightly higher average deviation of 0.48%, compared to 0.46% for the EDC 90/10 + 0.5 g poly acrylic fluid.

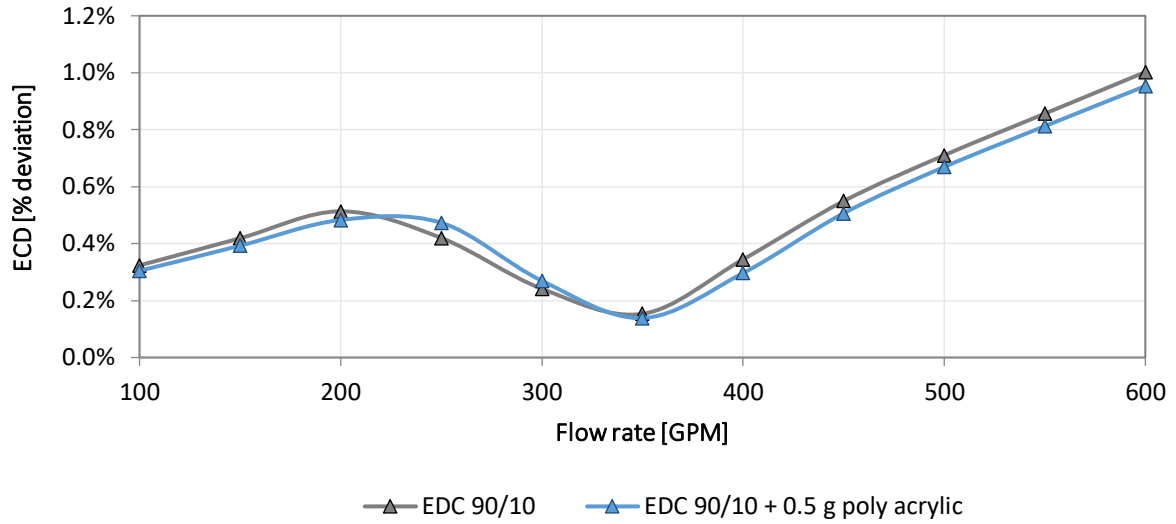


Figure 6.22: ECD percentage deviation between the 22°C and 100°C simulation for each of the two fluids

## 6.5 Torque & Drag Simulations

From the theory part, the importance of the torque and drag were emphasized, as values exceeding either the tensile limit or the torsional limit can result in a drill-string failure in the wellbore. Torque and drag are generally most critical in horizontal and deviated wells, as the drill-string is more prone to contact with the wellbore walls, resulting in a higher frictional resistance. A fluid with a lower coefficient of friction will provide better lubricity for the drill-string and the drill bit, potentially increasing the measured depth (MD) of drilling.

The torque and drag simulations were performed in order to evaluate the performance of the nanoparticles with regards to the drilling fluid's lubrication properties. For the torque and drag simulations, the following criteria were used to evaluate the frictional resistance in the system; effective tension, torque and stress trip out. The effective tension is plotted in **figure 6.23**, while the torque and stress trip out plots can be found in **APPENDIX D – FRICTION MEASUREMENT AND TORQUE & DRAG SIMULATIONS**.

Based on the results from the frictional tests of nano modified water-based fluids, addition of the MoS<sub>2</sub> nanoparticles reduced the coefficient of friction. By reducing the coefficient of friction, this will lubricate the drill-string and the drill-bit, which will cause a reduction in the torque and drag values.

### 6.5.1 Simulation Arrangement

All torque and drag simulations were performed in WellPlan™, which is a part of the Landmark software. The simulation well, illustrated in **Figure D.8** in appendix D, had a 13 3/8" casing with casing shoe at 4012.5 ft and a 12.615" deviated, open hole section. The depth of the open hole section was varied in order to investigate the maximum depth that was possible to drill by the use of different drilling fluids. For the reference fluid, the depth of the open hole section was determined to be 13 600 ft. The drill-pipe used in the simulations had a 5" OD and 4.86" ID. The rotation speed was set to 100 RPM, with tripping in and tripping out speed of 60 ft/min.

### 6.5.2 Torque and Drag Simulation Evaluation

For the simulations, the effective tension when tripping in and tripping out was found to be the limiting factors for the drill-string. From this point on, the depth of the wellbore, as well as the length of the drill-string, was continuously increased in order to investigate at which depth the tripping in or the tripping out curve would exceed the tensile limit. The depth at where one of the two curves exceeds the tensile limit curve, is determined to be the maximum measured drilling depth with that specific drilling fluid.

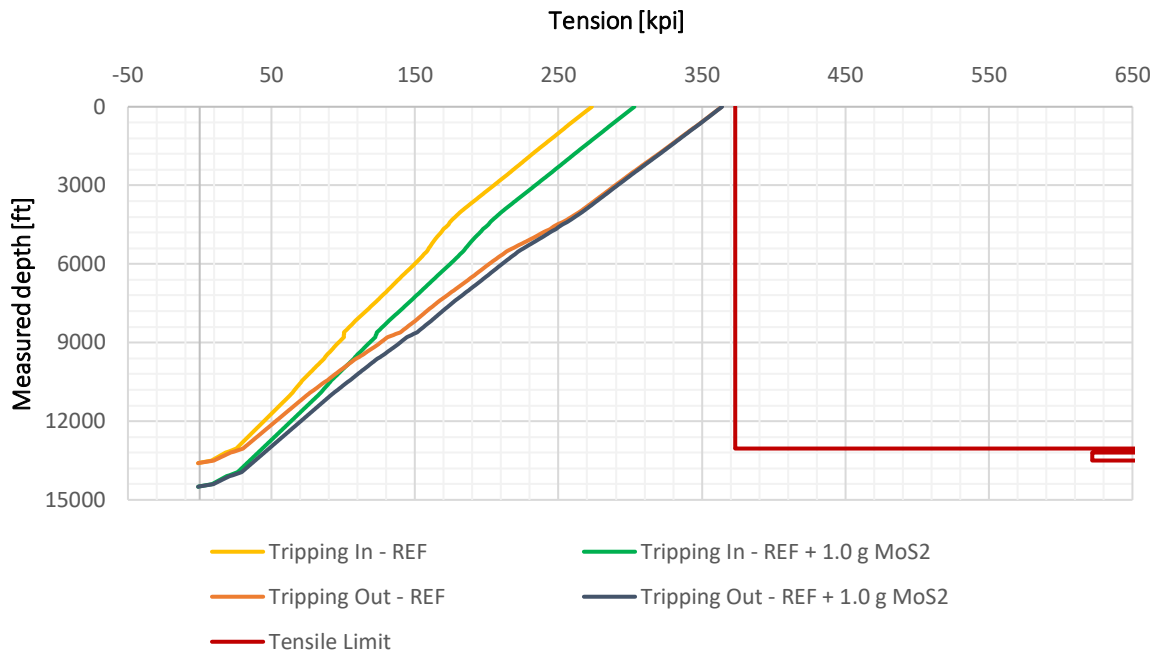


Figure 6.23: Drag chart for the Reference and the Reference + 1.0 g Molybdenum Disulphide fluids

Based on the findings from the drag chart in figure 6.23, the drill-string was able to drill down to 13 600 ft MD with both the reference fluid and nano modified fluid. However, 13 600 ft was found to be the maximum measured drilling depth for the reference fluid. If one drilled any further with the reference fluid, the tripping out curve would have exceeded the tensile limit causing a failure of the drill-string. When conducting extensive drill-string analysis with the REF + 1.0 g MoS<sub>2</sub> fluid, it was found that the measured depth limit was at 14 500 ft, as seen in figure 6.24. This indicates that the addition of 1.0 gram of molybdenum disulphide would increase the drill-string’s achievable measured drilling depth by 900 ft, or 6.62%, compared to drilling with the reference fluid.

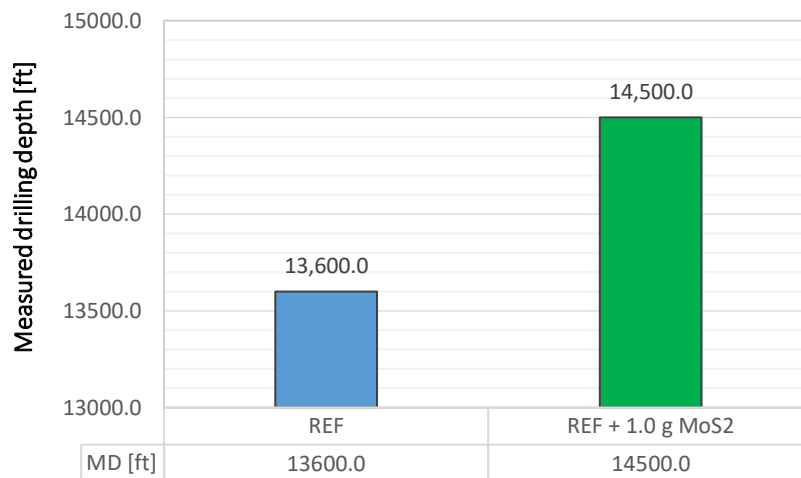


Figure 6.24: Maximum measured drilling depth

## 7 SUMMARY AND DISCUSSION

Chapter 7 summarizes the experimental work and the simulation studies. It presents one part summarizing the drilling fluid characterization, one part outlining the hydraulic performance and one section commenting on the measurement limitations and uncertainties.

### 7.1 Drilling Fluid Characterization

There are several ways of characterizing drilling fluids, but in this thesis the characterization of drilling fluids has been performed by the use of rheological measurements and viscoelastic, barite sag and friction testing. The rheological measurements were performed using an Ofite model 800, 8-speed viscometer and the fluids were tested at various temperatures in order to investigate the fluids' dependency of temperature in terms of fluid properties. The water-based fluids were measured at 22°C, 50°C and 80°C, while the oil-based fluids were additionally tested at 100°C.

The viscoelastic properties of the drilling fluids were investigated by the use of an Anton Paar MCR 302 rheometer, performing oscillatory amplitude and temperature sweep tests. The barite sag potential was evaluated by performing experiments in both static and dynamic environments. Lastly, torque & drag and pump pressure & ECD simulations were performed in order to evaluate the frictional and hydraulic performance of some selected drilling fluids. The hydraulic performance will be summarized and discussed in **Chapter 7.2**.

#### 7.1.1 Characterization of Flat Rheology Water-Based Drilling Fluids

The initial rheological measurements were performed to investigate the effect of lignosulfonates on water-based drilling fluid systems. As the results in **Figure 5.1** showed, the viscometer response decreased as a function of increased amount of added lignosulfonates. This behaviour was expected, as lignosulfonates is used as a disperser for clay particles, hence, decreasing the fluid viscosity.

However, the main reason lignosulfonates were added, was to analyze how the drilling fluid properties, in particular the yield stress, were affected as the fluid temperature was increased. As displayed in **Figure 5.2**, the yield stress became progressively more stable as the amount of added lignosulfonates increased. From the initial tests that were conducted with fluids containing 0.2-0.5 grams of added LS, and additionally one extreme case containing 2.0 grams LS, it was found that the fluid exhibiting the most stable and strongest yield stress most likely was somewhere in between 0.5 and 2.0 grams of added lignosulfonates.

Further, a fluid containing 1.0 gram of lignosulfonates was tested, in order to restrict the testing interval to be somewhere between 0.5 and 1.0 or 1.0 and 2.0 grams. From the results, displayed in **Figure 5.3**, it was found that the addition of 1.0 gram LS exhibited better yield stress values than 2.0 grams. Therefore, it was decided that the interval for additional testing was to be 0.6-0.9 gram of added lignosulfonates. Ultimately, the fluid containing 0.9 gram of added lignosulfonates exhibited the largest yield stress value, which also was stable as the temperature was increased. A summary of the yield stress values for some given fluids are presented in **table 7.1** below.

**Table 7.1:** Calculated yield stress values, based on Robertson-Stiff model, for given lignosulfonates WBM

Fluid temperature	Ref	Ref + 0.9 g LS	Ref + 1.0 g LS	Ref + 2.0 g LS
22°C	16.3	6.71	6.04	3.13
50°C	19.7	6.51	5.65	2.75
80°C	20.2	7.16	5.61	3.10

From the viscoelastic oscillatory amplitude testing of the water-based fluids it was observed that all the fluids behaved like viscoelastic gels for smaller strain values. This is determined by the relative position of the storage and loss modulus curves, where in this case the storage modulus was located above the loss modulus for smaller strain values. The linear viscoelastic range was determined to be less than 2% strain for all the fluids. A general trend identified from the amplitude sweep tests was that the value of both the storage and loss modulus of the fluids decreased with increasing lignosulfonates contents, also gradually reducing the yield stress. The flow point, the change from behaving like a viscoelastic gel to behaving like a viscoelastic liquid, was also decreasing with increasing LS contents, clearly indicated in **Figure 5.9**. Thus, further indicating a reduction in fluid viscosity as a function of increased lignosulfonates contents.

### 7.1.2 Characterization of MoS<sub>2</sub>-Nanofluid - Ex-situ vs In-situ Treatment of Flat Rheology WBM

The best performing water-based fluid system, the reference fluid plus 0.9 gram of lignosulfonates, was treated with 0.10 wt%, 0.19 wt% and 0.29wt% of MoS<sub>2</sub> nano-solution in order to investigate if this could improve the fluid's lubricity.

The results from the rheological measurement of the drilling fluids containing various amount of MoS<sub>2</sub> nanofluid showed no linear trend indicating either increasing or decreasing viscometer response with increasing amount of MoS<sub>2</sub>. When comparing the viscometer response from the ex-situ treated to the in-situ treated fluids, the response for both treatment methods were quite similar, indicating very small differences in the rheological properties.



However, from the viscoelastic amplitude sweep testing of the ex-situ and in-situ treated fluids, it was found that the ex-situ fluids exhibit larger values for both storage and loss modulus with respect to the reference fluid, as seen in **Figure 5.13**. Additionally, it was found that the in-situ treated fluid systems produced storage and loss modulus values less than of the reference fluid. These findings suggest that the ex-situ nano treated fluid system possess higher potential for storing energy, hence better gel characteristics.

The results from the frictional testing of the nano modified fluids showed that the addition of nanoparticles did reduce the coefficient of friction in five out of six fluids. Based on the test results, it is quite evident that the addition of nanoparticles should be done ex-situ in order to obtain the best outcome, as seen from **table 7.2**, where the percentage change of the coefficient of friction is displayed.

**Table 7.2:** Percentage change of the coefficient of friction with regards to the reference fluid

	REF + 0.5 g MoS <sub>2</sub>	REF + 1.0 g MoS <sub>2</sub>	REF + 1.5 g MoS <sub>2</sub>
In-situ	-0.50%	-35.3%	8.20%
Ex-situ	-29.9%	-40.2%	-21.2%

The addition of nanoparticles, ex-situ, resulted in an average reduction of the coefficient of friction of 30.4%, while the in-situ addition resulted in an average reduction of only 9.2%. Based on these results, the reference fluid and the (REF + 1.0 g MoS<sub>2</sub>)<sub>ex-situ</sub> fluid were both simulated for torque and drag. These simulations showed how the coefficient of friction affects the achievable measured depth of drilling. A minor modification of the reference fluid, with 0.19 wt% added MoS<sub>2</sub>, resulted in an increase in drilling depth of 900 ft with respect to the maximum measured depth of drilling.

### 7.1.3 Characterization of Oil-Based Drilling Fluids

#### 7.1.3.1 Characterization of M-I Swaco Oil-Based Drilling Fluids

The rheological testing of the M-I Swaco fluids were performed in order to investigate how different oil-water-ratios affected the viscometer response. From **Figure 5.14** it is observed that the response decreases as a function of increased OWR, even though the 90/10 fluid exhibit higher response values than both the 70/30 and the 80/20 fluid. Further, when analyzing the yield stress of these fluids, the trend indicates lower yield stress as a function of increased oil-water-ratio, as seen from **Figure 5.15**.

Based on the calculated yield stress values and the measured electrical stability of the 60/40, 70/30 and 80/20 fluids, it was decided to experiment with various amounts of additional emulsifier in order to

make the fluids thermally stable. From the experimental studies, it was found that the addition of 2.2 wt% One-Mul was enough to cause the fluids to exhibit stable yield stresses as a function of increased temperature, as presented in **Figure 5.17**. A summary of the yield stress values for these fluids, and additionally the largest yield stress difference,  $\Delta YS_{\max}$ , for each of the fluids are presented in **table 7.3**.

**Table 7.3:** Calculated yield stress values, based on Herschel-Bulkley model, for modified OBMs exhibiting stable values

Fluid temperature	60/40 One-Mul	70/30 One-Mul	80/20 One-Mul
22°C	9.32	6.96	6.59
50°C	8.42	5.55	6.78
80°C	8.30	5.56	6.80
100°C	7.64	5.67	6.91
$\Delta YS_{\max}$	1.68	1.41	0.32

Results gained from the oscillatory amplitude sweep tests of the M-I Swaco fluids was somewhat difficult to interpret, as the storage and loss modulus curves crossed each other more than once for all of the fluids except the 90/10 fluid. However, for all of the fluids, the storage modulus curve was located above the loss modulus curve at small strain values, indicating that the fluids behave like viscoelastic gels at these lower strain values. The linear viscoelastic range was different for all of the OWRs, with the smallest LVE ending at approximately 0.05% strain for the 70/30 fluid.

The shear yield stress, yield strain and the shear stress flow point were all attained by using the same procedures as for the water-based drilling fluids. The results did not indicate any linear trend of either increasing or decreasing yield stress/flow point as a function of increasing OWR. This might be due to inadequate mixing, resulting in an inhomogeneous fluid mixture, inconsistency in measurements or errors with, or uncalibrated, equipment. However, the tests were run several times in order to make sure that the results were repeated, and all the tests produced similar results every time.

From the temperature sweep test analysis, it looked like the 70/30 and the 80/20 fluids exhibited a dual performance, with flow point at approximately 42°C and 32°C, respectively, and then going back to gel like characteristics when reaching 54°C and 55°C. For the 60/40 and 90/10 fluids, the damping factor was below 1 for all given temperatures, indicating viscoelastic gel like behaviour.

The static barite sag testing of the M-I Swaco's drilling fluids showed no indications of barite sag issues, as all static sag factors were found to be below the sag factor limit of 0.53. However, for the dynamic sag testing, the dynamic sag factors for both the 80/20 and the 90/10 fluids were found to be well above

the sag factor limit, exhibiting values at 0.550 and 0.561, respectively. To solve this problem, it was investigated if the addition of the polymer poly acrylic could reduce the sag potential. Based on the results from the testing of the 90/10 fluid, it was found that the addition of 0.5 gram in 300 grams of reference fluid was proven to be enough to produce a fluid that exhibited a higher  $G'/G''$ -ratio and a dynamic sag factor below the sag factor limit, hence a sag-preventive fluid.

### 7.1.3.2 Characterization of UiS Formulated Oil-Based Drilling Fluids – EDC 90/10 OBM

For the UiS formulated oil-based drilling fluids the rheological measurements showed almost identical results for the EDC 90/10 reference fluid and the poly acrylic modified fluids. This is clearly illustrated in **Figure 5.29**, where the largest difference between a reading at the same RPM for all of the fluids is equal to 6.5 lbf/100ft<sup>2</sup>. There is no trend found in the rheological values as a function of added poly acrylic. As a result of very similar viscometer response, the calculated yield stresses are also very much alike for all the fluids, where all of them exhibit very low, but temperature stable yield stress values.

From the viscoelastic amplitude sweep tests of the EDC 90/10 fluids, some interesting results were obtained. For the reference fluid EDC 90/10, the loss modulus curve was located above the storage modulus curve for the whole period of the test, indicating that the fluid behaves like a viscoelastic liquid and that the fluid is incapable of storing energy. Since the storage and loss modulus curves never cross over for the reference fluid, this means that it does not possess a flow point. The lack of flow point is also determined from **Figure 5.32**, where the phase angle curve never crosses the flow point limit at 45°, but is situated above it.

The amplitude sweep test results for the poly acrylic modified EDC 90/10 fluids exhibits viscoelastic gel properties at low strain values. As the strain is gradually increased, the fluids changes behaviour from viscoelastic gels to viscoelastic liquids and the flow point can be determined. The shear stress flow points that are obtained exhibit an increase in value as the amount of poly acrylic is decreased. These findings indicated that the EDC 90/10 + 0.5 g poly acrylic is cable of storing more energy and is stronger than the other EDC 90/10 fluids.

From the initial static barite sag testing, the EDC 90/10 reference fluid was found to have problems with sagging of weight materials. Both the static and dynamic barite sag test results of this fluid produced sag factor values above the sag factor limit of 0.53, indicating a barite sag potential. By adding various amounts of poly acrylic to the reference fluid, the fluid was progressively exhibiting higher strength when reducing the amount of poly acrylic from 1.5 grams to 0.5 gram with an increment of 0.5 gram for each new fluid system. The EDC 90/10 + 0.5 g poly acrylic was the only fluid that produced a sag factor

below the sag limit, supporting the results from the amplitude sweep tests that indicated that this was the strongest fluid with the greatest gel characteristics and highest probability of avoiding sag issues.

#### 7.1.4 Evaluation of Yield Stress

In order to properly evaluate the value of the yield stress for all the fluids, four different evaluation methods have been considered and compared. As mentioned in **Chapter 2.4**, research and scientific work performed by H. Barnes have suggested that the yield stress is better represented by a region, rather than a single point. However, for all practical purposes, a single point was used to determine the yield stress in this thesis, as this is more useful when comparing the values relative to each other.

Summaries of the yield stress values for all fluids, and all evaluation methods, are given in **table 7.4**, **table 7.5** and **table 7.6** below. As seen from these tables, the values are widely spread between each of the different evaluation methods, for all of the fluids. The yield stress values for the Herschel-Bulkley, the Robertson-Stiff and the Bingham Plastic model are all calculated from the viscometer readings obtained at 22°C, given in **APPENDIX A – RHEOLOGICAL MEASUREMENTS**. The Bingham plastic yield point is included because this value is widely used in the oil industry, as it is easily obtained. However, it is important to emphasize that this value is considerably overestimated but gives a fair indication of the yield stress value. The viscoelastic shear yield stress,  $\tau_{ys, VE}$ , and the shear stress flow point,  $\tau_{fp}$ , are both obtained from the viscoelastic amplitude sweep tests.

Based on the results from the viscoelastic amplitude sweep tests, there are different ways of interpreting the yield stress. As described in **Chapter 5.1.2**, a common way of determining the yield stress is to consider the end of the LVE region, as this represents the end of the linearity and indicates a structural breakdown. However, the linear viscoelastic range is prone to subjective interpretation, which might favor the use of the flow point as the yield stress. The flow point is determined as the point where  $G' = G''$  and indicates the transition from a viscoelastic gel to a viscoelastic liquid. There is a significant gap between the values of  $\tau_{ys, VE}$  and  $\tau_{fp}$  and this zone between these two points is often referred to as the transition zone, as it represents the transition from viscoelastic gel to viscoelastic liquid like behaviour.

**Table 7.4:** Summary of yield stress values from different evaluation methods and flow point for lignosulfonates WBMs

Fluid	$\tau_{ys, VE}$ [Pa]	$\tau_{ys, R-S}$ [Pa]	$\tau_{ys, B-P}$ [Pa]	$\tau_{fp}$ [Pa]
Ref	4.09	7.83	9.49	10.54
Ref + 0.2g LS	2.88	6.18	7.78	8.57
Ref + 0.3g LS	1.57	5.11	6.90	7.04
Ref + 0.4g LS	1.14	4.36	5.80	6.11
Ref + 0.5g LS	0.42	4.10	5.39	5.66
Ref + 0.6g LS	0.79	3.44	3.86	4.35
Ref + 0.7g LS	0.56	3.16	3.83	3.76
Ref + 0.8g LS	0.53	2.93	3.67	3.84
Ref + 0.9g LS	0.40	3.22	3.81	3.57
Ref + 1.0g LS	0.73	2.90	3.79	3.76
Ref + 2.0g LS	0.01	1.50	1.82	2.72

**Table 7.5:** Summary of yield stress values from different evaluation methods and flow point for OBMs provided by M-I Swaco

Fluid	$\tau_{ys, VE}$ [Pa]	$\tau_{ys, H-B}$ [Pa]	$\tau_{ys, B-P}$ [Pa]	$\tau_{fp}$ [Pa]
60/40	0.40	5.37	6.84	1.08
70/30	0.11	3.74	4.76	0.23
80/20	0.13	2.96	4.17	0.63
90/10	0.23	2.83	4.20	2.75

**Table 7.6:** Summary of yield stress values from different evaluation methods and flow point for OBMs formulated at UiS

Fluid	$\tau_{ys, VE}$ [Pa]	$\tau_{ys, R-S}$ [Pa]	$\tau_{ys, B-P}$ [Pa]	$\tau_{fp}$ [Pa]
EDC 90/10	N/A	0.60	0.87	N/A
EDC 90/10 + 0.5 g poly acrylic	0.0019	0.59	0.83	0.048
EDC 90/10 + 1.0 g poly acrylic	0.0012	0.62	0.64	0.033
EDC 90/10 + 1.5 g poly acrylic	0.0017	0.64	0.78	0.003

## 7.2 Hydraulic Performance

The hydraulic performance of both the water-based and oil-based drilling fluids were analyzed by simulating the EDC and the pump pressure in a vertical wellbore of 10 000 feet. This subsection will discuss the effect of:

- Lignosulfonates in water-based fluid systems on pump pressure and ECD
- One-Mul addition in oil-based fluid systems on pump pressure and ECD
- Poly acrylic in oil-based fluid systems on pump pressure and ECD

### 7.2.1 Hydraulic Performance of Water-Based Drilling Fluids

For the water-based drilling fluids, the total pressure drop was reduced as a function of added lignosulfonates. As seen in **table 7.7**, the pump pressure is reduced by a total of 431 psi at a pump rate of 100 GPM by modifying the reference fluid with 0.9 gram of lignosulfonates and reduced by a total of 595 psi when modified with 2.0 grams of lignosulfonates. These pressure differences decrease as the pump pressure is increased, but even at the highest flow rate simulated, at 600 GPM, the 0.9 g LS fluid produces 177 psi less pressure drop relative to the reference fluid. Less pressure drop is beneficial, as it means that the fluid requires less pump pressure in order to be circulated through the drilling fluid circulation system.

The reason for the reduction in pump pressure can be explained by the fact that lignosulfonates works as a disperser, creating a less viscous fluid, resulting in less frictional pressure drop. From the right-hand side of **table 7.7** one can see that the relative change in pressure loss is larger for the 2.0 grams LS fluid at 100 GPM, but lower at the 600 GPM pump rate. This might indicate that 2.0 gram of added lignosulfonates constitutes a better concentration compared to the 0.9 gram fluid in terms of pump pressure. By looking at the total pressure loss in **table 7.8**, this suggestion is confirmed, as the 2.0 gram LS fluid requires a pump pressure that is 2210 psi less than of what the 0.9-gram LS fluid requires.

**Table 7.7:** Pressure loss for WBMs at selected flow rates and relative change in pump pressure for WBM fluids at 80°C

Pump rate	Ref [psi]	Ref + 0.9 g LS [psi]	Ref + 2.0 g LS [psi]	$\Delta P_{\text{Ref, Ref + 0.9 g LS}}$ [psi]	$\Delta P_{\text{Ref, Ref + 2.0 g LS}}$ [psi]
100 GPM	733	302	138	431	595
600 GPM	1190	1013	1083	177	107

**Table 7.8:** Total pressure loss for water-based mud systems

	Ref	Ref + 0.9 g LS	Ref + 2.0 g LS
$\Delta P_{\text{total}}$ [psi]	11464	6337	4127

In terms of the ECD, it is interesting to analyse the difference in ECD between the two simulated temperatures. As seen in **table 7.9**, Ref + 2.0 g LS exhibits the most stable ECD when analysing at the average change in ECD. However, when analysing the temperature effect of ECD at 100, 300 and 600 GPM respectively, one can see that Ref + 0.9 g LS exhibits the smallest ECD fluctuations, hence, providing the most temperature stable ECD of the three fluids.

**Table 7.9:** Change in ECD at the same flow rate but different temperature and absolute average change in ECD

	Ref [ppg]	Ref + 0.9 g LS [ppg]	Ref + 2.0 g LS [ppg]
$\Delta$ ECD at 100GPM	-0.109	-0.049	-0.033
$\Delta$ ECD at 300GPM	-0.093	-0.062	-0.018
$\Delta$ ECD at 600GPM	-0.070	-0.051	0.178
$\Delta$ ECD average	0.088	0.059	0.057

## 7.2.2 Hydraulic Performance of Oil-Based Drilling Fluids

### 7.2.2.1 Hydraulic Performance Evaluation of M-I Swaco OBMs

For the M-I Swaco oil-based drilling fluids there is a trend indicating that the One-Mul modification decreases the pressure loss in varying extents, as observed in **table 7.10**. The total pressure loss reduction of the One-Mul modified 70/30 fluid is three times larger than the total pressure loss reduction of the 80/20 fluid. The general information gained from this simulation is that the addition of more One-Mul, emulsifier, reduces the total amount of pump pressure required to pump the fluid through the drilling fluid circulation system.

**Table 7.10:** Pressure loss at selected pump rates and total pressure loss for One-Mul modified oil-based drilling fluids

Pump rate	60/40 [psi]	60/40 One-Mul [psi]	70/30 [psi]	70/30 One-Mul [psi]	80/20 [psi]	80/20 One-Mul [psi]
100 GPM	447	365	434	254	339	305
600 GPM	1469	1348	1254	1138	1169	1108
$\Delta P_{total}$	9285	8485	8353	6831	7419	6961

As for the ECD, it is observed, from **table 7.11**, that the ECD of the 70/30 fluid is reduced quite significantly when compared to the 60/40 and 80/20 fluids. For the 70/30 fluid the reduction in ECD is quite constant for all pump rates, while for the 60/40 fluid the change in ECD is decreasing with increasing flow rate and opposite for the 80/20 fluid, with increasing change in ECD with increasing flow rate. These observations indicate that the addition of One-Mul reduces the ECD, but not equally for different oil-water-ratios or different pump rates.

**Table 7.11:** Relative change in ECD between reference and One-Mul modified fluid and the absolute average change in ECD

	60/40 [ppg]	70/30 [ppg]	80/20 [ppg]
$\Delta$ ECD at 100GPM	-0.114	-0.212	-0.042
$\Delta$ ECD at 300GPM	-0.049	-0.225	-0.050
$\Delta$ ECD at 600GPM	-0.016	-0.229	-0.062
$\Delta$ ECD average	0.049	0.225	0.052

### 7.2.2.2 Hydraulic Performance Evaluation of UiS Formulated OBMs

For the UiS formulated oil-based drilling fluids, the pump pressure and ECD was analyzed as a function of added poly acrylic. The EDC 90/10 reference fluid and the best system, EDC 90/10 + 0.5 g poly acrylic, were simulated at both 22°C and 100°C. As seen from **table 7.12**, the pump pressure is almost identical for the two fluids at the same temperatures, indicating that the addition of 0.5 gram of poly acrylic have little effect on the hydraulic performance of the fluid system. The simulated pump pressure at 22°C is moderately larger than the pump pressure required at 100°C.

**Table 7.12:** Pump pressure at selected pump rates for two different temperatures

Fluid	EDC 90/10 [psi]		EDC 90/10 + 0.5 g poly acrylic [psi]	
	22°C	100°C	22°C	100°C
100 GPM	89	68	89	71
300 GPM	422	352	423	354
600 GPM	1427	1169	1420	1175

However, when analyzing the pump pressure change with regards to temperature, as displayed in **table 7.13**, there is a trend indicating that the pump pressure difference,  $\Delta P$ , between the two simulated temperatures is increasing as the pump rate increases, for both of the fluids. Instead of analyzing the pump pressure change it self, but rather looking at the percentage change, the values are quite similar for all pump rates, with a maximum deviation of 7% between different flow rates.

**Table 7.13:** Relative change in pump pressure with regards to temperature ( $P_p^{22^\circ\text{C}} - P_p^{100^\circ\text{C}}$ ) and percentage change

Pump rate	$\Delta P_{\text{EDC 90/10}}$ [psi]	$\% \Delta P_{\text{EDC 90/10}}$	$\Delta P_{\text{EDC 90/10 + 0.5 g poly acrylic}}$ [psi]	$\% \Delta P_{\text{EDC 90/10 + 0.5 g poly acrylic}}$
100 GPM	21	24%	18	20%
300 GPM	70	17%	69	16%
600 GPM	258	18%	245	17%



For the ECD simulations, the values were almost identical for both of the EDC 90/10 and the EDC 90/10 + 0.5 g poly acrylic fluids at both temperatures simulated. The ECD is slightly reduced when the temperature is increased and the change in ECD increases from 350 GPM up to 600 GPM, as illustrated in **table 7.14**. These simulations indicate that the EDC 90/10 + 0.5 g poly acrylic exhibits more constant changes in ECD and that it has a lower average change in ECD, which is positive, as it indicates that the fluid is more stable in terms of temperature fluctuations.

**Table 7.14:** Relative change in ECD ( $ECD_{100^{\circ}C} - ECD_{22^{\circ}C}$ ) and the absolute average change in ECD

	EDC 90/10 [ppg]	EDC 90/10 + 0.5 g poly acrylic [ppg]
$\Delta ECD$ at 100GPM	-0.047	-0.044
$\Delta ECD$ at 300GPM	-0.035	-0.040
$\Delta ECD$ at 600GPM	-0.154	-0.147
$\Delta ECD$ average	0.076	0.072

## 7.3 Measurement Limitations and Uncertainties

This subsection will give some general information about measurement limitations and uncertainties, as well as try to pin-point the potential uncertainties related to the experimental work performed in this thesis. With regards to the hydraulics simulations, all the assumptions are stated back in **Chapter 6.2** and **Chapter 6.3**. As the sole purpose of the simulations was to compare the fluid systems relative to each other, these assumptions were reasonable enough to produce the desired data.

### 7.3.1 Uncertainty and Limitations

In order to produce reliable and representative measurement results, it is of utmost importance that the tests are easily reproducible. For all types of measurements, there will be some degree of uncertainty in the produced data, as no equipment or instrument is capable of producing 100% reliable data. The accuracy and reliability of the produced data is dependent of the total number of measurements and/or tests performed. As time was the limiting factor, most of the data presented in this thesis was attained by conducting one or two repetitive measurements/tests.

### 7.3.2 Viscometer Measurements

As previously mentioned, all the rheological measurements were performed by the use of a conventional Ofite model 800, 8-speed viscometer. All tests were performed by operating with the same procedures in order to prevent or minimize the probability of errors and mismeasurements. However, there will always be some factors that are more difficult to control than others. Some of these factors which might have influenced the viscometer readings are:

- **Inhomogeneous fluid mixture**
  - Could result in fluctuating viscometer response, as the fluid will change properties as to what part of the fluid that is measured
- Potential **barite sag** during measurement
  - Leading to higher solids concentration in the bottom of the viscometer cup, causing the viscometer to measure a fluid that is less viscous than the actual fluid of interest
- Potential **temperature fluctuations** during the measurement
  - Potential temperature changes could cause either higher viscometer response at lower temperatures, or lower viscometer response at higher temperatures

If the recorded rheological data is affected by any of the factors mentioned above, this would also have affected the hydraulics simulations, as they are based up on the viscometer data.

### 7.3.3 Rheometer Measurements

All the measurements conducted with the Anton Paar MCR 302 rheometer are prone to inaccuracy when performed in oscillatory mode, particularly at low torques. Some of the measurements performed in this these recorded very noisy data at low strain values, emphasizing this potential problem. For these measurements, all fluids were prepared and pre-mixed following the same procedure for each fluid, in order to make sure that the tests were carried out at equal conditions. Some of the elements that may have influenced the rheometer measurements are:

- **Instrument not 100% level**
  - May prevent the test sample from being in contact with both plates during the measurement and prevent the test from being performed with two parallel plates, as is required in order to get reliable viscoelastic data
- **Inhomogeneous fluid mixture**
  - Could result in fluctuating data points, as some part of the fluid will behave more like a viscoelastic liquid and some of it might behave more like a viscoelastic gel

As a result of noisy data during the measurement of some particular fluids, these data points were removed and the remaining, more reliable data were used for further fluid characterization.

### 7.3.4 Barite Sag Measurements

The dynamic barite sag measurements were all performed using the Ofite model 800 viscometer, the M-I Swaco sag shoe and the heating apparatus. In order to produce as reliable and accurate data as possible, it was important to conduct all the measurements following the test pre-sets, including; constant shear rate of 100 RPM for 30 minutes and fluid temperature of 50°C. However, the barite sag measurement may have been affected by:

- **Pre-test sagging**
  - Causing a potentially higher solids concentration than actual
- **Temperature fluctuations**
  - Could result in higher or lower degree of sagging, depending on whether the temperature is increased or decreased

Either way, these factors were avoided in the best possible manner by pre-mixing the fluid of interest after heating, before testing, and by keeping the fluid temperature as constant as possible by the use of the heating apparatus.

## 8 CONCLUSION

The primary objectives of this thesis were;

- to formulate thermally stable rheology drilling fluids,
- formulate a sag preventive oil-based drilling fluid,
- analyze the frictional performance of nanofluids in the best water-based fluid system and
- perform drilling fluids rheology modelling, hydraulics and torque & drag performance simulation studies.

Based on the results from the experimental work and the simulations studies, the following two subsections will provide some reasonable conclusions that have been drawn regarding the formulation and modification, by the application of polymers and/or nanoparticles, of both water-based and oil-based drilling fluids.

### 8.1 Conclusions for Water-Based Drilling Fluids

#### 8.1.1 Effect of Lignosulfonates

- ✓ Results from the rheological measurement of the water-based fluid systems indicated that the addition of 0.17 wt% of the polymer lignosulfonates provided the most thermally stable fluid system.
- ✓ The findings from the oscillatory amplitude sweep tests showed that the addition of lignosulfonates gradually decreased the flow point, yield stress and the storage/loss-ratio as the amount of polymer in the fluid mixture increased.
- ✓ Hydraulic simulations indicated that the application of lignosulfonates in water-based drilling fluid systems enhanced the hydraulic performance of the fluid. The addition of 0.17 wt% of lignosulfonates reduced the total pressure loss with a total of 5127 psi, equal to a 44.7%, compared to the reference fluid, hence reducing the pump pressure required to pump the fluid through the drilling fluid circulation system.
- ✓ ECD simulations indicated that the lignosulfonates water-based drilling fluid system provided the smallest fluctuations in ECD as the temperature was increased, with an average change of 0.059 ppg, hence supporting the conclusion of temperature stable rheology drawn from the rheological measurement.

### 8.1.2 Effect of MoS<sub>2</sub>-Nanofluid

- ✓ Addition of 0.19 wt% of molybdenum disulphide to the thermally stable fluid system resulted in a total reduction of the coefficient of friction by 35.3% when added in-situ and a reduction of 40.2% when added ex-situ.
- ✓ As a result of the reduced coefficient of friction, the torque and drag simulations showed that the maximum measured drilling depth was increased with 6.12%.

## 8.2 Conclusions for Oil-Based Drilling Fluids

### 8.2.1 Effect of Emulsifier One-Mul

- ✓ Rheological measurement results of the M-I Swaco oil-based drilling fluids showed that modification of the fluid systems by addition of 2.2 wt% One-Mul made the 60/40, 70/30 and 80/20 fluid systems' yield stresses stable with increased fluid temperature.
- ✓ Pump pressure simulations indicated that the addition of 2.2 wt% One-Mul resulted in reduced total pump pressure for all the fluids, with the 70/30 fluid experiencing the highest reduction of 1522 psi, equal to 18.2%.
- ✓ ECD simulations of the M-I Swaco oil-based drilling fluids indicated that the addition of 2.2 wt% One-Mul reduced the ECD for all fluids, but in varying extent. The fluids had average reductions of 0.049 ppg, 0.225 ppg and 0.052 ppg for the 60/40, 70/30 and 80/20 fluid respectively.

### 8.2.2 Effect of the Polymer Poly Partial Sodium Salt (Poly Acrylic)

- ✓ The combined results of  $G'/G''$ -ratio and the dynamic sag factor showed that the application of 0.17 wt% of poly acrylic to the 90/10 M-I Swaco reference fluid system strengthened the fluid's sag preventive characteristics. The sag factor was reduced by 5.7% and the  $G'/G''$ -ratio was increased by 16.2%.
- ✓ Combination of oscillatory amplitude sweep test results and dynamic sag test results indicated that the addition of 0.17 wt% of poly acrylic to the EDC 90/10 reference fluid system enhanced the fluid's ability to prevent sagging. The sag factor was reduced by 9.3% and the  $G'/G''$ -ratio was increased by 68.7%.

## BIBLIOGRAPHY

- [1] SPE, "Petrowiki.org," 2 June 2015. [Online]. Available: [https://petrowiki.org/Drilling\\_fluid\\_types](https://petrowiki.org/Drilling_fluid_types). [Accessed 9 January 2019].
- [2] H. Nazami, "Polymers in Our Daily Life," *BiolImpacts*, pp. 73-74, 16 June 2017.
- [3] Z. Khanam, V. Singh and M. G. H. Zaidi, "Nano in Our Daily Life," *Everyman's Science*, pp. 90-95, June 2015.
- [4] K. P. Hoelscher, G. De Stefano, M. Riley and S. Young, "Application of Nanotechnology in Drilling Fluids," in *SPE International Oilfield Nanotechnology Conference*, Noordwijk, 2012.
- [5] ikon Sience, "ikonSience.com," [Online]. Available: <https://www.ikonscience.com/solutions/drilling>. [Accessed 2019 January 2019].
- [6] V. Chilingarian G and P. Vorabutr, *Drilling and drilling fluids*, Amsterdam: Elsevier science publishing company inc, 1983.
- [7] B. Bloys, N. Davis, B. Smolen, L. Bailey, L. Fraser and M. Hodder, "Designing and Managing Drilling Fluid," *Oilfield Review*, pp. 33-43, April 1994.
- [8] Society of Petroleum Engineers, "PetroWiki," 26 April 2018. [Online]. Available: [https://petrowiki.org/PEH:Drilling\\_Fluids#Challenges\\_Related\\_to\\_Drilling\\_Fluid](https://petrowiki.org/PEH:Drilling_Fluids#Challenges_Related_to_Drilling_Fluid). [Accessed 2 May 2019].
- [9] D. Power and M. Zamora, "Making a Case for AADE Hydraulics and the Unified Rheological Model," in *Drilling & Completion Fluids and Waste Management*, Houston, Texas, 2002.
- [10] Schlumberger, "Schlumberger," [Online]. Available: [https://www.glossary.oilfield.slb.com/en/Terms/l/lost\\_circulation.aspx](https://www.glossary.oilfield.slb.com/en/Terms/l/lost_circulation.aspx). [Accessed 2 May 2019].
- [11] O. Skjeggstad, *Boreslamteknologi*, Bergen: Alma Mater Forlag AS, 1989.
- [12] G. Kolle and R. Mesel, *Brønnvæsker*, Nesbru: Vett og Viten AS, 1998.
- [13] K. Van Dyke, *Drilling fluids, mud pumps and conditioning equipment*, Austin, Texas: Petroleum Extension Service, Division of Continuing Education, University of Texas at Austin, 1998.

- [14] Schlumberger, "Schlumberger.com," [Online]. Available:  
[https://www.glossary.oilfield.slb.com/Terms/b/base\\_oil.aspx](https://www.glossary.oilfield.slb.com/Terms/b/base_oil.aspx). [Accessed 4 February 2019].
- [15] S. Devereux, **Drilling Technology in Nontechnical Language**, Second Edition, Tulsa, Oklahoma, USA: PennWell Corporation, 2012.
- [16] O. Aunan, A. Fjogstad, H. Hoset, P. I. Norky, J. Rostad E, A. Saasen and E. Westgård, "Application of Ilmenite as Weight Material in Water Based and Oil Based Drilling Fluids," *Annual Technical Conference and Exhibition* , pp. 1-5, 30 September 2001.
- [17] M-I Swaco, **Drilling Fluids Engineering Manual**, M-I Swaco - A Schlumberger Company, 2009.
- [18] Schlumberger, "Schlumberger," [Online]. Available:  
<https://www.glossary.oilfield.slb.com/en/Terms/h/hpht.aspx>. [Accessed 12 March 2019].
- [19] R. Bland, Y. Gonzalez, F. Harvey, G. Mullen and M. Pless, "HP/HT Drilling Fluid Challenges," in *Asia Pacific Drilling Tehcnology Conference and Exhibition* , Bangkok, 2006.
- [20] P. A. Bern, P. J. Hearn, K. S. Slater and M. Zamora, "The Influence of Drilling Variables on Barite Sag," SPE , Colorado, USA, 1996.
- [21] P. M. Hanson, G. T. T. K. Rachal and M. Zamora, "Investigation of Barite "Sag" in Weighted Drilling Fluids in Highly Deviated Wells," in *Annual Technical Conference and Exhibition of the Society of Petroleum Engineers*, New Orleans, 1990.
- [22] H. Ebelhoft, B. Neustadt, E. van Oort, K. Slater, M. Zamora and C. Zurdo, "Barite Sag: Measurement, Modeling, and Management," in *Asia Pacific Drilling Technology Conference*, Jakarta, 2000.
- [23] A. Saasen, "Sag of Weight Material in Oil Based Drilling Fluids," in *Asia Pacific Drilling Technology* , Jakarta, 2002.
- [24] D. E. Jamison and W. R. Clements, "A New Test Method To Characterize Setting/Sag Tendencies of Drilling Fluids in Extended Reach Drilling," pp. 109-113, 1990.
- [25] H. A. Barnes, "Very Shear-thinning or "Yield Stress" Fluids," in *A Handbook of Elementary Rheology*, Wales, Univeristy of Wales, Institution of Non-Newtonian Fluid Mechanincs, 2000, pp. 71-76.

- [26] R. Ewolt, J. Maxey, G. McKinley and P. Winter, "Yield Stress: What is the "True" Value?," in *AADE Fluids Conference and Exhibition* , Houston, Texas, 2008.
- [27] L. Long, X. Xianguan, S. Jinsheng, Y. Xubo and L. Yingmin, "Vital Role of Nanomaterials in Drilling Fluid and Reservoir Protection Applications," in *Abu Dhabi International Petroleum Exhibition and Conference* , Abu Dhabi, 2012.
- [28] G. De Stefano, J. Friedheim, K. P. Hoelscher and S. Young, "Nanotechnology Application in Drilling Fluids," in *Offshore Mediterranean Conference and Exhibition* , Ravenna, Italy, 2013.
- [29] R. I. Tanner, *Engineering Rheology*, Oxford: Oxford University Press, 2000.
- [30] Schlumberger, "Schlumberger.com," [Online]. Available: [https://www.glossary.oilfield.slb.com/en/Terms/y/yield\\_point.aspx](https://www.glossary.oilfield.slb.com/en/Terms/y/yield_point.aspx). [Accessed 10 January 2019].
- [31] J. Vlachopoulos, "Research Gate," January 2003. [Online]. Available: [https://www.researchgate.net/figure/Velocity-shear-rate-and-shear-stress-profiles-for-flow-between-two-flat-plates\\_fig2\\_266472193](https://www.researchgate.net/figure/Velocity-shear-rate-and-shear-stress-profiles-for-flow-between-two-flat-plates_fig2_266472193). [Accessed 14 January 2019].
- [32] Drilling Formulas, "Drilling Formulas," 14 February 2016. [Online]. Available: <http://www.drillingformulas.com/types-of-flow-and-rheology-models-of-drilling-mud/>. [Accessed 15 January 2019].
- [33] The University of Waikato, "Science Learning Hub," 12 April 2010. [Online]. Available: <https://www.sciencelearn.org.nz/images/1846-shear-thinning-and-shear-thickening-liquids>. [Accessed 15 January 2019].
- [34] T. Hemphill, W. Campos and A. Pilehvari, "Yield-power Law Model More Accurately Predicts Mud Rheology," *Oil and Gas Journal* , pp. 45-50, 23 August 1993.
- [35] R. E. Robertson and H. A. Stiff, "An Improved Mathematical Model for Relating Shear Stress to Shear Rate in Drilling Fluids and Cement Slurries," *Society of Petroleum Engineers Journal*, pp. 31-36, February 1976.
- [36] Kelly, "Viscoelasticity," in *Solid Mechanics Part I* , 2015, pp. 283-342.
- [37] B. Bui, J. Maxey, S. Z. Miska, M. E. Ozbayoglu, A. Saasen, N. E. Takach and M. Yu, "Viscoelastic Properties of Oil-Based Drilling Fluids," *Annual Transactions of the Nordic Rheology Society, VOL 20*, pp. 33-47, 2012.



- [38] Aalto University, *Rheology and Viscoelasticity*, Helsingfors, Finland: Aalto University.
- [39] M. Ystenes, "Store Norske Leksikon," 26 June 2014. [Online]. Available: [https://snl.no/Hookes\\_lov](https://snl.no/Hookes_lov). [Accessed 17 January 2019].
- [40] T. G. Mezger, *The Rheology Handbook: For users of rotational and oscillatory rheometers*. 2nd revised edition, Hannover: Vincentz Network, 2006.
- [41] R. J. Larsen, D. A. Weitz and H. M. Wyss, "Oscillatory Rheology," *G.I.T Laboratory Journal* 3-4, pp. 68-70, 2007 .
- [42] D. Power, A. Tehrani and M. Zamora, "Role of Rheology in Barite Sag in SBM and OBM," in *AADE Drilling Fluids Conference* , Huston, Texas, 2004.
- [43] API, *Rheology and Hydraulics of Oil-well Fluids*, Washington, DC: API Publishing Services , 2010.
- [44] B. Dye, N. Hansen, R. Leaper, L. Moroni and M. Otto, "Meeting Deepwater Challenges with High Performance Water Based Mud," in *AADE Drilling Fluids Technoical Conference*, Houston, Texas, 2006.
- [45] J. Maxey, "Rheological Analysis of Static and Dynamic Sag in Drilling Fluids," *Annual Transactions of the Nordic Rheology Society*, 2007.
- [46] A. Cliffe, J. Froud-Williams, I. Onwuzulike and M. A. Tehrani, "New Laboratory Technique for Barite Sag Measurement," in *Offshore Mediterranean Conference and Exhibition* , Ravenna, Italy, 2011.
- [47] A. & E. Whittaker, *Theory and Application of Drilling Fluid Hydraulics*, Boston: International Human Resources Development Corporation, 1985.
- [48] B. Guo and G. Liu, *Applied Drilling Circulation Systems*, United States: Gulf Professional Publishing, 2011.
- [49] J. Sadigov, "Comparisons of Rheology and Hydraulics Prediction of Mud Systems in Concentric and Eccentric Well Geometry," University of Stavanger, Stavanger, Rogaland, 2013.
- [50] Schlumberger, "Schlumberger.com," [Online]. Available: <https://www.glossary.oilfield.slb.com/Terms/e/e.cd.aspx>. [Accessed 18 February 2019].

- [51] C. F. Ellis, F. B. Growcock, Shmidt and D. D, "Electrical Stability, Emulsion Stability, and Wettability of Invert Oil-Based Muds," *SPE Drilling and Completion*, pp. 39-46, March 1994.
- [52] M. Burby, C. G. Enyi, P. C. Ihenacho and G. G. Nasr, "50/50 Oil-Water Ration Invert Emulsion Drilling Mud Using Vegetable Oil as Continous Phase," *International Journal of Chemical and Molecular Engineering* , p. 300, 2016.
- [53] M. G. Reitsma, R. G. Cain, D. Smith, S. Biggs and N. W. Page, "Lateral Force Microscopy: A Tool For Tribology," in *ISRM International Symposium*, Melbourne, Australia, 2000.
- [54] E. Kaarstad, B. S. Aadnøy and T. Fjelde, "A Study of Temperature Dependent Friction in Wellbore Fluids," in *SPE/IADC Drilling Conference*, Amsterdam, 2009.
- [55] M. Belayneh, *PET580 Advanced Drilling Compendium*, Stavanger: University of Stavanger , 2018.
- [56] T. V. Aarrestad and H. Blikra, "Torque and Drag - Two Factors in Extended-Reach Drilling," *JPT*, pp. 800-803, 1994.
- [57] Instron, "Instron," Illinois Tool Works Inc. , [Online]. Available: <https://www.instron.us/en-us/our-company/library/glossary/t/torsional-strength>. [Accessed 13 May 2018].
- [58] H. Fossen, "Store Norske Leksikon," 14 February 2009. [Online]. Available: <https://snl.no/bentonitt>. [Accessed 25 February 2019].
- [59] G. Bedekovic, A. Kutlic and I. Sobota, "Bentonite Processing," University of Zagreb, Zagreb, 2012.
- [60] C. Cryer, "Fitz Chem," [Online]. Available: <https://www.fitzchem.com/bentone-38.html>. [Accessed 11 March 2019].
- [61] H. M. King, "Geology.com," [Online]. Available: <https://geology.com/minerals/barite.shtml>. [Accessed 26 February 2019].
- [62] Schlumberger.com, "Schlumberger," [Online]. Available: [https://www.glossary.oilfield.slb.com/Terms/s/soda\\_ash.aspx](https://www.glossary.oilfield.slb.com/Terms/s/soda_ash.aspx). [Accessed 26 February 2019].
- [63] Total Fluids, "Safety Data Sheet - EDC 95-11," Total Fluids , France.
- [64] ExxonMobil, "Escaid Fluids," ExxonMobil, 2015.

- [65] M-I Swaco, "Schlumberger," [Online]. Available: [https://www.slb.com/-/media/Files/miswaco/ps-drilling-fluids/one\\_mul.pdf?la=en&hash=07FE77412666C601B815CC15C2C4FEBFFBF2C467](https://www.slb.com/-/media/Files/miswaco/ps-drilling-fluids/one_mul.pdf?la=en&hash=07FE77412666C601B815CC15C2C4FEBFFBF2C467). [Accessed 11 March 2019].
- [66] M-I Swaco, "Schlumberger," [Online]. Available: <https://www.slb.com/-/media/Files/miswaco/ps-drilling-fluids/lime.pdf?la=en&hash=2FD5F24971492980C016D52C63F7FFCC7B40F0A7>. [Accessed 11 March 2019].
- [67] Qmax, "Qmax," [Online]. Available: <http://www.qmax.com/mud/Calcium%20Carbonate.pdf>. [Accessed 11 March 2019].
- [68] M-I Swaco, "Schlumberger," [Online]. Available: [https://www.slb.com/-/media/Files/miswaco/ps-drilling-fluids/versatrol\\_t.PDF?la=en&hash=C22A262F32832BA82ECDE39C2408044DFB0AA28F](https://www.slb.com/-/media/Files/miswaco/ps-drilling-fluids/versatrol_t.PDF?la=en&hash=C22A262F32832BA82ECDE39C2408044DFB0AA28F). [Accessed 11 March 2019].
- [69] L. E. Helseth, "snl.no," 8 October 2019. [Online]. Available: <https://snl.no/polymerer>. [Accessed 27 February 2019].
- [70] Baker Hughes, *Drilling Fluids Reference Manual*, 2006.
- [71] M-I Swaco, "Duo-Vis," M-I Swaco, Houston, Texas, 2011.
- [72] R. Flatt and I. Schober, in *Understanding the Rheology of Concrete*, Woodhead Publishing Series in Civil and Structural Engineering, 2012, pp. 144-208.
- [73] Sigma-Aldrich, "Poly (acrylamide-co-acrylic) partial sodium salt," [Online]. Available: <https://www.sigmaaldrich.com/catalog/product/aldrich/511471?lang=en&region=NO>. [Accessed 22 March 2019].
- [74] A. El-Diasty and A. M. S. Ragab, "Application of Nanotechnology in the Oil and Gas Industry: Latest Trends Worldwide and Future Challenges in Egypt," in *North Africa Technical Conference & Exhibition*, Cairo, Egypt, 2013.
- [75] National Center for Biotechnology Information, "PubChem Database," [Online]. Available: <https://pubchem.ncbi.nlm.nih.gov/compound/14823>. [Accessed 25 April 2019].

- [76] A. R. Lansdown, **Molybdenum Disulphide Lubrication**, Amsterdam: Elsevier Science , 1999.
- [77] Anton Paar GmbH, "Anton Paar," [Online]. Available: <https://www.anton-paar.com/kren/products/details/rheometer-mcr-102-302-502/>. [Accessed 7 March 2019].
- [78] M. Hurum, "Extended Reach Drilling using RDM - Heavy Over Light Solution," UiS, Stavanger, 2015.
- [79] M. A. A. Alvi, M. S. A. Belayneh and B. S. Aadnøy, "The Effect of Micro-sized Boron Nitride (BN) and Iron Trioxide (Fe<sub>2</sub>O<sub>3</sub>) Nanoparticles on the Properties of Laboratory Bentonite Drilling Fluid," in *SPE Norway One Day Seminar*, Bergen, 2018.
- [80] M. Belayneh, B. S. Aadnøy and T. Sharman, "Dynamic and Static Sagging Characterization and Performance of Four Oil Based Muds," in *International Conference on Ocean, Offshore and Arctic Engineering*, South Korea, 2016.
- [81] A. Saasen, L. Dawei and C. Marken, "Prediction of Barite Sag Potential of Drilling Fluids from Rheological Measurements," in *SPE/IADC Drilling Conference*, Amsterdam, 1995.
- [82] M. V. Ohcoa, "Analysis of Drilling Fluid Rheology and Tool Joint Effect to Reduce Errors in Hydraulics Calculations," Texas A&M University , Texas, USA, 2006.
- [83] Ofite, "ofite.com," 19 October 2017. [Online]. Available: <http://www.ofite.com/publications/instructions/121-130-22-instructions/file>. [Accessed 2 April 2019].

# APPENDICES

## APPENDIX A – RHEOLOGICAL MEASUREMENTS

**Table A.1:** Ofite viscometer readings for WBM with 0 grams, 0.2 grams and 0.3 grams of added lignosulfonates

Fluid name (WBM)	Ref			Ref + 0.2 g LS			Ref + 0.3 g LS		
	22°C	50°C	80°C	22°C	50°C	80°C	22°C	50°C	80°C
Fluid Temperature	22°C	50°C	80°C	22°C	50°C	80°C	22°C	50°C	80°C
Shear Rate [RPM]	-	-	-	-	-	-	-	-	-
600	51.5	50	50.5	45.5	45.5	47.5	44	43.5	36.5
300	39.5	39.5	40	35	35	36	32.5	33	30
200	32.5	34.5	34.5	29	29.5	33	27	28	27.5
100	27	28	29	23	25	28	22	22	22.5
60	24	26	27	19.5	23	25.5	18	20	21
30	20.5	23.5	24	18	21	23.5	15.5	16.5	18.5
6	16.5	19.5	20	13	17	20	11.5	12.5	15.5
3	16	19	19.5	12.5	16	19.5	10.5	12	15

**Table A.2:** Ofite viscometer readings for WBM with 0.4 grams, 0.5 grams and 2 grams of added lignosulfonates

Fluid name (WBM)	Ref + 0.4 g LS			Ref + 0.5 g LS			Ref + 2.0 g LS		
	22°C	50°C	80°C	22°C	50°C	80°C	22°C	50°C	80°C
Fluid Temperature	22°C	50°C	80°C	22°C	50°C	80°C	22°C	50°C	80°C
Shear Rate [RPM]	-	-	-	-	-	-	-	-	-
600	40.5	37	33.5	45	34	34	40.5	19	15.5
300	29.5	29	27.5	31.5	27.5	28.5	21.5	17.5	11.5
200	24.5	25.5	25	24.5	23.5	25.5	15.5	12.5	10
100	18.5	20.5	20.5	18.5	19.5	21	11	9.5	7
60	16	18.5	18.5	15.5	16.5	19	8.5	6.5	6
30	13.5	16.5	16.5	13	15	17	6.5	5.5	4.5
6	9.5	12	13.5	9	11.5	14.5	4	3.5	3.5
3	9	11.5	13	8.5	11	14	3	3	3

**Table A.3:** Ofite viscometer readings for WBM with 0.6 grams, 0.7 grams, 0.8 grams and 0.9 grams of added LS

Fluid name (WBM)	Ref + 0.6 g LS			Ref + 0.7 g LS			Ref + 0.8 g LS			Ref + 0.9 g LS		
Fluid Temperature	22°C	50°C	80°C	22°C	50°C	80°C	22°C	50°C	80°C	22°C	50°C	80°C
Shear Rate [RPM]	-	-	-	-	-	-	-	-	-	-	-	-
600	45	35	32	38.5	31	31	37	31.5	31	38	32	31
300	27	22	23	23.5	21.5	22.5	24	22	23	24	21.5	23
200	20	18	19.5	18.5	19	19.5	18.5	17.5	20	19	18	19
100	15	14	15.5	14.5	14	15	13.5	13.5	13.5	13.5	14.5	14
60	12.5	12	14	12	12	12.5	12	10.5	12.5	12.5	11.5	13.5
30	11	10.5	11.5	9.5	10.5	11.5	9.5	9	10.5	10.5	11	11
6	7.5	8	9	7	8	8	6.5	7.5	7.5	7	7	7.5
3	7	6.5	6.5	6.5	7	7.5	6	7	7	6.5	6.5	7

**Table A.4:** Ofite viscometer data for the nano modified water-based fluid, *in-situ*

Fluid name (WBM)	REF + 0.5 g MoS <sub>2</sub>			REF + 1.0 g MoS <sub>2</sub>			REF + 1.5 g MoS <sub>2</sub>		
Fluid Temperature	22°C	50°C	80°C	22°C	50°C	80°C	22°C	50°C	80°C
Shear Rate [RPM]	-	-	-	-	-	-	-	-	-
600	39.5	32.5	31.5	39	29	30.5	39.5	31.5	30.5
300	22.5	21.5	22	21	19.5	21	22.5	20	21
200	17	17	17.5	16.5	16	16	18	16	17
100	12.5	12.5	13	11.5	11.5	12	13	12	12.5
60	10.5	10.5	11	9.5	9.5	10	10.5	10	10.5
30	8.5	9	9.5	7.5	7.5	8	8.5	8.5	9
6	6	6	6.5	5	5.5	6	6	6	6.5
3	5.5	5.5	6	4.5	5	5.5	5	5	6

**Table A.5:** Ofite viscometer data for the nano modified water-based fluid, *ex-situ*

Fluid name (WBM)	REF + 0.5 g MoS <sub>2</sub>			REF + 1.0 g MoS <sub>2</sub>			REF + 1.5 g MoS <sub>2</sub>		
Fluid Temperature	22°C	50°C	80°C	22°C	50°C	80°C	22°C	50°C	80°C
Shear Rate [RPM]	-	-	-	-	-	-	-	-	-
600	36	30	27.5	33.5	29	27.5	37	30	27
300	22	20	19.5	20.5	19.5	19.5	22	20.5	19
200	17	16	16	16	15.5	15.5	17	16.5	16
100	12	11.5	12	11.5	11	12	12.5	12	12
60	10	10	10.5	9.5	9.5	10	10	10	10
30	8	8	8.5	7.5	8	8.5	8	8	8.5
6	5	5	6	5.5	5.5	6.5	5.5	5.5	6.5
3	4.5	4.5	5.5	4.5	4.5	5.5	4.5	5	6

**Table A.6:** Ofite viscometer readings for OWRs of 60/40 and 70/30

Oil Water Ratio	60/40				70/30			
Fluid Temperature	22°C	50°C	80°C	100°C	22°C	50°C	80°C	100°C
Shear Rate [RPM]	-	-	-	-	-	-	-	-
600	151	126.5	108	82	93	72	68.5	56.5
300	86.5	73.5	62.5	48.5	53.5	42	41.5	38.5
200	63	54.5	47	39.5	39	32.5	32.5	30.5
100	39	35	31.5	28	25.5	22	21.5	22
60	29.5	26.5	24	23	19.5	17	17	18.5
30	21	20	19	19	15	15	14	15
6	12	12	12	13	8.5	9	9	11
3	11.5	11	11	12	8	8	8	10.5

**Table A.7:** Ofite viscometer readings for OWRs of 80/20 and 90/10

Oil Water Ratio	80/20				90/10			
Fluid Temperature	22°C	50°C	80°C	100°C	22°C	50°C	80°C	100°C
Shear Rate [RPM]	-	-	-	-	-	-	-	-
600	73	63	58	50.5	103	82	71.5	54.5
300	42.5	38.5	36	33.5	56.5	45.5	40	33
200	32	30	27.5	26.5	41.5	35	31	25
100	21	20.5	19	19	27.5	23	20.5	18
60	16	16	16	15.5	20	16.5	16	13.5
30	13	11.5	13.5	12	13.5	12.5	12	10.5
6	7.5	7.5	8	8.5	7.5	7.5	7	7
3	6.5	6.5	6.5	8	6.5	5.5	5.5	5.5

**Table A.8:** Ofite viscometer readings for EDC 90/10 and EDC 90/10 + 0.5 g poly acrylic

Fluid	EDC 90/10				EDC 90/10 + 0.5 g poly acrylic			
Fluid Temperature	22°C	50°C	80°C	100°C	22°C	50°C	80°C	100°C
Shear Rate [RPM]	-	-	-	-	-	-	-	-
600	62	44	32.5	28	61.5	41	33	29.5
300	31.5	22.5	16.5	15	31.5	21.5	18	16
200	22.5	16	12	11	21.5	15	12.5	11.5
100	12.5	9	7	6.5	12.5	8.5	7	6.5
60	8.5	6	5	5	8	5.5	5	5
30	5.5	4	3	3	5	3.5	3	3
6	2	2	1.5	1.5	2	2	2	1.5
3	1.5	1.5	1	1	1.5	1.5	1.5	1



**Table A.9:** Ofite viscometer readings for EDC 90/10 + 1.0 g poly acrylic and EDC 90/10 + 1.5 g poly acrylic

Fluid	EDC 90/10 + 1.0 g poly acrylic				EDC 90/10 + 1.5 g poly acrylic			
	22°C	50°C	80°C	100°C	22°C	50°C	80°C	100°C
Fluid Temperature	22°C	50°C	80°C	100°C	22°C	50°C	80°C	100°C
Shear Rate [RPM]	-	-	-	-	-	-	-	-
600	65	37.5	32	28.5	57.5	42	34	29.5
300	33.5	18.5	16.5	14.5	29	22.5	18	16.5
200	22	12.5	11.5	10.5	21	14	12	11.5
100	12	7	6.5	6	11	8	7	7
60	8	5	4.5	4.5	7.5	5.5	5	4.5
30	4.5	3	3	2.5	4.5	3.5	3	3
6	2	1.5	1.5	1.5	2	2	2	2
3	1.5	1	1	1	1.5	1.5	1.5	1.5

**Table A.10:** Ofite viscometer readings for 90/10 + 0.5 g poly acrylic and 90/10 + 1.0 g poly acrylic

Fluid	60/40 One-Mul				70/30 One-Mul			
	22°C	50°C	80°C	100°C	22°C	50°C	80°C	100°C
Fluid Temperature	22°C	50°C	80°C	100°C	22°C	50°C	80°C	100°C
Shear Rate [RPM]	-	-	-	-	-	-	-	-
600	149	108	81.5	72.5	107.5	74	59.5	50.5
300	84	59.5	50.5	47	61.5	44.5	37	32
200	62.5	45.5	39.5	37	45.5	33	28.5	24.5
100	39.5	31	28	26	29	21.5	19	17
60	30	24	22	21	21.5	16.5	15	13.5
30	21.5	18	17	16	15.5	12	11.5	10.5
6	11	10.5	10.5	10.5	8.5	7	7	7
3	10	9	9	8.5	7.5	6	6	6

**Table A.11:** Ofite viscometer readings for the 80/20 One-Mul fluid

Fluid	80/20 One-Mul			
Fluid Temperature	22°C	50°C	80°C	100°C
Shear Rate [RPM]	-	-	-	-
600	80.5	64	54.5	45.5
300	48	39	34.5	30.5
200	36	28.5	26.5	23.5
100	23.5	19.5	18	16.5
60	18	15.5	14.5	13.5
30	13	11.5	11,5	10.5
6	8	8	8	7.5
3	7	7	7	7

## APPENDIX B - VISCOELASTICITY

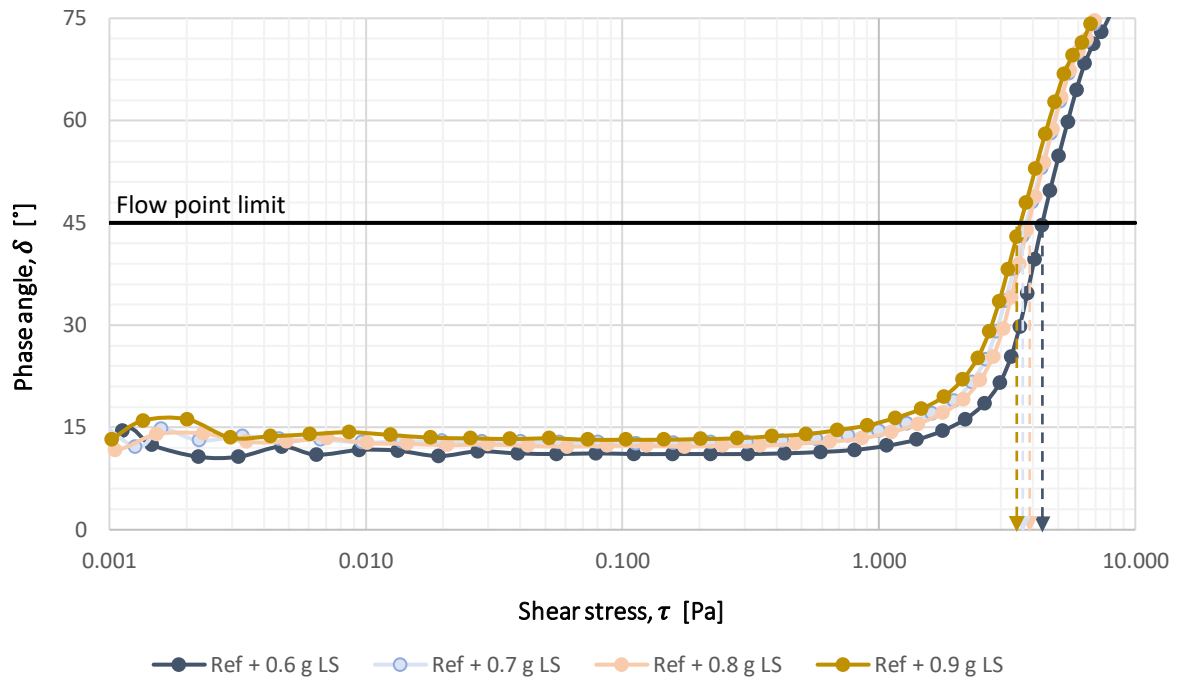


Figure B.1: Phase angle vs. shear stress for WBM containing 0.6-0.9 grams of added lignosulfonates

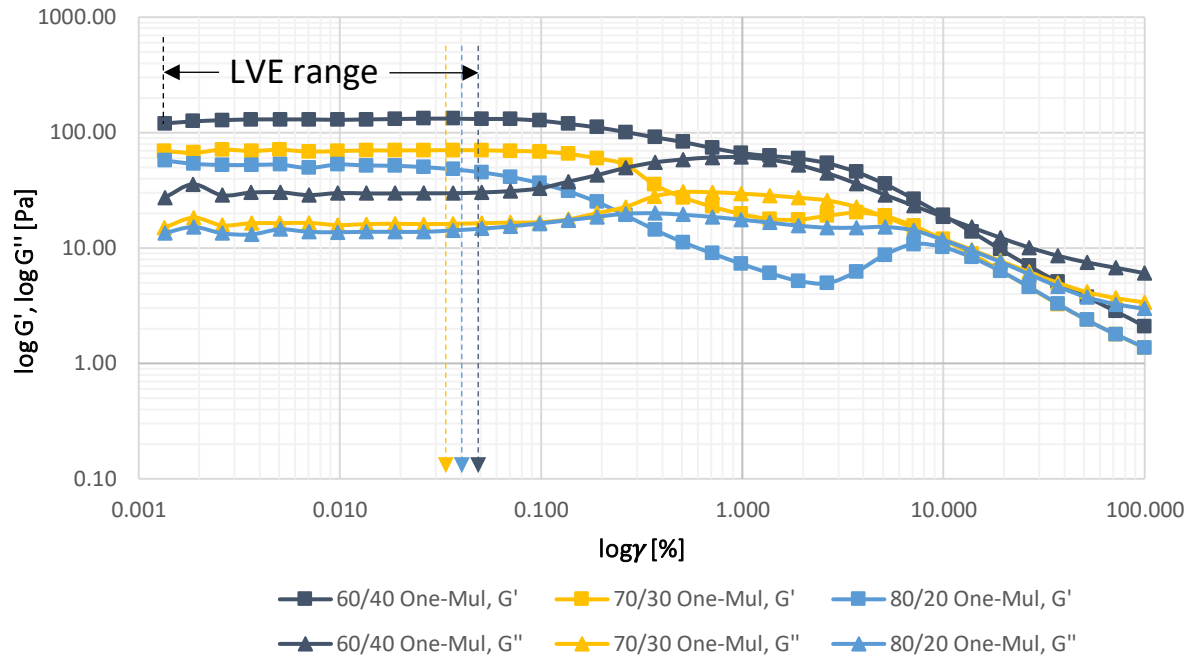


Figure B.2: Storage and loss modulus vs. strain for OWRs of 60/40, 70/30 and 80/20 containing additional One-Mul

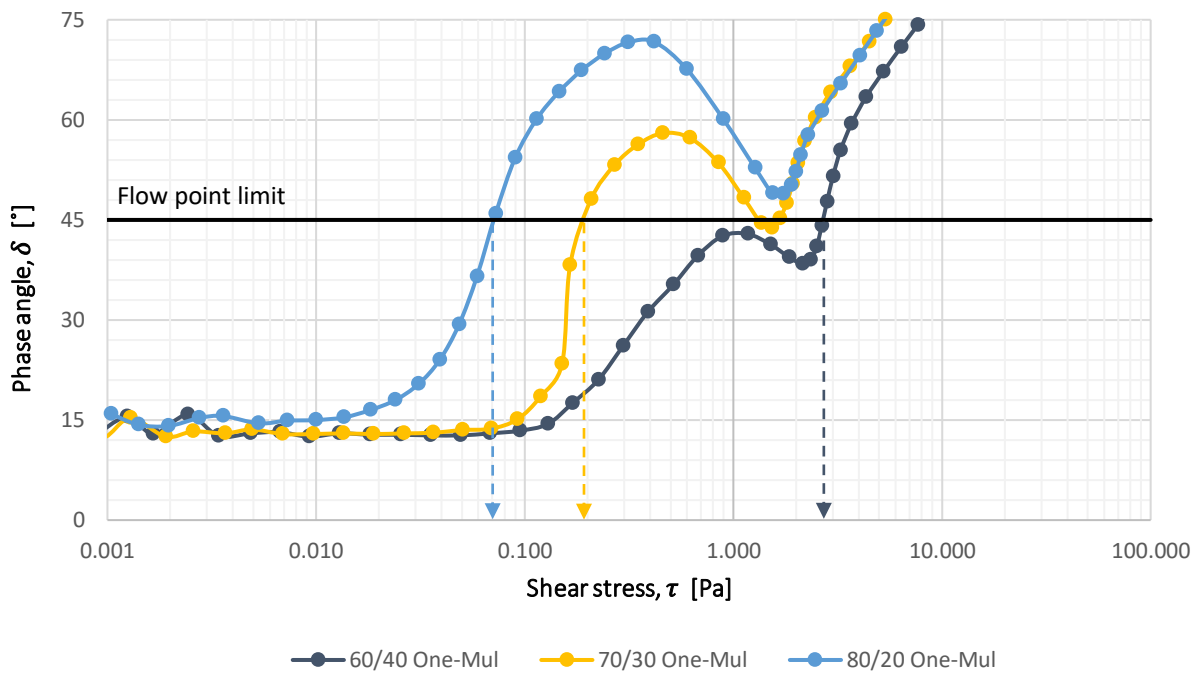


Figure B.3: Phase angle vs. shear stress for OWRs of 60/40, 70/30 and 80/20 containing additional One-Mul

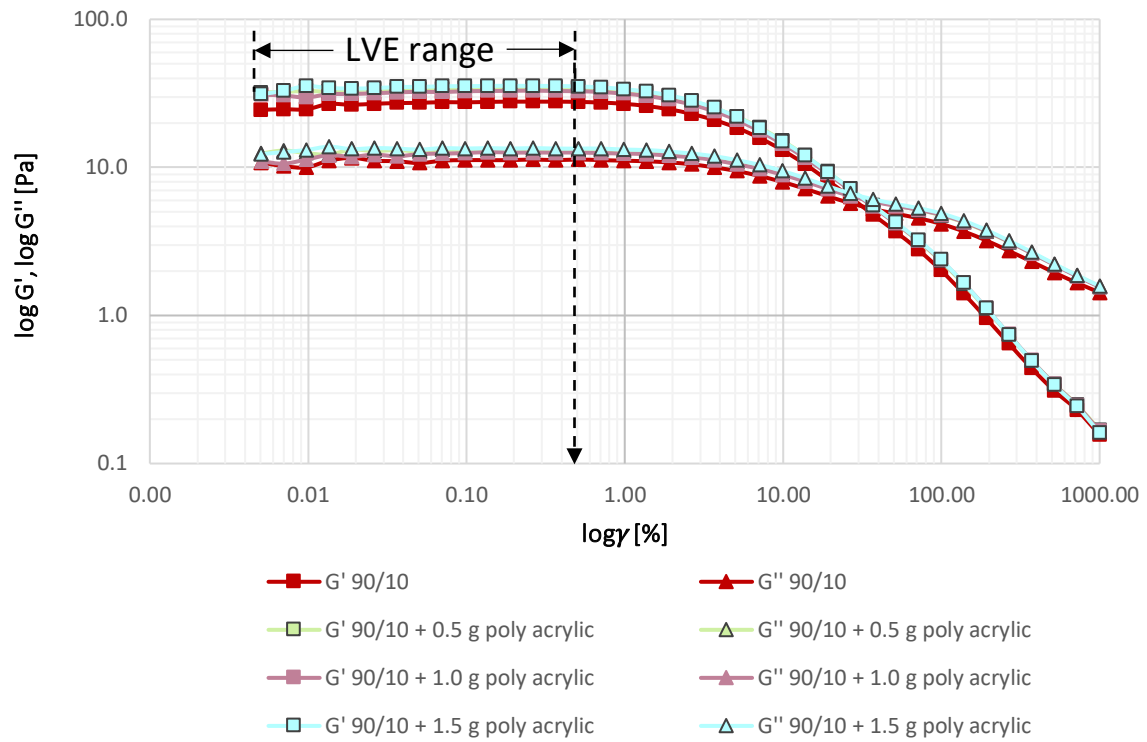


Figure B.4: Storage and loss modulus vs. strain for the 90/10 fluid and the 90/10 fluids modified with poly acrylic

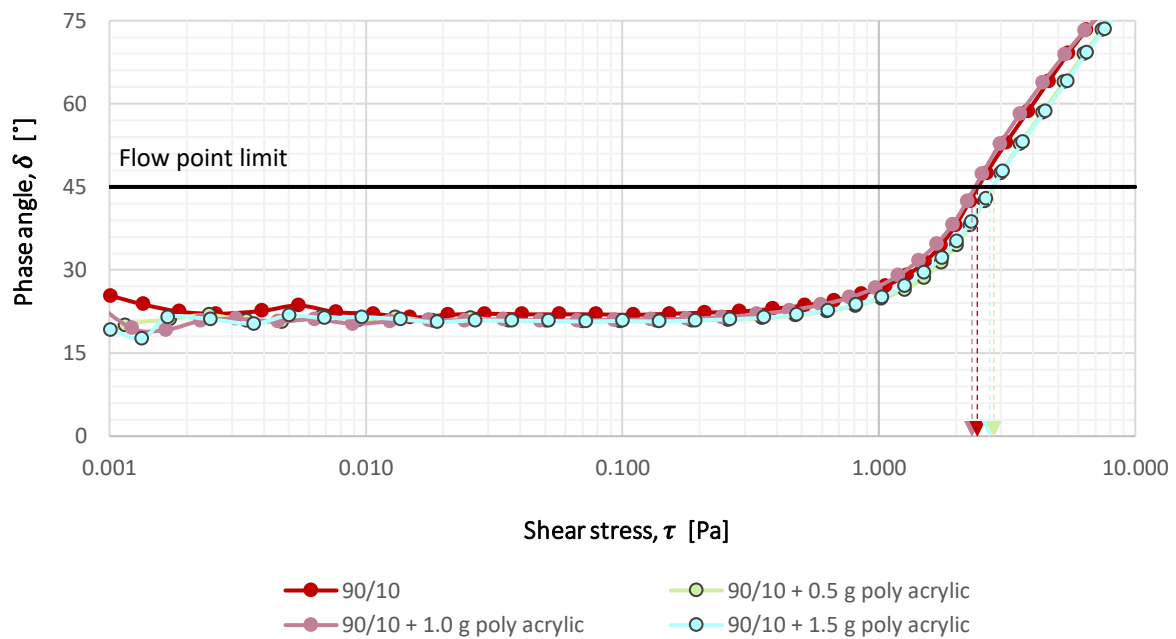


Figure B.5: Phase angle vs. shear stress for the 90/10 fluid and the 90/10 fluids modified with poly acrylic

## APPENDIX C – BARITE SAG

**Table C.12:** Summary of dynamic sag measurement data for the M-I Swaco fluids

Fluid	$W_{\text{initial}}$ [g]	$W_{\text{final}}$ [g]	Sag Factor	wt% additive	$\Delta MW$ [SG]
60/40	28.88	30.42	0.527	0.00	0.08
70/30	29.81	31.50	0.528	0.00	0.09
80/20	29.18	32.11	0.550	0.00	0.15
90/10	29.01	32.54	0.561	0.00	0.18

**Table C.13:** Summary of dynamic sag measurement data for the 90/10 fluids

Fluid	$W_{\text{initial}}$ [g]	$W_{\text{final}}$ [g]	Sag Factor	wt% additive	$\Delta MW$ [SG]
90/10	29.01	32.54	0.561	0.00	0.18
90/10 + 1.5 g poly acrylic	29.31	32.37	0.552	0.50	0.15
90/10 + 1.0 g poly acrylic	29.70	32.09	0.540	0.33	0.12
90/10 + 0.5 g poly acrylic	29.86	31.60	0.529	0.17	0.09

**Table C.14:** Summary of dynamic sag measurement data for the EDC 90/10 fluids

Fluid	$W_{\text{initial}}$ [g]	$W_{\text{final}}$ [g]	Sag Factor	wt% additive	$\Delta MW$ [SG]
EDC 90/10	35.05	40.08	0.572	0.00	0.25
EDC 90/10 + 1.5 g poly acrylic	34.24	38.91	0.568	0.50	0.23
EDC 90/10 + 1.0 g poly acrylic	35.47	38.64	0.545	0.33	0.16
EDC 90/10 + 0.5 g poly acrylic	34.12	35.45	0.519	0.17	0.07



Figure C.6: OWR 90/10 EDC fluid after static sag test

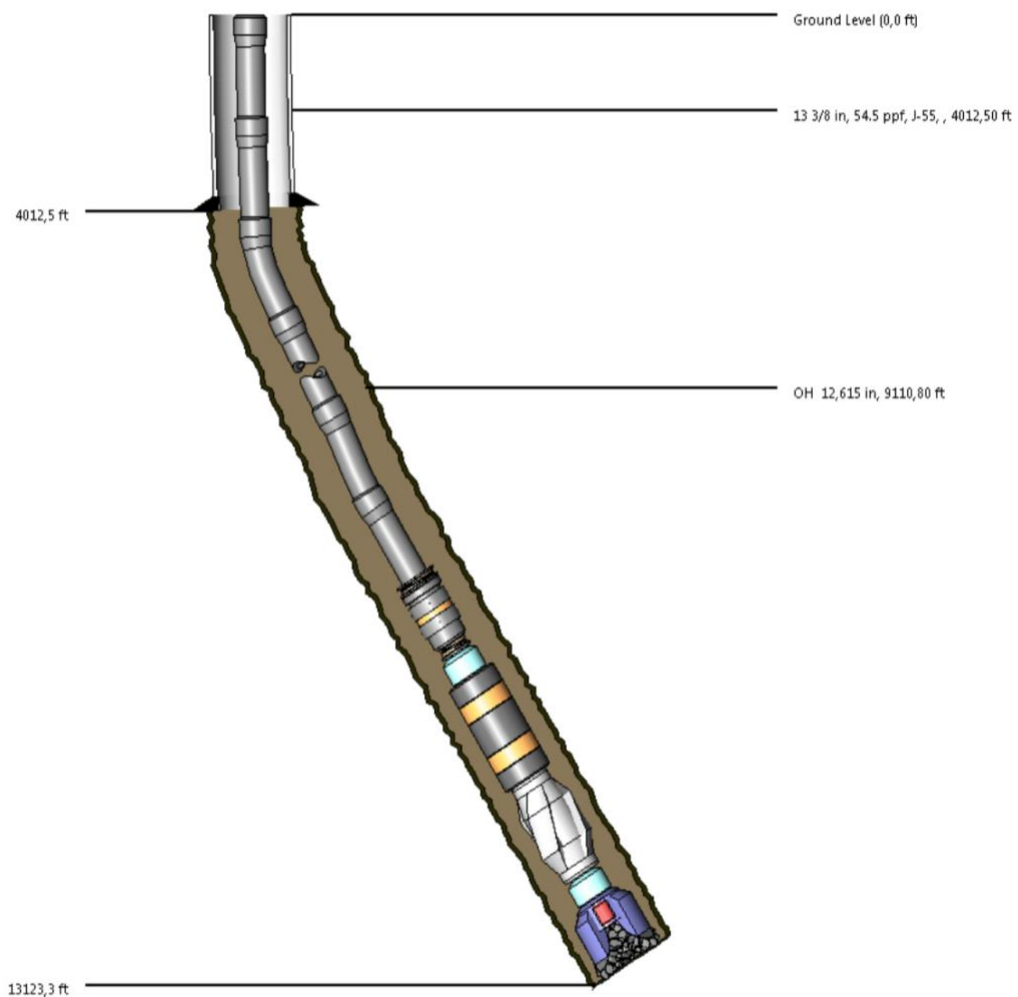


Figure C.7: OBMs from M-I Swaco after aging

## APPENDIX D – FRICTION MEASUREMENT AND TORQUE & DRAG SIMULATIONS

**Table D.15:** Average values for the coefficient of friction for the various fluid systems

Fluid	REF	REF + 0.5 g MoS <sub>2</sub>	REF + 1.0 g MoS <sub>2</sub>	REF + 1.5 g MoS <sub>2</sub>
In-situ	0.184	0.183	0.119	0.199
Ex-situ	0.184	0.129	0.110	0.145



**Figure D.8:** Illustration of the simulation well used for torque and drag simulations



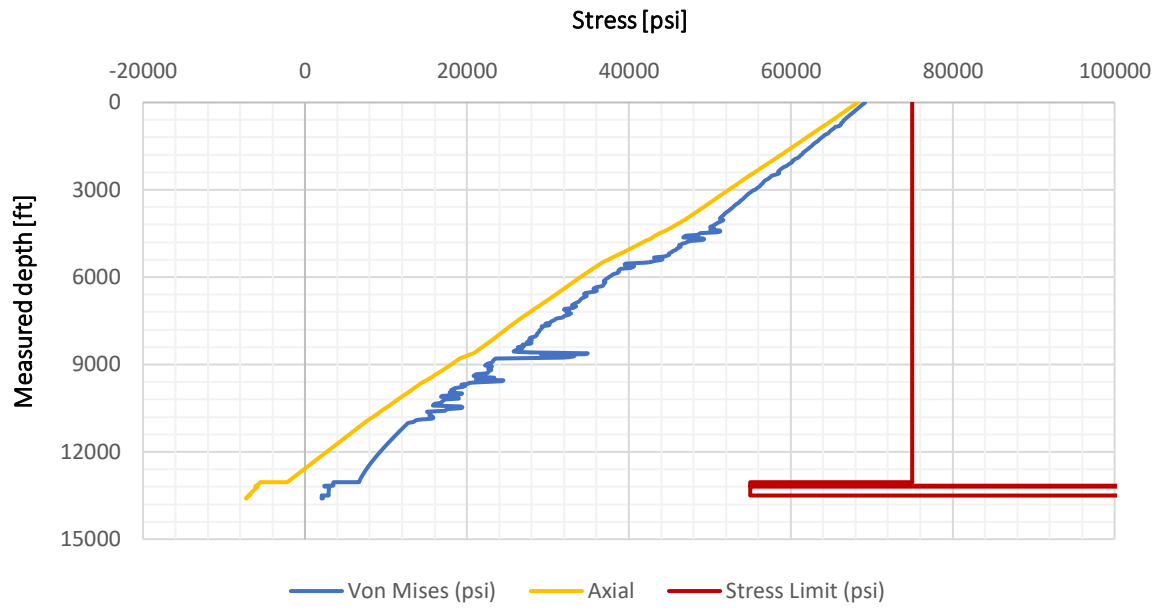


Figure D.9: Stress trip out for the reference fluid

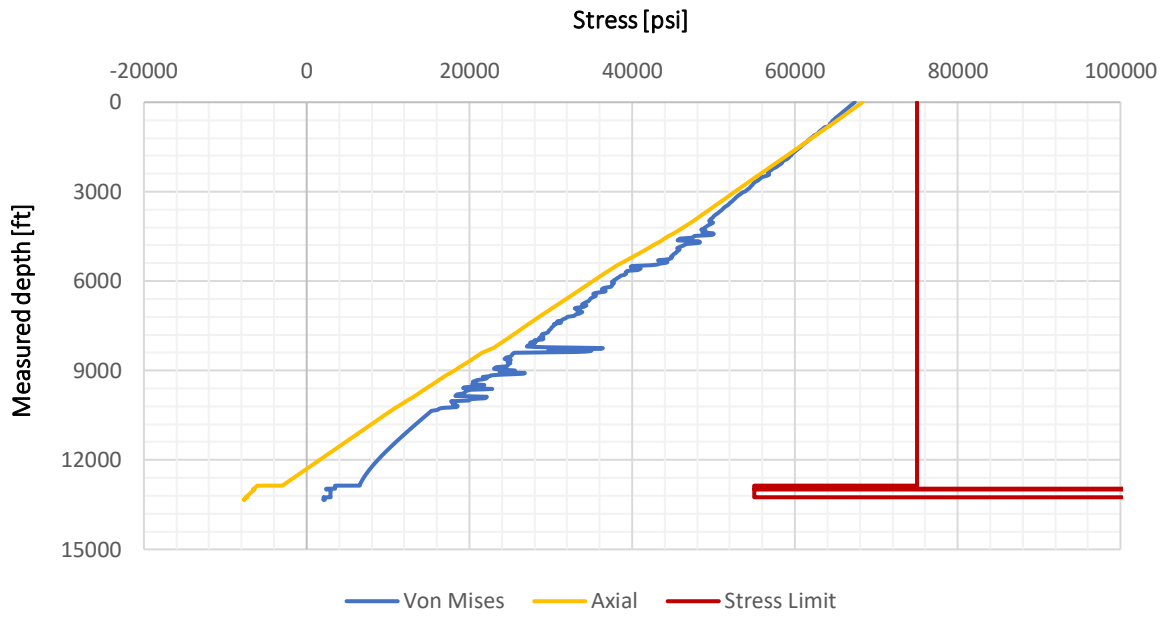


Figure D.10: Stress trip out plot for the reference + 1.0 g MoS<sub>2</sub> fluid

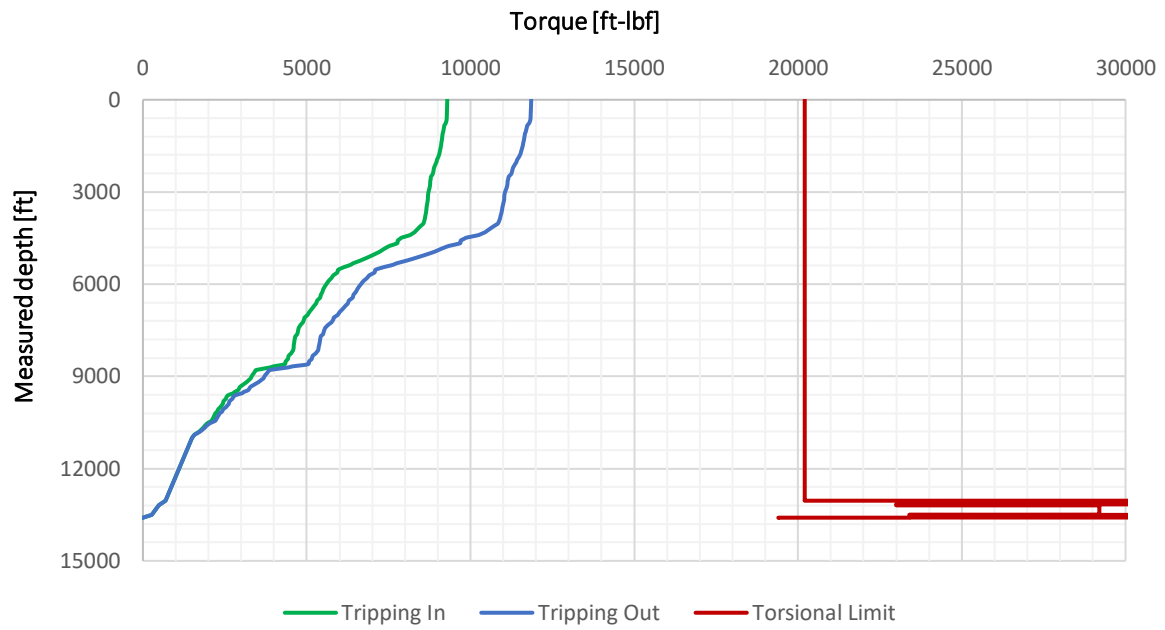


Figure D.11: Torque plot for the reference fluid

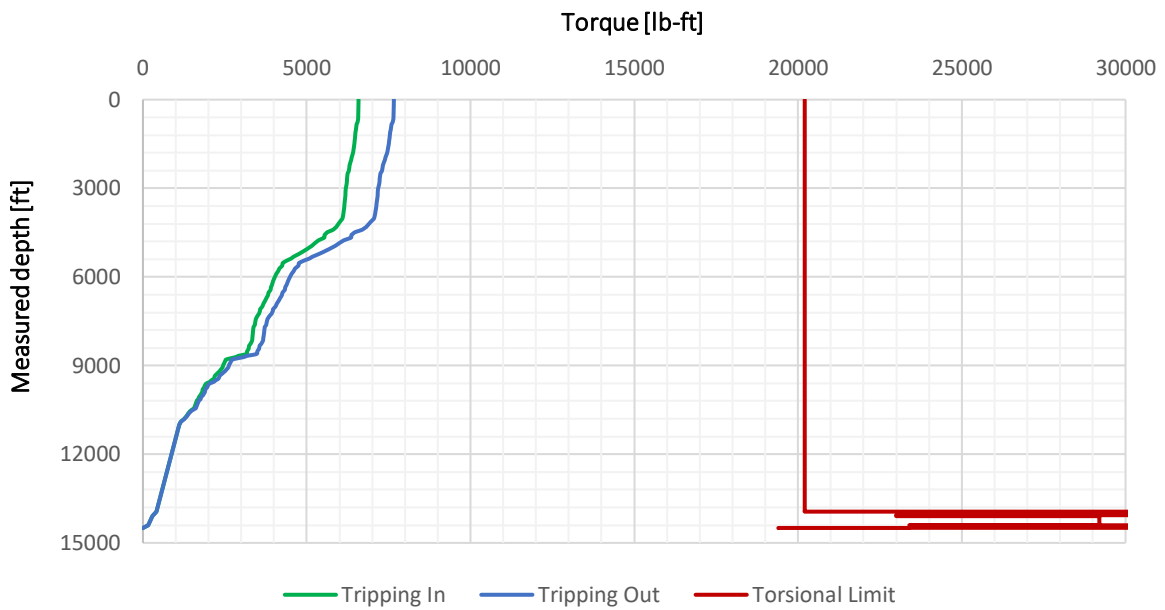


Figure D.12: Torque plot for the reference + 1.0 g MoS<sub>2</sub> fluid